UNIVERSITY OF Southampton

University of Southampton Research Repository

Copyright © and Moral Rights for this thesis and, where applicable, any accompanying data are retained by the author and/or other copyright owners. A copy can be downloaded for personal non-commercial research or study, without prior permission or charge. This thesis and the accompanying data cannot be reproduced or quoted extensively from without first obtaining permission in writing from the copyright holder/s. The content of the thesis and accompanying research data (where applicable) must not be changed in any way or sold commercially in any format or medium without the formal permission of the copyright holder/s.

When referring to this thesis and any accompanying data, full bibliographic details must be given, e.g.

Thesis: Author (Year of Submission) "Full thesis title", University of Southampton, name of the University Faculty or School or Department, PhD Thesis, pagination.

Data: Author (Year) Title. URI [dataset]

University of Southampton

Faculty of Engineering and Physical Sciences

Chemistry

A Systematic Study into the Influence of Aromatic Stacking Interactions and Fluorine Substituent Effects on Molecular Organic Crystal Assembly

by

Eleanor Marie Dodd

Thesis for the degree of Doctor of Philosophy

April 2020

University of Southampton

Abstract

Faculty of Engineering and Physical Sciences

Chemistry

Thesis for the degree of Doctor of Philosophy

A Systematic Study into the Influence of Aromatic Stacking Interactions and Fluorine Substituent Effects on Molecular Organic Crystal Assembly

by

Eleanor Marie Dodd

This thesis reports the aromatic stacking interactions observed within a system of related fluorinated organic compounds, fluorinated benzylideneanilines (or fluoroanilines). A comprehensive library of fluoroaniline structures was assembled to systematically study the effect of fluorine substitution primarily on the aromatic stacking interactions, but also the complementarity with any other non-covalent intermolecular interactions. Through controlled, iterative changes to the number and position of fluorine substituents in the molecule, it is possible to examine the shifting preference for different aromatic interaction configurations.
The entire library of structures was structurally characterised through single crystal X-ray diffraction analysis. The structures are categorised into groups based on their crystal assembly, intermolecular geometry and spatial packing similarity. A subset of these structures was selected for quantitative analysis of the intermolecular interactions by high resolution data collection and quantum crystallographic methods. Topological analysis of the experimental electron density field gradient using Quantum Theory of Atoms in Molecules and complementary theoretical calculations using the interaction energy approach reveal the nature of these interactions. These analyses compute energies for intermolecular interactions from which the observed crystal structure assembly can be rationalised.
The primary results of this study characterise the influence of fluorine substituents on the molecular packing in the crystal. Significantly, these findings show that contrary to popular belief, this influence is not necessarily due to atom-atom intermolecular interactions, but rather to dipole-dipole direct substituent interactions between stacked aromatic rings. This study also generated many more results which characterise the nature of these interactions and when combined with the categorisation of packing motifs this provides a framework within which molecular assembly in this system can be rationalised. From this it is possible to identify the nature of interactions which are clearly dominant and provide a means for characterising other interactions which are not structure-directing.

Table of Contents

Table of Tables

Table of Tables

Table of Tables

Table of Tables

Table of Tables

Table of Figures

Table of Figures

Table of Figures

Table of Figures

List of Accompanying Materials

Key data underpinning this thesis can be found in the attached appendices, as indicated when discussed in the related sections of the text. A full set of Accompanying Materials has been deposited in the University of Southampton research data repository and has been assigned the Digital Object Identifier DOI: 10.5258/SOTON/D1348

https://doi.org/10.5258/SOTON/D1348

These materials comprise:

Crystallographic Information Framework files (CIFs) for all structures determined; these contain experimental data collection parameters, structure solution and refinements details, structure factors and a complete description of the crystal structure parameters.

Raw diffraction data for high resolution experiments, accompanied by the results of property calculations on the electron density and CIFs containing multipole refinement parameters.

Similarity parameter data and coordinate files for the similarity motifs determined by XPac.

Outputs from the PIXEL calculations on intermolecular energies.

Hirshfeld surface data and enrichment ratio calculations.

Research Thesis: Declaration of Authorship

Print name:	Eleanor Marie Dodd

Title of thesis:	A Systematic Study into the Influence of Aromatic Stacking Interactions and Fluorine Substituent Effects on Molecular Organic Crystal Assembly

I declare that this thesis and the work presented in it are my own and has been generated by me as the result of my own original research.

I confirm that:

1. This work was done wholly or mainly while in candidature for a research degree at this University;
2. Where any part of this thesis has previously been submitted for a degree or any other qualification at this University or any other institution, this has been clearly stated;
3. Where I have consulted the published work of others, this is always clearly attributed;
4. Where I have quoted from the work of others, the source is always given. With the exception of such quotations, this thesis is entirely my own work;
5. I have acknowledged all main sources of help;
6. Where the thesis is based on work done by myself jointly with others, I have made clear exactly what was done by others and what I have contributed myself;
7. None of this work has been published before submission

Signed:

Date:

Acknowledgements

Funding from EPSRC, through the National Crystallography Service and University of Southampton Doctoral College.

European Crystallographic Association for providing a grant that allowed me to attend the Erice International School of Crystallography 52nd Course in Quantum Crystallography.

My supervisor Prof. Simon Coles for his support and guidance throughout my time at the University of Southampton.

Dr. Graham Tizzard, Dr. Peter Horton, Dr. Mateusz Pitak and Dr. Tony Keene, who taught me the ins and outs of crystallography. Sarah Milsted for her pragmatism and advice. All of the NCS team and Coles group for their kindness and support.

Dr. Terry Threlfall for the synthesis and crystallisation of hundreds of fluoroanilines over the course of this project. Phil Adler, Sam Ling and Liam Oliver for the data collection of a not insignificant number of these crystals.

My fellow Ph.D and masters students (Phil, Lucy, Joe, Wilma, Rob and Gopikka), particularly Ningjin for her friendship and boundless encouragement in the last stages of my project.

Dr. Amber Thompson, my tutor at the Durham Intensive Teaching School in X-Ray Structure Analysis, whose tutorship and counsel was invaluable at a difficult point in my progression as a crystallographer and researcher.

Matt Reeves, University of Edinburgh, for his PIXEL advice and friendship.

And of course my family (Mum, Dad, Lawrence, Lexie) and friends, whose continued belief and support kept me going. And finally, my partner Oliver who has been with me through all of it.

Definitions and Abbreviations

1D – One dimensional

2D – Two dimensional

3D – Three dimensional

^{19}F NMR – Fluorine 19 Isotope Nuclear Magnetic Resonance: a spectroscopic technique

A – Acceptor

Å – Angström

AO – Angled Overlap

B – Benzene

B/HFB – Co-crystal of benzene and hexafluorobenzene

BCP – Bond critical point

CCDC – Cambridge Crystallographic Data Centre

CCP – Cage critical point

CIF – Crystallographic Information Framework

Co-crystals - Crystals with two or more components of different chemical moieties

CP – Critical Point

CSD – Cambridge Structural Database

D – Donor

DFT – Density Functional Theory

DNA – Deoxyribonucleic Acid

EML – Espinosa-Molins-Lecomte approach

ESP – Electrostatic Potential

HFB – Hexafluorobenzene

H-t-H – Head-to-Head overlap

H-t-T – Head-to-Tail overlap

IAM – Independent Atom Model

IUPAC – International Union of Pure and Applied Chemistry

KAP – Kitaigorodskii's Aufbau Principle

NCI – Non-covalent Interaction

NLO – Non-linear Optics

PIXEL – A program for semi-classical density sums interaction energy calculations

RCP – Ring Critical Point

QTAIM – Quantum Theory of Atoms in Molecules

XPac – A program for evaluating the spatial similarity between crystal structures

Chapter 1 Introduction

1.1 Crystal Engineering

The crystalline solid state is significant in many chemical disciplines, encompassing materials science, protein biology and the characterisation of synthetic products.

For example, in the pharmaceutical industry, crystal forms are more stable than their amorphous equivalents and so molecular crystals are preferred as pharmaceutical products[1]. There are, however, a multitude of other properties arising from the crystal structure that might affect the success of a potential drug. The crystal arrangement can influence the solubility, bioavailability, tabletability and mechanical properties that would affect the manufacture of the drug[1,2]. The understanding and control of these properties is, therefore, vital to producing an effective drug. Here the principles of crystal engineering provide the tools to success[1,3].

Crystal engineering is a field of research dedicated to the design of crystal structures with desirable properties. This is accomplished through an understanding of intermolecular interactions and their role in the assembly of the crystal structure[4,5]. These intermolecular interactions are defined by the functional groups present in the molecules or moieties in the crystal. Tuning these functional groups, in terms of both size and chemical properties, can therefore affect the orientation and conformation of the nearest neighbours to a molecule in the solid lattice and thereby determine the nature of the crystal packing.

At its highest level, crystal engineering can relate the molecular structure to both the crystal structure and the bulk properties of the material. This opens pathways to broader applications, such as in organic semiconductors, optoelectronics and biophysics. The ability to design mechanical properties in functional materials is one of the major goals of modern crystal engineering[6].

The understanding of how the structural features of the molecules contribute to the assembly of the crystal remains fundamental to all levels of crystal engineering.

1.1.1 Crystal Assembly

Crystal assembly is principally directed by close-packing considerations[4,7,8]. Thermodynamic principles dictate that the most stable crystal structure is obtained by packing the molecules as close to one another as possible, maximising intermolecular contact and minimising void space[9]. This is the basis of close-packing principles as put forward by Kitaigorodskii[10,11].

Kitaigorodskii's theory describes the "bumps and hollows" of the molecular surface. Ideal packing arrangements are obtained through the complementary fitting of these features between neighbouring molecules, an idea emphasized by Pauling and Delbrück[8,12]. Therefore, the geometric properties of the molecule are crucial to understanding the crystal assembly.

It is important to note that, for any given molecule the most thermodynamically stable crystal structure may not crystallise as readily as other morphologies. Crystal nucleation and growth are kinetically controlled and less stable but faster growing nuclei are likely to dominate the observed crystal structures. The deviation from ideal close-packing and the change in energy between these structures tend to be small. Numerous metastable structures can co-exist alongside the thermodynamically favourable structure, as demonstrated by polymorphism[13–18].

Energetically stabilising intermolecular interactions, such as hydrogen bonding, can also result in deviations from ideal close-packing. In particular, interactions with strong directionality can have a profound effect on the orientation of molecules[4,8,10,19]. These atom-to-atom interactions can be abstracted as anchors or tethers between specific points on neighbouring molecules[20].

Additionally, when rationalising crystal packing structure it is important to consider the electrostatic energy. Although they are more dominant in ionic crystals, electrostatic interactions are still a significant factor in the assembly of molecular crystals. The electrostatic energy is minimised where like-to-like interactions are avoided; bump to hollow and acceptor to donor configurations are more favourable[8].

The interplay of these cooperative and competing factors leads to a complex picture of crystal assembly. Advancement in computational chemistry has made crystal structure prediction from the molecule more viable; predictions are increasingly accurate[9,16,21–23]. However, it can still be useful to use models such as Kitaigorodskii's Aufbau principle in order to rationalise the structures observed.

Kitaigorodskii's Aufbau principle (KAP) is an extension of close-packing principles and describes the conceptual construction of a crystal in stages[24–26].

> "The following is the most useful way for dealing with packing in molecular crystals. We must first of all deduce all possible methods of constructing chains of molecules (formations extending in one dimension) and then demonstrate what layers are possible (formations extending in two dimensions), followed finally by considering layer stacking in the crystal (a formation extending in three dimensions)"
>
> **A. I. Kitaigorodskii, 1961**[11]

As described, the first step is the formation of chains from the molecules under certain symmetry operations. These chains coalesce into sheet sub-structures which are then assembled to form the full crystal structure. This approach relies on an understanding of crystal structure symmetry and the geometric constraints of the organic molecule being studied. The concepts of symmetry will be explored in Section 2.1.1.

KAP utilises geometry, thermodynamics and symmetry to build up a picture of the crystal structure. The approach can be used to visualise different components of the structure, identifying various motifs such as the chains and sheets.

These motifs highlight the intermolecular interactions between the molecules[25]. Identifying the combination of different interactions present provides a valuable insight into the network of interactions which form the three-dimensional crystal structure.

The structural control that these interactions enact upon the crystal are of the upmost importance to the field of crystal engineering. These atom-to-atom interactions can be manipulated and engineered to produce a crystal structure with desired properties once there is an understanding of their directionality and strength[4,6,25].

1.1.2 Non-Covalent Interactions

The term non-covalent interaction (NCI) is used in both supramolecular chemistry and crystal engineering to describe all intermolecular interactions occurring between molecules. Non-covalent interactions are very weak compared to covalent bonds. The bond dissociation energy of a covalent bond is about 400 kJ mol^{-1} whereas the strength of interaction for most non-covalent interactions is -5 kJ mol^{-1} or less (with the exception of strong hydrogen bonds, which can achieve -15 kJ mol^{-1})[27]. The term refers to both attractive and repulsive interactions but is generally used in the description of energy stabilising contributions[5,28–30].

The total energy of a crystal lattice is the sum of all non-covalent interactions, encompassing Coulombic forces, charge, polarization, dipole-dipole interactions, hydrogen bonding, and dispersive forces[31]. These interactions can be categorised in a number of ways, most broadly as either atom-atom or molecule-molecule interactions.

Crystal engineering often places an emphasis on highly directional atom-atom interactions such as hydrogen bonding or halogen bonds[29]. These atom to atom interactions are habitually treated as analogous to covalent chemical bonds though they are orders of magnitude weaker. These interactions will often be denoted in the form X – H ··· A to define an intermolecular "bond"[19]. It is important to acknowledge that proximity of neighbouring atoms does not necessitate that an

atom-atom intermolecular interaction is present. Such relationships may be near to neutral or repulsive and should be considered as “short contacts” in the absence of qualitative data for the energy of the supposed interaction.

Molecule-molecule interactions, by contrast, are more nebulous; there are no specific atom locations associated with the interaction. Instead, the interactions are described by the charge distributions of the molecules and how these influence one another[19]. Dispersion is the clearest example of molecule-molecule interactions.

Dispersive energies arise from the interaction of transient dipoles in both polar and non-polar species. These instantaneous dipole moments are the result of fluctuations in the electron density distribution in the molecule. The strength of the dispersive energy is proportional to the polarizability of the molecule[32]. Polarizability of an atom expresses how tightly outer electrons are controlled by the nucleus. Tight control over the outer electrons leads to low polarizability as electron density fluctuation in response to an external electric field will not be as great. Dispersion is ubiquitous in molecular crystal structures as all molecules are polarizable to some extent.

Geometric features of the crystal structure are often used as a guide to indicate the presence of particular intermolecular interactions. Whilst this is useful to determine hydrogen bonding and other prominent atom-atom interactions it can lead to misinterpretation and neglects important contributions, such as dispersion, that are not necessarily highlighted by geometric features[33,34].

In short, the requirements and relative stabilising energy of all various intermolecular interactions drive the geometry of the crystal packing and not the other way around.

1.1.3 Hydrogen Bonding

For the purposes of molecular crystal engineering, hydrogen bonding is considered to be the fundamental interaction for directing the crystal structure[4,35]. The majority of design strategies are based on strong hydrogen bonds due to their capacity for directionality and pattern recognition.

The hydrogen bond is a concept that has existed for approximately a century and covers a broad range of different interactions. An official definition was given by IUPAC in 2011

> “The hydrogen bond is an attractive interaction between a hydrogen atom from a molecule or a molecular fragment X–H in which X is more electronegative than H, and an

atom or a group of atoms in the same or a different molecule, in which there is evidence of bond formation."

International Union of Pure and Applied Chemistry[36]

Hydrogen bonds are generally denoted in the form X – H ··· A, as with other intermolecular interactions. The hydrogen bond acceptor (A) is usually electronegative and must have an accessible source of electron charge, e.g. a lone pair of electrons. The most common hydrogen bond acceptor atoms are oxygen, nitrogen and sulphur.

The pattern recognition of hydrogen bonds is integral in many biological structures, such as DNA (Deoxyribonucleic Acid) and enzyme-substrate complexes. The bond angle between X – H ····· A in the hydrogen bond tends towards 180°, potential energy of the bond drops off sharply with deviation from a linear bond; hence their directionality[32,37].

The hydrogen bond is comprised of several energetic contributions. The definition specifies that X be more electronegative than H. This indicates the Coulombic character, which is important to the directionality of the hydrogen bond. (The more electronegative the donor atom X the stronger this electrostatic character is likely to be as a result of a more positively charged H atom.) Polarization, charge transfer and dispersion are also present in the bond, but are arguably of lesser importance to the bond due to a weaker influence at long range and a smaller impact to the directionality[35,36].

One of the most common hydrogen bonds is formed between O – H groups and O, as observed between H_2O molecules in liquid water and ice. Hydrogen bonding is highly influential in the structure of ice[27]. The many hydrogen bonds within ice form an open framework leading to a structure with lower density than that of liquid water. The prevalence of energy stabilising hydrogen bonds compensates for the loss of dispersion contributions from optimal close-packing.

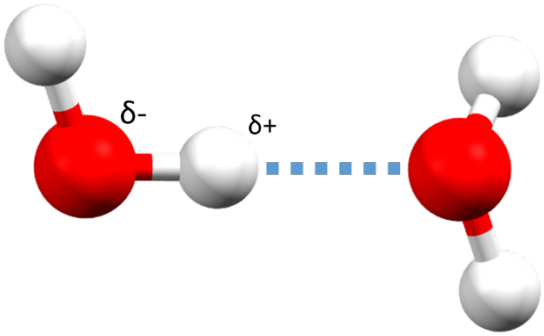

Figure 1.1 Hydrogen bonding in crystalline H_2O i.e. ice. The partial charge of the oxygen and hydrogen atoms is indicated for the hydrogen bond donor. Oxygen from another water molecule acts as the hydrogen bond acceptor.

A variety of other weak intermolecular interactions contribute to the energy and arrangement of the crystal structure. While these interactions are acknowledged in the rationalization of a structure, they have not been as commonly used to inform design strategies. However, in recent years there has been an increased interest in this aspect of crystal engineering and whether weaker intermolecular interactions can meaningfully contribute to crystal and synthon design.

1.1.4 Supramolecular Synthons

Designing a strategy for the formation of a particular crystal structure is a complex task. The crystal structure is not related to the molecular structure by obvious and simple means. Desiraju describes crystal structures as an emergent property; a property which a complex system has but the members of the system do not have[4]. Given these difficulties, it can be useful to draw an analogy between crystal engineering and the better understood field of organic synthesis. Organic synthesis concerns itself with the chemistry of the covalent bond and the mechanisms by which atoms bond to form molecules. A target molecule is synthesised through the correct combination of molecular building blocks known as synthons[38].

Crystal structures can be considered as supramolecular constructs[39] and so have equivalent building blocks known as supramolecular synthons. These supramolecular synthons are built around non-covalent interactions.

> "supermolecules are to molecules and the intermolecular bond what molecules are to atoms and the covalent bond"
>
> **J. Lehn, 1988** [40]

Retrosynthetic analysis in organic synthesis is the process of identifying synthons present in the target structure and using them to select suitable starting materials and pathways by which to synthesise the molecule. Likewise, reverse engineering can be employed to analyse target networks and determine precursor molecules which would yield suitable supramolecular synthons through intermolecular interaction[38]. This approach can be applied to crystal engineering as intermolecular interactions, like covalent bonds, are kinetically controlled[4].

A supramolecular synthon is a structural unit containing molecules or molecular fragments held by intermolecular interactions. The value of the supramolecular synthon for crystal engineering depends on how well it conveys structural motifs and interactions seen in the whole crystal structure[4,41,42]. The synthon must also express the interactions prominent in crystal formation. These tend to be directional interactions, typically hydrogen bonds and those that have the most influence at long range.

A synthon must be stable and predictable to be of mechanistic relevance to design rather than purely a descriptor of observed structure[5,42]. The identification of viable synthons for crystal design should arise from an understanding of intermolecular interaction hierarchies. The hierarchy expresses which interactions will have preference when there are competing forces. Statistical studies of large databases of crystal structures (e.g. the Cambridge Structural Database[57]) have been employed to determine such hierarchies and the patterns commonly observed in hydrogen bonding[43,44]. While based on empirical evidence, these studies are reliant on the measurement of close contact distances and angles to identify the fundamental interactions. Geometric models of this nature are valuable, but it is important that they have a chemical founding. There are many instances of molecular pairings in observed crystal structures which have negligible or even repulsive energy associated with them[45].

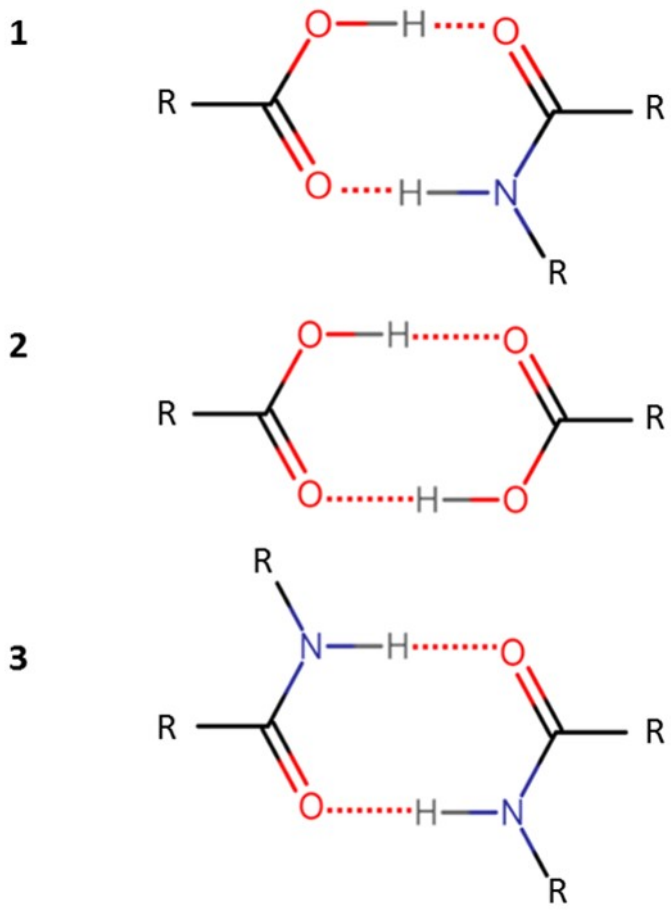

Figure 1.2 Examples of simple synthon dimers connected by strong hydrogen bonds.

1 Heterosynthon between carboxylic acid and carboxylic amide

2 Homosynthon of two carboxylic acids

3 Homosynthon of two carboxylic amides

In a 2012 paper, Dunitz and Gavezzotti calculated the relative energies of several recognised synthon dimers[37]. They found that carboxylic acid, O – H ····· O, and pyrazole, N – H ····· N, ranked highest with a binding energy approximately equal to -35 kJ mol^{-1}. These where followed by carboxylic amides, N – H ····· O, and alcohols, O – H ····· O, with binding energies of approximately -30 and -25 kJ mol^{-1}, respectively.

Dunitz and Gavezzotti also calculated the energies for molecular pairs with recognisably weak interactions. They described such synthons as neutral – adding relatively little stabilisation energy to the cohesion of the molecules. However, they also calculated energies for synthon pairs in which these weak interactions were present alongside much stronger interactions. They observed that the energy associated with the molecular pairing was approximately equivalent to the sum of these interactions. This suggests that, despite competition, weaker interactions can be additive; a complementary effect also noted by other studies[46].

While this effect can aid in molecular cohesion and provide more avenues for crystal design strategies it also adds another layer of complexity to synthon transferability. Synthon transferability (or in-transferability) is one of the complications of synthon design strategies. Even with a knowledge of interaction hierarchies it is difficult to apply synthon design to an organic molecule with multiple function groups[37,42]. Such difficulties result in "synthon polymorphism" by which a particular synthon design can produce more than one distinct supramolecular structure[47,48]. Other limitations of synthon engineering arise from solvent inclusion in the crystal and unforeseen interaction in co-crystallisation[5].

In most cases, even with small rigid organic molecules, an experimental structure cannot be fully rationalised by one motif of robust synthons. Instead a more holistic view of many different interaction contributions, both weak and strong, must be considered to develop a more detailed understanding of the crystal assembly[21,46].

1.1.5 Weak Non-Covalent Interactions

The importance of weak non-covalent interactions has received greater recognition in recent years. Increasingly, research has been focused on the understanding of weaker interactions for designing crystals in the absence of strong hydrogen bonding donors or acceptors[49–53]. The cumulative stabilisation of many weak interactions can account for deviation from close-packing in crystal structures without strong NCI.

There have also been studies into the cooperative effect of weaker NCI alongside strong hydrogen bonds[46,54]. The capacity of weaker NCI to behave cooperatively allows for novel design strategies

in which a crystal structure can be subtly manipulated. For example, the control of hydrogen bond strength and ratio can be used to influence crystal assembly. Following this strategy, a hierarchy of hydrogen bonds is constructed from an assortment of strong and weak hydrogen bonds present in a given system. Then by varying the ratio of strong to weak interactions the system can be finely tuned for a target supramolecular structure[55,56].

For the most part, weak noncovalent interactions are still conceived of in terms of localised atom to atom bonds. This representation favours the importance of electrostatic interactions between specific atoms over more diffuse attractive forces. This bias can lead to misinterpretation of stabilising contributions – in particular, disregarding dispersion as a key component in weak noncovalent interactions.

Whilst flawed, the atom to atom model is still useful as a way of identifying and categorising the variety of weak NCI, such as weak hydrogen and halogen bonding. The atom to atom model should be applied to weaker interactions with caution and an acknowledgement of unseen energetic contributions. Again, without calculations of interaction energy an observed close contact cannot be distinguished as an attractive, as opposed to a repulsive or neutral influence.

1.1.5.1 Weak Hydrogen Bonding

Weak hydrogen bonds are of widespread interest to crystal engineering, in particular, organic hydrogen bonds i.e. C – H ··· X (X = O, N, F, Cl, Br), given their prevalence in organic crystals. These organic hydrogen bonds are categorised within the same criteria as traditional hydrogen bonding, although carbon is much closer to hydrogen in electronegativity. They also behave similarly to traditional hydrogen bonding geometrically and spectroscopically[7]. Although, weaker interaction energies result in less rigid and longer bonds, which are therefore less directional.

While the presence of C – H ··· X close contacts are unavoidable in most organic crystals, studies of the Cambridge Structural Database[57] show that the frequency at which they occur is significantly greater than predictions based on chance[7]. Notably, C – H ··· Cl and C – H ··· F interactions occur much more often than would be expected, suggesting a small stabilising influence not one which is merely neutral or repulsive. Results from theoretical and semi-empirical studies generally support this view[19,58,59].

Organic hydrogen bonds of the form C – H ··· π have also been reported. In these interactions the π electrons of the aromatic system act as a source of electron density for the bond[29,60]. Here the weak interaction is constructed between the hydrogen bond donor and the molecular region associated with the aromatic π system, a slight departure from the purely atom to atom bonding model[19].

1.1.5.2 Halogen Bonding

Halogen bonding is a competitive counterpart to hydrogen bonding often present in organic crystals[61–63]. The term covers any noncovalent interaction in which a halogen acts as an acceptor of electron density but was formally defined by IUPAC in 2013.

> "A halogen bond occurs when there is evidence of a net attractive interaction between an electrophilic region associated with a halogen atom in a molecular entity and a nucleophilic region in another, or the same, molecular entity"
>
> **International Union of Pure and Applied Chemistry**[64]

The halogen bond is typically expressed in the form R – X ··· Y where R – X is the halogen bond donor and X is a halogen atom with an electrophilic (positive) region and Y is the halogen bond acceptor. The halogen's region of positive electrostatic potential is referred to as the "σ-hole"[65,66].

The presence of this positive region in many halogens is somewhat unexpected given their electronegativity. The σ-hole arises from anisotropy of charge distribution within the atom. When the halogen forms a covalent bond its electronic charge is polarised towards the bond. This causes diminished electron density in the outer region along the direction of the bond and increased electron density in the equatorial region. The extent of this anisotropy is, therefore, heavily dependent on the polarizability of the halogen[65].

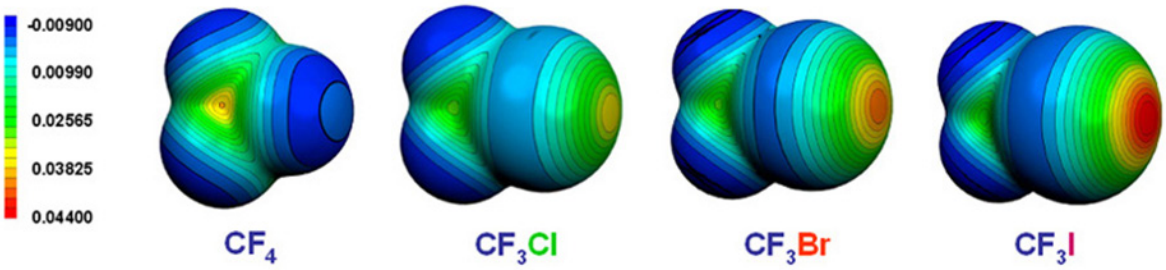

Figure 1.3 Diagram of the electrostatic potential of different halogens. The σ-hole is visible to the right side for Cl, Br and I. Red represents the most positive regions on the scale. This diagram copied from "Halogen Bonding: the σ-hole"[66].

Since the halogen simultaneously possesses a positive σ-hole and a negative equatorial region, it is also possible to form halogen to halogen bonds.

The strength of the halogen bond is determined by the strength of the σ-hole; the greater the polarizability and the lesser the electronegativity of the halogen the more positive the σ-hole. This leads to a hierarchy of halogens from least to most capable of halogen bonding F < Cl < Br < I, as reflected in Figure 1.3.

Like hydrogen bonds, halogen bonds form relatively strong interactions between molecules and possess long-range directionality. Halogen to halogen contacts form in two distinct geometric arrangements: the symmetrical contact type I and the orthogonal contact type II[67]. Type I and type II contacts are fundamentally different in their chemistry[68,69]. The geometry of type I is the result of the two halogen atoms minimising repulsion of contact by approaching at neutral regions of their electrostatic potential surface. Whereas, type II involves the orthogonal approach of the σ-hole and the negative equatorial region. As such, only type II contacts are considered true halogen bonds, following the IUPAC definition.

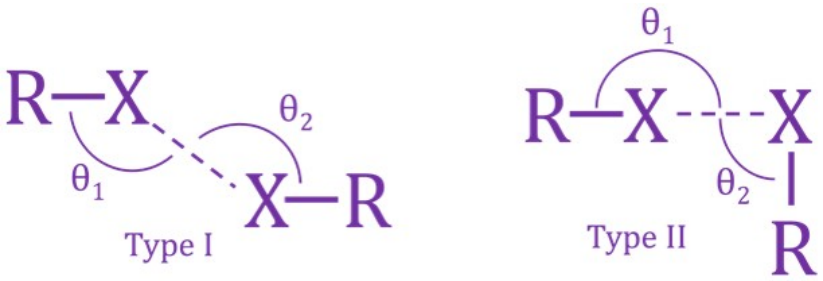

Figure 1.4 The two different halogen contacts. In type I θ_1 and θ_2 are approximately equal. In type II θ_1 is approximately equal to 180° and θ_2 is approximately equal to 90°[61,69].

This orthogonal orientation offers interesting opportunities for crystal design and the halogen bond is acknowledged as a reliable force for the construction of targeted supramolecular complexes[70,71]. The influence of type II halogen bonds are competitive with that of hydrogen bonds and have an advantage over weaker hydrogen bonds in terms of strength and long range directionality[61,72].

Fluorine is generally considered to be unable to participate in halogen bonding. Fluorine has a low polarizability and usually there is no σ-hole visible in electrostatic potential maps[73], Figure 1.3. However, there is evidence to suggest fluorine can be involved in "halogen-like" interactions – this is discussed further in Section 1.2.4.

1.1.5.3 Aromatic Rings

Aromatic rings also participate in non-covalent interactions, though typically these interactions are very weak. Nonetheless, intermolecular interactions between aromatic rings are integral to molecular recognition in many biological processes[74,75]. Examples include: the structure of proteins[60]; the base-pair stacking of nucleic acids such as in duplex DNA[76] and protein–ligand complexation[77]. The presence of aromatic rings in chemical supramolecular systems provide another avenue for crystal design.

These interactions are generally described as π – π stacking. The term is something of a misnomer as it suggests a preference for parallel face-to-face stacks of flat rings[78]. This is often not the case; benzene, as well as many other simple aromatics, generally crystallise in a herringbone arrangement with edge-to-face rings[19,78–80]. There are three distinct orientations associated with favourable interactions in simple aromatics: T-shape edge-to-face, parallel stacks, and parallel displaced (slipped) stacks[80–82].

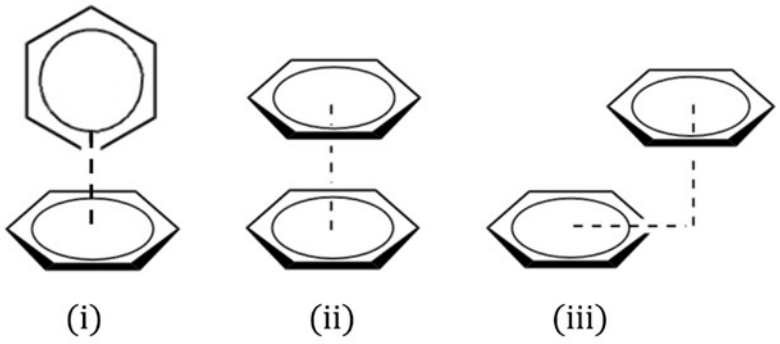

Figure 1.5 Three core configurations of benzene ring packing. i) edge-to-face ii) Parallel stacked, face-to-face iii) Parallel displaced, face-to-face.

In 1990, Hunter and Saunders put forward a simple physical model to describe this behaviour[83]. The authors proposed that favourable π – π attraction was the product of π – σ attraction and π – π repulsion between the rings. They noted that most aromatics exhibit a quadrupole moment leading to a region of negatively charged π electrons above and below the face of the aromatic ring and partial positive charge on the periphery of the ring[84–86]. The direct face-to-face contact of two quadrupoles of this type would be repulsive and avoided in preference for other geometries.

These initial models of interaction have been refined over the years and interpretation of aromatic interactions is now more simply framed by consideration of electrostatics between the π systems and π-electron densities[86–88].

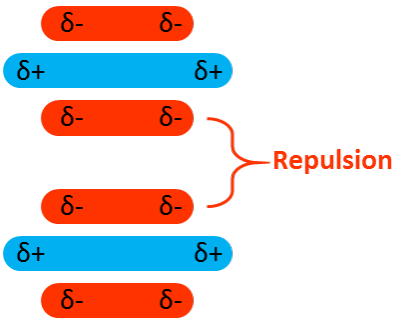

Figure 1.6 Simple electrostatic scheme of a benzene dimer in parallel stacked arrangement. Repulsion between negatively charged π-electron densities has been highlighted.

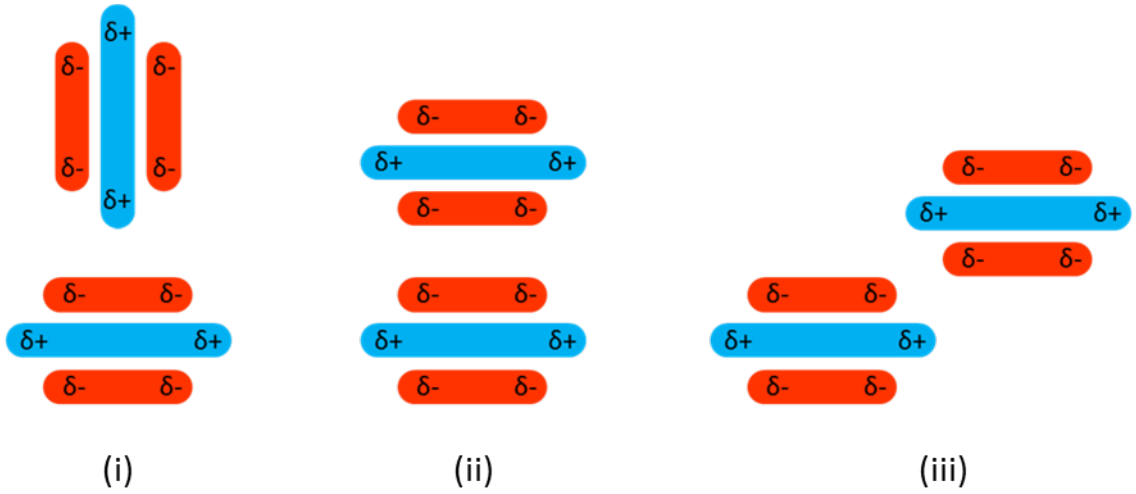

Figure 1.7 Simple electrostatic scheme for the three core stacking arrangements of simple aromatic rings. i) edge-to-face ii) Parallel stacked, face-to-face iii) Parallel displaced, face-to-face.

As the scheme in Figure 1.7 shows, both edge-to-face (i) and parallel displaced face-to-face (iii) arrangements minimise the π-electron repulsion[87]. Energetic calculations from various studies[19,81,89] confirm that the edge-to-face and parallel displaced arrangements are significantly more stabilising than parallel stacks for benzene dimers.

The total stabilisation energy of these interactions is the sum of the electrostatic, dispersive and repulsive energies. These forces, as well as solvophobic effects, drive the geometries for aromatic ring stacking[86,90]. Attraction between the rings is still significant at some distance, which indicates that a substantial part of the attraction comes from long-range forces such as dispersion and electrostatics[81]. Dispersion is found to be the main contributor to the attraction between aromatic rings[88,91]. While electrostatic interaction makes for a smaller part of the stabilising energy, it is highly orientation dependant, even at long-range. The interplay of these two forces is responsible for the directionality of aromatic ring stacking.

For instance, the parallel stacked face-to-face (ii) interaction is a predominantly dispersive interaction, which maximises the surface contact between the aromatic rings, but it results in a reduced contribution from electrostatic stabilisation and an increase in repulsion. While the edge-to-face (i) arrangement minimises the π-electron repulsion it also reduces the surface contact between the rings. The parallel displaced face-to-face (iii) interaction represents a balance between these two, which both maximises for dispersion and offsets the rings to reduce repulsion and promote electrostatic attraction. This arrangement generally results in the greatest attractive force of the three[19,81,89].

Aromatic ring interactions are by no means limited to these three archetypes. Most attractive aromatic non-covalent interactions will lie somewhere between these standard arrangements despite a loss of optimal stabilisation energy between dimers[19,80]. From these observations it should be apparent that the chosen arrangement of the rings in the crystal structure is sensitive to small changes in the chemical environment. Therefore, there are many opportunities for crystal engineering via the exploitation of aromatic interactions[74,79,86,92].

Aromatic interactions can be influenced by bulky substituents, solvation, inclusion of heteroatoms in the aromatic ring and halogenation – particularly fluorine, which has a profound effect due to its electronegativity[74,79,87,91–99]. Fluorinated aromatics will be discussed further in Section 1.2.2.

1.1.5.4 Fluorine in Weak Non-Covalent Interactions

In all of the NCI discussed in this section, fluorine seems to be an exceptional case.

1. Organic fluorine is a weak hydrogen bond acceptor despite its electronegativity.
2. Fluorine does not appear to participate in conventional halogen bonding.
3. Fluorine dramatically influences aromatic-aromatic interactions

In a short 2004 review, Dunitz referred to organic fluorine as the “odd man out” and this certainly seems to be the case[100].

Weak non-covalent interactions are still very poorly understood compared to covalent bonding and traditional hydrogen bonding. There is a great need for further study to successfully use these interactions to influence crystal structure and properties. Intermolecular interactions involving organic fluorine are in particular need of further study. But if understood, their exceptional nature should prove to be a rich avenue for crystal engineering

1.2 Organic Fluorine

Organic fluorine is currently a topic of great interest in crystal engineering and the number of studies dedicated to it increase year on year[101–103]. The properties of organic fluorine can be used to develop new materials through crystal design. Applications extend to liquid crystals, plastics, dyes, organic electronics, catalysts, agrochemicals and pharmaceuticals[101,103], for example the substitution of hydrogen for fluorine in potential drug compounds.

Lightly fluorinated compounds tend to have the same biological recognition as their hydrogen analogues; the steric characteristics of fluorine are similar to those of hydrogen. However, the biological activity can be drastically changed by the substitution. The strength of the C – F bond and the strong electronegativity of fluorine affect the absorption, transport and metabolism of

the potential drug. In general, the fluorinated analogue is more resistant to metabolic degradation. Therefore, fluorine substitution could aid the development of otherwise unstable drugs[102,104].

Evidently, the physiochemical properties of organic fluorine can have a profound influence on the intermolecular forces at play in a crystal structure. To harness these properties for crystal engineering it is important to understand how organic fluorine interacts with neighbouring molecular species and how these interactions can be tuned and adapted for purpose.

1.2.1 Understanding the C – F Bond

The characteristics of fluorine and the C – F bond are both exceptional and fundamental to the behaviour of organic fluorine.

Fluorine is the most electronegative of all the elements, with a value of $\chi = 4.0$ on the Pauling scale[105]. Pauling calculated the electronegativity by considering the partial ionic character of bonded atoms. The electrostatic component of the bond between two atoms A – B is proportional to the difference in electronegativity between A and B, $|\chi a - \chi b|$.

Table 1.1 Selected electronegativity values and differences with respect to carbon[105]

Atom	**χ**		**Bond**	**$\lvert\chi a - \chi b\rvert$**
H	2.1		C – H	0.4
C	2.5		C – C	0
F	4.0		C – F	1.5

As shown in Table 1.1, the difference between carbon and fluorine is 1.5, a comparatively large value, which reveals the highly polarised nature of the C – F bond. Due to this polarisation, the C – F bond has a large dipole which will interact with other dipoles that come into close contact[106]. These electrostatic interactions are a key factor in the intermolecular behaviour of organic fluorine.

The C – F bond is also one of the strongest covalent bonds observed in organic chemistry. The bond dissociation energy of C – F is 441.0 kJ mol^{-1} compared to the weaker C – H bond, which has a dissociation energy of 413.4 kJ mol^{-1} [106]. This strength can be rationalised by considering the significant contribution of electrostatic attraction to the bond.

Due to its highly electronegative nature, the lone pairs on fluorine are largely unavailable for resonance. The 2p valence electrons are held tightly by the nuclear charge of fluorine and so the energy required to remove an electron from a fluorine atom is very high (-1679 kJ mol^{-1}) [106]. Despite the dipole providing fluorine with a significant amount of the electron density ($C^{\delta+} – F^{\delta-}$), fluorine has a low polarizability and is generally thought to be a poor hydrogen bond acceptor.

1.2.2 Interactions between Phenyl and Fluorinated Phenyl

The substitution of hydrogen for organic fluorine in an aromatic ring has a significant impact on the aromatic ring interactions and the electrostatics of the ring. This is highlighted by studying co-crystals of fluorine substituted and un-substituted phenyl groups.

Both benzene (B) and hexafluorobenzene (HFB) rings are arranged in herringbone, edge-to-face, motifs in their crystal structures[74,75,102]. However, the 1:1 mixture of benzene and hexafluorobenzene crystallises into face-to-face stacks. First synthesised by Patrick and Prosser in 1960, the co-crystal (B/HFB) has a higher melting point than either of its two constituent parts, indicating a higher lattice energy for this structure[107]. The co-crystal (B/HFB) exhibits a parallel stacked structure in which the molecules alternate along the stack to form columns, Figure 1.8.

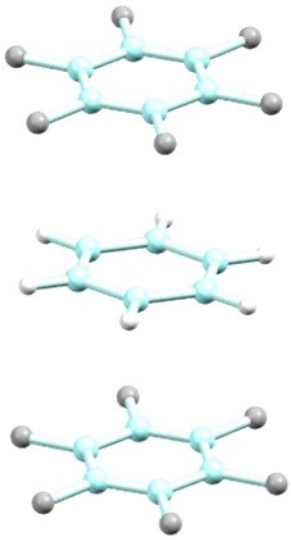

Figure 1.8 Parallel stacked benzene and hexafluorobenzene[108].

1.2.2.1 Quadrupole – Quadrupole Model

Historically, this observation has been rationalised by considering the quadrupole – quadrupole moment interaction between benzene and hexafluorobenzene[84,87,94,109]. The quadrupole moment of benzene is large and negative in sign (-29.0 × 10^{-40} C m^2)[74,84,87,94,100]. The electronegativity of fluorine draws electron density to the periphery of the ring, reversing the sign of the quadrupole

moment, but retaining a similar strength (31.7×10^{-40} C m^2)[74,84,87,94,100]. Parallel stacking of the rings should maximise the electrostatic interaction between the two quadrupole moments.

However, this rationale has been called into question[91,98,100]. It has been noted by Dougherty and Dunitz, among others, that using a multipole expansion to evaluate electrostatic interactions between molecules is only valid at large interaction distances[91,98,100,110]. For benzene and hexafluorobenzene the intermolecular distance between the rings is smaller than the quadrupole dimensions[98]. Therefore, the quadrupole – quadrupole model can be dismissed as insufficient for understanding interactions between the adjacent, stacked molecules. Despite this, the quadrupole model persists as the default rationalisation for aromatic attraction in many articles.

1.2.2.2 π-Polarisation Model

The stacking arrangements of phenyl and perfluorophenyl rings have also been rationalised by considering the substituents' effect on the π-electron distribution. Electron withdrawing groups, such as fluorine, deplete the π-electron density in the aromatic ring. Whereas, electron donating groups will increase the π-electron density associated with the aromatic ring. Depletion of π-electron density creates an 'electron-poor' face, which will exhibit less repulsion when parallel stacked with an unsubstituted ring. The opposite is true for donation to π-electron density, which creates an 'electron-rich' face. Thereby, substituents can modulate the strength of attraction or repulsion by polarisation of the aromatic rings[53,87,90,111,112].

By this mechanism, as with the quadrupole – quadrupole moment interaction, parallel stacked dimers between phenyl and perfluorophenyl should maximise the electrostatic interaction between the π-electron rich face of the unsubstituted ring and the π-electron depleted face of the perfluorinated ring, Figure 1.9. These are referred to as "aromatic donor-acceptor interactions"[78].

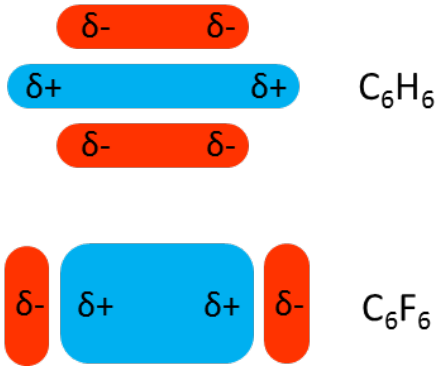

Figure 1.9 Simple electrostatic scheme used to rationalise the alignment of benzene and hexafluorobenzene through contact of π-electron rich and π-electron poor surfaces.

In this model, the polarising effect of certain substituents are presumed to affect the whole aromatic π-system through resonance. Electrostatic potential (ESP) surfaces are often used to support this interpretation[88,112–114].

The ESP is a measure of the potential interaction of a molecule with a positive test charge at a given point in space. Negative electrostatic potential corresponds to an attractive interaction with the charge, while positive electrostatic potential indicates repulsion. Typically, the ESP is mapped onto the electron density isosurface of a molecule[88,113].

The ESP map of benzene shows a negative region above the aromatic ring, while the map of hexafluorobenzene shows a positive region above the ring (an increase in electrostatic potential relative to benzene), Figure 1.10. Such observations in ESP are often interpreted as evidence of a change in the delocalised π-electron density of the aromatic ring[112,114].

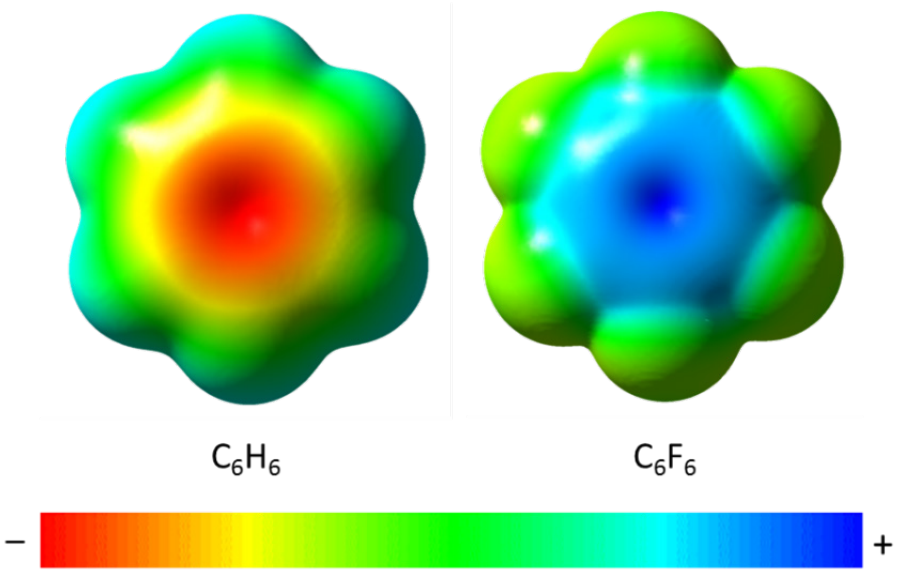

Figure 1.10 Electrostatic potential (ESP) surface of benzene and hexafluorobenzene.

This arises from a misinterpretation of ESP surfaces. The ESP map is not a depiction of local charge across the isosurface, instead the ESP at a given point depends on the electron density of the entire molecule and is sensitive to through-space effects of near-by substituents. Therefore, although a negative region on an ESP surface often will correspond to an electron-rich region, it can never be assumed that a specific ESP value is the result of local changes in electron density[88,113]. As an outcome of this misinterpretation, the ESP above the ring has been used as a measure of the extent to which an aromatic face is ‘electron-rich’ or ‘electron-poor’, and then used to predict the relative strength of the stacking interaction.

While the presence of electron withdrawing and electron donating groups certainly do change the electron density in the central aromatic π-system, more and more research suggests that this is not the primary force governing the influence of substituents on stacking arrangements.

1.2.2.3 Direct Substituent Interaction Model

Instead of substituent induced changes to the aromatic π-system, the direct interaction model proposes that the effect of substituents on aromatic stacking is the result of direct electrostatic interactions between the substituents and the unsubstituted ring.

Substituent effects are found to be consistent with the interaction of substituent dipoles with the local C – H dipoles on the opposing ring[115,116]. These electrostatic interactions are the dominant force controlling how substituents influence aromatic stacking. For instance, in the benzene : hexafluorobenzene (B/HFB) co-crystal the direct interactions occur between the C – F dipoles on hexafluorobenzene and C – H dipoles on benzene.

The advantages of the direct interaction model over both the π-polarisation model and the quadrupole – quadrupole model are exemplified by investigation of trifluorobenzenes. The ESP of the 1,3,5-trifluorobenzene ring is approximately neutral, Figure 1.11, likewise, the quadrupole moment of 1,3,5-trifluorobenzene is very small[74,100,115].

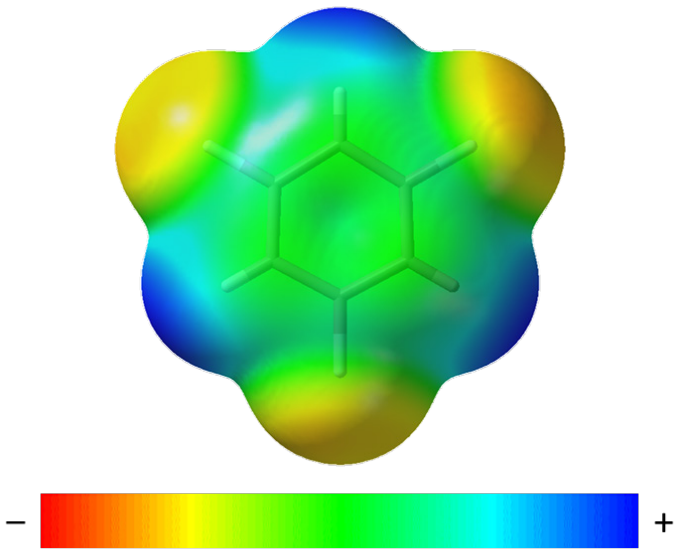

Figure 1.11 Electrostatic potential (ESP) surface of 1,3,5-trifluorobenzene.

Both the π-polarisation model and the quadrupole – quadrupole model would suggest that a face-to-face dimer of 1,3,5-trifluorobenzene would have a small associated stabilisation energy. Whereas, in fact, anti-parallel stacks of 1,3,5-trifluorobenzene are analogous to strong stacking interactions between benzene and hexafluorobenzene[91,115]. A similar observation is made for anti-

parallel stacks of 1,2,3-trifluorobenzene, which also has a neutral ESP above the ring and a negligible quadrupole moment. In all of these fluorinated systems the rings are oriented such that the C-H bonds are located roughly above the C-F bonds. This stacking arrangement maximises the electrostatic attraction between the local C – F dipoles and C – H dipoles of the opposite ring.

These results are consistent with PIXEL energetic calculations for fluorinated benzene systems from the 2003 paper, "Molecular Shape and Intermolecular Liaison: Hydrocarbons and Fluorocarbons" [91]. The paper describes how calculations predicted a stabilising energy for all dimer arrangements in which F atoms and H atoms where juxtaposed i.e. C-H bonds were located above/below C-F bonds. However, the paper does also note that the calculated dimers did not closely match observed arrangements seen in the crystal structures. All of the calculated dimers adopted a face-to-face nondisplaced arrangement at their minimum energy. Whereas, the crystal structures often have lateral displacement or relative rotation of rings. This was rationalised as the result of improved inter-stack packing.

Preference for parallel displacement could also be the result of close-packing within the same stack. Aromatic rings can achieve a shorter vertical separation through displacement – when the 'hollow' in the centre of the aromatic ring (visible in the isosurface) is aligned with a carbon atom from the other ring, the rings can come into closer contact[98]. Equally, computational studies of molecular orbitals suggest that overlap between lobes is maximised when the rings are displaced[117].

1.2.2.4 Crystal Engineering with Fluorinated Phenyl Groups

The direct interaction model provides intuitive predictions for substituent effects and is in general agreement with DFT and PIXEL interaction energy calculations. The model is useful for understanding the structures of partially fluorinated aromatic stacks and rationalising them through the same local dipole interactions as phenyl : perfluorophenyl co-crystals.

The strong interaction between phenyls and perfluorophenyls is widely recognised and the stacking motif has been successfully applied as a synthon in numerous crystal design strategies[74,75,86,92,95,118–124].

In the direct interaction model, substituent effects are broadly additive[115]. Therefore, incrementally increased substitution and specific placement of fluorine could be used to finely tune a molecule for a target synthon.

1.2.3 The Organic Fluorine Hydrogen Bond

The nature of the organic fluorine – hydrogen bond has been under scrutiny for over three decades. Unlike fluoride, F^-, which is one of the strongest confirmed hydrogen bond acceptors due to its electronegativity[125,126], the electronegativity of organic fluorine results in poor availability of the fluorine lone pairs[106], as discussed in Section 1.2.1.

1.2.3.1 Initial Database Studies

In early investigations of organic fluorine hydrogen bonds a number of database searches were carried out. In 1983 and 1994 Glusker and colleagues identified short contacts between organic fluorine and hydrogen when searching the Cambridge Structural Database[127,128]. They recognised that the interaction was very weak but might still have an influence on crystal packing. In 1996 Howard and O'Hagan conducted a similar search, specifically examining the capability of organic fluorine as a hydrogen bond acceptor[129]. They found that viable interactions were extremely rare and proposed that fluorine is a very weak hydrogen bond acceptor. Following this Dunitz and Taylor published the famously titled "Organic Fluorine Hardly Ever Accepts Hydrogen Bonds" based on their own investigations of the Cambridge Structural Database (CSD) and the Brookhaven Protein Data Bank[130]. They wrote that such interactions were only observed in "exceptional molecular and crystal environments". In a much later paper, Taylor went on to describe organic fluorine as "a donor's last resort"[131].

In the twenty years since these early studies a great many more crystal structures with organic fluorine hydrogen short contacts have been added to the database. A 2016 database study identified 117 crystal structures with only C, H and F atoms[132]. However, these still amount to a tiny proportion of the CSD, which now exceeds one million crystal structures[133], and it can be difficult to infer meaningful results for a small set of (supposedly) exceptional interactions.

These studies have relied on purely geometric information to identify possible interactions. As such, many of these short contacts have been dismissed as merely incidental and the inevitable by-product of close-packing requirements and the abundance of organic fluorine in the structure[130,134].

While this may be true for many fluorine - hydrogen short contacts, studies of the relative frequency of interactions across the Cambridge Structural Database have shown that C – H ··· F interactions occur much more often than could be expected by chance[7,135]. This suggests a need for further investigation into their nature rather than dismissal.

1.2.3.2 Identification

There is now a great deal of experimental evidence supporting the existence and importance of organic fluorine hydrogen bonds[102,126,136–140]. However, many of the interactions in these papers are identified based on the van de Waals radii of the atoms concerned and their calculated distances.

Proximity of organic fluorine and hydrogen can suggest the presence of an attractive interaction but, in of itself, is not enough to confirm a weak hydrogen bond[141]. Crystallographic evidence alone is not sufficient to fulfil the IUPAC criteria for a hydrogen bond. Confirmation of organic fluorine as a weak hydrogen bond acceptor will require a combination of evidence from different techniques.

Spectroscopic methods such as microwave spectroscopy and ^{19}F NMR have been used to reveal the presence of a hydrogen bond[58,142]. There is a large chemical shift observed in the ^{19}F NMR when a hydrogen bond is formed directly with fluorine. The degree of the shift can indicate a relative value for the proton transfer associated with the formation of the hydrogen bond[58,143].

The combination of crystallographic data and theoretical calculations can also aid identification of a true hydrogen bond. Density Functional Theory (DFT) calculations and semi-empirical calculations, such as PIXEL, can help ascertain whether an observed close contact is a stabilising interaction and not a repulsive one[58,59,99,126,132,144,145]. Theoretical calculations and methods will be discussed further in Section 2.2.

While geometric evidence alone is insufficient proof of a hydrogen bond, close examination of the geometry can inform whether a close contact conforms to established observations of hydrogen bond angles. Geometric analysis is also important to assess the directionality of the contacts[126,135].

Few instances of organic fluorine hydrogen bonds have been characterised to the degree required to satisfy the IUPAC definition but there are some examples in the literature. In 2014, Shang et al. used DFT calculations in conjunction with crystallographic data to show that C(sp^2)– H ··· F – C(sp^2) hydrogen bonding was stabilising the folded conformations of aromatic triazole foldamers[146]. They calculated the energy minima for their various compounds and found that the folded conformations (held by C – H ··· F – C hydrogen bonds) were lower in energy than their unfolded counterparts. They also showed that for the un-fluorinated analogues the unfolded conformer was more stable. The authors concluded that the C – H ··· F – C hydrogen bonds provide enough stabilization to balance the destabilization that arises from electrostatic repulsion and steric strain of the folded conformer.

Through this and other studies the interaction has been sufficiently proven to exist and researchers who previously challenged the importance of C – H ··· F – C have come to recognise it as a viable, if weak, hydrogen bond[126,147].

1.2.3.3 Structural Influence

With the legitimacy of the organic fluorine hydrogen bond established, investigation should turn to ascertaining its directionality and power to influence a structure.

Geometric analysis reveals that, like conventional hydrogen bonding, C – H ··· F – C interactions have a preference for higher bond angles, approaching 180°[135,142]. In 2018, Saha et al. performed a population density analysis for a set of structures, selected from the CSD, with only C, H, O, and F atoms. They analysed the population density of the C – H ··· F – C interaction at different H ··· F distances and bond angles. They found that the maximum population density was at the higher angle range, 170 – 180°, and that as the angle deviated from this ideal the H ··· F distance increased. The authors also noted that the C – H ··· F bond angle was more prominently affected by the directionality than the H ··· F – C bond angle. They attributed this to the properties of the F atom, which is larger and closer to being isotropic and so less sensitive to direction than H atoms. At very short H ··· F distances both angles prefer linearity but at longer distances the H ··· F – C angle often adopts a bent geometry[135].

The propensity of organic fluorine (C – F) to act as a hydrogen bond acceptor has been measured against other weak hydrogen bond acceptors, utilising crystallographic data. It has been found that C – F competes unfavourably in the presence of these alternative acceptors[128,131,132,135,148]. However, C – H ··· F – C interactions have been identified in molecular crystals alongside other weak and strong hydrogen bonds[59,135,144,149]. They can, it seems, act cooperatively, but not competitively.

Further classification of the C – F bonding propensity found that hybridisation of the carbon modulated the acceptor capability. Through both crystallographic analysis and theoretical calculations, it has been established that F – C(sp^3) is a better acceptor than F – C(sp^2)[142,149,150]. The aromatic C(sp^2) – H ··· F – C(sp^2) interaction is still meaningfully attractive, as demonstrated by Shang et al., discussed in Section 1.2.3.2. It is these interactions which are likely to occur laterally in aromatic systems using F substitution to augment aromatic stacking.

While the strength of C – H ··· F – C interactions is decidedly weak they do appear to have directionality, especially at shorter H ··· F distances[135,144].

1.2.4 Fluorine Halogen Bond

As touched on in Section 1.1.5.2, fluorine is generally considered to be unable to participate in halogen bonding. However, there is growing evidence that fluorine can be involved in "halogen-like" interactions[73]. In systems with no other strong nucleophilic groups, only C, H and F atoms, the F ··· F interaction is of particular interest.

Despite contention over its existence, a number of studies have concluded that the F ··· F interaction is due to a stabilising force and not merely the product of close packing[151–153]. The F ··· F interaction could be an important tool for crystal design but is still little understood and atypical among other halogen – halogen interactions[153–156]. As well as being the least polarisable halogen, it has been noted that F is more likely to bond to H than another F; it is the only halogen for which this is true[139,144].

Even though F ··· F interactions are very weak they have a strong directionality[154,155]. The most favourable configuration is generally found where both C – F ··· F angles are equal to 90°[152,155], Figure 1.12. This "mutually orthogonal" configuration is distinct from other halogen bonds although it bears resemblance to both traditional halogen bonding types. In a 2016 study of F ··· F directionality, Karnoukhova et al. found that a pure type II configuration had a very similar optimised F ··· F distance (≈ 2.82 Å) but was nearly half as energetically stabilising compared to the "mutually orthogonal" configuration[155].

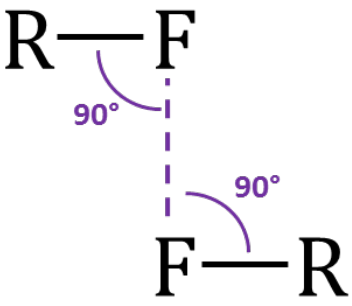

Figure 1.12 Mutually orthogonal configuration for F ··· F "halogen-like" interactions.

F ··· F interactions are very weak and should be considered distinct from halogen bonds and they do not compete favourably, even against very weak F ··· H interactions. Despite this, they may offer some small influence on the structure and should not be dismissed.

1.3 Conclusions

In this first chapter, the key concepts of crystal engineering have been introduced with a focus on the non-covalent interactions involving organic fluorine. The nature of phenyl – fluorophenyl

aromatic bonding, C – H ··· F – C interactions and F ··· F interactions have been discussed with an emphasis on their role in crystal structure formation and energetic contribution.

The aromatic bonding between fluorinated and unsubstituted rings is recognised as a strong synthon in crystal design. If utilising fluorine to control ring stacking (in isolation of strong hydrogen bond acceptors) C – H ··· F – C and F ··· F interactions are likely to occur simultaneously. While the directionality of C – H ··· F – C and F ··· F interactions have been well established, the capacity for these interactions to be structure determining is called into question by their weak stabilisation energies.

However, the process of crystal assembly is not simple and the most thermodynamically stable crystal is not always the most crystallisable. The first stages of crystallisation are driven by kinetic forces. Weak but directional non-covalent interactions, such as C – H ··· F – C, may have a significant influence on the initial molecular self-recognition in the absence of strong synthons[157,158]. Only as crystal growth continues does dispersion become dominant over these atom-atom specific interactions. Thus, one can speculate that weak but directional interactions can have a significant structural influence, even in a crystal of predominately dispersive energy stabilisation.

To investigate this influence, and the relative strengths of fluorine-based non-covalent interactions, a variety of experimental and theoretical methods need to be employed.

Chapter 2 Analytical Methods

In this chapter, different methods for the analysis of crystal structures will be explored. Particular emphasis is placed on X-ray diffraction as the fundamental technique for crystal structure determination. An overview of the background theory will be given along with a discussion of complementary techniques utilised in this project. This will include a brief introduction to the theory behind specific quantum crystallographic approaches for the analysis of electron density and interactions within the crystalline state.

2.1 Crystallography

Crystallography is the study of molecular and crystalline structures and properties[159]. Crystals are formed from highly ordered arrangements of repeated chemical units. The crystal structure is often conceptualised as an infinite lattice of these repeating chemical units. In the study of molecular crystals, crystallographic methods are employed not only to establish molecular structure and conformation, but also the relative atomic coordinates and symmetry relationships between the molecules that form the lattice.

Concepts of symmetry are essential to understanding the crystal array, and the symmetry of the crystal lattice dictates that of the diffraction patterns observed from X-ray experiment, while the intensity of diffracted X-rays is related to the molecular structure and composition (via the electron density).

2.1.1 Symmetry

2.1.1.1 The Unit Cell and Lattices

The regular repeating pattern of a crystal structure can be represented succinctly by defining a unit cell. The unit cell is a structural unit that describes the full symmetry of the repeating chemical moieties in the smallest possible volume. The unit cell is defined by the three cell lengths *a, b* and *c* and three angles α, β, and γ.

For a primitive lattice the lattice points (repeated chemical moieties) lie on the vertices of the unit cell. There are seven different crystal systems that correspond to the observed primitive lattices – triclinic, monoclinic, orthorhombic, tetragonal, rhombohedral, hexagonal and cubic. The unit cells of different crystal systems must comply with different symmetry constraints and can be

identified by the relative values of the unit cell parameters. For example, in a cubic system the three unit cell lengths, a, b, and c, are all equal; as are the angles, α, β, and γ = 90°.

Lattices of higher symmetry in the same crystal system are described by unit cells with additional lattice points. These are termed centred lattices. Lattices are assigned different letters to represent their centring: P is used to symbolise primitive lattices, while I, F and A/B/C are used to symbolise body centred, all-face centred, and one-face centred lattices, respectively. All regular crystal structures can be described by fourteen different lattices, defined by a combination of both the crystal system and the centring type; these are known as the Bravais Lattices[160].

2.1.1.2 Symmetry Elements

Unit cells in a lattice are related to one another by translation symmetry only. However, within the unit cell, and therefore the crystal structure, a variety of symmetry operations may relate the chemical moieties to one another. Different symmetry elements are valid within different crystal systems.

Common symmetry operations include proper (1-, 2-, 3-, 4-, 6-fold) and improper rotations. An improper rotation is the combination of a rotation and an inversion centre and can have the same range of orders as proper rotations. A mirror plane can also be described as a two-fold improper rotation. In Hermann–Mauguin notation this would be denoted as $\bar{2}$ (or more commonly the *m* symbol is actually used*)* to represent the two-fold rotation, 2, and the inversion centre, $\bar{x}$. Similarly, an inversion centre with 360° rotation is denoted as $\bar{1}$. Hermann–Mauguin notation is used throughout as it allows for the description of both point and translation symmetry.

The combination of compatible proper rotations and improper rotations leads to 32 unique crystallographic point groups. Higher symmetry crystal systems are able to accommodate higher symmetry point groups as shown in Table 2.1.

Table 2.1 Crystallographic Point Groups organised by crystal system. The essential symmetry of the crystal system has also been given. Centrosymmetric point groups have been highlighted in bold.

System	**Essential Symmetry**	**Point Groups**
Triclinic	None	1, $\bar{\mathbf{1}}$
Monoclinic	2 or *m*	2, *m*, **2/*m***
Orthorhombic	222 or *mm*2	222, *mm*2, ***mmm***
Tetragonal	4 or $\bar{4}$	4, 422, $\bar{4}$, **4/*m***, 4*mm*, $\bar{4}$2*m*, **4/*mmm***

System	Essential Symmetry	Point Groups
Trigonal	3 or $\bar{3}$	3, $\mathbf{\bar{3}}$, 32, 3*m*, $\mathbf{\bar{3}/m}$
Hexagonal	6 or $\bar{6}$	6, 622, $\bar{6}$, **6/*m***, 6*mm*, $\bar{6}2m$, **6/*mmm***
Cubic	23	23, **2/*m* $\bar{3}$**, 432, $\bar{4}3m$, ***m*$\bar{3}$*m***

Within these crystallographic point groups, symmetry operations occur relative to a fixed point in space. However, within a crystal structure these symmetry operations can also be accompanied by movement in space, combining proper and improper rotations with translation. These are known as glide planes and screw axes.

A glide plane is constructed from a mirror reflection coupled with a translation. Glide planes are denoted based on the plane of reflection and direction of the translation. Glide planes are observed either parallel to one unit cell direction, producing *a*, *b*, or *c* glide planes, or parallel to a combination of cell directions, producing *n* or *d* glide planes.

A screw axis is constructed from a proper rotation and translation. They are denoted n_m where *n* is the type of rotation and *m* divided by *n* is the translation across the unit cell. For example, the operation 2_1 is a 2-fold rotation followed by a translation of ½ the unit cell parallel to the rotation axis.

The inclusion of these symmetry operations with the 32 point groups and the 14 Bravais lattices produces the crystallographic space groups, which describe the symmetry within a crystal structure.

2.1.1.3 Crystallographic Space Groups

There are 230 unique crystallographic space groups, although most organic crystal structures populate only a handful of these.

Space groups are identified following a particular notation to describe the central symmetry and lattice properties. The name begins with a capital latter that corresponds to the lattice centring. This is followed by the point group of the system with the inclusion of any glide planes and screw axes. There are point group symmetry elements associated with each axis; however, some of these are omitted from the notation if they have no effect on the crystal symmetry. The crystal system of a particular space group can be inferred from the point group.

The most common space group for organic crystal structures is $P2_1/c$, a primitive monoclinic cell with a 2_1 screw axis perpendicular to b and a glide plane perpendicular to the b axis with a translation along the c axis.

All of the crystallographic space groups are listed in the International Tables for Crystallography, Vol A. along with projections of these space groups[161]. These projections illustrate the symmetry operations within the cell and how they relate the molecules or chemical moieties to one another. In these projections, various symbols are used to identify different symmetry operations. For instance, the symbol ( ) represents a 2_1 screw axis, while a small unfilled circle represents an inversion centre.

Figure 2.1 illustrates the projection of symmetry operations for $P2_1/c$ as given in the International Tables for Crystallography, Volume A. The position of the four chemical fragments in the unit cell are represented by the larger unfilled circles. The presence of an apostrophe indicates an inverted fragment. The + and – symbols indicate whether a fragment is above or below the plane of the page. The arrow running parallel to the c axis and labelled $\frac{1}{4}$ indicates the presence of the c glide plane.

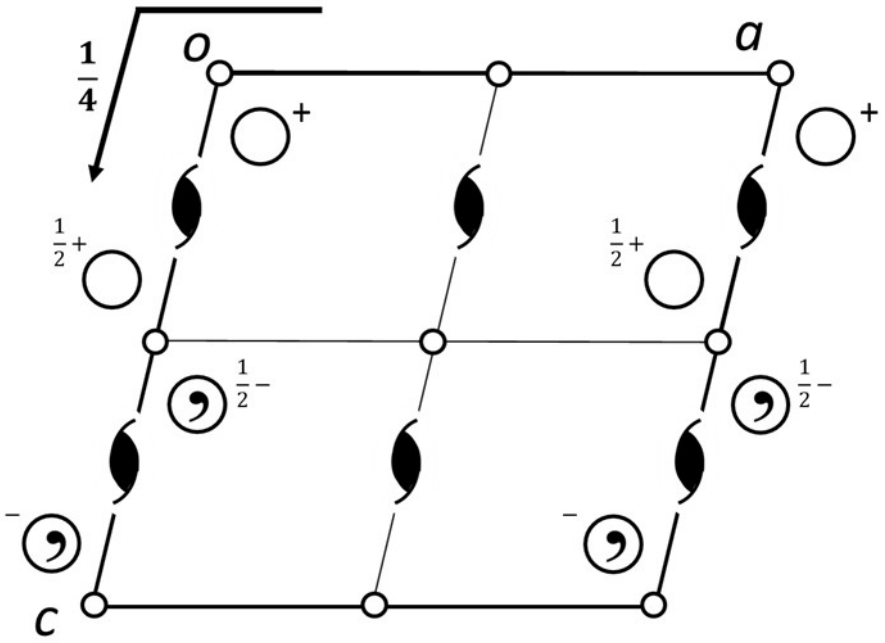

Figure 2.1 Projection of the symmetry operations present in space group $P2_1/c$, viewed down the *b* axis. The origin, *a* axis and *c* axis are labelled *o*, *a* and *c*, respectively.

All crystallographic symmetry can be described and categorised through the use of these space groups; they are crucial to understanding the arrangement of molecules within a crystal structure and the diffraction behaviour of different crystals.

2.1.2 Single Crystal X-Ray Diffraction

2.1.2.1 X-Ray Diffraction

Diffraction is the bending or redirecting of waves when they meet an obstacle or opening of a comparable size to the wavelength. Atomic radii are roughly comparable in size, ≈0.3 – 3.0 Å, to the wavelength of an X-ray beam. The X-ray diffraction produced by interaction with one atom would be insignificant and effectively undetectable. However, the ordered nature of a crystal array magnifies the effect and makes it possible to measure the diffracted X-rays.

X-ray beams are scattered by their interaction with the valence electrons of the atoms. The scattered waves interfere either constructively or destructively to produce a diffraction pattern. Reflections are observed where the conditions for constructive inference are met. The geometric requirements for these conditions were determined by William and Lawrence Bragg and are described by Bragg's Law[162], Equation 2.1.

Equation 2.1 Bragg's Law

$$2d_{hkl}\sin\theta = n\lambda$$

In Equation 2.1, θ is the angle of incidence for the beam or Bragg angle, λ is the wavelength of the X-rays and d_{hkl} is the distance between the planes of the crystal lattice. The value $n\lambda$ is the additional path length that must be travelled by a wave passing through the crystal lattice. The geometric principles for this equation are demonstrated in Figure 2.2.

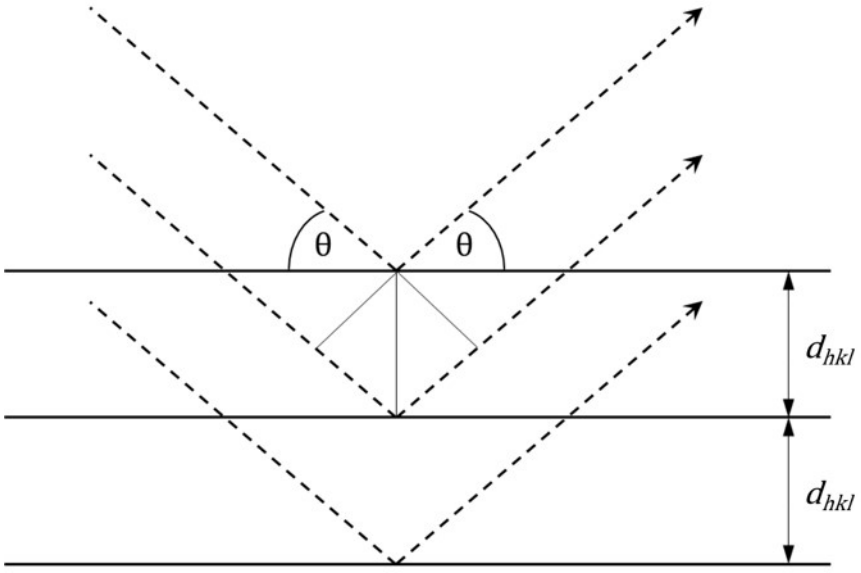

Figure 2.2 Illustration of the principle of Bragg's Law within the crystal lattice.

Constructive interference is observed when the additional path length is equal to an integer multiple of the wavelength; the Bragg's equation is satisfied when n is an integer. The integer value of *n* is usually treated as 1, as the Miller indices, *h*, *k*, *l,* corresponding to the observed reflection can be used to account for multiples of the wavelength.

The diffracted beams form a lattice of reflections, with defined positions and intensities, referred to as the diffraction pattern. This lattice has a reciprocal relationship to the crystal lattice. Measurement of the reciprocal lattice can reveal information about the distances in the real lattice. The symmetry elements present in the crystal structure will also be reflected in the diffraction pattern. However, observation of the geometry and symmetry of the reciprocal lattice does not reveal information about the atoms and their location within the unit cell.

The intensities of the observed reflections are related to the electron density within the unit cell. These diffraction intensities are investigated in order to determine molecular structure and the arrangement of atoms within the unit cell.

2.1.2.2 Structure Factors and Electron Density

Each reflection in a diffraction pattern is labelled by the three Miller indices, *h*, *k*, and *l,* which describe the lattice plane corresponding to that reflection. The diffracted wave associated with each reflection can be numerically defined by the amplitude of the wave, $|F|$, and the phase, ϕ. If the wave is described as a vector with the amplitude $|F|$ as the length and an angle of ϕ from the origin defining the direction, it can be written as a single complex number F, known as the structure factor, Equation 2.2.

Equation 2.2 Derivation for the structure factor from the amplitude and phase of a wave.

$$F = |F|\,(\cos\phi + i\ \sin\phi)$$
$$F = |F| \cdot\ e^{i\phi}$$

$F(hkl)$ is the structure factor for a reflection of indices *h*, *k*, and *l*. It is necessary to make a summation of all the reflections to describe the structure factor; each part of the structure contributes to every reflection observed, Equation 2.3.

Equation 2.3 Structure factor equation. f_j describes the effect of atomic scattering.

$$F(hkl) = \sum_{j=1}^{N} f_j\, e^{2\pi i(hx_j + ky_j + lz_j)}$$

The structure factor and the electron density of the crystal (electron density distribution in the unit cell) are related by a Fourier transformation, Equation 2.4.

Equation 2.4 Structure factor equation in relation to the electron density.

$$F(hkl) = \int_{cell} \rho(xyz)\, e^{2\pi i(hx_j + ky_j + lz_j)} dV$$

The Reverse Fourier transformation returns the electron density from the structure factors, Equation 2.5.

Equation 2.5 Electron density equation.

$$\rho(xyz) = \frac{1}{V} \sum_{h,k,l} F(hkl) \cdot e^{-2\pi i(hx+ky+lz)}$$

This equation can also be separated in to the wave amplitude and phase components, Equation 2.6.

Equation 2.6 Electron density equation with separated amplitude and phase components of the structure factor.

$$\rho(xyz) = \frac{1}{V} \sum_{h,k,l} |F(hkl)| \cdot e^{i\phi(hkl)} \cdot e^{-2\pi i(hx+ky+lz)}$$

The value for the electron density in the unit cell is calculated by summation of all diffracting beams with their corresponding wave amplitudes and phases.

The amplitude of the waves are recorded in the diffraction pattern as the relative intensities of the reflections, $I \propto |F|^2$, but phase information is lost. Consequently, the reverse Fourier transform cannot be calculated directly from results of the diffraction experiment. This is known as “the phase problem”. The phase problem must be resolved in order to determine electron density and hence the crystal structure.

2.1.2.3 Crystal Structure Solution

Various methods have been employed to overcome the phase problem in order to solve the crystal structure. The three most prominent methods are Patterson syntheses, direct methods and charge flipping[163].

Patterson methods work more successfully when one or a few of the atoms have significantly more electron density than the rest, so-called “heavy atoms”. In the Patterson method the phase problem is resolved by taking the squared amplitudes of the observed diffraction, $|F_o|^2$, and setting all of the phases to zero. The resulting Fourier transform produces a Patterson synthesis or function, Equation 2.7[164].

Equation 2.7 The Patterson function

$$P(xyz) = \frac{1}{V}\sum_{h,k,l}|F_o(hkl)|^2 \cdot e^{-2\pi i(hx+ky+lz)}$$

The Patterson function produces a map of the vector relationships between pairs of atoms in the structure. The Patterson maps show the approximate position of atoms relative to each other. Heavy atoms produce significantly large peaks in the map, once these are recognised it becomes possible to determine the other atoms by relative position.

Direct methods are suited for crystals both with and without heavy atoms[165]. Direct methods begin by selecting the reflections that contribute the most to the Fourier transform and assigning a probable combination of phase relationships for those reflections. The probable phases are chosen following a number of constraints set by the relationships between phase and amplitude and the physical restriction of the electron density properties. Namely, electron density must be positive or zero, and electron density will be concentrated in certain regions (atoms)[163]. The Fourier transform is calculated with these probable phases and the observed amplitudes. This produces a first approximation for the electron distribution, which is then improved by adjusting the input phases over cycles of refinement.

Charge flipping and similar methods utilise dual-space iterative phasing algorithms to determine the crystal structure. These algorithms find a solution to the phase problem by making modifications in both direct and reciprocal space, alternating between the two[166]. Charge flipping is the most recent method for structure determination and has largely superseded historic methods.

After an initial solution has been calculated the basic structure must be completed and refined; there may be missing atomic positions or unassigned electron density. This partial structure becomes the first structure model. A new structure factor is calculated from the model structure, F_c. The accuracy of the model is improved by adjusting atomic parameters to minimise the difference between F_c and the structure factor of the observed data, F_o.

The residual factor is widely used to assess the accuracy of a model, Equation 2.8. A lower residual represents a better fit between the observed and modelled structure factors.

Equation 2.8 Residual factor equation

$$R = \frac{\sum\big||F_o| - |F_c|\big|}{\sum|F_o|}$$

The atomic parameters are adjusted and fed back into a revised model. The process is repeated over several cycles until the least-squares refinement converges and the best fit for the crystal structure is obtained.

Equation 2.9 Least-squares refinement. Convergence is achieved when the least-squares sum is brought to a minimum. *w* represents the weighting of the contribution from each reflection.

$$\sum w(F_O^2 - F_C^2)^2$$

Standard crystallographic studies utilise the independent atom model (IAM) to model the electron density. The model assumes that the electron density is spherical and accumulated around the atomic nuclei[167].

The atomic parameters optimised by least-squares refinement are the three atomic coordinates *x, y, z* and the atomic displacement parameters *U*. Anisotropic vibration is modelled by six *U* values for each atom, these describe the vibration for three axis and three off-axis directions. The final step in refinement is assigning the hydrogen atoms, these are typically described by three atomic coordinates and only a single isotropic displacement parameter[168].

The IAM is sufficient for the majority of crystallographic studies. The models provide precise atomic positions for the crystal structure. From these positions, and derived bond lengths and angles, a substantial amount of structural analysis is possible. Beyond the unit cell, the crystal lattice structure is also modelled from the application of symmetry. This provides useful insight into the way the molecules pack, and therefore interact, in the crystal structure.

However, there are limitations to the applicability of this model. The IAM is unable to accurately describe electron density distribution in chemical bonds and other interactions, as the electron density is assigned exclusively to atomic nuclei[169]. While bond length is usually a good indicator of strength, atomic coordinates cannot be relied upon to deduce accurate bond energy.

2.1.3 Charge Density Analysis

The spherical model employed in the IAM is not sufficient to describe the non-spherical distortion of electron density distribution caused by atomic bonding. A number of approaches have been developed to better model the atom-centred electron density that deviates from the spherical. This is known as the deformation density, which is derived from separately considering core and valence electron density and which can be modelled using multipolar techniques.

2.1.3.1 Multipolar Expansion

The most widely recognised multipolar expansion is the Hansen-Coppens model, Equation 2.10[170]. The electron density of the atom, ρ_{atom}, is divided into three components. These components correspond to the spherical core density, the spherical valence density and the aspherical deformation valence density.

Equation 2.10 The Hansen-Coppens expansion.

$$\rho_{atom}(\boldsymbol{r}) = P_{core}\rho_{core} + P_{val}\kappa^3\rho_{val}(\kappa r) + \sum_{l=0}^{l_{max}} \kappa'^3 R_l(\kappa' r) \sum_{m=0}^{l} P_{lm\pm} Y_{lm\pm}(\theta, \varphi)$$

In this equation, the P_{core} and P_{val} terms represent the core and valence electron populations, respectively; κ and κ' are dimensionless expansion-contraction scaling parameters; R_l represents the normalised Slater-type radial functions; $Y_{lm\pm}$ represents the spherical harmonics with their respective multipole population parameter, $P_{lm\pm}$.

The aspherical deformation valence density (the summation terms at the end of the expansion equation) describes the deviations in electron density caused by the presence of molecular bonding.

Multipolar refinement involves a much greater number of parameters for least-squares refinement than standard (IAM) crystallographic methods. This produces a more accurate model of the charge density, provided that the X-ray diffraction data is of high enough quality; high resolution, 100% completeness and high redundancy to refine against the greater number of parameters.

2.1.3.2 High Resolution Data

The resolution of X-ray diffraction data is defined by the highest angle resolvable peak. Reflections observed further to the edge of the diffraction pattern, at a higher angle, indicate that a higher degree of accuracy is possible for the structure refinement.

Standard crystallographic experiments aim to collect atomic resolution data; good atomic resolution would be approximately 0.8 Å. This resolution is sufficient to define precise atomic position from their electron density using standard refinement techniques.

However, in order to distinguish thermal vibrational effects from charge deformation a resolution of at least 0.5 Å is required[171]. Low temperature is also required to measure accurate and minimised thermal displacement parameters. Additionally, the scattering power of valence electrons decreases rapidly with decreasing resolution compared to that of the core electrons[172].

High quality and well-diffracting crystals are necessary for collecting high resolution data suitable to underpin charge density analysis.

Through the multipolar refinement of high resolution data, the charge density distribution can be assessed for topological features and quantitatively analysed to give insight into the nature of interactions within the crystal.

2.1.3.3 Quantum Theory of Atoms in Molecules

The electron charge distribution contains invaluable information about the interactions between atoms and a wide array of techniques exist to extract this information.

Bader's Quantum Theory of Atoms in Molecules (QTAIM) employs topological analysis of the electron density field gradient to derive a number of associated properties[173,174]. These include: the electron density, the Laplacian of electron density, electrostatic potential and critical points in the topology.

In QTAIM theory, electron density is partitioned and assigned to different atoms. These atomic basins are defined by zero-flux boundaries in the electron density gradient field vector[175]. From this definition individual atom properties can be determined, such as the atomic charge, which is calculated by integration of electron density within the boundary, known as the atomic basin.

The bonds between these atomic basins are also defined by topological analysis of the charge density and its gradient vector. Extrema values of the electron density, ***ρ(r)***, are of particular note and are referred to as critical points.

2.1.3.3.1 Critical Points

Critical points (CPs) are topological features in the electron density, which occur at saddle points between electron density gradient vectors, maxima or minima. These points are found where the gradient vector approaches zero, $\nabla\rho(\boldsymbol{r}) = 0$.

There are four types of topologically stable critical points. They are characterised by the rank, ω, of the Hessian matrix, which is the number of non-zero eigenvalues and the signature, σ, which is the algebraic sum of the signs of the eigenvalues.

- **(3, -3)**: all curvatures are negative, corresponding to a local maximum in the electron density distribution. This is a "nuclear attractor" and in a molecule these occur only at the nuclei.
- **(3, -1)**: two curvatures are negative and one is positive, corresponding to a saddle point. This is known as a bond critical point (BCP).

- **(3, +1)**: two curvatures are positive and one is negative, these occur inside a ring of bonded atoms. This is known as a ring critical point (RCP).
- **(3, +3)**: all curvatures are positive, corresponding to a local minimum in the electron density distribution. This is known as a cage critical point (CCP).

According to Bader's QTAIM, a bond critical point will always be present where there is an interaction between two atomic nuclei[173,176,177]. The location of a critical point indicates the atoms involved, while the electron density, $\rho(\boldsymbol{r}_{BCP})$, and the Laplacian of electron density, $\nabla^2\rho(\boldsymbol{r}_{BCP})$, reveal the nature of the bond.

Shared shell interactions, such as covalent bonding, result in an overlap of the electron density of the participating atoms; there is an accumulation of charge. Therefore, there is a high $\rho(\boldsymbol{r}_{BCP})$ at the bond critical point and $\nabla^2\rho(\boldsymbol{r}_{BCP}) < 0$. In contrast, a low $\rho(\boldsymbol{r}_{BCP})$ and $\nabla^2\rho(\boldsymbol{r}_{BCP}) > 0$ indicates a closed-shell interaction such as a hydrogen bond or a van der Waals interaction; the electron density is locally depleted at ***r***.

2.1.3.3.2 Local Energy Density

The energetic properties of the interactions can also be derived from the values of $\rho(\boldsymbol{r}_{BCP})$ and $\nabla^2\rho(\boldsymbol{r}_{BCP})$. Using Abramov's formula[178], the local kinetic energy density, $G(\boldsymbol{r}_{BCP})$, the local electrostatic potential energy, $V(\boldsymbol{r}_{BCP})$, and the total energy density, $H(\boldsymbol{r}_{BCP})$, can be calculated for a closed shell interaction following the Espinosa-Molins-Lecomte (EML) approach[179]. These calculations are outlined in Equations 2.11 to 2.13.

Equation 2.11 Calculation of the local kinetic energy density. $\rho(\boldsymbol{r}_{BCP})$ is given in atomic units.

$$G(\boldsymbol{r}_{BCP}) = \left(\frac{3}{10}\right)(3\pi^2)^{\frac{2}{3}}\rho(\boldsymbol{r}_{BCP})^{\frac{5}{3}} + \left(\frac{1}{6}\right)\nabla^2\rho(\boldsymbol{r}_{BCP})$$

Equation 2.12 Calculation of the local electrostatic potential energy. $\rho(\boldsymbol{r}_{BCP})$ is given in atomic units.

$$V(\boldsymbol{r}_{BCP}) = \left(\frac{\hbar^2}{4m}\right)\nabla^2\rho(\boldsymbol{r}_{BCP}) - 2G(\boldsymbol{r}_{BCP})$$

Equation 2.13 Calculation of the total energy density.

$$H(\boldsymbol{r}_{BCP}) = G(\boldsymbol{r}_{BCP}) + V(\boldsymbol{r}_{BCP})$$

These values prove useful in the classification of the interactions and rationalisation of the bond properties.

Experimental charge density studies are exceptionally useful in characterising the atom-atom interactions associated with bond critical points. However, many closed shell interactions cannot be identified using this method as they are not atom-centred. Instead, theoretical methods can be employed to investigate theoretical charge distribution in the crystal.

2.2 Theoretical Analysis of Crystal Structure Energies

Theoretical methods have become an increasingly available, accessible and reliable means of calculating interactions and material properties, benefiting from advances in computation speed and theory in the last two decades.

Quantitative calculations of intermolecular interactions energies can be derived from the theoretical charge distribution. These are useful for highlighting diffuse molecule-molecule interactions, which are not identified in experimental charge density analysis.

In a number of these methods, the calculated energies can be partitioned into different energetic contributions, which is useful for further characterising the observed interactions, Equation 2.14. For instance, a large Coulombic energy component indicates the presence of electrostatic forces in the interaction.

Equation 2.14 Energy partitioning in the PIXEL method. The energy terms represent the Coulombic energy, E_{coul}, polarisation energy, E_{pol}, dispersion energy, E_{disp}, and exchange-repulsion energy, E_{rep}.

$$E_{tot} = E_{coul} + E_{pol} + E_{disp} + E_{rep}$$

The most prominent theoretical analysis method used in this study is the PIXEL method.

2.2.1 PIXEL

The PIXEL[19,180,181] method is also known as the Semi-Classical Density Sums approach. It is a semi-empirical method of molecule-molecule energy calculation. The electron densities of separate molecules are obtained from quantum mechanical molecular orbital calculations and experimentally derived atomic coordinates.

The electron densities are treated as a three-dimensional array of electron density units, referred to as pixels. Each of the pixels is assigned to an atom for which the nuclei to pixel distance is less

than the atomic radius. The electron density is thereby ascribed different parameters, such as polarizability, based on its assigned chemical environment. The symmetry in the crystal is applied to the positions of all pixels and nuclei in order to produce a cluster of molecules. The intermolecular interaction between two molecules is calculated by summation of pair-wise pixel-pixel interactions. These molecule-molecule interactions are partitioned into different energy contributions, Equation 2.14.

2.2.1.1 Coulombic Energy

The Coulombic interaction between two charged entities is described by Equation 2.15, in which *Q* represents a charge and *r* is the distance between the charged entities.

Equation 2.15 Calculation for Coulombic energy.

$$E_{coul} = \frac{Q_1 Q_2}{4\pi\varepsilon_0 r}$$

In the PIXEL method the Coulombic energy for the interaction between two molecules is calculated by the summation of all pixel-pixel, pixel-nuclei and nuclei-nuclei Coulombic attraction terms[182].

2.2.1.2 Polarisation Energy

Polarisation energy, also known as induction, is the result of electron density deformation from an applied electric field. The induced dipole moment, μ, is proportional to the strength of the applied electric field, ε, multiplied by the molecular polarizability, α, Equation 2.16.

Equation 2.16 Equation for calculating the dipole moment.

$$\mu = \alpha\varepsilon$$

The linear polarisation energy at a pixel *i* is calculated from the total electric field exerted by the surrounding molecules, ε_i, the polarizability, α_i, and the induced dipole, μ_i, Equation 2.17[183].

Equation 2.17 Linear polarisation energy equation.

$$E_{pol} = -\frac{1}{2}\,\mu_i\varepsilon_i = -\frac{1}{2}\,\alpha_i{\varepsilon_i}^2$$

A dampening term is added to PIXEL calculations to reduce physically unrealistic contributions.

The polarisation energy between two molecules in the PIXEL method is calculated by the summation of polarisation terms for all associated electron density pixels. The total polarisation

energy of the crystal is calculated separately by the summation of all molecular polarisation energies.

2.2.1.3 Dispersion Energy

The dispersion energy calculation is based on the London formulation, Equation 2.18[184].

Equation 2.18 The London formulation for calculating dispersion energy between two molecules of polarizability α and ionization energy E_{ION}.

$$E_{disp} = -\frac{3}{4}\frac{(E_{ION}\alpha^2)}{\left[(4\pi\varepsilon^0)^2(R_{ij})^6\right]}$$

In the PIXEL method, the intermolecular dispersion energies are calculated by summation of pixel-pixel terms in a London-type expression[180,181]. Again, a dampening function, f(R), is included to avoid singularities due to short pixel-pixel distances, R_{ij}. The "oscillator strength", E_{OS}, replaces the ionisation energy, E_{ION}, in more recent versions of PIXEL. Therefore, the expression for the dispersion energy between two molecules, A and B, is given by Equation 2.19.

Equation 2.19 PIXEL equation for dispersion energy between two molecules, A and B.

$$E_{disp,AB} = \left(-\frac{3}{4}\right)\sum_{i,A}\sum_{j,B}\frac{E_{OS}f(R)\alpha_i\alpha_j}{\left[(4\pi\varepsilon^0)^2(R_{ij})^6\right]}$$

The total dispersion energy of the crystal is calculated as the sum of all the two-body molecule-molecule interactions divided by two, Equation 2.20.

Equation 2.20 Summation for total dispersion energy in a crystal.

$$E_{disp} = \frac{1}{2}\sum\sum E_{disp,AB}$$

2.2.1.4 Repulsion Energy

The repulsion energy in PIXEL is calculated from the overlap, S_{AB}, of the electron densities of two molecules, A and B, Equation 2.21 and 2.22.

Equation 2.21 PIXEL equation for repulsion between two molecules. $\Delta\chi_{AB}$ is the difference in Pauling electronegativity and K_1 and K_2 are disposable parameters.

$$E_{rep,AB} = (K_1 - K_2\,\Delta\chi_{AB})S_{AB}$$

Equation 2.22 Electron density overlap for molecules A and B. Summation of overlapping pixel electron densities, ρ, over pixel volume, V.

$$S_{AB} = \sum_{i,A} \sum_{j,B} [\rho_i(A)\rho_j(B)]V$$

Similar to the calculation for total dispersion energy, the total repulsion energy in a crystal is calculated as the sum of all two-body molecule-molecule overlaps divided by two, Equation 2.23.

Equation 2.23 Summation for total repulsion energy in a crystal.

$$E_{rep} = \frac{1}{2} \sum \sum E_{rep,AB}$$

2.2.2 Hirshfeld Surface Analysis

Hirshfeld surfaces provide another means to theoretically investigate the intermolecular interactions in a crystal. They are often used as a tool for visualising the space occupied by a molecule within the crystal structure, but their properties also have further reaching applications.

The Hirshfeld surfaces began their development as a method to partition the crystal electron density into molecular fragments[185]. F. L. Hirshfeld's stockholder partitioning scheme[186] for the definition of atoms in molecules was applied to the partitioning of molecules in crystals. A density weight function was defined for a molecule in a crystal, Equation 2.24[187]. The promolecule density term is the sum over the atoms in the molecule of interest, while the procrystal density term is the sum over the crystal.

Equation 2.24 Weight density function defining a molecule in a crystal.

$$\boldsymbol{w}_A(\boldsymbol{r}) = \sum_{i\varepsilon\, molecule\ A} \rho_i{}^{at}(\boldsymbol{r}) \Big/ \sum_{i\varepsilon\, crystal} \rho_i{}^{at}(\boldsymbol{r})$$

$$= \boldsymbol{\rho}_{promolecule}(\boldsymbol{r}) / \boldsymbol{\rho}_{procrystal}(\boldsymbol{r})$$

The Hirshfeld surface is defined by $\boldsymbol{w}_A(\boldsymbol{r})$= 0.5. This isosurface defines the volume of space where the promolecule electron density exceeds the electron density of all neighbouring molecules. Therefore, the Hirshfeld surface is defined by both the molecule and its nearest neighbours rather than being dependant on molecule electron density in isolation. This relationship encodes information about intermolecular interactions into the properties of the surface.

The distances from the surface to the nearest nucleus inside the surface (internal distance, d_i) and outside the surface (external distance, d_e) can be mapped onto a 2D plot, known as a fingerprint plot. These plots are useful for analysis and comparison of different short contacts between nuclei

in related crystal structures. A break-down of the different elements contributing to the plots can indicate which atom-atom interactions are preferred.

The propensity for certain atom-atom contacts can also be explicitly calculated through the calculation surface enrichment ratios for the Hirshfeld surface.

2.2.2.1 Surface Enrichment

The surface enrichment ratio for a particular atom-atom close contact represents the propensity for those atoms to form close contacts. The ratio is obtained by comparing the contacts observed in the real crystal with a theoretical crystal structure, in which all contacts are equally likely to form.

The enrichment ratio for a contact X ··· Y is calculated using the following procedure[188]:

The proportion of surface contacts involving atoms X and Y, C_{XY}, is a reported value in Hirschfeld surface internal and external distance analysis. The molecular surface coverage of atom X, S_x, is calculated by summation of the surface contacts involving X, Equation 2.25.

Equation 2.25 Calculation of molecular surface coverage for element X.

$$S_X = C_{XX} + \frac{1}{2}\sum_{Y \neq X} C_{XY}$$

The factor ½ is used because C_{XY} describes both X ··· Y and Y ··· X contacts with atoms both internal and external to the Hirshfeld surface. The summation of all molecular surface coverage ratios should equal unity, $\sum_X S_X = 1$.

The random contact coverage term, R_{XY}, is defined as if all contacts are evenly distributed across the molecular surface. The value is obtained by probability products of the molecular surface coverages, Equation 2.26.

Equation 2.26 Calculation of the random contact proportions, R_{XX} and R_{XY}.

$$R_{XX} = S_X S_X \qquad and \qquad R_{XY} = 2 S_X S_Y$$

As for C_{XY}, the R_{XY} proportion describes both X ··· Y and Y ··· X contacts, hence the presence of the factor of 2 in the R_{XY} equation.

The enrichment ratio, E_{XY}, for the contacts involving atoms X and Y is defined as the ratio between the proportion of observed contacts in the crystal and the theoretical proportion of random contacts, Equation 2.27.

Equation 2.27 Calculation of the surface enrichment ratio.

$$E_{XY} = C_{XY}/R_{XY}$$

A surface enrichment ratio > 1 indicates an enriched contact; the contact is observed more often than would be expected by chance. Conversely, a surface enrichment ratio < 1 indicates an impoverished contact; the contacts is observed less often than would be expected by chance.

2.3 Conclusions

Single crystal X-ray diffraction is a powerful analytical technique for determination of molecular and crystal structures. Standard crystallographic experiments generate precise atomic positions suitable for geometric analysis of the molecules and crystal packing.

High resolution X-ray diffraction coupled with multipolar refinement can relate further information about the electron density within the crystal. Following QTAIM, topological analysis of this electron density can identify and quantify intermolecular interactions within the structure.

Additionally, the PIXEL method for analysis of molecule-molecule interaction energies has been described. This technique views intermolecular interactions through a different lens. Interactions between molecules are constructed from the calculated Coulombic, polarisation, dispersion and repulsion energy contributions.

The methods described in this chapter will be employed in combination, so as to supplement standard crystal structure data with insights into intermolecular interactions from different perspectives. By comparing and contrasting the information derived from these approaches, this thesis will present a deep analysis of the driving forces behind crystal structure assembly in the compound family being investigated.

Chapter 3 Aims and Methodology

3.1 Aims

Chapter 1 outlines the increasing interest in weaker intermolecular interactions for crystal engineering. Fluorine was highlighted as it exhibits exceptional behaviour in organic molecular crystal structures. In particular, fluorine has a dramatic influence on the strength of aromatic stacking interactions.

The aim of the work presented in this thesis is to improve understanding of aromatic stacking interactions augmented by fluorine substitution, particularly by the utilisation of systematic experimental data. The ultimate application of this would be to inform crystal design strategies, utilising small modifications in fluorine substitution on an aromatic ring to influence the crystal assembly.

The direct substituent interaction model will be used to rationalise aromatic stacking interactions in this work. While fluorine is not very polarisable, there is a strong dipole in the C – F covalent bond. The interaction of dipoles proposed in the direct substituent interaction model explains the influential effect of F in aromatic-aromatic interactions. The model also suggests that substituent effects are broadly additive. Therefore, both incremental increase in fluorine substitution and variation in the specific placement should cause observable changes in the crystal packing. If present, these effects could be observed by geometric analysis of relative aromatic ring positions and verified by changes in calculated molecule-molecule interaction energies. Successful implementation of this analysis would also provide experimental support for the direct substituent interaction model.

Performing this comparative structural analysis requires a large data set of related molecular crystal structures with systematically varied fluorine substitution patterns, as outlined in the following sections. This analysis will utilise the techniques described in Chapter 2, predominately focusing on geometric analysis from standard resolution atomic coordinates. A subset of these crystal structures will also be the subject of charge density analysis, PIXEL calculations and surface enrichment analysis.

As stated in section 1.3, the use of fluorine to control ring stacking behaviour creates opportunities for C – H ··· F – C and F ··· F interactions to form, in the absence of strong hydrogen bond acceptors. These interactions have been shown to demonstrate weak stabilising energies

and directionality, but their influence in crystal assembly has been largely dismissed. The properties of these interactions will also be analysed in this work.

3.1.1 Objectives

The main objectives of this thesis can be summarised by the following questions:

1. *Are fluorine-augmented aromatic stacking interactions structure directing?*
2. *Is there experimental evidence for the direct substituent interaction model?*
3. *How does the placement of fluorine substituents affect aromatic stacking interactions?*
4. *Can C – H ··· F – C or F ··· F interactions influence the crystal assembly and are they competitive with other interactions in the structure?*

3.2 Fluoroanilines

As stated, comparative structural analysis requires a large data set of related molecular crystal structures with systematically varied fluorine substitution patterns. A suitable molecular system for analysis must be able to support different degrees of substitution and the parent molecule must be easily altered to modify the position of these substituents. Additionally, the absence of strong hydrogen bond acceptors is required for the observation of C – H ··· F – C and F ··· F interactions.

In this work, analysis was performed on the crystal structures of a large data set of partially fluorinated (E) N-benzylideneanilines, abbreviated to fluoroanilines.

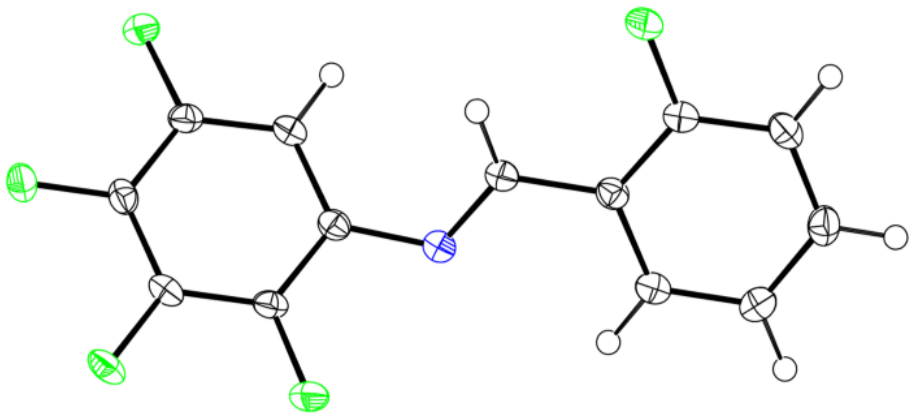

Figure 3.1 Example of a partially fluorinated (E) N-benzylideneaniline with 5 F substituents spread across the two aromatic rings.

3.2.1 Advantages of Fluorinated (E) N-Benzylideneanilines

There are a number of advantages to using these fluoroanilines in this analysis:

- Tunability

  These fluoroanilines are highly tuneable for different substituent patterns and are easily synthesised; they are the synthesis product of the addition of one aniline ring and one benzylidene ring. These two rings can be independently substituted with fluorine to the desired number and location.

- Range of Substitution

  The independent substitution of the rings offers a large range of unique substitution patterns. Each ring has 32 possible different arrangements of fluorine substitution, when varying their locations and number from 0 to 5.

- Flexibility

  While the molecule is constructed from two rigid phenyl rings, the skeleton of the molecule has a certain amount of flexibility; the phenyl rings can freely rotate in solution. Therefore, the molecule has a (limited) capacity to twist and flex according to the needs of the directing interactions in crystal assembly or in response to repulsion. This could amplify the observable effects of these interactions.

- Packing Ability

  It is also advantageous if molecules can easily pack as this reduces additional variables involved in the crystal assembly; crystal packing could be hindered by complicated non-planar molecules or molecules with large steric groups. These fluoroanilines are small organic molecules with no bulky steric groups.

3.2.2 Previous Fluoroaniline Studies

Fluoroanilines have been utilised in other studies to probe the strength and influence of weak C – H ··· F – C interactions. Notable examples include the work of Kaur, Panini, Chopra and Choudhury.

In a collaborative paper by these four authors in 2012[189], a small set of mono- and di-fluorinated benzylideneanilines were synthesised and investigated. They concluded that the weak C – H ··· F – C interactions contributed towards the crystal lattice energy in the absence of strong hydrogen

bond acceptors. The potential structural influence of these interactions was discussed in relation to their directionality. However, there is little attention given to rationalising the crystal packing arrangement as a result of the specific position of the fluorine substituents.

In a subsequent paper by Kaur and Choudhury[190], in 2014, the structural influence of the fluorine in fluoroaniline crystals was examined further. This study highlighted a number of potentially structure directing C – H ··· F – C interactions and demonstrated that replacing F in these positions with another halogen, such as Cl or Br, lead to the formation of a different crystal packing arrangement. They also performed QTAIM analysis on some of these interactions (using computational wave functions rather than experimental high-resolution data). These analyses found bond critical points between the interacting atoms. The study identified interactions between the azomethine hydrogen and fluorine as being particularly stabilising, with energies equivalent to other weak hydrogen bonds, such as C – H ··· N and C – H ··· O.

In 2015 Kaur and Choudhury investigated a set of tetra-fluorinated benzylideneanilines and conducted a database search of the CSD to identify possible synthons constructed from C – H ··· F – C interactions[191]. They concluded that these interactions were capable of forming frequently occurring supramolecular synthons. The azomethine hydrogen to fluorine interaction was highlighted as one of the stronger participating features in the synthons (synthon I). Again, stabilisation energies and bond critical points were identified using computational methods rather than experimental high-resolution data. Specific comment was made on the effect of fluorine substitution position. In particular, synthon I was always observed when fluorine was in the *ortho*-position (2 position) on the aniline ring and either the 3, 4 or 3, 5 positions on the benzylidene ring.

Throughout these papers, little discussion is made regarding the aromatic stacking interactions, although some potential C – H ··· π interactions are highlighted in the 2012 paper.

In an earlier paper by researchers Zhu, Zhu, Jin and Li in 2005, fluoroanilines were investigated in a study of phenyl – perfluorophenyl aromatic stacking interactions[124]. Co-crystals of differently substituted fluoroanilines were used to investigate the influence of F. The observed structures packed such that perfluorinated aromatic rings overlapped with unsubstituted aromatic rings. Melting points of the starting materials and co-crystal demonstrated that the aromatic face-to-face interactions between perfluorinated benzylideneaniline and unsubstituted benzylideneaniline had a stabilising effect. However, the scope of this paper was limited to two co-crystal structures.

In order to meaningfully evaluate the more nuanced behaviours of fluorine augmented aromatic stacking, a larger data set is required. The direct substituent interaction model dictates that the specific position of fluorine substitution will have a significant influence on the aromatic stacking as well as atom-atom interactions involving the fluorine substituent. Many different iterations of similarly substituted fluoroanilines must therefore be systematically compared.

3.3 Systematic Structural Dataset

3.3.1 Database Searches

A large dataset of crystal structures is beneficial when seeking to identify trends of behaviour. Crystallographic database searches are often conducted to generate a large body of structural results for comparison. Some examples of these studies are discussed in Section 1.2.3.1, these were database searches probing the prevalence and nature of C – H ··· F – C interactions.

While the collective insight of large structural databases is undeniably useful[133], database searches have their limitations, particularly in the investigation of weak intermolecular interactions[192]. The databases are generally compiled of isolated entries from different studies, and, as such, they do not provide a continuous set of related compounds, particularly where small incremental changes in molecule structure are required. This continuity is essential for identifying and rationalising the cause of structural differences between compounds. A systematic approach is required.

3.3.2 Structural Systematics

Structure directing changes can be more readily identified by a systematic approach in structural comparisons. These systematic comparisons can give useful insights into the determining factors in crystal assembly[158].

Systematic studies of crystal structures, such as the work proposed in this thesis, require a large dataset of related molecular crystals with many variants. The scope of these systematic studies is sometimes limited by the number of possible variants for a particular system.

The fluoroaniline system has a vast number of possible variants, which can be exploited to construct a select database of these closely related molecules.

3.3.3 Systematic Library

In order to study the effects of F substitution, a select database of fluoroaniline crystal structures will be constructed for this project. Unlike conventional databases, this systematic library will be designed specifically for this molecular system, with each component being synthesised, crystallised and structurally characterised in order to become part of the library for this study.

As discussed, fluoroanilines have a vast number of possible variant substitution patterns. There are 32 unique fluorine substitution patterns for each aniline and benzylidene ring. Multiplication of the two yields 1024 possible unique molecular structures. It is important that the library can systematically and clearly display this chemical landscape.

Firstly, a numbering scheme and conventions must be established to describe the substitution patterns of the molecular structure, Figure 3.2. Crystal structures of studied fluoroanilines will be labelled according to the substitution pattern on the aniline ring and the benzylidene ring, respectively. For example, the structure presented in Figure 3.3 would be denoted as structure (234 – 256). This scheme will be used throughout this project.

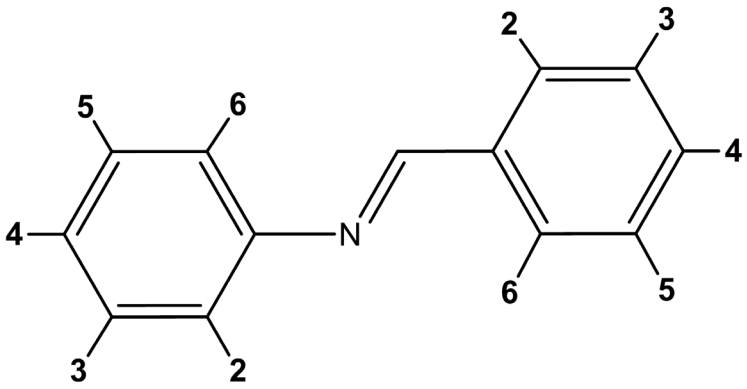

Figure 3.2 Numbering scheme for the F substitution patterns of fluoroanilines.

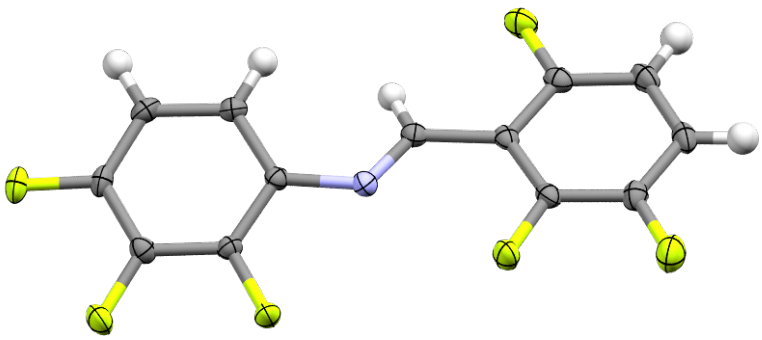

Figure 3.3 Fluoroaniline molecule in structure (234 – 256).

The systematic library will be constructed around this framework, using the aniline and benzylidene substitution pattern to define a position in a matrix. This matrix will then be populated by crystal structures available for comparative analysis, see Section 4.1.

3.4 Methodology

In order to achieve the objectives of this project, the following categorisation and characterisation methods will be employed:

1. Structures in the systematic library will be categorised into different visually determined packing descriptions.

2. The geometric relationships between overlapping aromatic rings will be characterised for the structures within each packing group, using standard resolution atomic coordinates.

3. The spatial similarity between structures will be assessed and these relationships presented.

4. Notable subsets of structures will be selected for further analysis using various methods to identify and analyse intermolecular interactions, such as experimental charge density analysis, PIXEL energy calculations and Hirshfeld surface enrichment ratios.

Chapter 4 Structural Analysis and Categorisation

Initial analysis of the structural library focuses on aromatic ring interactions observed in the various structures. The aim is to investigate, characterise and relate the aromatic overlap relationships and the larger structural arrangement of the molecules and, subsequently, associate the specific fluorine substitution pattern with energetic stabilisation and propensity for certain aromatic ring configurations.

Therefore, for this analysis, the most important chemical features of the molecular structures are the fluorine substitution pattern and the distinction between the aniline and benzylidene aromatic rings. To highlight these features the fluorinated trans-N-benzylideneaniline molecules are displayed in a simplified form. The fluorine atoms are highlighted in green. The hydrogen atoms in each molecule are hidden and non-fluorine atoms have been coloured according to their association with either the aniline or benzylidene ring; aniline atoms are coloured purple while benzylidene atoms are coloured orange, Figure 4.1.

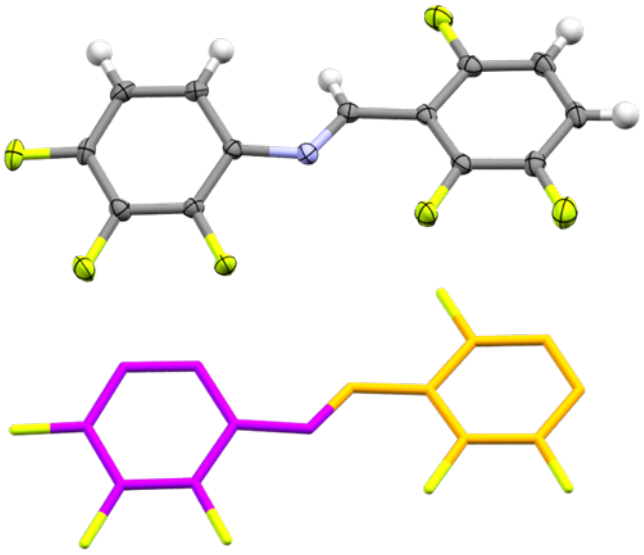

Figure 4.1 Structure (234 – 256). Top: ellipsoid representation. Bottom: simplified representation highlighting the fluorine substitution pattern and distinction between the aromatic rings.

The simplified representation also displays atoms using a thick wireframe rather than ellipsoids. This further aids clarity in the structural diagrams, especially when analysing large structural motifs.

Structural analysis in this chapter begins with an overview of the structural library and categorisation of the structures into fundamental groups determined by visually apparent spatial arrangements.

4.1 Structural Matrix

The structural library contains 118 unique molecular crystal structures (plus one additional structure for (2356 – 4), which exhibits two polymorphs). These samples were synthesised and crystallised by Dr. Terry Threlfall. X-ray diffraction data for the crystals were collected in collaboration with Dr. Phillip Adler, Liam Oliver, Sam Ling and myself, as detailed in the appendices. All structures were determined and refined by myself. The crystal data for all structures can be found in the appendices.

These structures encompass a large number of the possible fluorinated benzylideneaniline molecules, however, there are still gaps in the chemical landscape. An overview of the experimentally obtained structures is presented in the Structural Matrix, Table 4.1. The crystal structures are presented across the matrix as filled squares, using fluorine substitution patterns as coordinates.

The numbering scheme, detailed in Section 3.3.3, is translated to the axes of the matrix. The aniline ring fluorine substitution pattern is listed along the y axis, while the benzylidene ring fluorine substitution pattern is listed along the x axis.

The matrix has certain columns and rows shaded out. These pertain to inaccessible crystal structures as the starting materials for the synthesis of these structures were unavailable or prohibitively expensive.

The matrix displays the population of structures across the chemical landscape. Overall there is good coverage of the structures, including those with a greater number of fluorine substituents.

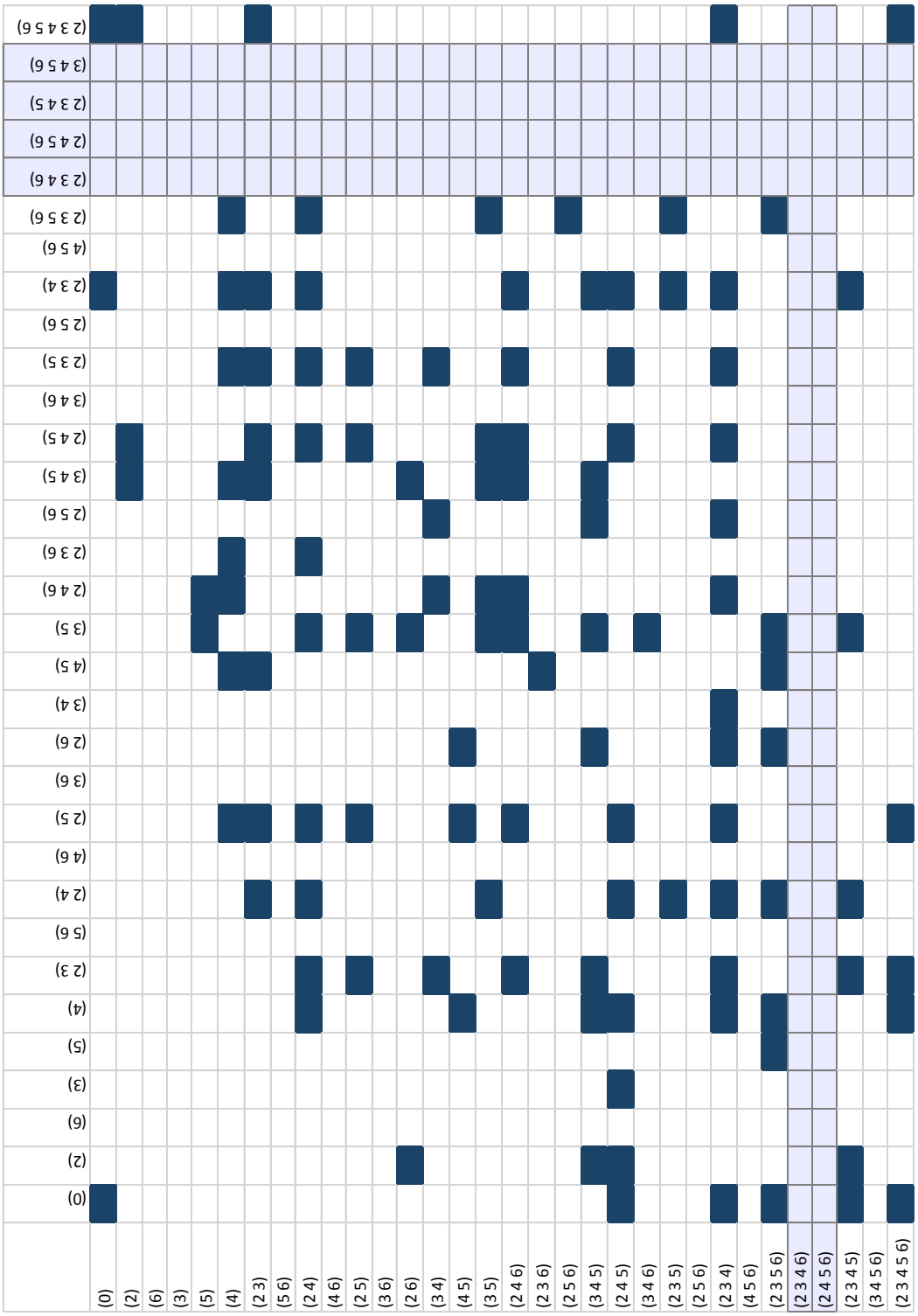

Table 4.1 Structural Matrix: Depiction of the structures presented in the structural library. The y axis displays the aniline fluorine substitution pattern, while the x axis displays the benzylidene fluorine substitution pattern.

4.1.1 Visually Determined Packing Descriptors

The crystal structures have been separated into categories based on visual inspection and identification of their most distinct packing motifs. By using this method, seven different packing groups have been categorised.

Table 4.2 Population of Visually Determined Packing Groups

Packing Description	**Members of group**
Head-to-Head Stack	28
Head-to-Tail Stack	40
Staggered Overlap	4
Interwoven	7
Angled Overlap	17
Grid	7
Other	15

These groups are purely topological, so they do not impart any information about the chemistry, i.e. intermolecular interactions, in the crystal structure. However, they do offer initial insights into the packing behaviour of the fluorine substituted aromatic rings in this system.

A more detailed description of each packing group is given in the following subsections. The figures in this section represent an archetype structure for each packing system, as such no fluorine atoms are shown.

4.1.1.1 Stacking Motifs

Two of these packing groups share the same overall stack topology but have been separated based on the orientation of the molecules. They are categorised as follows: ‘Head-to-Head’, in which stacked molecules are aligned in the same direction with respect to the aniline and benzylidene rings; and ‘Head-to-Tail’, in which stacked molecules are in anti-parallel alignment with respect to the aniline and benzylidene rings, Figure 4.2. Both motifs also exhibit lateral displacement of the stacked aromatic rings. This is in agreement with other experimental results for fluorinated phenyl ring stacking, as described in Section 1.2.2.3, and is also observed in the Staggered Overlap and Interwoven packing groups.

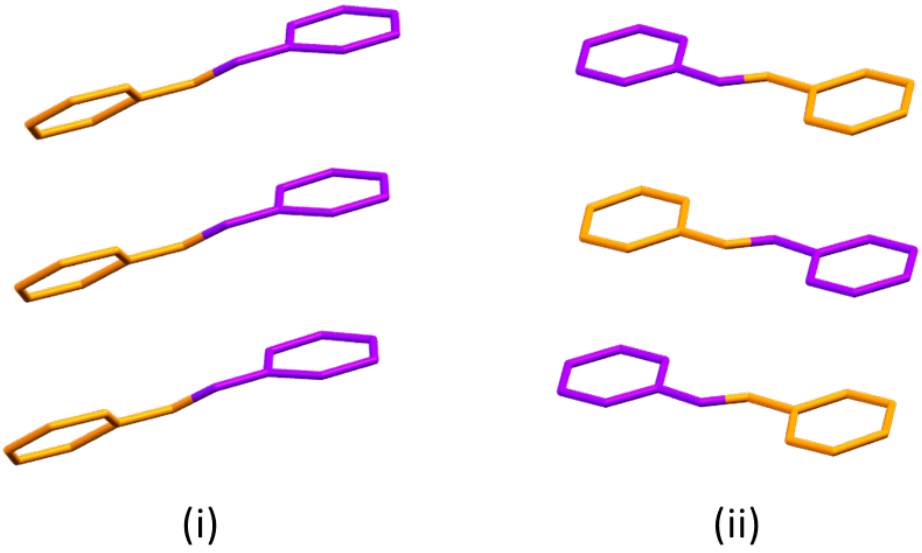

Figure 4.2 Archetype representations of (i) Head-to-Head stacking motif, (ii) Head-to-Tail stacking motif.

These groups are both characterised by the central one-dimensional stacking motif. The majority of crystal structures in this study adopt one of these stacking motifs, with a preference towards Head-to-Tail stacks. This is largely consistent with the expected behaviour of aromatic ring stacking, although the presence of like-to-like (parallel Head-to-Head) stacks is somewhat unexpected in fluorinated systems. In parallel Head-to-Head stacks the substituted fluorine atoms are necessarily juxtaposed and, as such, one might expect large repulsion from their close proximity. It would appear the effect is mitigated by other factors, which are explored further in Section 4.2.2 and Section 4.2.7.

While the Head-to-Tail stacking motif is the most obvious configuration for favourable overlap of the fluorinated aromatic rings, several alternative configurations present themselves in the subsequently identified groups.

4.1.1.2 Staggered Overlap

In this subset of structures the central motif is the offset overlap or 'Staggered Overlap' of the aromatic rings between neighbouring molecules. While there are only four members in this small group, the parallel stacking of rings make this motif distinct among the other structures.

In these structures the molecules are aligned in the same direction and translation of the molecules results in the parallel head-to-tail stacking between the aromatic rings, Figure 4.3. Each molecule in the structure has aromatic ring overlap with four other molecules, giving rise to two unique interactions. These propagate in two directions to produce a sheet of overlapping molecules.

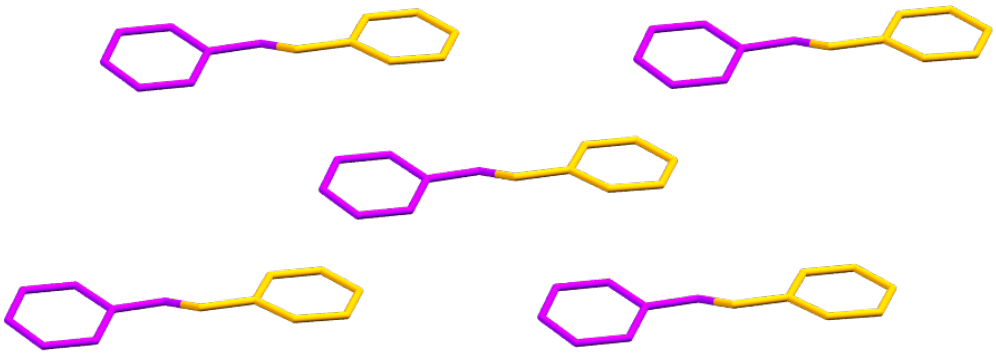

Figure 4.3 Archetype representation of the Staggered Overlap motif.

The stacking is deemed parallel as the molecules are related to one another through translation operations only and orientated in the same direction. This is opposed to anti-parallel head-to-tail stacking, in which the rings are related through inversion or rotation – such as in the Head-to-Tail stacking group.

This mode of stacking is observed in other planar aromatic molecules and is variously referred to as brick-wall, brick layer stacking, brickwork and brick packing[74,79,123,138]. The title 'Staggered Overlap' has been used in this work in order to differentiate from other structural motifs which might equally be described in terms of brickwork patterns. One such set of structures is the Interwoven group.

4.1.1.3 Interwoven

In the Interwoven group there is also offset overlap between aromatic rings. The Interwoven structures are formed of anti-parallel dimer pairs which are arranged in offset stacks. Unlike the Staggered Overlap motif, the offset overlap in these structures is in an anti-parallel head-to-head configuration, in which the aromatic rings are related through inversion. The molecules within the anti-parallel dimer pairs are also related to one another through inversion, and therefore head-to-tail.

The head-to-head arrangement of the offset overlapping rings does not necessarily lead to close contact of the fluorine atoms in these structures due to their anti-parallel configuration.

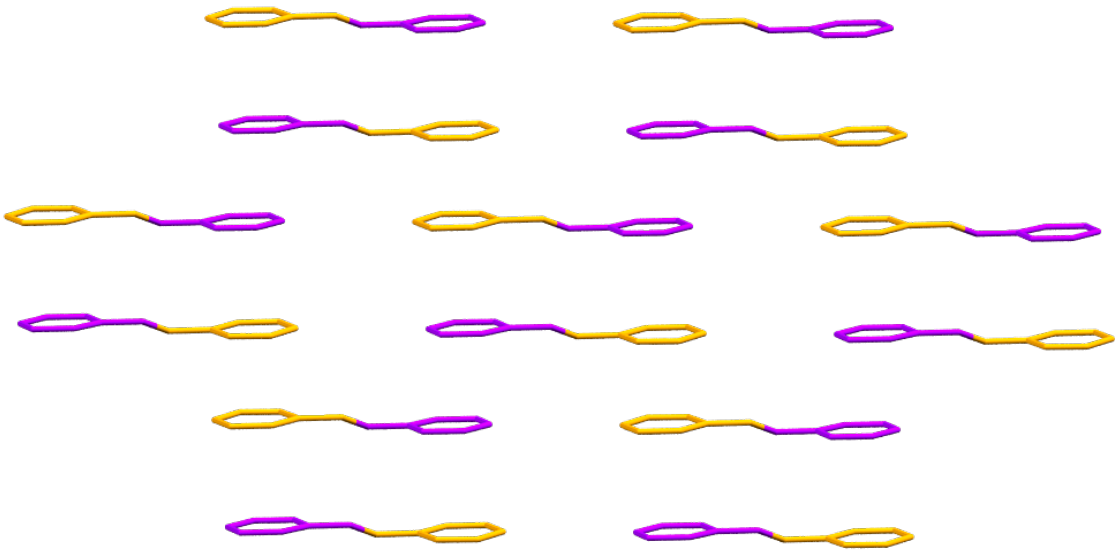

Figure 4.4 Archetype representation of the anti-parallel pairs and head-to-head overlap in the Interwoven structures.

In the first structures identified with this pattern of anti-parallel dimer pairs, adjacent layers of molecules were oriented perpendicular to one another, Figure 4.5. This gave the appearance of interwoven molecules, for which the group is named.

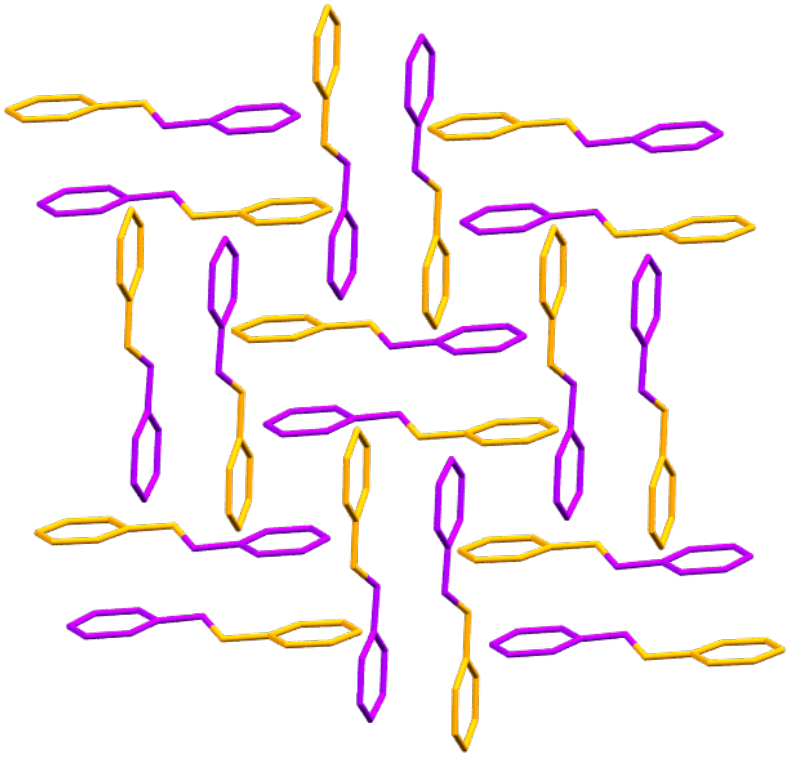

Figure 4.5 Perpendicular arrangement of adjacent layers in selected structures within the Interwoven Group.

4.1.1.4 Angled Overlap

Unlike the others, this structure is typified by molecules angled over one another creating a saw-tooth pattern, Figure 4.6. The structures in this group are identified by this distinctive central pattern. The arrangement in this motif allows two head-to-tail overlaps with each molecule angled over two neighbours. The configuration of aromatic rings is not parallel nor is it strictly anti-parallel in the same way other structures have been described; the angled overlap is a unique and unanticipated configuration.

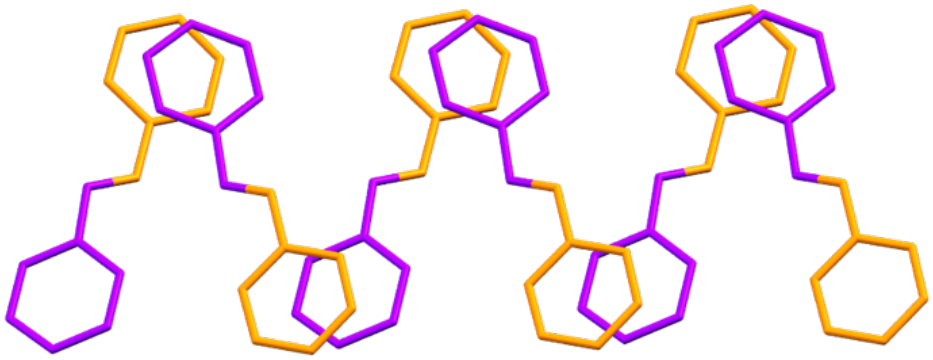

Figure 4.6 Archetype representation of the Angled Overlap motif.

The larger assembly of the structures are not as directed by this central motif as in the Interwoven packing descriptions. While there are isostructural subsets within the group, the one dimensional angled overlap motif does not seem to be as influential on the long-range packing. Therefore there is a broad spectrum of different structures which fall within this categorisation.

4.1.1.5 Grid Structures

This group is partially characterised by the distance between the molecules, which is much greater than other structural groups identified here. Initial inspection of structures suggests they should be categorised as Head-to-Head stacks. However, the molecules are significantly separated and displaced such that there is no meaningful overlap between aromatic rings.

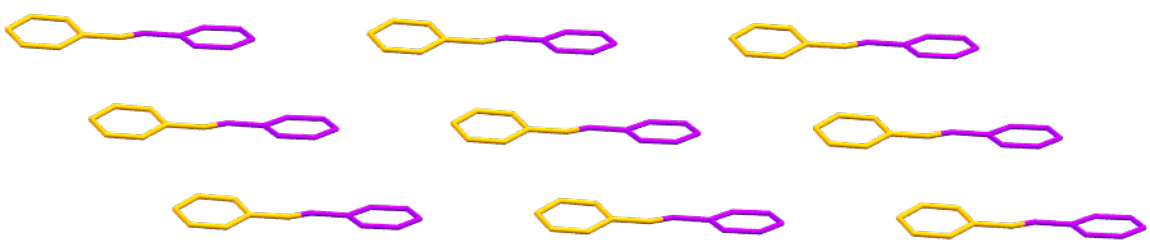

Figure 4.7 Archetype representation of Grid structure separated stacks.

Another structural feature of this group is the arrangements of adjacent layers of molecules, which orient themselves perpendicular to one another. As these layers repeat, they begin to give the appearance of a net or grid, Figure 4.8.

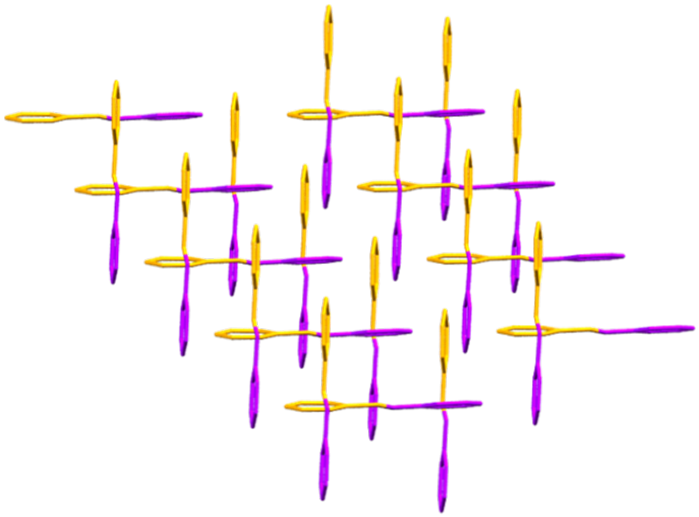

Figure 4.8 Perpendicular arrangement of three adjacent layers in the Grid structures.

4.1.1.6 Other

While the broad visual packing descriptions are able to account for most of the structures a small proportion, 15 of the 118 structures, could not be categorised in this way as they exhibited packing arrangements which did not conform to the broader groups.

Some of these uncategorised structures are found to bear similarity to one another, often with a related substitution pattern. For example, (23 – 25) and (25 – 25) both exhibit a herringbone-like pattern built from anti-parallel dimer pairs, Figure 4.9.

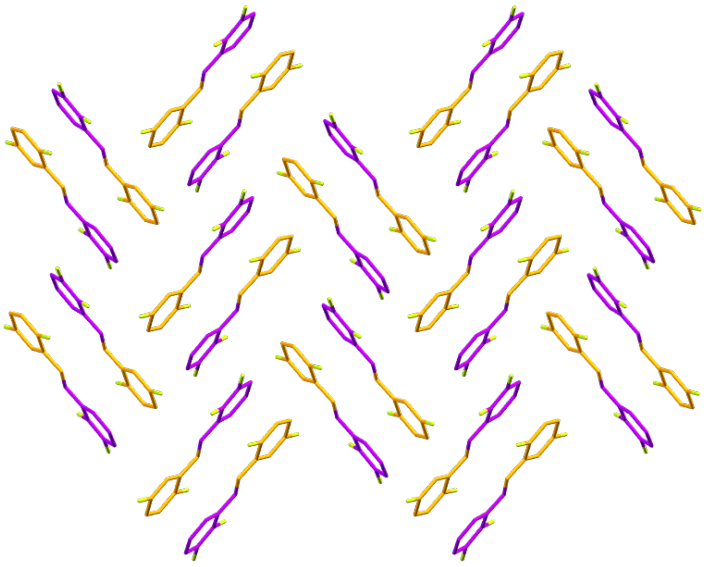

Figure 4.9 Herringbone-like arrangement of structure (23 – 25).

As well as aromatic ring overlap within the dimers, overlap between the aniline rings of adjacent pairs is also observed. This is similar to the anti-parallel head-to-head overlap seen in the Interwoven group although here the head-to-head arrangement only proliferates along one side of the dimers, creating a diagonal stack. Closer inspection of the structure also reveals that, unlike the herringbone arrangement of benzene or hexafluorobenzene[79,144], the diagonal stacks are shifted such that no edge-to-face aromatic overlap interactions are possible.

While difficult to account for when assessing the matrix as a whole, the structures in this group are of interest as examples of unexpected or anomalous behaviour. Comparison of the packing arrangements and substitution patterns observed in these structures with those of similar molecules could give unique insight into the directing forces behind the deviation.

4.1.2 Visual Packing Description Matrix

The results of this structure categorisation were plotted on a new matrix, in which colours have been used to define the different packing groups, Table 4.3.

This Visual Packing Description Matrix highlights the spread of various packing arrangements across the structural library. Relationships between the fluorine substitution pattern and these broad packing descriptions are not immediately apparent.

The structures with the highest levels of fluorine substitution adopt predominately uncategorised arrangements. Head-to-Head stacks appear to be less prevalent at higher numbers of fluorine substitution, although there are still exceptions to this, such as structure (235 – 2356).

The term complementary is used to describe benzylideneanilines substituted such that fluorine atoms are juxtaposed with hydrogen atoms when the molecules are stacked Head-to-Tail. These structures appear to favour this head-to-tail conformation, for example structure (236 – 45). By contrast, structures in which the fluorine substitution is identical on both rings exhibit no Head-to-Tail stacked structures, instead preference appears to be for Head-to-Head and uncategorised arrangements, for example structure (35 – 35) adopts a Head-to-Head configuration.

These broad observations of structural trends offer some insight into the relationship between fluorine substitution and crystal structure. However, the directing forces and principal interactions present in these structures cannot be inferred from the visual packing descriptions or their distribution across the matrix. More detailed investigation of the different structural arrangements is required.

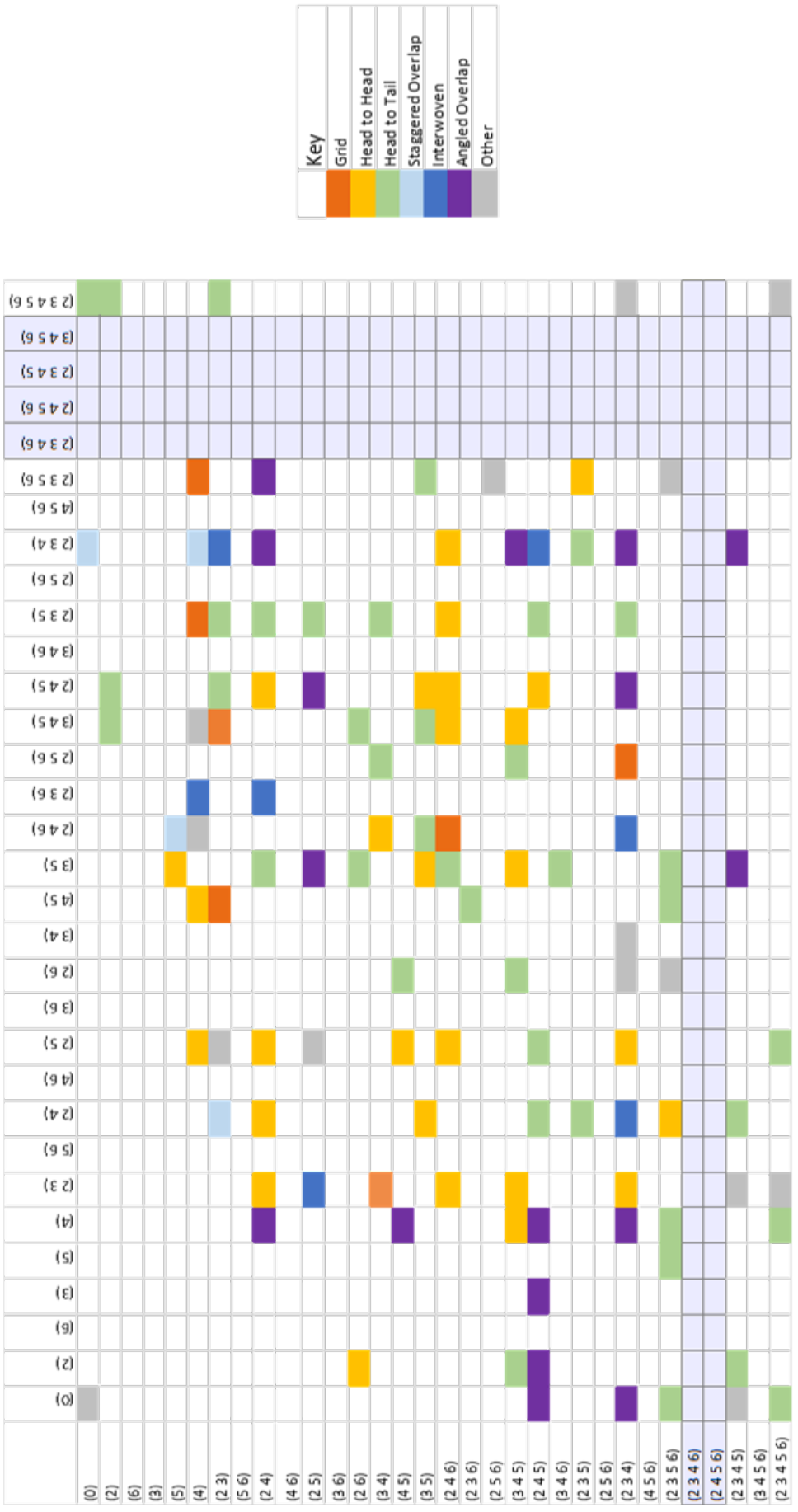

Table 4.3 Visual Packing Description Matrix: depiction of the visual packing groups associated with the various structures within the structural library. Key on the right defines the colour for each group.

4.2 Geometry

As discussed in Chapter 1, investigation of the geometric features in a crystal structure can be used to indicate the presence of intermolecular interactions. These are usually prominent atom-atom interactions such as strong hydrogen bonds, which are identified through short contact distances and favourable bond angles for interaction. Though often overlooked, geometric analysis can also provide insight into the more diffuse molecule-molecule interactions such as aromatic stacking.

In this section the spatial relationships between overlapping phenyl rings are analysed to determine the strength and directing power of various modes of "π – π" intermolecular interactions. The experimental crystal structures are analysed systematically, studying molecules pairwise to identify unique phenyl-phenyl relationships within the structures.

As with geometric evidence for atom-atom interactions, this analysis cannot provide proof of intermolecular interaction or interaction strength without support from energetic calculations. However, ring separation distance and the degree of lateral displacement can be used to infer lesser or greater energetic contributions arising from aromatic ring overlap, highlighting structures of interest for pairwise molecule-molecule energetic calculations in later analysis.

4.2.1 Geometric Descriptors

The structural geometry was measured for pairs of molecules with overlapping phenyl rings, recording the distances and angles between them.

The aromatic rings were used to define parameters for comparison. For each phenyl ring the positions of the six carbons were used to calculate a least squares plane. Similarly, these six atoms were used to define a centroid describing the centre of mass for each phenyl ring.

For a given aromatic ring overlap the following geometric properties were measured: centroid separation; lateral displacement of centroids or 'translation' distance; plane separation distance and the intermolecular dihedral angle between the rings.

4.2.1.1 Intermolecular Dihedral Angle

The intermolecular dihedral angle is the angle between the planes of the phenyl rings associated with each aromatic overlap relationship. A low intermolecular dihedral angle is considered more favourable for aromatic ring stacking overlap. As discussed in Section 1.1.5.3, dispersion is the main contributor to attraction between aromatic rings[88,91]. A parallel or near parallel relationship maximises the surface contact between aromatic rings and improves the dispersive interaction.

4.2.1.2 Intermolecular Distances

The centroid separation is simply the distance between the centroids of each phenyl ring in the aromatic overlap, Figure 4.10. Likewise, the plane separation is the distance between the planes associated with each ring. The plane separation is measured from the centroid of one ring to the plane associated with the other overlapping ring. If the intermolecular dihedral between rings deviates from 0 this gives two values for the plane separation. An average of these values is calculated to give the plane separation for the unique overlap relationship.

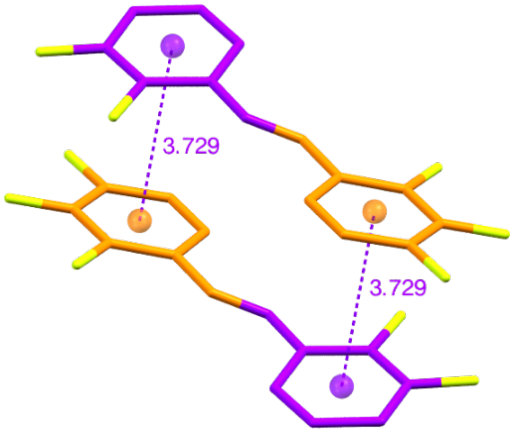

Figure 4.10 Centroid to centroid distance between overlapping rings in structure (23 – 234).

Parallel translation distance, also referred to as plane to plane shift, describes the lateral displacement of one phenyl ring along the plane of the overlapping ring. As with the plane separation, this results in two values for each unique overlap in instances where the planes between the overlapping rings are not parallel. An average of these values is calculated to give the lateral displacement of the individual aromatic interactions.

4.2.1.3 Relationship between Lateral Displacement and Plane Separation

A number of computational studies have identified that aromatic stacking motifs with lateral displacement are generally more favourable than fully eclipsed face-to-face stacking[98,117]. This is supported by observations of experimental crystal structures which show a preference for twisted or parallel-displaced stacks[91].

As discussed in Section 1.2.2.3, parallel displacement of the rings generally results in a shorter plane separation i.e. closer stacking. In a 2018 computational study, Lutz and Bayse identified that translation of the aromatic rings enhanced the interpenetration of the electron densities and reduced the repulsion between molecular orbitals, such that the benzene derivatives could stack closer together[117]. They also found that different substituents affected the length of the optimal lateral displacement. In particular, hexafluorobenzene stacks exhibited shorter optimal translation

distances than benzene stacks due to the influence of fluorine substitution on the molecular orbitals.

Therefore, the translation and plane separation values are expected to vary across the different structures as fluorine substitution will affect the optimal translation associated with the closest stacking. Manipulation of ring separation and stacking distance through fluorine substitution would be a valuable tuneable property for crystal engineering; stacking distances are important to the design of many crystal systems, such as discotic liquid crystalline materials[193].

However, molecular orbital calculations for all of the fluoroanilines is beyond the scope of this work. Even with such calculations, the overlap between molecular orbitals is small and it would be difficult to disentangle the influence of fluorine substitution in order to give a robust rule for stacking distance manipulation. This is an experimental and not a computational study, as such the most thermodynamically optimal configuration may not be the one observed, especially when the forces involved are very small. Additionally, direct substituent effects between rings are expected to significantly influence the packing motifs.

Instead, translation and plane separation distances are recorded for the various geometric groups with the hope of identifying trends in relation to the packing motifs. The degree of fluorine substitution, i.e. the number of F atoms, is not expected to directly relate to the optimal translation distance or plane separation; the position of the F atoms will have a more significant impact on the overlap between molecular orbitals as well as direct substituent effects.

As a baseline for comparison, the average plane separation for overlapping rings is approximately 3.40 Å across the structure library with a standard deviation of 0.07 Å. The translation distances are much more varied, in agreement with the discussion above. Lateral displacement of rings much exceeding 2.79 Å (the approximate width of a phenyl ring) are unlikely to relate to significantly stabilising aromatic ring overlap. If ascribing to the molecular orbital model set out by Lutz and Bayse, this distance would mean that there could be no overlap between the molecular orbitals of the two rings and therefore no inter-ring density. Likewise, electrostatic models of aromatic interactions would suggest that this degree of separation would prohibit significant attraction between the rings.

4.2.1.4 Intramolecular Measurements

In addition to these intermolecular geometric descriptors, the intramolecular dihedral angles of the fluoroanilines were also measured. The intramolecular dihedral angle is the angle between the planes derived from the two aromatic rings within the same molecule, Figure 4.11.

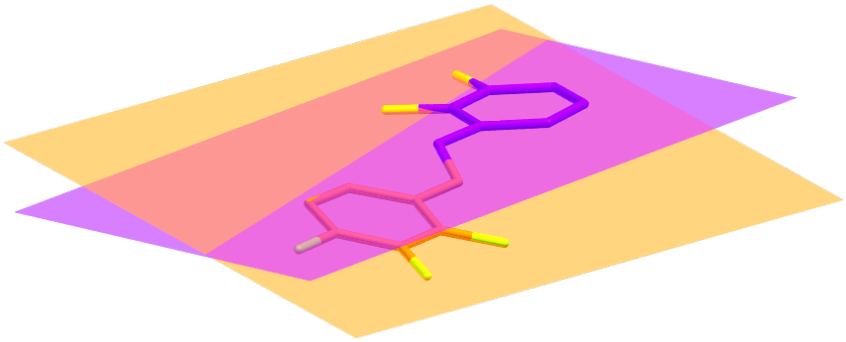

Figure 4.11 Two planes derived from the phenyl rings in one molecule from structure (23 – 234). Planes are coloured corresponding to the aniline or benzylidene ring.

The conformation of the trans-N-benzylideneaniline molecules are closely inter-related to the electronics of the system, namely, non-planarity disrupts pi-electron conjugation across the molecule[194,195]. Trans-N-benzylideneanilines have been extensively studied for their application in optics, such as non-linear optics (NLO)[196]. Conjugation of the pi-system is a necessary requirement for such applications.

As such the intramolecular dihedral angle is an important descriptor for the molecular conformation as it expresses the degree of planarity, and therefore the possible conjugation across the system.

The fluorinated trans-N-benzylideneanilines in the structural library presented generally resist planarity. This is also the case for unsubstituted trans-N-benzylideneaniline. The aniline ring in N-benzylideneanilines is twisted out of the C-N=N-C plane by 55° and the benzylidene ring twisted in the opposite direction by 10°, giving an intramolecular dihedral angle of 65° [197]. Whereas, analogues of N-benzylideneaniline, E-stilbene and azobenzene, adopt a near planar conformation. This is generally rationalised by considering the competing influence of the energy stabilisation of lone-pair electron conjugation and the repulsive interactions of non-bonded atoms in close proximity.

Several studies have utilised protonation of the nitrogen as a means of improving the planarity[194,195]. However, it has also been demonstrated that it is possible to manipulate the planarity of these aniline systems through substitution of the aromatic rings[196].

In the instance of fluorinated derivatives of trans-N-benzylideneaniline the electron withdrawing effect of fluorine strongly influences the electronic structure and the aromaticity of the molecules. Aromaticity studies of fluorine substituted aromatics demonstrate that fluorine reduces the availability of σ-electrons for electron delocalisation across the molecule[198,199]. In particular, ring-current calculations show a decrease in current strengths with increasing

fluorination. These current strengths are a reliable indicator of electron delocalisation, assessing the pathways for electron transport in conjugated molecules.

Other research papers suggest that fluorine substitution can compensate for a loss of aromaticity expected from the introduction of a heteroatom into an aromatic framework[200,201]. It was proposed that the strong electron negativity of fluorine could draw the electrons located on the heteroatom onto the central ring. These studies also found that the position of the substituent relative to the heteroatom had a significant effect; the aromaticity is enhanced when the fluorine is closer to the heteroatom. This is in contrast to the ring current strength approach, which suggests position has little impact on the fluorine effect, but that increasing the extent of fluorination leads to further electron depletion of the other atoms.

Fluorine is a strong σ acceptor and a weak π donor. Studies which observe an increase in aromaticity with fluorination may be using methods that are more sensitive to change in π orbitals. Whereas, studies of ring-current strengths explicitly observe the total current to measure the conjugation in the molecule[198].

Consequently, the propensity of fluorinated trans-N-benzylideneaniline to adopt a non-planar conformation can be easily rationalised by considering the decrease in energetic stabilisation afforded by planarity. As such, planarity observed in these molecules may not be a particularly reliable indicator of electron delocalisation and conjugation.

Instead, low intramolecular dihedral angles might indicate a system with low 'strain' – molecules in which there is limited intramolecular repulsion between non-bonded atoms.

More broadly, analysis of the molecular conformation across the different structures in the library will further establish the traits of different packing motifs and how these properties relate to fluorine substitution. For example: does substitution in certain positions prohibit planarity through repulsion of fluorine in close proximity to atoms in the opposite ring? Does this dihedral angle limit accessible packing motifs?

4.2.1.5 Nitrogen Separation

The nitrogen separation distance was also recorded for structures that adopted stacking configurations.

The 2005 paper by S. Zhu et al. speculated that the electrostatic repulsion from the lone pair of the nitrogen atom was a major contribution to the variation in fluoroaniline structures[124]. Therefore, the nitrogen separation has been calculated in order to investigate if proximity of nitrogen affects the structural arrangement or orientation of the molecules.

Additionally, comparison of the nitrogen separation distance relative to the centroid separation revealed further traits of different stacked arrangements, highlighting symmetry elements between the stacking molecules.

4.2.1.6 Geometric Grouping

Systematic comparison of these geometric descriptors across the crystal structures yielded sub-sets in which similar local geometries were grouped together. These sets loosely correlated with the visual packing descriptions, linking the larger topology to the local arrangement of molecules.

The full table of geometric measurements for each structure can be found in Appendix C, sorted by geometric group.

4.2.2 Stacking Patterns

As in the visually determined packing descriptions, these groups are characterised by the central stacking motif. Assessment of geometric properties within the Head-to-Head and Head-to-Tail stacking groups suggests a further division into subsets based on geometry and symmetry, into which both head-to-head and head-to-tail structures fall. These subsets are differentiated by the relationships between common centroid distances, consistency between intramolecular and intermolecular dihedral angles and the symmetry elements present. There are four distinct geometric groups of stacking structures.

4.2.2.1 Stacking Group 1

A full table of geometric data for Stacking Group 1 is presented in Appendix C, C.1.1.

All structures in this geometric group are categorised as Head-to-Head stacks, although not all of the Head-to-Head stack structures conform to this local packing arrangement.

The most prominent feature of Stacking Group 1 is the singular centroid separation distance, which proliferates down both ‘columns’ of overlapping phenyl rings. This distance is also equivalent to the nitrogen separation, Figure 4.12. This separation distance is consistent for all like-to-like atom separations between the stacked molecules. The molecules within the stacks are related by translational symmetry only and the intermolecular dihedral angle is therefore equal to zero.

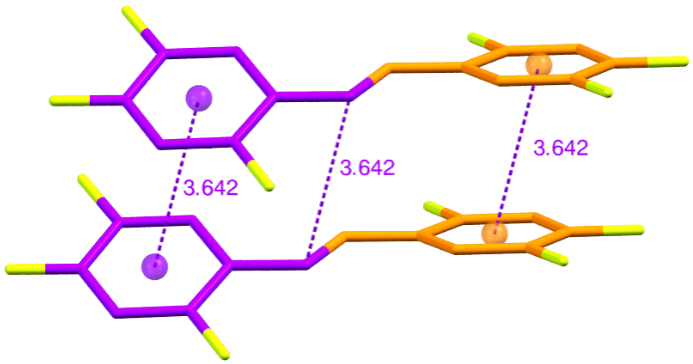

Figure 4.12 Structure (245 – 245) showing the centroid separation and nitrogen separation between stacked molecules, in units of Å.

Whilst the centroid separation distance is consistent throughout the stack, it should be noted that the plane separation and lateral displacement are different between the aniline and benzylidene ring overlaps.

In the example of structure (245 – 245) the aniline-to-aniline ring overlap has an associated lateral translation of 1.465(4) Å and a plane separation of 3.3348(17) Å, while the benzylidene-to-benzylidene ring overlap has a shorter lateral translation of 1.260(4) Å and a longer plane separation of 3.4174(16) Å, Table 5. All structures in this group are Head-to-Head and so the overlap relationships between stacked rings is always either aniline-to-aniline or benzylidene-to-benzylidene.

Table 4.4 Geometric data for structure (245 – 245) of Stacking Group 1, in which row A represents the aniline-to-aniline overlap and row B represents the benzylidene-to-benzylidene overlap.

Structure Code		**Centroid Separation /Å**	**Translation /Å**	**Plane Separation /Å**	**Inter-molecular Dihedral /°**	**Intra-molecular Dihedral /°**	**Nitrogen Separation /Å**
245 – 245	A	3.6424(2)	1.465(4)	3.3348(17)	0.00(15)	31.52(10)	3.6424(2)
	B	3.6424(2)	1.260(4)	3.4174(16)	0.0(2)		

It follows from the discussion in section 4.2.1.3 that a greater lateral translation might allow a shorter plane separation. In the example of structure (245 – 245) both the aniline and benzylidene rings have the same fluorine substitution pattern and so the molecular surface should be comparable between the rings. As such, it is difficult to rationalise why there is a discrepancy between the stacks. Potential lone pair repulsion from nitrogen does not appear to be a factor as

the nitrogen separation has the same value as the centroid separation and the plane separation is shorter for the aniline-to-aniline ring overlap.

The extent of this discrepancy also varies across the group; for many structures there is only a slight difference between the values. For example, structure (35 – 24) has a lateral translation of 1.424(4) Å and 1.430(4) Å for aniline and benzylidene overlap respectively. The magnitude of the difference does not appear to correlate with the pattern or degree of fluorine substitution. Neither does it seem to be an artefact of the intramolecular dihedral angle.

The intramolecular dihedral angles for this group are in the range 30° to 50° with the exception of structures (345 – 345) and (45 – 25), which have a near planar dihedral of 1.2(4)° and 1.36(11)° respectively. As with the unsubstituted trans-N-benzylideneaniline, the aniline ring is generally twisted out of the azomethine (C-N=C-C) plane more than the benzylidene ring. A low intramolecular dihedral brings the atom in the 6 position on the aniline ring into close proximity of the azomethine hydrogen. This proximity introduces repulsive force into the molecular conformation. Therefore, it is likely that the planar conformations observed in (345 – 345) and (45 – 25) are supported by intermolecular interactions with adjacent molecules.

The intermolecular dihedral angle of zero between overlapping aromatic rings is likely to increase the molecular surface contact and maximise stabilisation from dispersion. This will mitigate a portion of the repulsive contribution of juxtaposed fluorine atoms.

As previously stated, all structures in Stacking Group 1 are Head-to-Head stacks but not all of the structures classified as Head-to-Head are in this group. The structure (246 – 345) falls into Stacking Group 4 – discussed in section 4.2.2.4. It is not immediately obvious why this substitution pattern favours Stacking Group 4.

4.2.2.2 Stacking Group 2

A full table of geometric data for Stacking Group 2 is presented in Appendix C, C.1.2.

In contrast to Stacking Group 1, all structures in this geometric group are stacked head-to-tail. Stacking Group 2 is characterised by two distinct aniline-to-benzylidene ring overlap relationships with two unique centroid separation distances. The two overlap configurations alternate down the columns while each stacked molecule pair exhibits one unique centroid separation distance for both aniline-to-benzylidene ring overlaps, Figure 4.13.

The intermolecular and intramolecular dihedral angles have the same value, Table 6. Consequently, the centroid separation distances are the same within a stacked pair; while not related by translation, as with Stacking Group 1, the intramolecular dihedral angle compensates

exactly for the intermolecular dihedral angle between stacked pairs. However, this effect cannot propagate down the columns and so the unique centroid distances alternate down the stack.

Table 4.5 Geometric data for structure (345 – 26) of Stacking Group 2, in which row 1 represents the first aniline-to-benzylidene overlap and row 2 represents the second aniline-to-benzylidene overlap between separate pairwise molecules.

Structure Code		**Centroid Separation /Å**	**Translation Average /Å**	**Plane Separation Average /Å**	**Inter-molecular Dihedral Angle /°**	**Intra-molecular Dihedral Angle /°**	**Nitrogen Separation /Å**
345 – 26	1	3.5948(3)	1.2345(7)	3.3759(4)	1.594(14)	1.594(14)	3.7868(12)
	2	3.6758(3)	1.1097(7)	3.5040(4)	1.594(14)		3.9926(11)

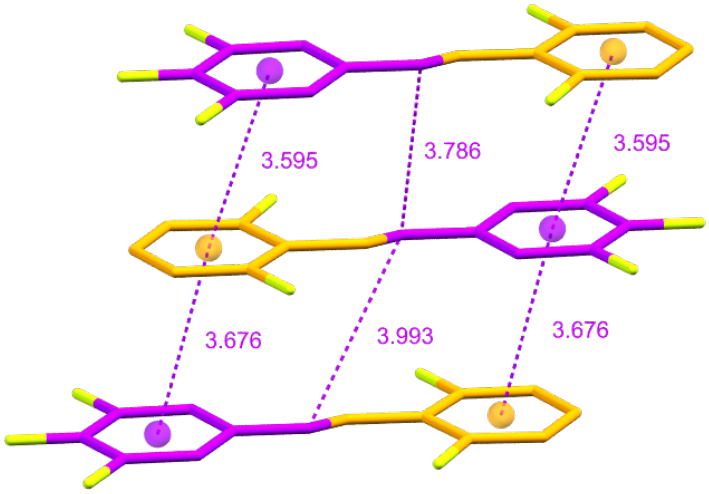

Figure 4.13 Structure (345 – 26) showing the centroid separation and nitrogen separation between stacked molecules, in units of Å.

In addition to remaining equal with the intermolecular dihedral angle, the intramolecular dihedral angles observed in this stacking group are comparatively small. The intramolecular angles range between 1° and 7°. Again, this low dihedral angle may suggest that the molecular conformation is supported by intermolecular interactions with adjacent molecules. However, as this near planar conformation is consistent throughout the group, it implies a link between the conformation and the local structural arrangement.

The stacked molecules are related by inversion, which describes the anti-parallel head-to-tail stacks. For these fluorine substitution patterns (structures present in Group 2), this maximises the direct electrostatic attraction between the local C – F dipoles and C – H dipoles of the opposite ring. This contribution helps balance the repulsive energy from close proximity and so low

dihedral angles become more viable, increasing molecular surface contact and maximising stabilisation from dispersion.

4.2.2.3 Stacking Group 3

A full table of geometric data for Stacking Group 3 is presented in Appendix C, C.1.3.

As with Stacking Group 2, all structures in Stacking Group 3 are arranged in head-to-tail stacks. Similarly, Stacking Group 3 is characterised by two distinct aniline-to-benzylidene ring overlap relationships with two unique centroid separation distances. However, in this sub-set the two overlap configurations are both present in any given stacked pair, such that the local geometric arrangement between any two stacked molecules is the same.

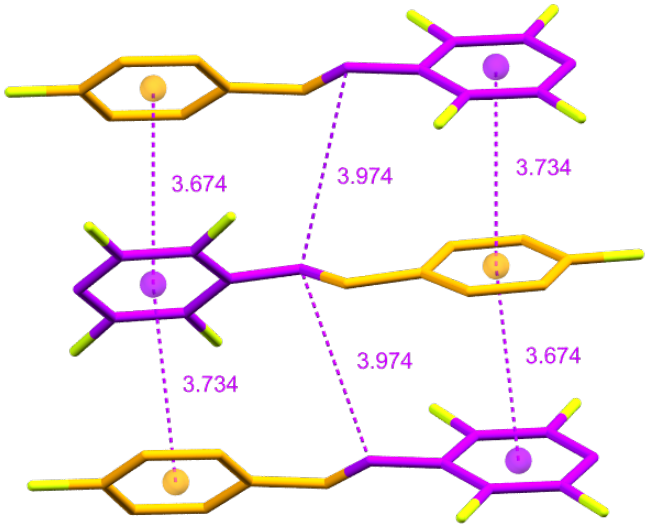

Figure 4.14 Structure (2356 – 4) showing the centroid separation and nitrogen separation between stacked molecules, in units of Å.

For example, in structure (2356 – 4) two distinct aniline-to-benzylidene ring overlap geometries are observed with associated centroid separation distances of 3.7336(2) Å and 3.6740(2) Å. Both of these aniline-to-benzylidene ring overlap conformations are present in each pair of stacked molecules, Figure 4.14.

The stacked molecules in this group are related by a 2_1 screw axis, which propagates down the centre of the stacking column. This rotational translation describes the alternation of the two different overlap geometries down the column, as well as within each individual molecule. Consequently, the nitrogen separation distance is identical between all stacks.

Similar to the inversion symmetry in Stacking Group 2, the screw axis results in anti-parallel head-to-tail stacks that maximise the direct electrostatic attraction between the local C – F dipoles and C – H dipoles of the opposite ring.

Table 4.6 Geometric data for structure (2356 – 4) of Stacking Group 3, in which row 1 represents the first aniline-to-benzylidene overlap and row 2 represents the second aniline-to-benzylidene overlap present in every pairwise stack.

Structure Code		**Centroid Separation /Å**	**Translation Average /Å**	**Plane Separation Average /Å**	**Inter-molecular Dihedral Angle /°**	**Intra-molecular Dihedral Angle /°**	**Nitrogen Separation /Å**
2356 – 4	1	3.7336(2)	1.5658(6)	3.3870(3)	4.929(11)	49.548(12)	3.9740(2)
	2	3.6740(2)	1.5633(5)	3.3216(3)	4.929(11)		

Unlike Stacking Group 2, the intermolecular and intramolecular dihedral angles are not equal. The intermolecular angle remains low for this group while the intramolecular angles are higher, in the range 25° to 60°. The higher end of this range is more consistent with the recorded intramolecular angle for unsubstituted trans-N-benzylideneaniline.

The geometric arrangement observed in Stacking Group 3 is the most common configuration for Head-to-Tail stacking, observed in 19 of the 40 Head-to-Tail structures.

4.2.2.4 Stacking Group 4

A full table of geometric data for Stacking Group 4 is presented in Appendix C, C.1.4.

The geometric arrangement of these molecules is markedly different from that of other stacking motifs. Whilst a small number of structures in the other stacking groups have an asymmetric unit with more than one fluoroaniline molecule, all structures in Stacking Group 4 have at least two molecules in the asymmetric unit, Z’ = 2.

The two molecules are chemically the same in each instance, but each have a unique conformation resulting from differences in the intramolecular dihedral angles. Necessarily there are no symmetry operators between the stacked molecules within the asymmetric unit. Neither is there any symmetry between the stacked molecules from one asymmetric unit to the next; the stacks are propagated by translation only, alternating between the two unique molecular conformations.

Consequently, there are four unique values for the centroid separation distances and two unique values for the nitrogen separation. To further illustrate this, in structure (23456 – 0) there are two pairwise stacked relationships between the unique molecular conformations, Figure 4.15. Each is associated with two aniline-to-benzylidene overlap relationships and a nitrogen separation between the molecules, Table 8.

Table 4.7 Geometric data for structure (23456 – 0) of Stacking Group 4, in which rows 1, 2, 3 and 4 represent the four aniline-to-benzylidene overlap relationships. Each row has two recorded intramolecular dihedral angles - describing the two unique molecular conformations in each stacking relationship.

Structure Code		**Centroid Separation /Å**	**Translation Average /Å**	**Plane Separation Average /Å**	**Inter-molecular Dihedral Angle /°**	**Intra-molecular Dihedral Angle /°**	**Nitrogen Separation /Å**
23456 – 0	1	3.641(3)	1.332(6)	3.386(3)	4.95(14)	45.40(13) 45.16(13)	3.904(5)
	2	3.623(3)	1.377(6)	3.349(3)	4.59(13)	45.40(13) 45.16(13)	3.904(5)
	3	3.759(3)	1.699(7)	3.353(4)	4.95(14)	45.40(13) 45.16(13)	3.725(5)
	4	3.770(3)	1.728(6)	3.348(4)	4.59(13)	45.40(13) 45.16(13)	3.725(5)

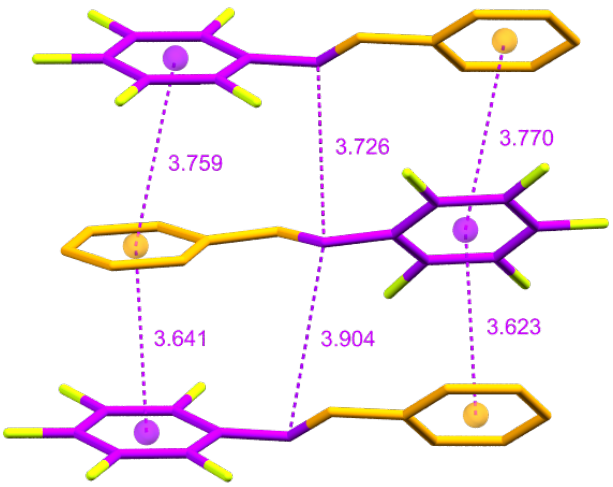

Figure 4.15 Structure (23456 – 0) showing the centroid separation and nitrogen separation between stacked molecules, in units of Å.

The alternation of intramolecular dihedral angles across molecules in the stack also gives rise to an alternation of intermolecular dihedral angles within the same stacked pair. A simplified expression of these patterns is given in Table 9.

Table 4.8 Simplified expression of the relationships between the values of different geometric descriptors in Stacking Group 4. Different letters are used to indicate identical values, i.e. X = X.

Centroid Separation /Å	**Intermolecular Dihedral/°**	**Intramolecular Dihedral/°**	**Nitrogen Separation /Å**
Distance 1	X	a b	α
Distance 2	Y	a b	α
Distance 3	X	a b	β
Distance 4	Y	a b	β

Unlike the other stacking groups described, Stacking Group 4 contains both Head-to-Tail and Head-to-Head structures. Although, only one Head-to-Head structure is present in this group, structure (246 – 345), Figure 4.16. This structure is a unique example of head-to-head stacking but it conforms well to the same geometric trends as Stacking Group 4.

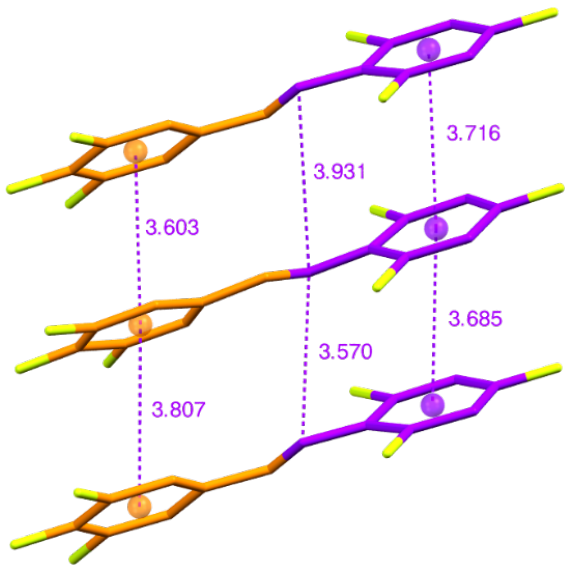

Figure 4.16 Structure (246 – 345) showing the centroid separation and nitrogen separation between stacked molecules, in units of Å.

Structure (246 – 345) has an unusual stacking arrangement between molecules within the asymmetric unit. In head-to-tail arrangements the azomethine linkers of stacked molecules are rotated or inversed such that they are not related to one another by translation. Whereas, the head-to-head arrangements of Stacking Group 1 exhibit stacking through translation only, such that the atoms of the azomethine linker and rings are juxtaposed with those of adjacent molecules.

In structure (246 – 345) the azomethine groups and aromatic rings are 'twisted' relative to one another, Figure 4.17. This unusual arrangement may alleviate repulsive effects from close contact of fluorine atoms and atoms in the azomethine group.

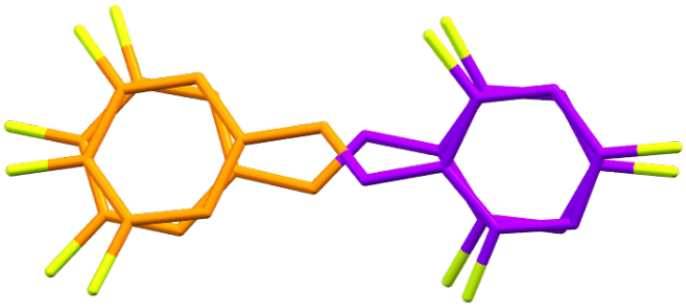

Figure 4.17 The asymmetric unit of structure (246 – 345) viewed down the stack.

For all structures in Stacking Group 4 the intramolecular dihedral angles are in the range 25° to 60°, similar to Stacking Group 3.

4.2.2.5 Stacking Geometry Summary

The Head-to-Head and Head-to-Tail stacking types were identified through visual inspection of the structures. The distinction between these stacking motifs remains important when studying the local geometry. The methods used to examine the geometric relationships between overlapping aromatic rings do not distinguish between aniline and benzylidene rings. Nevertheless, structures with head-to-head stacking motifs formed into crystal assemblies different from those with head-to-tail stacking motifs (with the exception of (246 – 345)).

The correlation between local geometry and stacking orientation supports the importance of substituent effects in aromatic ring stacking.

Structures with head-to-tail orientation exhibited a greater diversity of local structural arrangements – Stacking Groups 2, 3 and 4. This suggests the presence of subtler factors directing the assembly of these structures, likely influenced by particular fluorine substitution patterns.

4.2.3 Offset Overlap

The term “Offset Overlap” is used here to describe aromatic ring interactions in both the Staggered Overlap and Interwoven groups identified from visual inspection in Section 4.1.1. The two different overlaps observed in these groups are different in orientation; the aromatic ring interactions in the Staggered Overlap group have a parallel head-to-tail relationship whilst the offset overlap ring interactions in the Interwoven group are arranged anti-parallel head-to-head. In this section, however, the geometric comparison between different aromatic ring overlap is purely topological. Therefore, these conformations have been considered together.

The Grid structures might also be considered to contain offset overlap motifs. However, the molecules in these structures are significantly separated, such that favourable aromatic ring interactions are not feasible. Therefore, Grid structures have been discussed separately in Section 4.2.5.

It is notable that topological differences were observed between the offset overlaps in the Staggered Overlap and Interwoven groups, giving further support for the importance of substitution effects in these systems.

4.2.3.1 Staggered Overlap

A full table of geometric data for the Staggered Overlap group is presented in Appendix C, C.2.1.

Staggered Overlap structures exhibit parallel head-to-tail stacking between aromatic rings via significant lateral translation of the interacting molecules: offset overlap. Consequently, each molecule overlaps with four adjacent molecules, giving rise to two unique interactions. These might be considered separately as aniline-upon-benzylidene overlap and benzylidene-upon-aniline overlap and have a corresponding unique centroid separation distance, Figure 4.18.

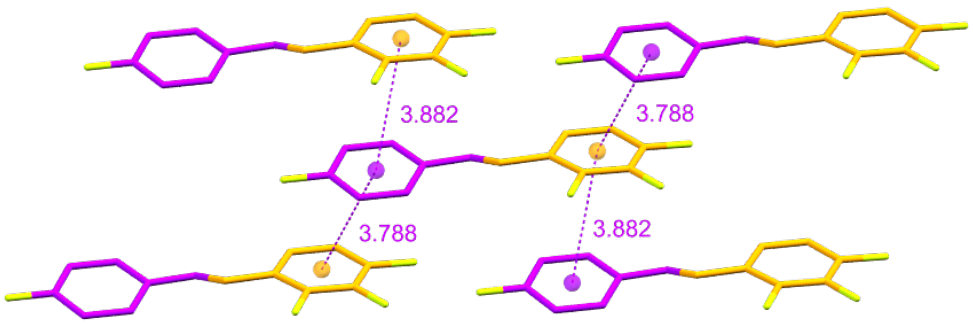

Figure 4.18 Structure (4 – 234) with centroid separation distances for the offset aromatic ring interactions, in units of Å.

Table 4.9 Geometric data for structure (4 – 234) of the Staggered Overlap group, in which rows 1 and 2 represent the first and second aniline-to-benzylidene overlap between staggered molecules.

Structure Code		**Centroid Separation /Å**	**Translation Average /Å**	**Plane Separation Average /Å**	**Intermolecular Dihedral Angle /°**	**Intramolecular Dihedral Angle /°**
4 – 234	1	3.7781(8)	1.571(2)	3.4467(13)	8.19(5)	8.19(5)
	2	3.8817(9)	1.986(2)	3.3246(16)	8.19(5)	

Although the molecules across the motifs are related by other symmetry elements present in the crystal, the overlapping rings in these structures are not directly symmetrically related other than by translation.

The overlapping rings in Stacking Group 1 are also related by translation symmetry only. In the case of those parallel head-to-head relationships the translation leads to an intermolecular angle of zero. However, in the Staggered Overlap group the parallel relationship is head-to-tail. Therefore, the intermolecular dihedral angle should be equivalent to the intramolecular dihedral angle, which is the angle relating the 'head' to the 'tail' within each molecule. This is concurrent with the observed values, Table 10.

Inspection of the geometric values in isolation suggests a closer similarity to Stacking Group 2, which also exhibit equivalent intermolecular and intramolecular angles and two unique overlap relationships. In Stacking Group 2 the stacked molecules are related by an inversion centre. The Staggered Overlap structures are centrosymmetric however the centres of inversion do not correspond to the parallel head-to-tail overlap relationships between molecules in the staggered overlap sheets, these symmetry operations only relate one sheet to another (with the exception of structure (23 – 24), which exhibits additional overlap relationships related by inversion).

4.2.3.2 Interwoven

A full table of geometric data for the Interwoven group is presented in Appendix C, C.2.2.

The Interwoven structures contain both offset overlap and stacking overlap relationships, Figure 4.19. Unlike the Staggered Overlap group, the offset overlap relationships in the Interwoven group are anti-parallel head-to-head. This configuration is unusual and leads to a head-to-head arrangement in which the fluorine atoms are not juxtaposed with their counterpart from the interacting ring. Therefore, there is not necessarily close contact between the fluorine atoms.

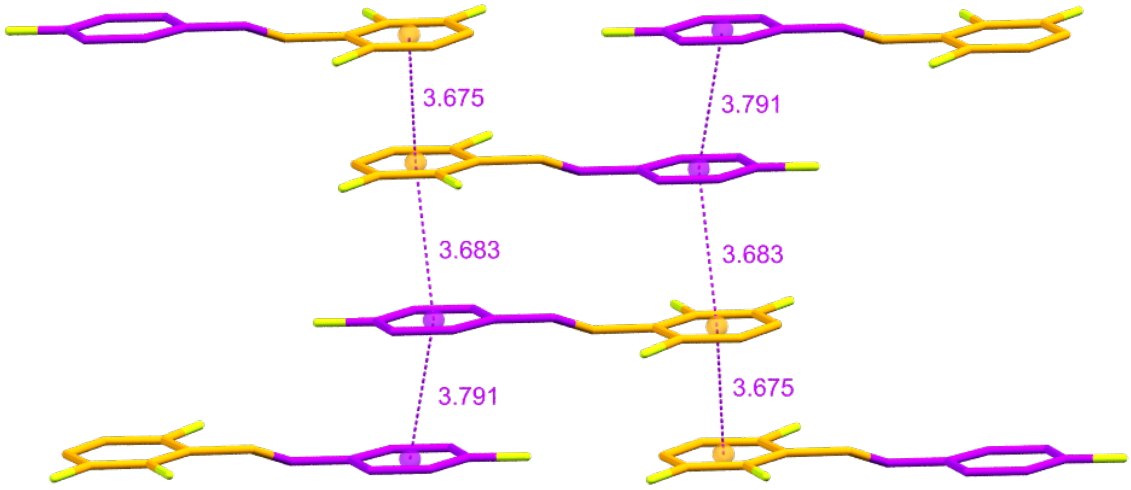

Figure 4.19 Structure (4 – 236) with centroid separation distances for the offset and stacked aromatic ring interactions, in units of Å.

These anti-parallel head-to-head aromatic rings are related to one another through inversion. This symmetry operation preserves an intermolecular dihedral angle of zero, Table 11.

Table 4.10 Geometric data for structure (4 – 236) of the Interwoven group. The H-t-T row shows the geometric parameters for the anti-parallel stacked dimer. Rows H-t-H 1 and 2 present the geometric parameters for the two unique offset overlap relationships.

Structure Code		**Centroid Separation /Å**	**Translation Average /Å**	**Plane Separation Average /Å**	**Inter-molecular Dihedral Angle /°**	**Intra-molecular Dihedral Angle /°**
4 – 236	H-t-T H-t-H 1 H-t-H 2	3.6833(16) 3.791(2) 3.675(2)	1.397(4) 1.522(5) 1.501(4)	3.408(2) 3.409(3) 3.354(3)	1.89(9) 0.0(3) 0.0(3)	1.89(9)

The Interwoven group also exhibits conventional stacking overlap in isolated anti-parallel dimer pairs. These are also related to one another by inversion and so have the same spatial arrangement as the stacks in Stacking Group 2. Likewise, the molecules in these structure have low intramolecular dihedral angles, approximately 2° to 16°.

4.2.3.3 Other

Offset overlap is also observed in structures outside the visual packing descriptions and the local geometry of these structures follows the same trends as observed in the other offset overlap structures.

For example, structures (23 – 25) and (25 – 25) (described in section 4.1.1.6, Figure 4.9) exhibit anti-parallel dimer pairs. These dimer pairs are related by an offset anti-parallel head-to-head overlap, as with the Interwoven group. As described previously, the head-to-head arrangement in these structures only proliferates along one side of the dimers, creating a diagonal stack or 'staircase', Figure 4.20.

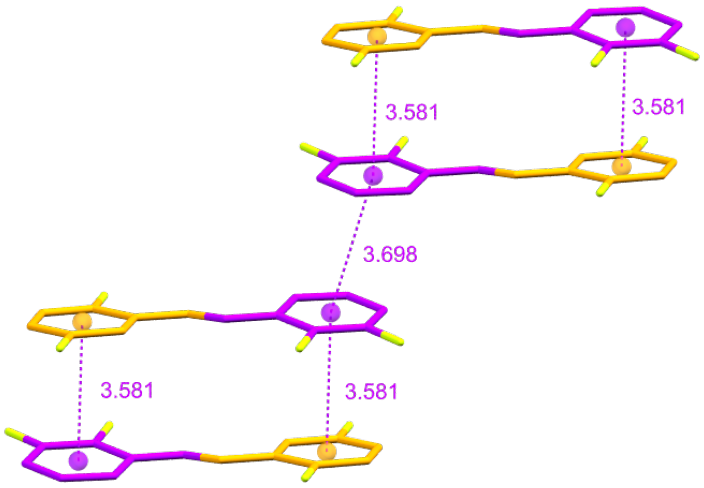

Figure 4.20 Structure (23 – 25) with centroid separation distances for the offset and stacked aromatic ring interactions, in units of Å.

Despite these topological differences, the geometric trends are the same. The overlapping molecules are related by inversion and so the intermolecular dihedral angle is zero for the head-to-head offset overlap and equal to the intramolecular dihedral angle for the stacked head-to-tail overlap, Table 12. (There is only one unique offset overlap in these structures as the offset motif only proliferates along one side.)

Table 4.11 Geometric data for structures (23 – 25) and (25 – 25). The H-t-T row shows the geometric parameters for the anti-parallel stacked dimer. The H-t-H row shows the geometric parameters for the anti-parallel head-to-head offset overlap.

Structure Code		**Centroid Separation /Å**	**Translation Average /Å**	**Plane Separation Average /Å**	**Inter-molecular Dihedral Angle /°**	**Intra-molecular Dihedral Angle /°**
23 – 25	H-t-T H-t-H	3.5808(9) 3.6984(14)	1.120(3) 1.405(3)	3.3965(12) 3.4211(18)	6.17(6) 0.00(8)	6.17(6)
25 – 25	H-t-T H-t-H	4.1084(7) 3.8067(9)	2.2527(18) 1.7469(17)	3.3577(14) 3.3822(12)	21.53(4) 0.000(3)	21.53(4)

Similarly, structure (234 – 26) does not conform to either of the offset overlap groups, Staggered Overlap or Interwoven, but does exhibit anti-parallel head-to-head offset overlap. Structure (234 – 26) is formed from alternating sheets of two distinct motifs and has two molecules in the asymmetric unit, each corresponding to the separate motifs. One sheet is formed from stacked molecules related by inversion, geometrically the same as Stacking Group 2, Figure 4.21.

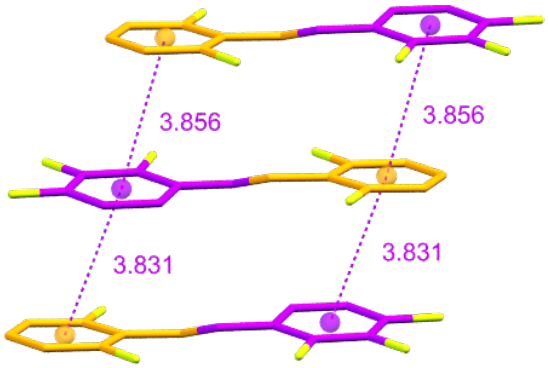

Figure 4.21 Stacking motif from structure (234 – 26), molecule "A" of the asymmetric unit. Centroid separation distances shown in units of Å.

The other alternating sheet is formed from offset overlap, which appears visually similar to the Staggered Overlap group. However, this motif is formed from head-to-head oriented anti-parallel overlapping rings in which the molecules are related by inversion, similar to the Interwoven structures, Figure 4.22.

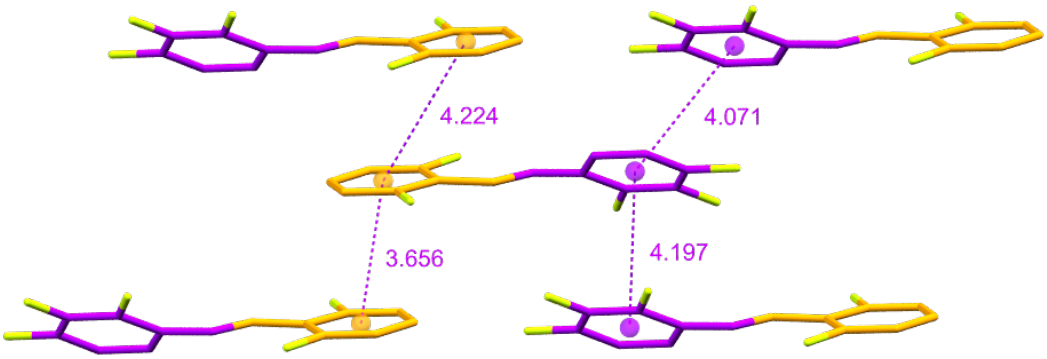

Figure 4.22 Offset overlap motif from structure (234 – 26), molecule "B" of the asymmetric unit. Centroid separation distances shown in units of Å.

Both motifs conform to the geometric trends observed in the other Offset Overlap structures and Stacking Group 2, Table 13.

Table 4.12 Geometric data for structure (234 – 26). Molecule A of the asymmetric unit exhibits the same stacking as Stacking Group 2 and so rows 1 and 2 refer to the different aniline-to-benzylidene overlaps between separate pairwise molecules.
The H-t-H rows of Molecule B show the geometric parameters for the anti-parallel head-to-head offset overlap, there are four unique overlap relationships for this motif. H-t-H A1 and A2 refer to aniline-aniline overlaps while H-t-H B1 and B2 refer to benzylidene-benzylidene overlaps.

Structure Code		**Centroid Separation /Å**	**Translation Average /Å**	**Plane Separation Average /Å**	**Inter-molecular Dihedral Angle /°**	**Intra-molecular Dihedral Angle /°**
234 – 26	1	3.8312(8)	1.657(2)	3.4531(12)	4.00(4)	4.00(4)
Molecule A	2	3.8560(8)	1.663(2)	3.4772(12)	4.00(4)	
234 – 26	H-t-H A1	4.0712(10)	2.325(2)	3.3420(15)	0.000(5)	33.99(4)
Molecule B	H-t-H A2	4.1971(10)	2.655(2)	3.2506(16)	0.0(2)	
	H-t-H B1	4.2241(11)	2.385(2)	3.4861(16)	0.00(8)	
	H-t-H B2	3.6555(11)	1.183(2)	3.4588(13)	0.000(5)	

4.2.3.4 Offset Overlap Summary

This group of structures highlights the importance of molecular orientation and how it is closely related to the local geometry.

The geometric relationships in this group are predicated on the presence of translational or inversion symmetry between the overlapping molecules. Through inversion or translation equivalent rings are parallel to one another, and so the orientation of the molecules determines the intermolecular dihedral angle. Where the phenyl rings are equivalent the dihedral angle must be zero and where they are non-equivalent they are related by the intramolecular dihedral angle.

These geometric trends are consistent for all offset overlaps, not just the Interwoven and Staggered Overlap groups. This is emphasised by the geometric analysis of uncategorised structures, such as (23 – 25), (25 – 25) and (234 – 26). Retrospectively, these rules also apply to Stacking Groups 1 and 2, in which molecules with aromatic ring interactions are related by translation or inversion.

4.2.4 Angled Overlap

As described in Section 4.1.1.4, the 'Angled Overlap' motif consists of two head-to-tail overlaps with each molecule angled over two neighbours, creating a saw-tooth pattern, Figure 4.23.

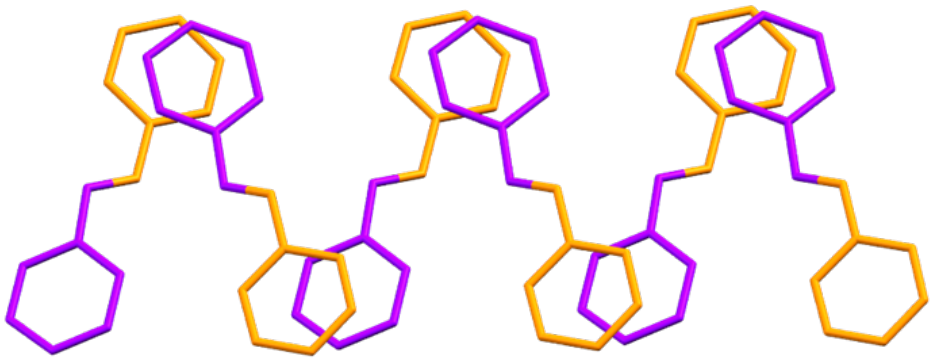

Figure 4.23 Archetype representation of the Angled Overlap motif.

This conformation of aromatic ring overlap is not strictly parallel or anti-parallel unlike interactions in other structures that have been studied. Whilst this conformation for aromatic ring interaction was unanticipated for this system there is a precedent in benzene:hexafluorobenzene co-crystals.

In these co-crystals the adjacent stacked molecules are both laterally displaced and mutually rotated[91]. This rotation possibly alleviates repulsion from close proximity of non-bonded atoms. Unlike most of the Angled Overlap structures, the rotated aromatic ring interactions in the co-crystal are formed between symmetry independent molecules (the benzene and hexafluorobenzene).

The angled overlap motif forms as a one-dimensional ribbon in the crystal structure. This motif does not greatly constrict the possible arrangements for the overall structure. As such there are a large variety of crystal structures observed in this packing group, as noted in the discussion of packing descriptions in Section 4.1.1.4.

Inspection of the aromatic stacking geometries in these structures also reveals variety in the local arrangement and the presence of additional overlap types. Therefore, the Angled Overlap structures have be separated into the sub-groups: Conventional Angled Overlap; Angled Overlap with Offset; Angled Overlap with Head-to-Tail Stacks and Angled Overlap with Twisted Stacks.

4.2.4.1 Conventional Angled Overlap

A full table of geometric data for the Conventional Angled Overlap group is presented in Appendix C, C.3.1.

In this sub-set of structures the angled overlap motif is the sole aromatic ring interaction observed. This is the most common arrangement for the Angled Overlap structures.

Two distinct local geometry types are observed in this group. In the first, there is one unique overlap relationship and corresponding centroid separation, for example in structure (234 – 4), Figure 4.24. In the second, there are two unique overlap relationships, for example structure (25 – 35), Table 14.

Table 4.13 Geometric data for structures (234 – 4) and (25 – 35). AO is an abbreviation for angled overlap. The labels AO 1 and AO 2 are used to distinguish the two unique overlap relationships in structure (25 – 35).

Structure Code		**Centroid Separation /Å**	**Translation Average /Å**	**Plane Separation Average /Å**	**Inter-molecular Dihedral Angle /°**	**Intra-molecular Dihedral Angle /°**
234 – 4	AO	3.7756(12)	1.651(3)	3.3955(19)	4.33(7)	32.59(7)
25 – 35	AO 1 AO 2	3.7603(13) 3.9246(13)	1.625(3) 1.985(3)	3.388(2) 3.386(2)	4.77(7) 4.77(7)	32.47(8)

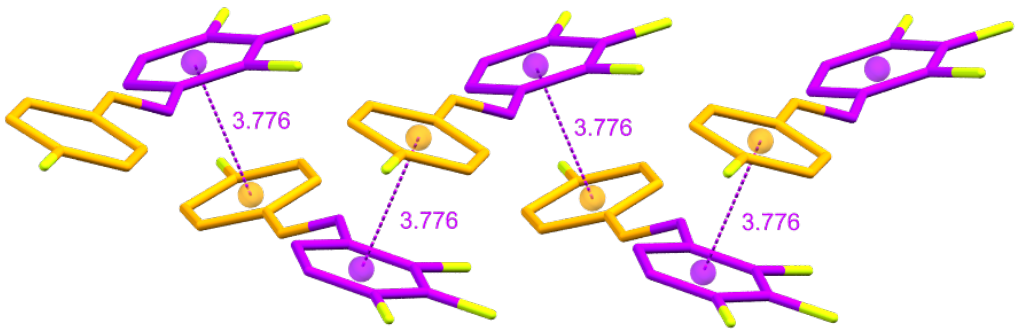

Figure 4.24 Angled overlap motif in structure (234 – 4) with centroid separation distances given in units of Å.

In both cases the overlapping molecules are related by rotation through a 2_1 screw axis. The screw axis runs between the layers of overlapping molecules, Figure 4.25. The only exception to this is the Z' = 2 structure (24 – 2356), in which the overlapping molecules are related by glide planes perpendicular to the plane of the molecules.

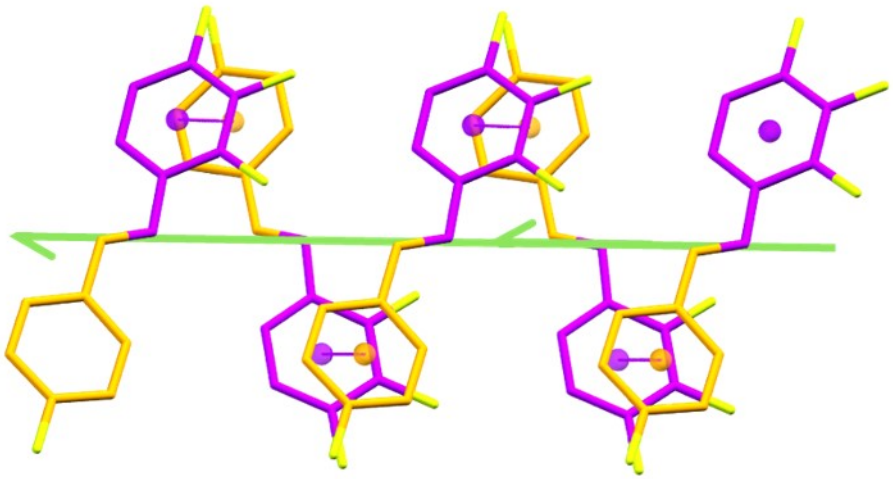

Figure 4.25 Position of the 2_1 screw axis between two layers of overlapping molecules in structure (234 – 4). The 2_1 screw axis is depicted here as a green arrow.

The intermolecular dihedral angles are low, in a similar range to other aromatic ring interactions studied here, approximately 0.5° - 5.5°. The intramolecular dihedral angles are in the approximate range 20° - 40°, with the exception of the Z' = 2 structure (24 – 2356), in which both molecules in the asymmetric unit have low intramolecular dihedral angles, 3.5(4)° and 4.0(4)°.

4.2.4.2 Angled Overlap with Offset

There is only one member in this sub-group, structure (25 – 245). Structures (2345 – 35) and (245 – 3) have a similar arrangement of molecules, however the 'offset' present is more similar to Grid geometries than the Staggered Overlap or Interwoven groups and as such there is not significant aromatic ring overlap.

Structure (25 – 245) follows the same geometric conventions of the previous angled overlap set with additional features from the presence of offset overlap.

Table 4.14 Geometric data for structure (25 – 245), AO is an abbreviation for angled overlap. The H-t-H row details the geometric data for the head-to-head offset overlap in this structure.

Structure Code		**Centroid Separation /Å**	**Translation Average /Å**	**Plane Separation Average /Å**	**Inter-molecular Dihedral Angle /°**	**Intra-molecular Dihedral Angle /°**
25 – 245	AO H-t-H	3.939(2) 3.604(3)	1.938(6) 1.370(6)	3.428(4) 3.334(4)	4.74(13) 0.0(3)	27.8(13)

Structure (25 – 245) has one unique angled overlap relationship and one unique offset overlap relationship, Table 15. As for the first sub-set, the overlapping molecules in the angled overlap motif are related by a 2_1 screw axis. The offset overlapping rings are arranged anti-parallel head-to-head, are related by an inversion centre and have an intermolecular dihedral angle equal to zero. This is consistent with the head-to-head aromatic interactions observed in the Interwoven group.

The angled overlap motif in this structure has an elongated centroid and plane separation compared to the staggered overlap and angled overlap relationships in other molecules.

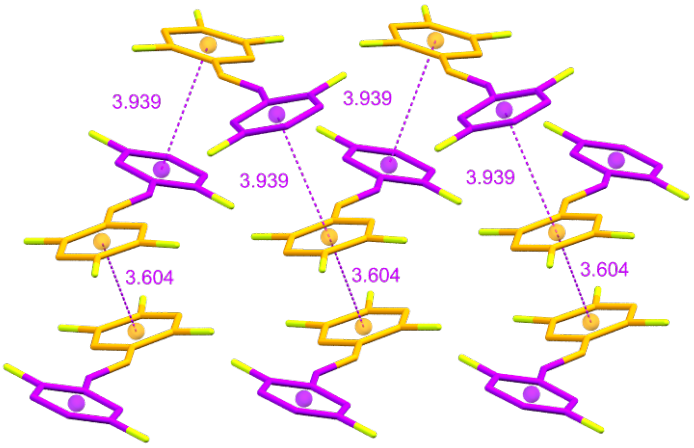

Figure 4.26 Angled overlap and offset overlap ring relationships present in structure (25 – 245). Centroid separation distances are given in units of Å.

4.2.4.3 Angled Overlap with Stacking Motifs

A full table of geometric data for the Angled Overlap with Stacking group is presented in Appendix C, C.3.3.

The addition of stacking motifs is quite common for the Angled Overlap group, they are present in 6 of the 17 structures. Of these, two structures exhibit conventional stacking motifs similar to Stacking Group 2, while the others adopt an unusual stacking arrangement tentatively described as twisted stacks.

In both cases the stacks do not proliferate along columns, instead they are present as dimer pairs – similar to the stacked molecules in the Interwoven group.

4.2.4.3.1 Head-to-Tail Stacks

Structures (234 – 245) and (2345 – 234) exhibited a more conventional head-to-tail stacking relationship in addition to the angled overlap motif.

Structure (2345 – 234) conforms to the conventions of both Conventional Angled Overlap and Stacking Group 2. The angled overlapping molecules are arranged head-to-tail and related by rotation through a 2_1 screw axis, whilst the stacked molecules are related by inversion and arranged anti-parallel head-to-tail with equal intermolecular and intramolecular dihedral angles, Table 16.

The local arrangement between stacks and angled overlap is similar for structure (234 – 245) however, the same symmetry relationships do not apply. Structure (234 – 245) has three molecules in the asymmetric unit and as such the overlapping molecules are symmetry independent.

Table 4.15 Geometric data for structure (2345 – 234), AO is an abbreviation for angled overlap. The H-t-T row details the geometric data for the anti-parallel head-to-tail stacking overlap.

Structure Code		**Centroid Separation /Å**	**Translation Average /Å**	**Plane Separation Average /Å**	**Inter-molecular Dihedral Angle /°**	**Intra-molecular Dihedral Angle /°**
2345 – 234	AO H-t-T	4.0355(9) 3.9220(9)	2.253(2) 1.596(3)	3.3477(17) 3.5216(15)	2.74(5) 23.45(5)	23.45(5)

The intermolecular angle between overlapping stacked molecules is unusually high in this structure. The centroid separations for both overlap motifs are also elongated compared to equivalent overlaps in related structural sub-sets. This suggests a less favourable aromatic ring interaction. This is rationalised by recognising the high degree of fluorination in these molecules – anti-parallel head-to-tail arrangement still leads to close proximity of fluorine atoms and the associated repulsion.

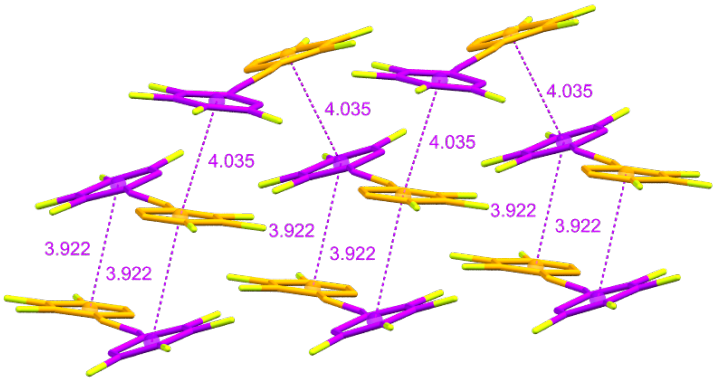

Figure 4.27 Angled overlap and stacking aromatic ring relationships present in structure (2345 – 234). Centroid separation distances are given in units of Å.

4.2.4.3.2 Twisted Stacks

The four other structures with angled overlap and stacking motifs adopted an unusual stacking arrangement. This arrangement is tentatively described as twisted stacking, Figure 4.28. Two of these structures exhibited anti-parallel head-to-head twisted stacks, while the other two exhibited anti-parallel head-to-tail twisted stacks.

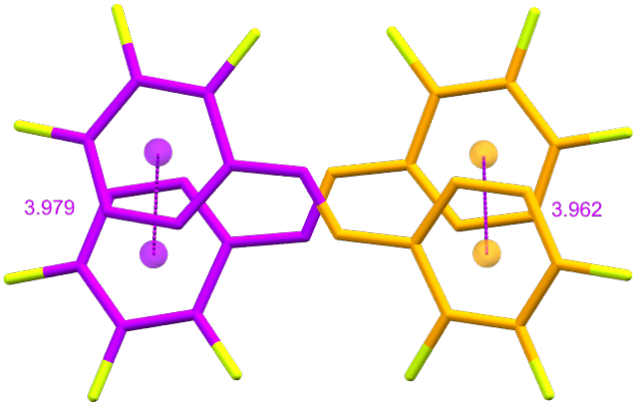

Figure 4.28 Anti-parallel head-to-head twisted stack in structure (234 – 234). Centroid separation distances are recorded in units of Å.

Both structures with head-to-head twisted stacks, (24 – 234) and (234 – 234), have two molecules in the asymmetric unit. Consequently, overlapping molecules are symmetry independent, and so both structures have two distinct twisted stack and angled overlap relationships, Table 17.

Table 4.16 Geometric data for structure (234 – 234), AO is an abbreviation for angled overlap. A and B distinguish between the two molecules in the asymmetric unit. AA AO therefore represents the angled overlap between the two A molecules. Rows AB H-t-H 1 and 2 detail the two distinct overlap relationships for the twisted stack.

Structure Code		**Centroid Separation /Å**	**Translation Average /Å**	**Plane Separation Average /Å**	**Inter-molecular Dihedral Angle /°**	**Intra-molecular Dihedral Angle /°**
234 – 234	AA AO	3.5820(8)	1.331(2)	3.3255(11)	1.20(5)	16.49(5)
Z’ = 2	AB H-t-H 1	3.9795(8)	1.796(2)	3.5511(13)	3.14(4)	19.13(5)
						16.49(5)
	AB H-t-H 2	3.9621(8)	1.859(2)	3.4977(13)	5.61(4)	19.13(5)
						16.49(5)
	BB AO	3.7011(8)	1.646(2)	3.3149(12)	2.02(4)	19.13(5)

The local arrangement of molecules in structure (234 – 234) is depicted in Figure 4.29, which highlights different packing motifs with coloured boxes around sections of the structure. This figure serves to represent both structure (234 – 234) and (24 – 234) as they are isostructural.

The two molecules in the asymmetric unit are labelled A and B. The angled overlap relationships in these structures are present between symmetry equivalent molecules related by rotation along a 2_1 screw axis. The upper purple box outlines the angled overlap motif for Molecule A equivalents, whilst the lower green box outlines the angled overlap motif for Molecule B equivalents. The central orange box outlines the head-to-head twisted stack relationships between the non-equivalent molecules A and B.

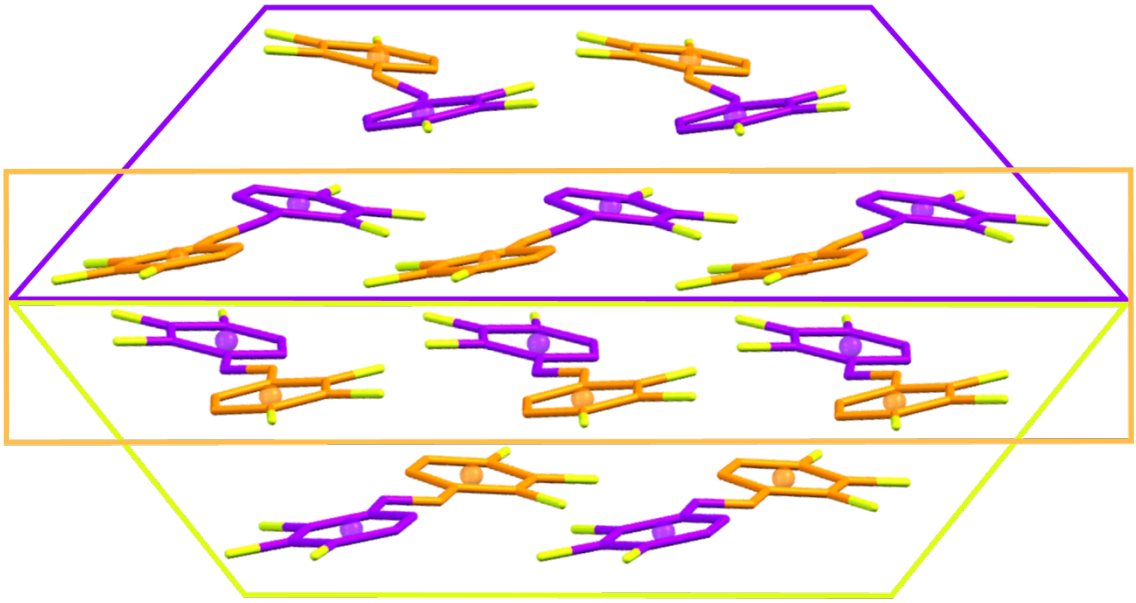

Figure 4.29 Structure (234 – 234) with highlighted sections to define different packing motifs. The upper purple and lower green sections show the two angled overlap motifs. The central orange box shows the twisted stack motif.

Both the twisted stacks and the angled overlap are arranged such that fluorine atoms are juxtaposed with hydrogen atoms of the interacting rings. Again, this is consistent with direct interaction models for substitute effects on aromatic stacking interactions. The juxtaposition of fluorine and hydrogen is also maintained in the two structures with head-to-tail twisted stacks.

One of these head-to-tail twisted stack structures, (245 – 0), has symmetry equivalent stacking molecules i.e. Z' = 1. In this structure the stacked molecules are related to one another by rotation through a 2_1 screw axis, which runs between the layers of the overlapping molecules – identical to the symmetry operator between angled overlap interactions. Consequently, the twisted stack motif could also be interpreted as a variant of angled overlap, in which the angled molecules are translated along the row, Figure 4.30.

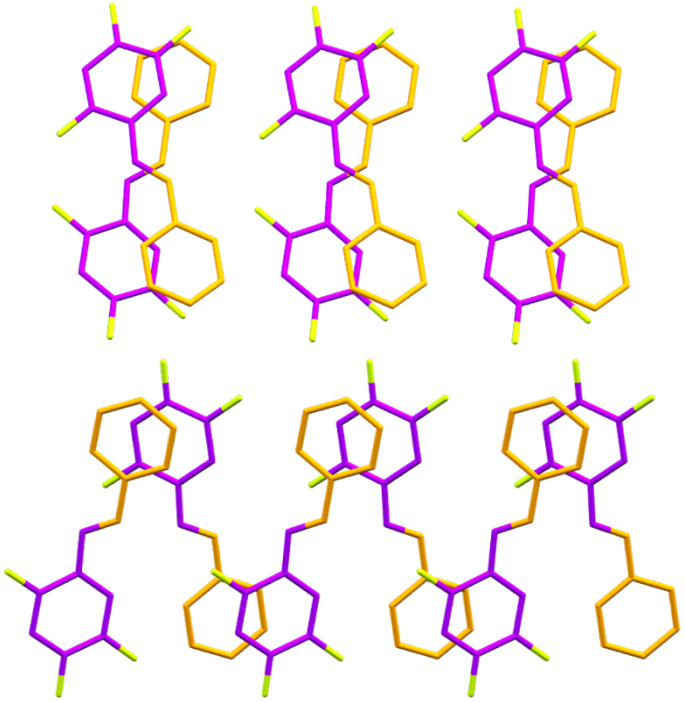

Figure 4.30 Visual comparison of the 'twisted stack' motif and angled overlap motif present in structure (245 – 0).

This interpretation is also substantiated by inspection of the geometric data. The intermolecular dihedral angles for head-to-tail angled overlap and head-to-tail 'twisted stack' overlap are equivalent for structure (245 – 0), Table 18.

Table 4.17 Geometric data for structure (245 – 0), AO is an abbreviation for angled overlap. The H-t-T row represents the geometric data for the twisted stack overlap.

Structure Code		**Centroid Separation /Å**	**Translation Average /Å**	**Plane Separation Average /Å**	**Inter-molecular Dihedral Angle /°**	**Intra-molecular Dihedral Angle /°**
245 – 0	AO	3.8091(13)	1.639(3)	3.4374(18)	3.01(7)	22.39(7)
	H-t-T	3.9356(12)	1.764(3)	3.5182(19)	3.01(7)	

In all examples of structures with angled overlap and twisted stacks the centroid separation and plane separation distances have been longer for the twisted stack interaction. This suggests a less favourable overlap relationship between the twisted stacks. It is therefore unclear why the molecular arrangement deviates from a conventional angled overlap structure. Especially if considering the twisted stack motif as a variant of angled overlap.

4.2.4.4 Other Angled Overlap

Angled overlap between aromatic rings is also present in structures which did not strictly conform to the Angled Overlap visual packing group. Structure (2345 – 0) is particularly interesting as it contains aromatic ring interactions between stacked molecules that have a local arrangement similar to angled overlap but are distinct from the twisted stack motif.

The stacked overlapping rings are rotated by approximately 10° around an axis defined by the shortest centroid to phenyl plane distance. This is similar to the rotation between rings in the angled overlap motif. Likewise, lateral displacement of the rings is also present in the overlap relationship. Structure (2345 – 0) has three molecules in its asymmetric unit so there are four unique overlap arrangements and values for this stacking motif, Figure 4.31 and Table 19.

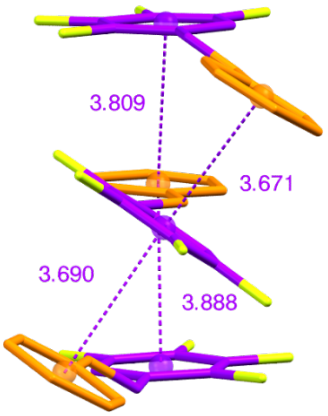

Figure 4.31 Stacking motif in the asymmetric unit of structure (2345 – 0), centroid separation distances given in units of Å.

Table 4.18 Geometric data for structure (2345 – 0), AO is an abbreviation for angled overlap. A, B and C distinguish between the three molecules in the asymmetric unit. AC AO 1 therefore represents the first angled overlap relationship between the A and C molecules. H-t-T rows detail the overlap relationship for the unusual stacking motif.

Structure Code		**Centroid Separation /Å**	**Translation Average /Å**	**Plane Separation Average /Å**	**Intermolecular Dihedral Angle /°**	**Intramolecular Dihedral Angle /°**
2345 – 0 Z' = 3	AC AO 1 AC AO 2	3.6729(10) 3.6848(10)	1.444(3) 1.540(3)	3.3772(14) 3.3480(14)	2.98(5) 3.29(6)	31.24(6) 31.62(6) 31.24(6) 31.62(6)

Structure Code		Centroid Separation /Å	Translation Average /Å	Plane Separation Average /Å	Inter-molecular Dihedral Angle /°	Intra-molecular Dihedral Angle /°
2345 – 0	AB H-t-T 1	3.8883(11)	1.730(3)	3.4820(15)	3.99(6)	31.24(6)
Z' = 3						31.22(6)
	AB H-t-T 2	3.6901(10)	1.312(3)	3.4430(14)	6.73(6)	31.24(6)
						31.22(6)
	BC H-t-T 1	3.6715(11)	1.380(3)	3.4023(14)	2.83(6)	31.22(6)
						31.62(6)
	BC H-t-T 2	3.8088(10)	1.590(3)	3.4606(15)	3.92(5)	31.22(6)
						31.62(6)

This structure also exhibits conventional angled overlap between the stacked asymmetric units, Table 19. The angled overlap motif connects the stacking units to one another, both those above and below and diagonally to non-adjacent neighbours, Figure 4.32.

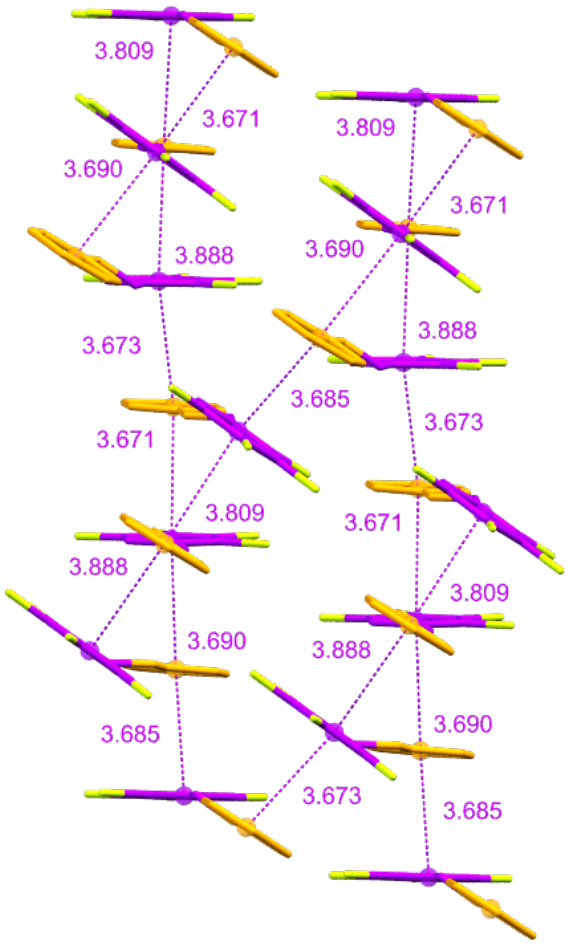

Figure 4.32 Arrangement of asymmetric units in structure (2345 – 0), stacking units interrelated by angled overlap motif. Centroid separation distances given in units of Å.

Unlike in the twisted stack motif, the rotated stack overlaps observed in this structure are comparable to the angled overlap relationships, in respect to topology. Whilst the angled overlap relationship still has a shorter plane separation distance, the centroid separation distances are very similar between the rotated stacks and angled overlap.

If all observed aromatic overlaps in this structure correspond to a stabilising interaction, then the arrangement of interconnected rotated stacks columns should result in a very energetically favourable and stable structure.

4.2.4.5 Angled Overlap Summary

Geometric analysis of the structures in this visual packing set differentiates them into several distinct sub-groups. In particular, the presence of additional overlap motifs has been used to define the groups.

Structures with more than one molecule in the asymmetric unit are very common for this packing type. The prevalence of aromatic ring interactions occurring between symmetry non-equivalent molecules makes it difficult to establish trends from the different geometric properties. This leads to complication in the relationships observed between intermolecular and intramolecular dihedral angles.

In this geometric analysis of overlaps between aromatic rings there is still a substantial reliance on the visual appearance of the arrangement to distinguish between related structures. Further analysis of these structures, calculating the spatial similarity between them should help to quantify these observed relationships.

4.2.5 Grid

The Grid structures have only elongated phenyl ring overlap between molecules with centroid separation distances that range from 4.481 Å to 4.845 Å and translation of the phenyl rings in the range 2.995 Å to 3.587 Å. This suggests the absence of significant aromatic ring interactions. Although, the plane separation distance is comparatively short for a select number of structures in this group, as low as 3.184 Å in the instance of structure (246 – 246).

The ‘near-overlap’ relationships in the Grid structures has been treated both as separated Head-to-Head stacks and extended Offset Overlap motifs. The aromatic rings are positioned poorly for either of these interactions, leading to the large centroid separation distances, Figure 4.33.

While favourable aromatic interactions do not seem feasible in these structures, the geometric properties still conform to the expected trends. Namely, the intermolecular dihedral angle is zero

for the head-to-head overlap and equivalent to the intramolecular dihedral angle for the head-to-tail overlap, Table 20. This is consistent with other structures in which the molecules are related by translation.

Table 4.19 Geometric data for structure (246 – 246). The H-t-H row represents overlap relationship for separated stacks while the H-t-T row represents the extended offset overlap.

Structure Code		**Centroid Separation /Å**	**Translation Average /Å**	**Plane Separation Average /Å**	**Intermolecular Dihedral Angle /°**	**Intramolecular Dihedral Angle /°**
246 – 246	H-t-H H-t-T	4.4806(3) 4.7959(9)	2.995(9) 3.587(8)	3.333(8) 3.184(10)	0.00(4) 2.39(5)	2.39(5)

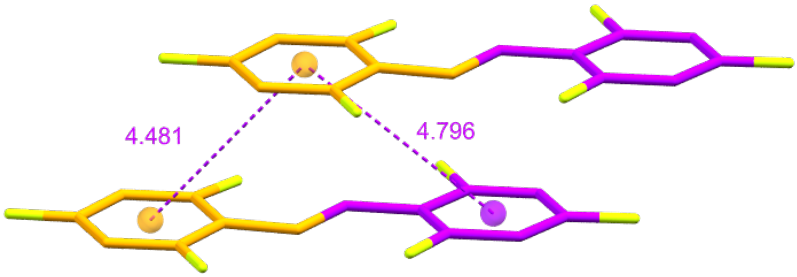

Figure 4.33 Local arrangement of molecules in the Grid structure (246 – 246). Centroid separation distances are given in units of Å.

Geometric data for the remainder of the Grid and related structures has been detailed in full in Appendix C, C.4.

4.2.6 Other

There are a number of structures not yet discussed which display interesting aromatic ring overlap arrangements but do not conform to any of the visual packing descriptions.

The geometric data for these remaining structures is presented in Appendix C, C.5.

Amongst these structures are a few that are particularly noteworthy:

1. Structures (0 – 0) and (23456 – 23456), which are at the two extremes of available fluorine substitution, do not display any viable aromatic ring interactions. Likewise, structure (4 – 246) does not display any overlap relationships between aromatic rings.

2. Structures (2345 – 23) and (23456 – 23) appear to adopt a stacking pattern similar to Stacking Group 3, in which the stacked molecules are related to one another by a 2_1 screw axis. However, in these structures the overlap relationships are unbalanced, such that one pair of overlapping rings is much closer than the other, Figure 4.34. The close overlap relationship has an associated centroid separation and lateral displacement comparable to other stacked relationships, however, the far relationship has an extended translation distance suggesting an absence of significant interaction between this second pair of aromatic rings, Table 21.

Table 4.20 Geometric data for structure (2345 – 23). H-t-T 1 represents the close stacking overlap, while H-t-T 2 represents the far stacking overlap.

Structure Code		**Centroid Separation /Å**	**Translation Average /Å**	**Plane Separation Average /Å**	**Intermolecular Dihedral Angle /°**	**Intramolecular Dihedral Angle /°**
2345 – 23	H-t-T 1 H-t-T 2	3.6531(10) 4.5805(12)	1.543(3) 3.339(2)	3.3097(15) 3.134(3)	3.34(5) 3.34(5)	43.33(6)

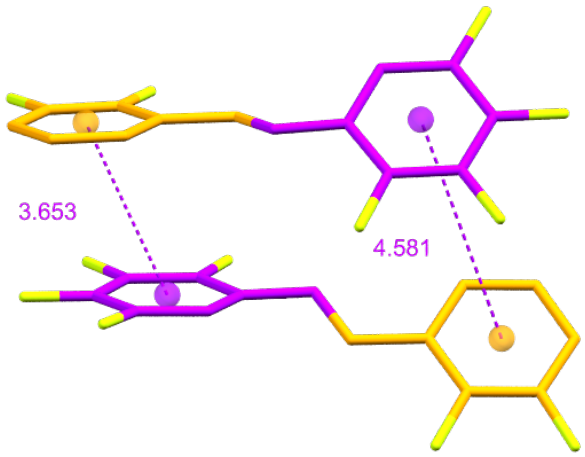

Figure 4.34 Unbalanced stacking relationship in structure (2345 – 23). Centroid separation distances are given in units of Å.

3. Structures (256 – 2356) and (2356 – 2356) both exhibit disorder in the azomethine linker between the fluorinated rings. This somewhat complicates the analysis of their local arrangement in respect to head-to-head versus head-to-tail overlaps. Despite this disorder, the intermolecular angles between overlapping molecules suggest that the aromatic interactions are head-to-head, this interpretation is the one presented, Table 22. Both of these structures exhibit offset overlap accompanied by a large intramolecular dihedral angle. This results in helical constructs propagating in one-dimensional tapes, Figure 4.35.

Table 4.21 Geometric data for structure (256 – 2356). H-t-H 1 and 2 describe the two offset overlap relationships in the helical motif.

Structure Code		**Centroid Separation /Å**	**Translation Average /Å**	**Plane Separation Average /Å**	**Inter-molecular Dihedral Angle /°**	**Intra-molecular Dihedral Angle /°**
256 – 2356	H-t-H 1 H-t-H 2	3.572(3) 3.574(3)	1.278(6) 1.277(6)	3.336(4) 3.336(3)	0.0(6) 0.00(5)	65.51(12)

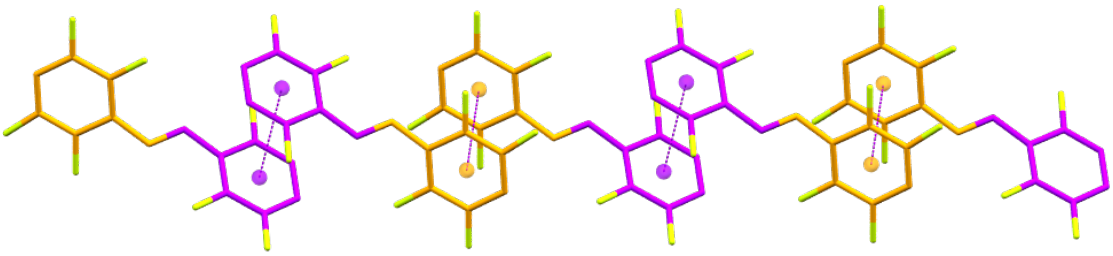

Figure 4.35 Helical motif of offset overlapping molecules in structure (256 – 2356).

The arrangement of the aromatic rings in these structures leads to close proximity of the fluorine atoms of opposite rings and the associated repulsive effects. This juxtaposition is inevitable in any overlap between the rings, be it head-to-head or head-to-tail, due to the substitution pattern and high degree of fluorination. One might expect an arrangement similar to that of structure (23456 – 23456), in which overlap of the rings is absent. It is curious, therefore, that the spatial arrangement of the molecules strongly indicates an energetically favourable interaction between the rings; the centroid and plane separation distances are both short compared to other offset overlap motifs.

As previously stated, the presence of disorder in the azomethine linker complicates analysis of these structures. Particularly, many energetic calculations are not possible with a disordered structural model.

4. Structure (2356 – 26) exhibits a unique ‘perpendicular’ aromatic ring overlap. In this ‘perpendicular’ interaction the aromatic rings are rotated by approximately 90° around an axis defined by the shortest centroid to phenyl plane distance, maintaining the low intermolecular dihedral angle between the planes of the rings, Figure 4.36.

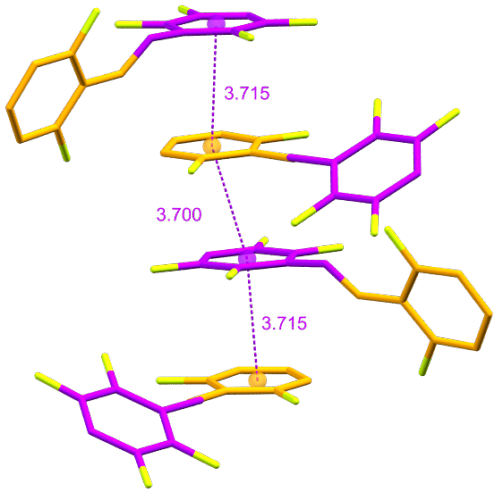

Figure 4.36 'Perpendicular' aromatic ring overlap in structure (2356 – 26). Centroid separation distances are given in units of Å.

Structure (2356 – 26) also exhibits head-to-tail stacking overlap that only occurs in one pair of aromatic rings in a molecular pair due to the difference in intramolecular dihedral angle between the two molecules in the asymmetric unit, Table 23. Anti-parallel head-to-head offset overlap is also present in this structure.

Table 4.22 Geometric data for structure (2356 – 26). A and B are used to distinguish between the two molecules in the asymmetric unit. AB H-t-T ⊥ represents the 'perpendicular' overlap between molecules A and B. AA H-t-H and BB H-t-H represent the anti-parallel head-to-head offset overlap relationships.

Structure Code		**Centroid Separation /Å**	**Translation Average /Å**	**Plane Separation Average /Å**	**Inter-molecular Dihedral Angle /°**	**Intra-molecular Dihedral Angle /°**
2356 – 26	AB H-t-T	3.7003(10)	1.425(3)	3.4139(14)	3.31(6)	67.31(6)
Z' = 2						31.62(6)
	AB H-t-T ⊥	3.7147(10)	0.978(3)	3.5824(13)	3.40(6)	67.31(6)
						31.62(6)
	AA H-t-H	3.7492(14)	1.426(3)	3.4673(16)	0.0(2)	67.31(6)
	BB H-t-H	3.9673(13)	2.112(3)	3.3586(18)	0.00(6)	31.62(6)

These structures in particular demonstrate the diversity of different packing arrangements observed across the fluoroaniline structure library. Whilst unique, there are still similarities between the aromatic ring interactions presented here and the motifs presented in the wider library. For instance, the 'perpendicular' overlap in structure (2356 – 26) is comparable to the angled overlaps observed in other structures, although the rotation is much larger.

All of the structures presented add to the overall picture of trends in the local geometry between aromatic rings.

4.2.7 Conclusion of Geometric Analysis

As previously stated in the introduction to this discussion of geometry, the structural groups identified by the comparison of geometric descriptors loosely correlate with visual packing descriptions – linking the larger topology to the local arrangement of aromatic ring interaction.

It should be acknowledged that some of the visual packing description groups are associated with more than one form of aromatic ring interaction. For example, the Interwoven structures contain both anti-parallel head-to-head offset overlap and dimer pairs exhibiting a head-to-tail stacking arrangement consistent with Stacking Group 2. In this geometric analysis the focus is on the local spatial arrangement of the different overlap types and how the geometric parameters might reflect energetic contributions arising from potential aromatic ring interactions. Although, some insight into the relationship between molecular conformation and the overall crystal assembly will also be gained.

The principal overlap arrangements identified in this analysis were as follows:

1. **Parallel Head-to-Head Stacking**, such as Stacking Group 1.

2. **Anti-parallel Head-to-Tail Stacking through inversion**, such as Stacking Group 2, Interwoven group and other variants, for example structure (234 – 26).

3. **Anti-parallel Head-to-Tail Stacking through a 2_1 screw axis**, such as Stacking Group 3.

4. **Anti-parallel Head-to-Tail Stacking between symmetry independent molecules**, such as Stacking Group 4 and other Z' = 2 structures.

5. **Parallel Head-to-Tail Offset Overlap**, such as the Staggered Overlap group.

6. **Anti-parallel Head-to-Head Offset Overlap**, such as the Interwoven group, Angled Overlap with Offset (25 – 245) and other variants, for example structures (234 – 26) and (256 – 2356).

7. **Angled Head-to-Tail Overlap**, such as the Angled Overlap group and other variants with rotated overlapping rings, such as structures (2345 – 0) and (2356 – 26).

8. ***Angled Head-to-Head Overlap***, only observed in the Twisted Stacks in Angled Overlap group and may not relate to an aromatic ring interaction.

   The Grid structures also exhibited aromatic ring arrangements which could be described as parallel head-to-head and parallel head-to-tail offset overlap, however these elongated conformations are unlikely to relate to an aromatic ring interaction.

Table 4.23 is a matrix view of the structural library which shows the distribution of different overlap types. Structures have been presented according to the overlap relationships exhibited regardless of the structures' categorisation in the visual packing descriptions or geometric groups. In the instance of a structure exhibiting more than one overlap type the structure has been coloured according to the key for both of those overlap relationships.

The Overlap Matrix highlights the prevalence of anti-parallel head-to-head offset overlap, which is present in the Interwoven structures as well as many of the previously uncategorised structures. The matrix also displays and distinguishes between different variations of Head-to-Tail stacking arrangements and reveals that, whilst the 2_1 screw axis head-to-tail relationship is the most common, the inversion related head-to-tail stacks appear to be the only stacking relationship compatible with other overlap types within the same structure.

Additionally, this matrix shows that the head-to-tail stacking structures of the complementary set exhibit a variety of head-to-tail overlap arrangements rather than one common motif.

Of all the overlap types identified, the different stacking orientations remain the most pertinent to traditional discussions of "π – π stacking" interactions – aromatic ring interactions. The Head-to-Tail stacking arrangements are the most consistent with the expected behaviour of aromatic ring stacking and the various stacking motifs are the most commonly observed overlap type in the structural library.

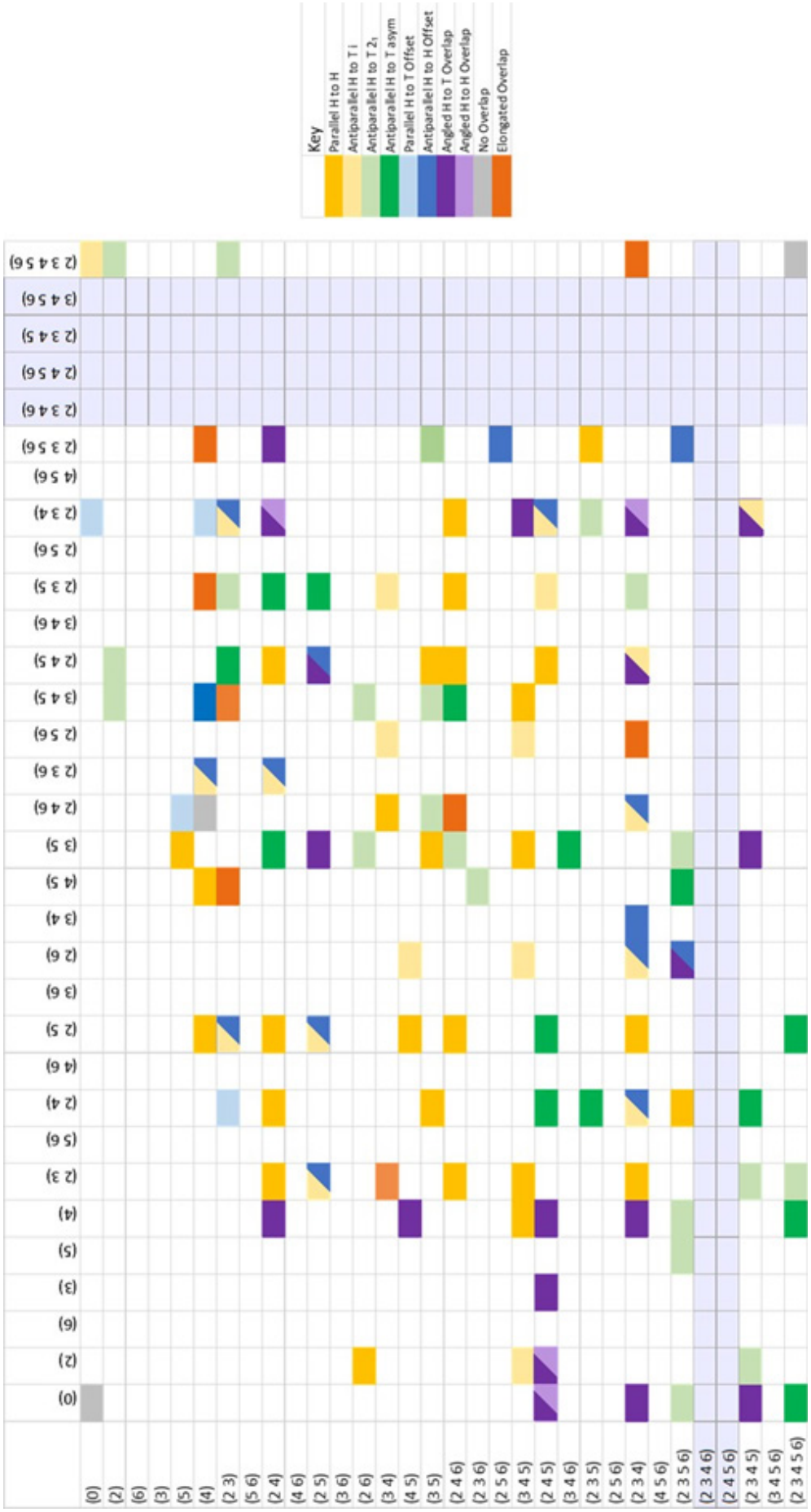

Table 4.23 Overlap Matrix: depiction of the different overlap types associated with the various structures within the structural library. Key on the right defines the colour for each overlap type.

4.2.7.1 Head-to-Head and Head-to-Tail Stacking

As previously discussed, the anti-parallel head-to-tail stacking motifs are the most apparent configuration for favourable overlap of fluorinated aromatic rings. This configuration promotes the direct electrostatic attraction between the local C – F and C – H dipoles of opposing rings by juxtaposing fluorine and hydrogen atoms. Different substitution patterns will change the favourability of the head-to-tail orientation.

For example, the head-to-tail arrangement of structure (34 – 235) brings the F and H atoms of opposing rings into close proximity with one another, however, there is an unavoidable juxtaposition of the two F atoms in the 3 position of the benzylidene and aniline rings, Figure 4.37. The direct substituent interaction model for aromatic stacking, described in Section 1.2.2.3, suggests that this juxtaposition will reduce the energetic stabilisation due to repulsion, although the overall energetic contribution of the aromatic ring interaction is still expected to be favourable.

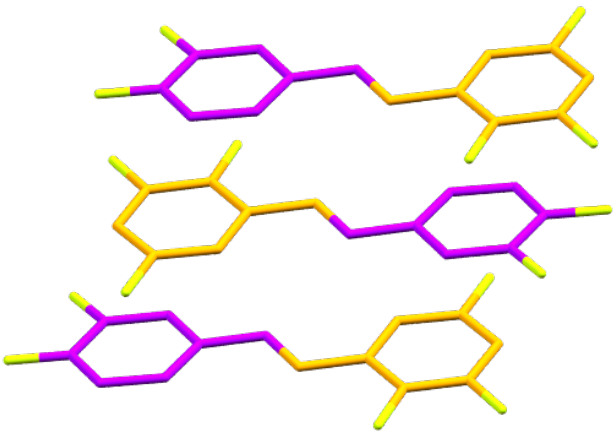

Figure 4.37 Head-to-tail stacking motif in structure (34 – 235).

The parallel head-to-head stacks are more difficult to rationalise. In these stacks the substituted fluorine atoms are necessarily juxtaposed with their equivalents on the opposing ring. Therefore, a large repulsion is expected due to their close proximity.

Lateral translation of the rings may slightly alleviate the repulsive forces, as will a longer plane separation distance. Comparison of the average values for translation and plane separation between the different stacking groups reveals that Head-to-Head structures (Stacking Group 1) have the largest average plane separation and a long average translation distance compared to the data set as a whole, however, these values are not significantly higher than for the other head-to-tail stacking groups, Table 4.24.

Table 4.24 Comparison of average lateral translation and plane separation for stacking groups.

Stacking Group	**Average Translation with standard deviation / Å**	**Average Plane Separation with standard deviation / Å**
Stacking Group 1	1.503 ± 0.100	3.419 ± 0.038
Stacking Group 2	1.264 ± 0.127	3.411 ± 0.042
Stacking Group 3	1.554 ± 0.326	3.384 ± 0.039
Stacking Group 4	1.443 ± 0.182	3.404 ± 0.059
Overall Stacking	1.469 ± 0.236	3.397 ± 0.051

Comparison of average translation and plane separation across the different stacking groups also reveals a trend in the Head-to-Tail structures. For these structures, translation and plane separation are inversely proportional to one another. Stacking Group 2 has the shortest translation distance and the largest plane separation while Stacking Group 3 has the longest translation and the smallest plane separation, Stacking Group 4 lies between these two. This trend is consistent with previous discussion of the relationship between lateral displacement and plane separation, Section 4.2.1.3. However, the Head-to-Head structures (Stacking Group 1) do not conform to the pattern – they exhibit a larger plane separation than expected given the lateral translation. This observation suggests the introduction of additional plane separation in these structures as a result of increased repulsion.

Geometric analysis of head-to-head and head-to-tail overlap stacking also reveals a consistent relationship between orientation of the stacks and the intermolecular dihedral angle. Symmetry equivalent head-to-head stacking molecules are related to one another by translation. Therefore, the intermolecular dihedral angle between them is equal to zero. While all of the aromatic ring overlaps have a low intermolecular dihedral angle, the head-to-head relationships are the only interactions between truly planar rings. This suggests an enhanced attractive dispersive interaction between the aromatic rings in these structures, though these dispersive forces might otherwise be mitigated by the introduction of greater lateral translation and plane separation.

Despite this beneficial planar arrangement, the geometric analysis of the head-to-head stacks still indicates that, while they are common in the structural library, they are not as energetically favourable as their head-to-tail counterparts. However, plane separation and translation distances only describe the local topology of the head-to-head stacking structures, there are likely to be many other factors directing the arrangement of the molecules into these types of stacks.

For instance, the planar intermolecular stacking may promote better close-packing in the overall structure.

Additionally, the head-to-head stack arrangement may be a more kinetically accessible structure during crystallisation. A head-to-head stacking conformation is not an unreasonable close-packing arrangement in the absence of significant repulsion, or a sufficiently attractive electrostatic interaction offered by another conformation.

The specific fluorine substitution pattern will affect the potential attraction offered by a head-to-tail conformation as well as the potential repulsion arising from juxtaposition of like-atoms. Energetic calculations are necessary to disentangle the different contributions of electrostatic attraction and repulsion and how they are modulated by fluorine substitution, this is explored in Section 5.2.

4.2.7.2 Evidence for Direct Substituent Effects

In this work, discussion about the influence of fluorine substitution on aromatic ring interactions is informed by the direct substituent interaction model. While there is an increasingly large body of computational data to support the direct substituent interaction model[88,114–116,202,203], the π-polarisation model is still widespread in the literature. Both models are outlined in more detail in Section 1.2.2.

Controversy remains between the two models as it is difficult to discern the nature of the electrostatic forces based on experimental evidence – whether the attraction arises from direct dipole interactions or resonance through the aromatic system. There remains a reliance on computational data.

Both models would suggest a disinclination for structures to adopt head-to-head stacking arrangements in preference for head-to-tail stacks, in which either aromatic donor-acceptor interactions are possible or an increased number of the direct interactions between C – H and C – F dipoles. In the π-polarisation model the aromatic donor-acceptor interactions would be most favourable in molecules with a large difference in the degree of fluorination between rings. For example structures (23456 – 0), (2345 – 2) and (2 – 23456) all conform to the predicted head-to-tail stacking orientation. However, these observations are also consistent with the direct substituent interaction model, as head-to-tail orientation of these molecules maximises the direct electrostatic attraction between the local C – F and C – H dipoles of the opposite ring due to their substitution pattern.

Despite the difficulties of obtaining insightful experimental evidence, observations of aromatic ring interactions in this structural library suggest a greater importance for specific substitution patterns rather than simply the degree of fluorination. For instance, the structures exhibiting anti-parallel head-to-head offset overlap provide support for the direct substituent interaction model. All head-to-head conformations of the aromatic rings will be similarly or less electrostatically favourable than head-to-tail conformations following the π-polarisation/resonance model. However, anti-parallel head-to-head overlap can still be more electrostatically attractive than a head-to-tail overlap following the direct substituent interaction model, provided that this conformation juxtaposes F and H atoms of the interacting rings.

Structure (234 – 34) is a prime example of this behaviour. Anti-parallel head-to-head offset of the aniline rings aligns fluorine substituents in the 2 and 3 positions with hydrogen in the 6 and 5 positions on the overlapping ring. Simultaneously, fluorine substituents in the *para* (4) position are distanced from one another in a manner which would not be possible in a stacked head-to-tail conformation as both rings have a *para* fluorine. This arrangement of the overlapping molecules provides better direct electrostatic attraction between the local C – F and C – H dipoles than a head-to-tail stack. The head-to-head conformation cannot be benefitting from any electrostatic interactions between aromatic electron-rich and electron-poor regions as the overall electrostatic potential of the aniline rings will be the same. Energetic calculations are required to confirm the assumption that this overlap interaction is attractive, Section 5.2.2.2.

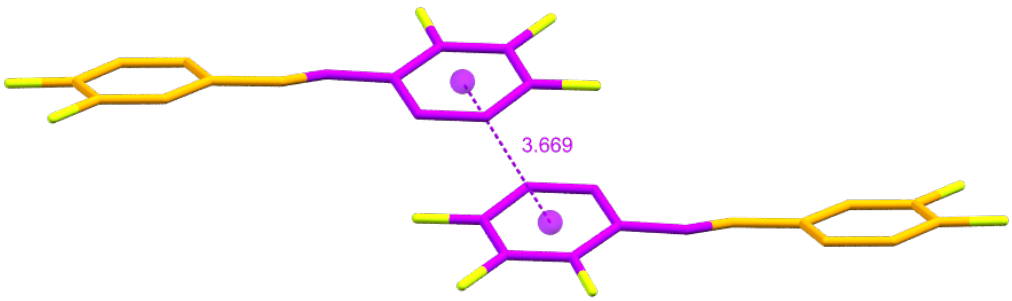

Figure 4.38 Anti-parallel head-to-head offset overlap motif in structure (234 – 34). Centroid separation distances are given in units of Å.

The π-polarisation/resonance model is not without merit and the increased fluorination of the aromatic rings will certainly modify the aromatic π-system and the electrostatic potential of aromatic regions. However, this is not the primary force directing the effect of fluorine substitution on aromatic ring interactions. There is more evidence here, and in other studies, to support the importance of direct substitution interactions, which are sensitive to the specific pattern of substitution not merely the number of electron-withdrawing substituents.

4.2.7.3 Intramolecular Dihedral Angles

Geometric analysis of the aromatic ring relationships also included measurement of the intramolecular dihedral angles for interacting molecules. It was found that the fluorinated trans-N-benzylideneanilines often resisted planarity and low intramolecular dihedral angles. As previously stated, in Section 4.2.1.4, a low intramolecular dihedral angle generally indicates that the energetic stabilisation from electron conjugation through the π-system outweighs the repulsion of non-bonded atoms in close proximity. However, the presence of the strongly electronegative fluorine reduces the availability of electrons for delocalisation. The propensity for of fluorinated trans-N-benzylideneaniline to adopt a non-planar conformation is easily rationalised by considering the decrease in energetic stabilisation afforded by planarity in these molecules.

In analysis of the unsubstituted trans-N-benzylideneaniline, structure (0 – 0), in this study an intramolecular angle of 62.63(5)° was recorded. Only four structures had larger dihedral angles: structures (256 – 2356), (2356 – 26), (2356 – 2356) and (23456 – 23456) with intramolecular dihedral angles of 65.51(12)°, 67.31(6)°, 70.58(5)° and 79.5(3)°, respectively. All of these structures were uncategorised in the visual packing descriptions and are described geometrically in Section 4.2.6 “Other”. These structures are also heavily substituted, and so, the large intramolecular angle can be reasonably attributed to repulsion from the numerous fluorine atoms in close proximity.

There is a large range of intramolecular dihedral angles observed in the structural library, and as well as these ‘high repulsion’ strained systems there are examples of nearly planar molecules. Rather than the stabilising effect of electron conjugation, low dihedral angles in these molecules might be attributed to favourable packing motifs. In particular, very low intramolecular dihedral angles are observed in structures with inversion centres relating overlapping molecules to one another, with dihedral angles in the range 0.80(6) to 16.10(13) °. A low dihedral angle may also suggest the presence of favourable atom-to-atom intermolecular interactions between adjacent molecules, which are only possible in those particular molecular conformations.

4.2.7.4 Concluding Remarks

Geometric analysis of the aromatic ring interactions has identified eight distinct overlap relationships. The plane separation and lateral translation distances indicate that these are predominately attractive aromatic interactions. Although, there are some exceptional cases; overlap interactions in the Grid structures would appear to be negligible as they only exhibit

elongated configurations, and aromatic overlap is absent in the un-fluorinated and per-fluorinated structures, (0 – 0) and (23456 – 23456).

The geometric data suggests a number of conclusions concerning the repulsion of parallel head-to-head stacks, which appear to be energetically suboptimal arrangements, and concerning the importance of direct substituent interactions in electrostatic attraction between overlapping molecules. These conclusions need to be substantiated by energetic calculations but the geometric data alone is strongly indicative.

This analysis has successfully established a number of conventions for various aromatic ring overlap relationships. For example, the head-to-tail overlap relationships related by inversion or translation will have equivalent intermolecular and intramolecular dihedral angles. Additionally, the analysis identified relationships between the local geometry of aromatic rings and the visually determined packing groups, this is apparent in the similarity between the Visual Packing Description Matrix and the Overlap Matrix.

However, geometric analysis has not been able to draw a strong association between the fluorine substitution pattern of the aromatic rings and the corresponding local structural arrangement, expressed by overlap types. The importance of specific substitution patterns is highlighted by this work, Section 4.2.7.2, but the comparison of substitution pattern to crystal packing is limited to the local arrangement.

A more refined comparison of structural similarity is required to draw more complex associations between structure and substitution pattern – one that can account for the structural arrangement of the overall crystal structure.

4.3 Structural Similarity

In this section, spatial analysis is employed to investigate the similarity of crystal structures. This analysis builds upon the geometric results, using the identified aromatic overlap types as a starting point. Spatial analysis compares the arrangement of the molecules beyond the local overlap arrangement. The structures are compared for common motifs such as end-to-end chains/tapes and side-to-side ribbons. These motifs describe the arrangement of molecules and how they propagate through the crystal structure.

4.3.1 Structural Motifs

Chain and sheet motifs are used in Kitaigorodskii's Aufbau principle to describe the conceptual construction of a crystal structure in stages, as discussed in Section 1.1.1. Identification of these

molecular motifs gives valuable insight into the formation of the crystal structures. Consequently, identifying motifs common between different crystal structures can indicate common directing influences in the assembly of these structures.

If structural similarity is also accompanied by similarity in fluorine substitution pattern one can begin to infer a connection between the specific positioning of fluorine and its influence on the crystal formation.

The degree of similarity between structures is primarily defined by the dimensionality of the shared motifs. Chains, ribbons and column stacks are 1-dimensional (1D), they propagate along one dimension, while sheets are 2-dimensional (2D). Isostructuralism is the highest degree of similarity; isostructural crystals share the same overall structure. It is also possible for crystals to exhibit 3-dimensional (3D) similarity but not be strictly isostructural, an example of this behaviour is described in Section 4.3.2.2.

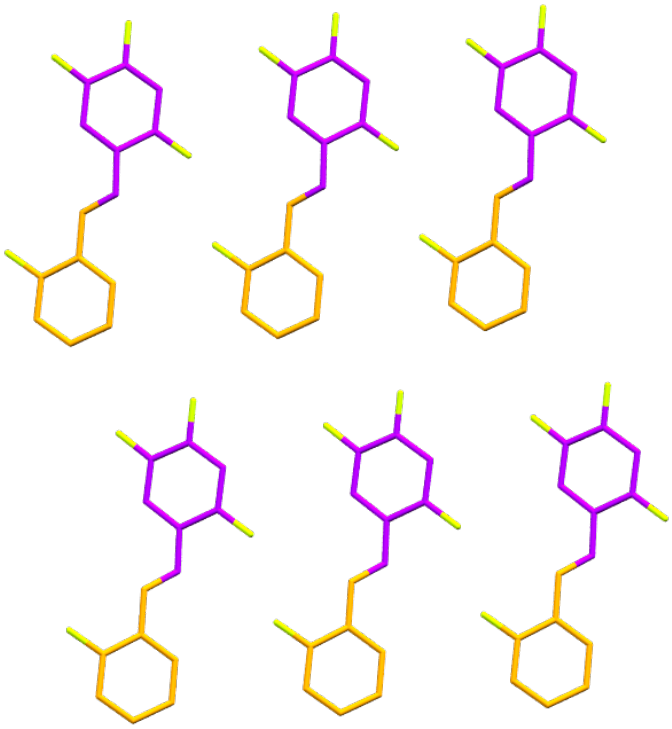

Figure 4.39 Sheet motif observed in the Angled Overlap structure (245 – 2). (A component of Angled Overlap Motif C – coordinate files can be found in the appendices).

The structures have been analysed in sub-groups based on the aromatic overlap types they exhibit. For this analysis the Grid structures have been largely excluded as they do not exhibit significant aromatic overlap.

The XPac analysis method has been used to analyse the structural similarity in this study.

4.3.2 XPac Analysis Method

The XPac program is designed to evaluate the similarity between molecular crystal structures of related molecules. The XPac method identifies "supramolecular constructs" common between the different structures. These are sub-components of the complete crystal structure, also referred to as motifs, which describe the crystal assembly. Supramolecular constructs are considered similar, and therefore comparable, if they consist of molecules of a similar structure assembled in the same arrangement.

For the purposes of similarity analysis, crystal structures are conceptualised as a central molecule with a shell of nearest neighbours forming a cluster. The molecules in the shell are generated by the application of observed symmetry operators to the central molecule (for Z' = 1 structures).

Similar cluster sub-units are then identified; these consist of the central molecule and a number of surrounding molecules in the shell. A supramolecular construct exists if all of the corresponding sub-units for a particular motif are similar.

The similarity is evaluated by comparing the angular parameters, δ_a and δ_p, of the supramolecular construct in the two similar structures where δ_a is the angular deviation and δ_p is the inter-planar angular deviation. An overall dissimilarity index, *X*, is calculated following the Equation 4.1.

Equation 4.1 XPac calculation for structural dissimilarity, *X*.

$$X = \Sigma(\delta_{a,i}{}^2 + \delta_{p,i}{}^2)^{\frac{1}{2}}$$

A stretch parameter, δ_d, is also reported, which describes the molecular centroid distance deviation. This parameter is not included in the overall dissimilarity index following the principle that the similarity of two arrangements is defined primarily by the angular relationships rather than the distance between objects[204].

A more thorough description of the XPac methodology is given in associated articles and case-studies from the program creators[204,205].

4.3.2.1 Interpreting XPac Results

XPac analysis on a family of molecules generates a list of pairwise comparisons describing the similarity of one structure to another. The crystal structures in this study have been analysed for similarity within subsets based on the overlap type identified in the geometric analysis section. This reduced the number of pairwise comparisons to be analysed based on pre-established distinctions between the structures.

There is no standard output file for XPac results, however, the program reports a number of parameters for each identified supramolecular construct. An example of a 3D isostructural relationship is presented in Table 4.25.

Table 4.25 Similarity parameters for the isostructural relationship between structures (2356 – 0) and (2356 – 4).

2356 – 0			**2356 – 4**
Dissimilarity Index: X = 3.0			
Stretch Parameter: D = 0.18 Å			
n = 18 neighbours			p = 14 points
Delta [a] = 1.2°			Delta [p] = 2.6°
Corresponding Lattice Vectors			
2356 – 0:			
1.00	0.00	0.00	= 5.967 Å
0.00	1.00	0.00	= 7.526 Å
0.00	0.00	1.00	= 23.622 Å
= 90.00°, 92.85°, 90.00°			
2356 – 4:			
-1.00	0.00	0.00	= 5.952 Å
0.00	1.00	0.00	= 7.387 Å
0.00	0.00	-1.00	= 24.359 Å
= 90.00°, 93.67°, 90.00°			

The dissimilarity index, *X,* and stretch parameter, δ_d, are described in the XPac analysis method. The number of neighbours refers to the number of molecules surrounding the central molecule – forming the supramolecular construct. The number of points refers to the atoms selected to represent the shared component of the related molecules. In this instance 14 atoms have been selected to represent the framework for the fluoroanilines; the 13 carbon atoms and the nitrogen, the fluorine and hydrogen substituents have been excluded as they will vary from molecule to molecule within the set. The values for delta[a] and delta[p] refer to the angular deviation, δ_a, and the inter-planar angular deviation, δ_p, respectively, as described in the XPac analysis method. The lattice vectors associated with the supramolecular construct in each structure are also reported.

The similarity parameters for the supramolecular constructs have been recorded for all pairwise comparisons between structures in the subsets (with the exception of 0D relationships), this data is presented in the appendices.

Groups of isostructural crystal structures can be easily identified but in such large sets of related structures it is difficult to visualise the 1D and 2D similarities and how these interconnect across each subset. A novel strategy for representing the similarity is required.

4.3.2.2 Similarity Diagrams

Clear presentation of the interconnectivity and shared similarity between structures is as important to understanding the similarity relationships as the quantitative results of the XPac analysis. For this purpose, similarity diagrams have been created for each overlap sub-set; these present the network of similar structures.

To represent the interconnected relationships between the structures, some aspects of graph theory have been appropriated and applied. Relationships are displayed as topological diagrams where crystal structures are treated as nodes (vertices) with connections (edges) drawn between them. The connections carry information about the degree of similarity between them. This is represented by the number of lines connecting the nodes: 1 for 1D and 2 for 2D. Isostructural arrangements are presented as the same node. Instances of 3D similarity, but not strict isostructuralism, are represented by three lines connecting the nodes.

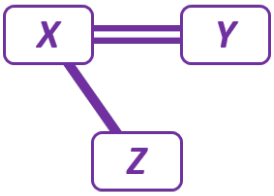

Figure 4.40 Similarity Diagram for structures X, Y and Z.

To illustrate, Figure 4.40 shows a similarity diagram for arbitrary structures X, Y and Z. Structure X is connected to Y by two lines, indicating a 2D similarity relationship. There is a single line connecting structure X and Z, indicating a 1D similarity relationship. No similarity relationships exist between structures Y and Z; they have no shared supramolecular constructs.

Different sub-sets exhibit different degrees of interconnectivity and similarity between structures. Consequently, some of the similarity diagrams have to obey different rules for clarity, such as removing the connections representing specific 1D motifs from the diagram. Such differences are noted in the discussion of each similarity diagram.

4.3.3 Stacking Patterns

4.3.3.1 Stacking Group 1

Stacking Group 1 structures are defined by a one-dimensional head-to-head stacking motif, which relates stacked molecules by translation along a column. This shared stack motif can be assumed between all structures in the group, as such this 1D motif has been omitted from the similarity networks for clarity.

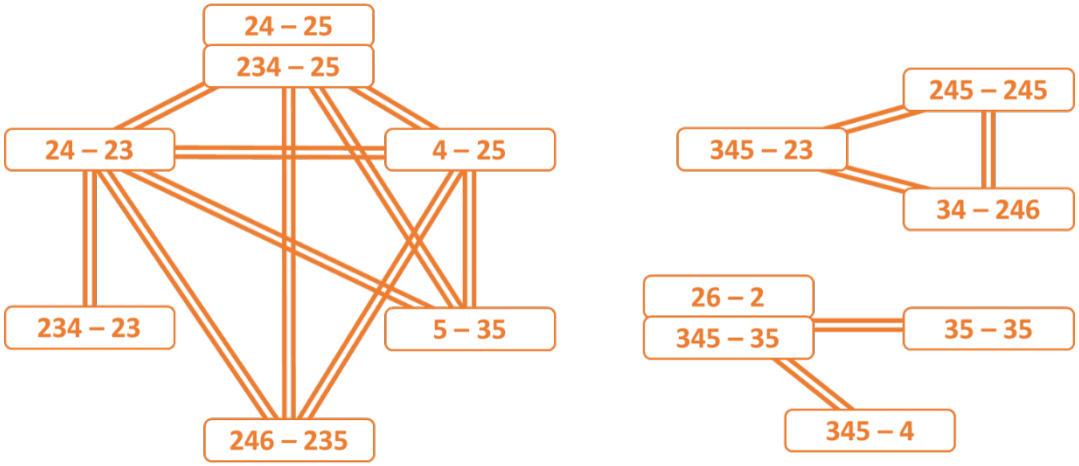

Figure 4.41 Similarity diagram for structures in Stacking Group 1. Only similarity relationships of 2D or more are highlighted. Structures with no similarity relationships greater than 1D have been omitted from the diagram.

The similarity diagram describes the additional motifs that are shared between structures. The various connections build a network, which highlights areas of reciprocal similarity. For instance, the group of six structures (24 – 23), (24 – 25), (234 – 25), (246 – 235), (4 – 25) and (5 – 35) are mutually similar – all are connected to one another by a 2D motif, Figure 4.41. Inspection of the structures reveals this motif to be an end-to-end or tape arrangement of the stacks herein labelled motif A, Figure 4.42.

Whereas, the 2D relationship between structures (24 – 23) and (234 – 23) is distinct from motif A. These structures both exhibit a side-to-side or ribbon arrangement of the stacks, motif B, in which adjacent stacks are related by a 2_1 screw axis. Structure (24 – 23) is, therefore, a combination of these two motifs.

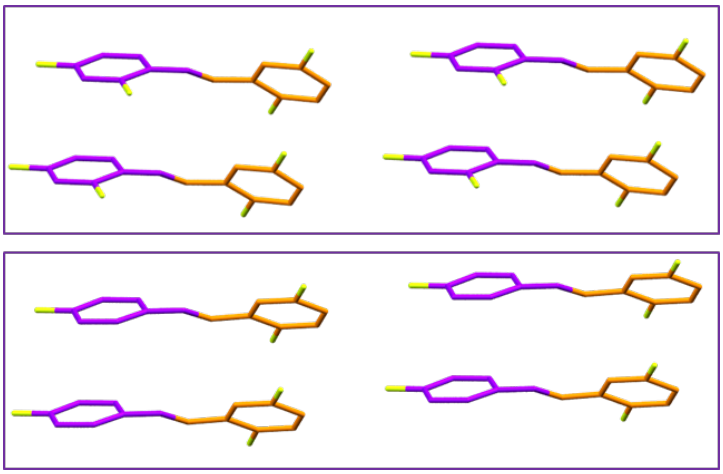

Figure 4.42 Motif A, a 2D end-to-end arrangement of stacks. Top: structure (24 – 25). Bottom: structure (4 – 25)

Structures (24 – 25) and (234 – 25) share three dimensional similarity and generally conform to definitions of isostructurality[206]; they share the same structural arrangement, symmetry group and have similar cell dimensions. Although, the molecules of (24 – 25) and (234 – 25) are positioned differently within the unit cell they are related to one another by reflection along the glide plane present in both structures.

The relationship between fluorine substitution pattern and crystal packing arrangement is much more apparent here than in the comparison of geometric local arrangement or inspection of the visual groups. The similarity in fluorine substitution patterns between the isostructural (24 – 25) and (234 – 25) is evident, with only the fluorine in the 3 position of the aniline changing. This suggests that the 3-aniline fluorine has less influence over the packing arrangement in these crystal structures, as the additional or subtraction of this fluorine atom does not significantly change the arrangement.

In this similarity network, there are a number of other examples of similar substitution patterns correlating with similar crystal structures. For instance, structure (4 – 25) shares 2D structural similarity with structures (24 – 25) and (234 – 25). However, shared fluorine positions is not a reliable indicator of structural similarity. Structures (26 – 2) and (345 – 35) are also isostructural, despite having no equivalent fluorine atoms.

Further investigation of the directing influence of specific fluorine substitution in structures (24 – 25), (234 – 25) and (4 – 25) is presented in Section 5.1.3.

In addition to the motifs A and B, the clusters on the right-hand side of the similarity network in Figure 4.41 exhibit three other motifs. Motif C, shared by structures (26 – 2), (345 – 35) and (345 –

4), is a ribbon arrangement of the stacks staggered such that the 'Head' of one molecule is side-to-side with the 'Tail' of adjacent molecules, Figure 4.43.

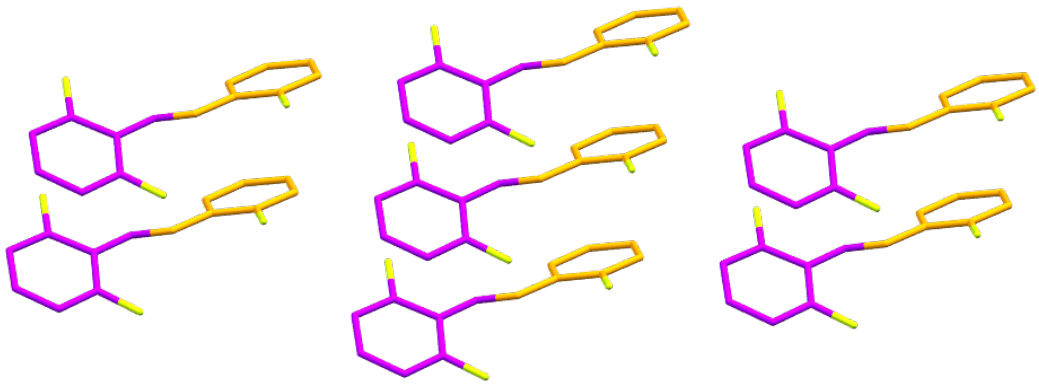

Figure 4.43 Motif C in structure (26 – 2) showing the staggered ribbon arrangement of stacks.

Motif D, shared by structures (26 – 2), (345 – 35) and (35 – 35), is a separate ribbon-stack motif. This motif is more complicated due to alternating rotation of adjacent stacks. Consequently, this motif cannot be easily depicted through 2-dimensional figures. Coordinate files for each motif have been provided in the appendices.

Structures (245 – 245), (34 – 246) and (345 – 23) are mutually similar through Motif E, which is a head-to-tail tape arrangement of stacks.

The full similarity parameters for these structural relationships can also be found in the appendices.

4.3.3.2 Stacking Group 2

Stacking Group 2 is a smaller subset of stacking structures, which are presented in the similarity diagram, Figure 4.44.

The structures in Stacking Group 2 are characterised by a shared set of geometric stacking properties. The stacks are formed of head-to-tail pairs; adjacent molecules in the stack are related to one another by inversion. The stacking arrangement can also be interpreted as stacks of anti-parallel dimers. The molecular pair with the shortest plane separation would be defined as the dimer within the stack.

Despite conforming to the symmetry and geometric trends of the group, the spatial arrangement of the dimer pairs is individual to each of the structures. Consequently, spatial analysis does not reveal a consistent stacking motif between all structures in Stacking Group 2. The variation in displacement and plane separation between dimer pairs produces geometrically similar stacks which fall outside of the XPac cut-off parameters used to identify spatial similarity. There are still

several instances of Stacking Group 2 structures with common stacking motifs, detailed in the following pages, however, there is no universal 1D stacking motif for the group – as observed in Stacking Group 1.

Instead, spatial analysis identifies the presence of the head-to-tail dimers. This 0D dimer motif is common between all of the Stacking Group 2 structures, although not presented in the similarity diagram.

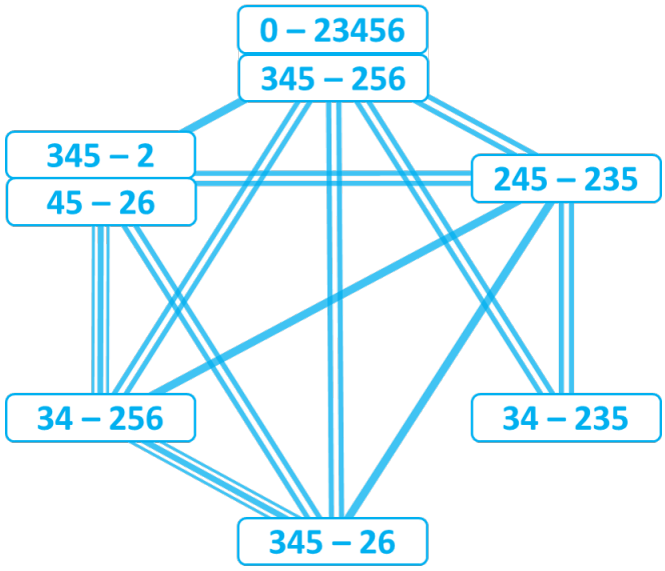

Figure 4.44 Similarity Diagram for structures in Stacking Group 2. A 0D dimer motif is shared between all structures but has not been presented in this diagram.

Notably, in this similarity diagram there are a number of examples of 3D similar structures that are not deemed isostructural. In particular, structures (34 – 256) and (345 – 26) are 3D similar but do not conform to isostructuralism. Whilst they have similar cell lengths the unit cells differ significantly in other regards.

Inspection of the lattice vectors associated with the 3D relationship reveals that the structures are related to one another by inversion, Table 26. Through manipulation of one of the structure files (by application of a -1 0 0 vector operation to atomic positions) an inverted analogue structure can be simulated, which is isostructural with the other unaltered structure. Both structures are in the space group $P\overline{1}$.

There is also a high dissimilarity index and stretch parameter associated with the 3D relationship between these two structures, which also suggests that they are not strictly isostructural, Table 26.

Table 4.26 Similarity parameters for the 3D similar relationship between structures (345 – 26) and (34 – 256).

345 – 26			**34 – 256**
Dissimilarity Index: x = 10.2			
Stretch Parameter: D = 0.50 Å			
n = 11 neighbours			p = 14 points
Delta [a] = 3.5°			Delta [p] = 9.3°
Corresponding Lattice Vectors			
345 – 26:			
1.00	0.00	0.00	= 7.044 Å
0.00	1.00	0.00	= 7.267 Å
0.00	0.00	1.00	= 11.973 Å
= 100.64°, 93.81°, 112.71°			
34 – 256:			
-1.00	0.00	0.00	= 7.013 Å
0.00	1.00	0.00	= 7.266 Å
0.00	0.00	1.00	= 12.171 Å
= 77.41°, 97.23°, 117.91°			

Additionally, spatial analysis identifies a 3D relationship between the isostructural pair (345 – 2) and (45 – 26) and structure (34 – 256), but only a 2D relationship between the pair and (345 – 26). This inconsistency in similarity is due to high dissimilarity values reaching beyond the cut-off parameters for this analysis. As a result, a lower but better fitting similarity relationship has been identified. Despite a network of 3D similar relationships connecting them, the four structures cannot be considered mutually isostructural.

Other such inconsistencies can be identified in the similarity diagram, Figure 4.44, which are also the result of high dissimilarity values. The full similarity parameters for all of these structures are reported in the appendices.

One might expect the isostructural pair (345 – 2) and (45 – 26) to be more structurally similar to (345 – 26) than (34 – 256) based solely on the similarity of fluorine substitution, but this is not observed. This can be rationalised by considering the potential influence of the ‘symmetrical’ substitution of (345 – 26) on the spatial arrangement. Here, ‘symmetrical’ substitution is used to describe the mirror equivalence of the fluorines; the meta-position fluorine atoms, 3 and 5, on the aniline ring are interchangeable by reflection as are the ortho-position fluorine atoms, 2 and 6, on the benzylidene ring.

The isostructural relationship between (0 – 23456) and (345 – 256) is also unexpected in terms of fluorine substitution patterns. Investigation of the energies associated with intermolecular interactions in these isostructural and 3D similar structures should help rationalise these observations.

In addition to the 3D similar and isostructural relationships, six other packing motifs are identified within Stacking Group 2. The coordinate files for each shared motif have been provided in the appendices.

4.3.3.3 Stacking Group 3

Of the stacking groups, Stacking Group 3 has the most spatial similarity between structures. There are several examples of isostructurality, 3D similar structures and mutually 2D similar networks.

As with Stacking Group 1 there is a shared 1D stack motif between all of the structures, which has not been depicted in the similarity diagrams for clarity. Additionally, Motif A is a 2D stack and ribbon motif which is shared by the majority of the structures. This high level of inter-similarity is difficult to depict within the similarity diagram. Instead, the structures that exhibit Motif A have been listed on the left-hand side of the diagram and the similarity network to the right depicts the remaining motifs and isostructural relationships, Figure 4.45.

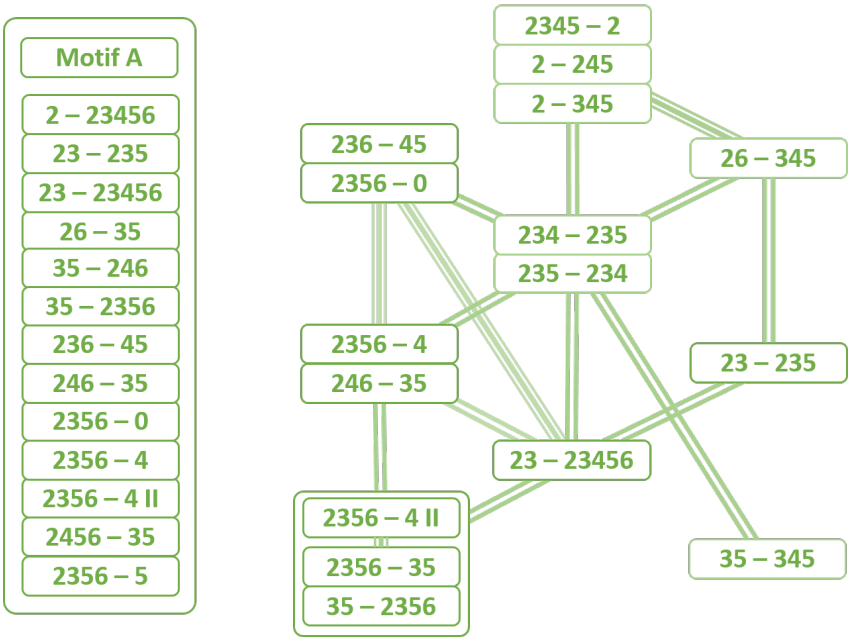

Figure 4.45 Similarity Diagram for Stacking Group 3. Structures that exhibit Motif A have been grouped on the left, additional relationships not expressed by Motif A are depicted in the network on the right.

The structures (236 – 45), (2356 – 0), (2356 – 4) and (246 – 35) are mutually isostructural. Structure (23 – 23456) is also isostructural with (236 – 45) and (2356 – 0), however, this structure has less spatial similarity with (2356 – 4) and (246 – 35) so only the 2D Motif A is observed between them.

The inversely substituted structures (234 – 235) and (235 – 234) are also found to be isostructural. Likewise the inversely substituted structures (2356 – 35) and (35 – 2356) are isostructural. These structures also exhibit a 3D similar relationship with (2356 – 4 II), a second phase of structure (2356 – 4). The structures (2345 – 2), (2 – 245) and (2 – 345) are also mutually isostructural with a 3D similar relationship to (26 – 345).

Among all of the crystal packing arrangements observed in the fluoroaniline structural library, Stacking Group 3 most adheres to the initial predictions of aromatic ring stacking as influenced by fluorine substitution. In Stacking Group 3 structures molecules form head-to-tail stacks, which both optimise the aromatic ring overlap and maximise the direct electrostatic attraction between the local C – F dipoles and C – H dipoles of the opposite ring. The influence of fluorine on the aromatic stacking and overall structural arrangement is highlighted by the spatial similarity between structures with similar fluorine substitution patterns, which is more evident in this stacking group than any other.

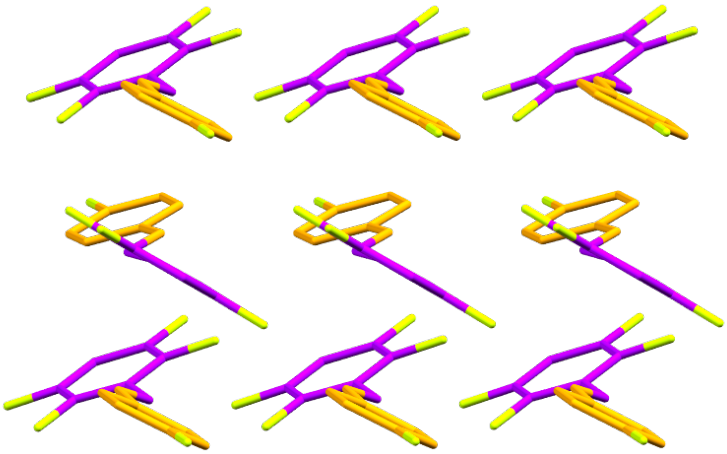

Figure 4.46 Depiction of the molecular arrangement in Motif A, shown for structure (2356 – 4).

Motif A is the most common shared motif between Stacking Group 3 structures, encompassing the majority of structures, Figure 4.46.

Five additional shared motifs were also observed in Stacking Group 3. Coordinate files and similarity parameters for each motif can be found in the appendices.

4.3.3.4 Stacking Group 4

Although visually similar, aromatic ring relationships in Stacking Group 4 were geometrically distinct from other stacking arrangements. In these structures aromatic ring overlap occurs between symmetry independent molecules. Consequently, the geometric properties are a product of asymmetry rather than an indicator of the spatial arrangement in the crystal structure. Spatial analysis of the group highlights a number of common motifs, displayed in the similarity network Figure 4.47, although many of these are limited to 1D relationships and only one instance of 3D similarity is observed. Coordinate files for the seven observed unique similar motifs can be found in the appendices alongside the similarity parameters for Stacking Group 4.

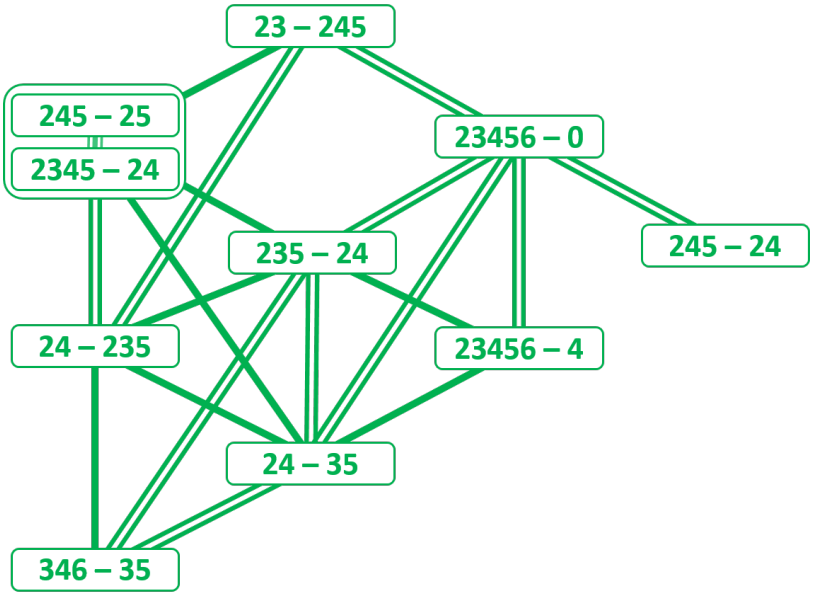

Figure 4.47 Similarity Diagram for Stacking Group 4.

Cross analysis of Stacking Group 4 to the other stacking groups reveals spatial similarity between the structures. The 3D similar pair (245 – 25) and (2345 – 24) share stack and tape motifs with the structures in Stacking Group 2 whilst the other structures in Stacking Group 4 share various stack and ribbon motifs with the structure in Stacking Group 3. Notably, (23456 – 4) is 3D similar with the Stacking Group 3 structures (35 – 2356) and (2356 – 35), Table 28.

Table 4.27 Similarity Parameters for the 3D similarity relationships between (23456 – 4) and (2356 – 35) and (35 – 2356).

23456 – 4			**2356 – 35**
Dissimilarity Index: x = 8.7			
Stretch Parameter: D = 0.34 Å			
n = 21 neighbours			p = 14 points
Delta [a] = 3.7°			Delta [p] = 7.5°
Corresponding Lattice Vectors			
23456 – 4:			
1.00	0.00	0.00	= 5.992 Å
0.00	0.00	1.00	= 7.464 Å
0.00	1.00	0.00	= 24.534 Å
= 90.00°, 90.00°, 91.54°			
2356 – 35:			
-1.00	0.00	0.00	= 6.250 Å
0.00	-1.00	0.00	= 7.378 Å
0.00	0.00	1.00	= 23.300 Å
= 90.00°, 90.00°, 90.00°			

23456 – 4			**35 – 2356**
Dissimilarity Index: x = 10.0			
Stretch Parameter: D = 0.36 Å			
n = 21 neighbours			p = 14 points
Delta [a] = 4.0°			Delta [p] = 8.8°
Corresponding Lattice Vectors			
23456 – 4:			
1.00	0.00	0.00	= 5.992 Å
0.00	0.00	1.00	= 7.464 Å
0.00	1.00	0.00	= 24.534 Å
= 90.00°, 90.00°, 91.54°			
35 – 2356:			
0.00	-1.00	0.00	= 6.270 Å
1.00	0.00	0.00	= 7.492 Å
0.00	0.00	1.00	= 23.680 Å
= 90.12°, 90.00°, 90.00°			

By nature of these structures containing more than one molecule in the asymmetric unit, similarity between long-range spatial arrangements are interrupted. For example, Motif F, present in the Z' = 3 structure (235 – 24), initially appears to be a 2D stack and ribbon motif similar to Motif A in Stacking Group 3. However, the side-to-side 'ribbon' component is interrupted by twisting of the third stack. Motif F is therefore a 1D motif and is best described as a trimer stack.

Closer inspection of structure (235 – 24) reveals a combination of stacking types. Two molecules in the asymmetric unit follow the conventions of Stacking Group 4 while the third molecule is involved in a separate stack in which molecules are related by a 2_1 screw axis, as for Stacking Group 3. The presence of two different aromatic stacking overlap relationships in the same structure suggests similar stabilisation energies associated with these arrangements. This structure offers an opportunity for comparison of energetic contributions from different stacking overlap types in which the fluorine substitution of the molecule remains constant.

4.3.4 Offset Overlap

The Staggered Overlap and Interwoven structures were considered together for this analysis as offset overlap arrangements are common between them. Similarity was observed between the two groups, although this was limited to 1D tape or ribbon motifs. These 1D similarity relationships are displayed in the similarity diagram, Figure 4.48. Staggered Overlap structures have been shown in pale blue, whilst Interwoven structures are shown in darker blue.

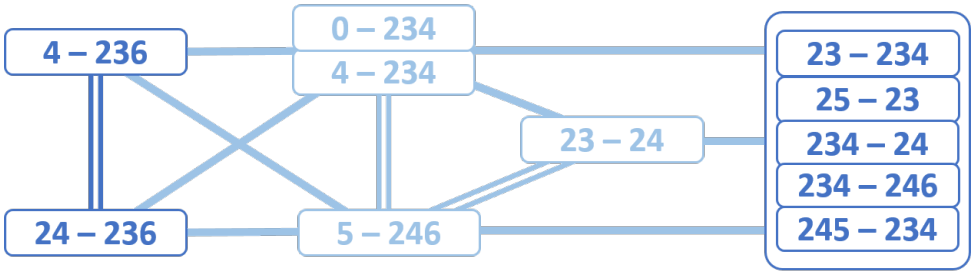

Figure 4.48 Similarity Diagram for both Staggered Overlap and Interwoven structures.

Within each group much higher spatial similarity was observed. The Interwoven structures are predominantly isostructural with the exception of structures (4 – 236) and (24 – 236). The Staggered Overlap structures also show high similarity with isostructuralism between (0 – 234) and (4 – 234) and overlapping motifs common between all structures. Coordinate files for the shared motifs can be found in the appendices alongside the similarity parameters for the Offset Overlap group.

The high degree of isostructuralism in the Interwoven group suggests that there is an optimal structural arrangement for these structures, which applies to a wide range of fluorine substitution patterns. The structural feature that distinguishes structures (4 – 236) and (24 – 236) from the main group is in the relationship between overlapped sheets. These arrangements appear to be supported by intermolecular atom-atom contacts, which are not present in the other structures.

As for structure (235 – 24) in Stacking Group 4, more than one overlap type is present in the Interwoven structures. Calculation of molecule-molecule intermolecular interaction energy in these structures provides another opportunity for direct comparison of overlap types with the same fluorine substitution pattern. In this instance, comparison of anti-parallel head-to-head offset overlap and anti-parallel head-to-tail inversion stacked overlap would be possible.

4.3.5 Angled Overlap

This group is defined by the presence of the angled aromatic ring overlap arrangement. As such, a 1D angled overlap ribbon motif is found consistently across the structures in this group, with the exception of the Z' = 2 structure (24 – 2356), which is spatially unique, and the Z' = 3 structure (234 – 245), which only forms 1D ribbon motifs as the aromatic ring overlap falls outside of the analysis cut-off parameters. These two types of 1D relationships have been omitted from the similarity diagram for clarity. The resulting similarity network shows clusters of related structures with limited interconnectivity to the rest of the crystal structures, Figure 4.49. These clusters are reflective of the different structural subsets.

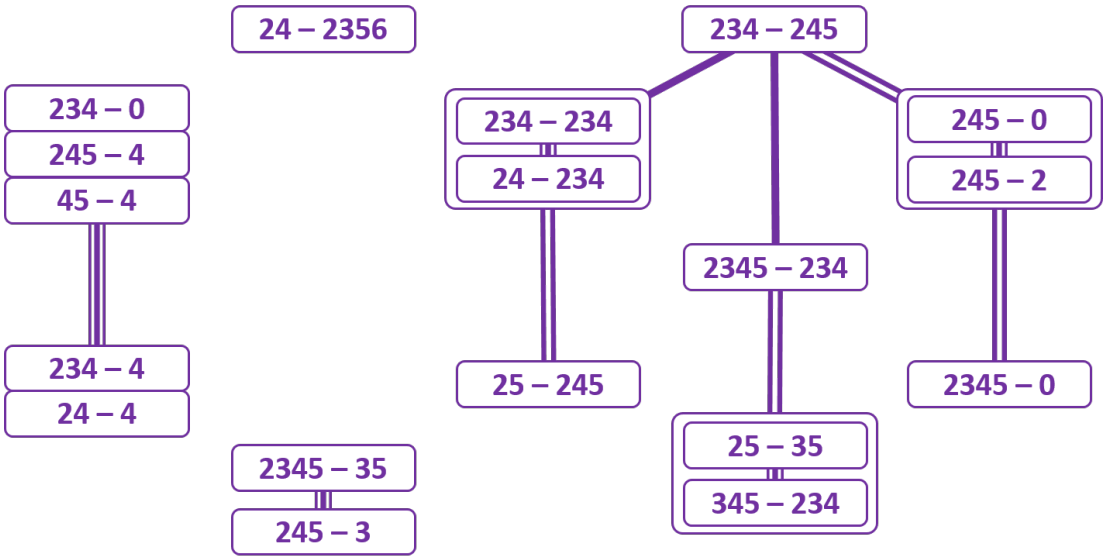

Figure 4.49 Similarity Diagram for Angled Overlap Group

The Angled Overlap group contains a number of structural subsets distinguished by the presence of additional overlap types. These subsets are well defined by the spatial analysis. A high degree of similarity is observed between the conventional angled overlap structures, for example the isostructural and 3D similar structures (234 – 0), (245 – 4), (45 – 4), (234 – 4) and (24 – 4).

Division into more specific subsets is also observed. Although geometrically related, structures with head-to-head twisted stacks, (234 – 234) and (24 – 234), are found to be spatially dissimilar to structures with head-to-tail twisted stacks, (245 – 0) and (245 – 2). Additionally, the uncategorised angled overlap structure (2345 – 0) shares 2D similarity with the head-to-tail twisted stack structures – reflecting the presence of twisted head-to-tail stacks in this structure.

Similarity parameters and coordinate files for all motifs are provided in the appendices.

4.3.6 Complementary Set

The term “complementary” is used to describe fluoroaniline molecules with substitution patterns that satisfy the maximum possible F and H dipole juxtapositions when arranged in head-to-tail stacks. Consequently, in these molecules there are always five fluorine atoms substituted in unique positions across the two aromatic rings. When oriented in head-to-tail stacks every fluorine atom is in juxtaposition with a hydrogen atom on the opposing ring. These structures generally conform to the predicted head-to-tail stacking, with the exception of structure (4 – 2356).

Observations of the Overlap Matrix in Section 4.2.7 identified that, while generally exhibiting head-to-tail stack arrangements, the aromatic overlap geometries varied across the complementary set. This has been highlighted by different colouration in the similarity diagram, Figure 4.50.

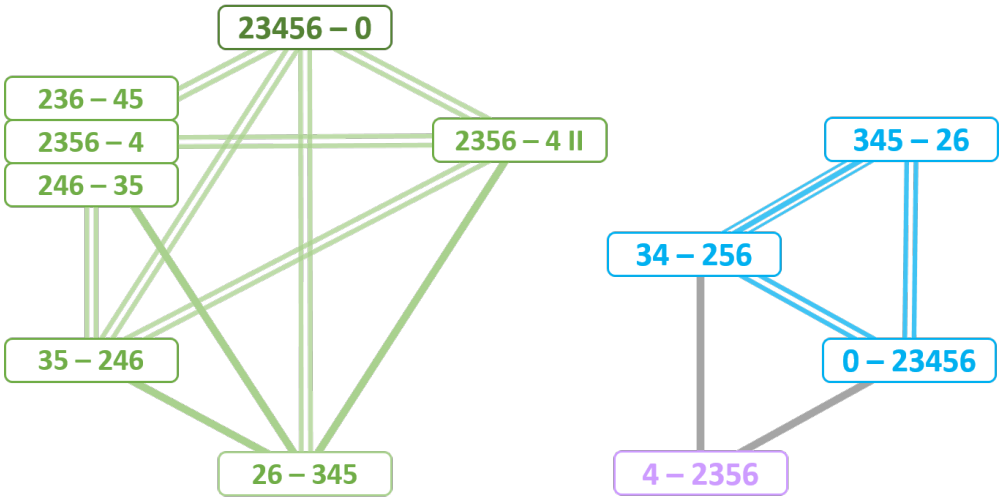

Figure 4.50 Similarity Diagram for the complementary set. Blue represents Stacking Group 2, light green represents Stacking Group 3, dark green represents Stacking Group 4 and violet represents Grid structures.

The distinction between different overlap geometries is also reflected in the spatial similarity analysis. Within the complementary set the Stacking Group 2 and Stacking Group 3 structures bear no similarity to one another. Although, the geometrically distinct structure (23456 – 0) does exhibit significant similarity to the Stacking Group 3 structures.

Motifs observed in the complementary set are generally repetitions of those seen in the stacking groups. The coordinate files and full similarity parameters for the complementary set can be found in the appendices.

Stabilisation from direct dipole – dipole interactions is expected to be approximately equal between complementary structures of the same overlap arrangement. Whilst the structures belonging to each overlap group exhibit a high degree of similarity, variation is still observed in the overall crystal packing; the structures are not mutually isostructural. This variation demonstrates the influence of specific substitution patterns on the structure.

The structural differences can be rationalised by considering the presence of atom-to-atom noncovalent interactions, which are dependent on the specific position of fluorine.

Additionally, the variation of π-electron density in the aromatic rings may become a more apparent influence in these structures where the direct dipole – dipole interactions are equivalent. As discussed in Section 1.2.2, the substitution of electron-withdrawing fluorine atoms will reduce the π-electron density of the aromatic rings. The effect is additive; the greater the number of fluorine atoms, the greater the influence on the electron density in the aromatic system. The resulting electrostatic attraction between electron rich and electron poor aromatic systems is less prominent than the direct substituent interactions and so is usually masked by them. The electrostatic attraction will be strongest between rings with the greatest difference in substitution, namely structures (23456 – 0) and (0 – 23456).

The separation of the head-to-tail complementary structures into Stacking Group 2 and Stacking Group 3 is starkly apparent from the similarity diagram. Examination of fluorine substitution patterns in the different groups reveals a common factor in related structures. Complementary structures exhibiting Stacking Group 3 aromatic overlap have a fluorine atom in the 2 ortho position on the aniline ring (with the exception of structure (35 – 246)). This fluorine position is absent in complementary structures exhibiting Stacking Group 2 aromatic overlap.

This observation is consistent with the presence of atom-to-atom intermolecular interactions. Close contact is observed between fluorine in the 2 position on the aniline ring (F2) and the azomethine hydrogen atom (H7) in the majority of Stacking Group 3 structures, those that contain F2. The close contact appears in the side-to-side ribbon motifs observed in these structures, Figure 4.51.

As discussed in Sections 1.2.3 and 1.3, while organic fluorine hydrogen bonds have been acknowledged as stabilising, the structure determining capability of C – H ··· F – C intermolecular interactions is not generally deemed significant due to their low energy stabilisation. Although, Kaur and Choudhury identified similar C – H ··· F – C intermolecular interactions in fluoroaniline crystal structures[190,191] and concluded that these interactions had the capacity to influence the crystal assembly in the absence of strong hydrogen bond acceptors.

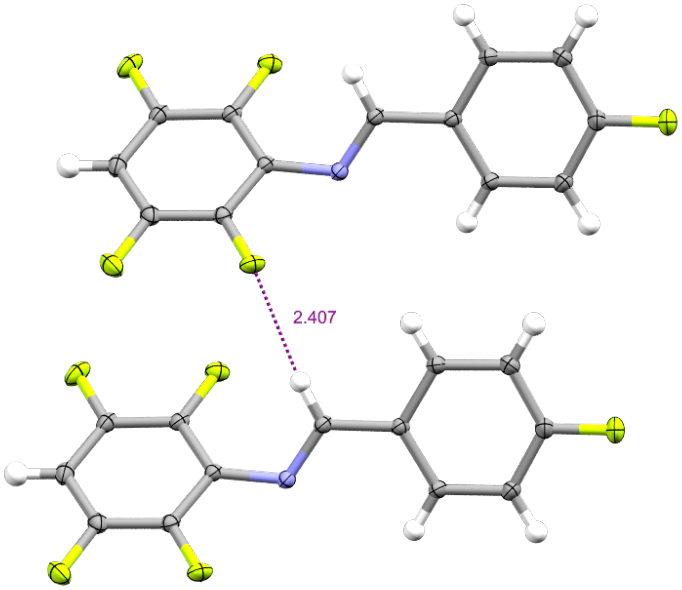

Figure 4.51 Close contact between F2 and H7 in structure (2356 – 4). Units are in Å. The contact distance (2.407 Å) is significantly shorter than the van der Waals radius for F ··· H (2.54 Å[207]).

In this study, energy calculations or charge density analysis of the Stacking Group 3 crystal structures would be able to confirm the presence and determine the strength of an attractive intermolecular interaction between F2 and H7.

4.3.7 Conclusions

Similarity analysis of the fluoroaniline structural library provides substantial supporting evidence for the correlation between the fluorine substitution pattern and the resulting crystal assembly.

Isostructural crystals in the structural library often have very similar substitution patterns, for example structures (2356 – 0) and (2356 – 4) in Stacking Group 3. Also, non-isostructural but similarly substituted structures often share 2D or 1D motifs, such as structures (24 – 25) and (4 – 25) in Stacking Group 1.

As discussed in Section 4.3.1, the presence of shared supramolecular constructs (shared motifs) between two structures is an indicator of similar directing forces in nucleation and crystal growth[204]. Investigation of these motifs can reveal potential intermolecular interactions directing their assembly.

While there is usually an emphasis in crystal engineering for identifying supramolecular synthons and close contacts for likely atom-to-atom non-covalent interactions[25,38], XPac analysis specifically identifies supramolecular constructs rather than synthons[204]. Supramolecular synthons imply the

presence of a definite bonding between the molecules whereas supramolecular constructs represent common strategies for crystal assembly regardless of the interaction between the molecules. This is useful for investigating structures that may be more reliant on dispersive forces such as those with prominent aromatic overlap interactions.

It is important to note that fluoroanilines with similar substitution patterns, but very different structures, have also been observed, including different aromatic overlap arrangements. Equally, isostructural fluoroanilines with significantly different substitution patterns have been observed.

This suggests that different substitution positions have different 'weight' in the crystal assembly. The specific positioning of fluorine may direct the crystal arrangement due to any of the following: repulsion with other proximate non-bonded fluorines; its effect on the pseudo symmetry of the molecule; its effect on the shape of the molecule or the potential for intermolecular atom-to-atom interactions.

Investigation of the complementary set highlights the importance of fluorine in the 2 position on the aniline ring (F2). While consideration of dispersive forces and the importance of aromatic overlap is foremost in the analysis of these structures, the directing power of F2 appears to be the result of a close contact between it and the azomethine hydrogen (H7). This potential atom-to-atom interaction seems formative in the overall structure of Stacking Group 3 structures, specifically Motifs A and B. With a few exceptions, Stacking Group 3 structures exhibiting Motif A or B have an F2 atom in the substitution pattern. Conversely, with the exception of (245 – 235), Stacking Group 2 structures do not have F2 in their substitution patterns.

Another example of differently weighted fluorine positions is observed in Stacking Group 1. Structures (24 – 25) and (234 – 25) are found to be isostructural; this suggests that the meta fluorine on the aniline (F3) has less influence over the crystal assembly as the addition or subtraction of this fluorine atom does not significantly change the arrangement. Whereas the removal of F2 does have an effect on the crystal packing, as demonstrated by the 2D similar structure (4 – 25).

Although these observations are strongly indicative, investigation of overlap geometry and structural similarity cannot provide sufficient evidence to identify the specific non-covalent interactions and dispersive forces responsible for directing the crystal assembly.

Standard resolution crystallography limits investigation of crystal structures to be purely reliant on atomic coordinates to draw conclusions. Analysis of the charge distribution between molecules is required to establish the presence of attractive intermolecular interactions and determine their stabilising energy. This can be achieved through high resolution X-ray diffraction experiments and

theory-based quantum crystallographic analysis. These methods are explored in the following chapter.

Chapter 5 Identification and Quantification of Non-Covalent Interactions

The structural analysis in the previous chapter highlights a number of potential non-covalent interactions. These include molecule-molecule interactions such as aromatic ring stacking and atom-atom interactions such as weak fluorine hydrogen bonds.

The structural analysis presented in Chapter 4 is reliant on atomic coordinates derived from standard resolution crystallography, the Independent Atom Model. However, confirmation of energetically stabilising non-covalent interactions requires charge distribution data. Charge distribution describes the electron density both localised to particular atoms and existing between atoms and molecules exhibiting interaction characteristics.

Charge distribution can be assessed experimentally through high resolution X-ray diffraction and charge density analysis utilising the quantum theory of atoms in molecules (QTAIM). Alternatively, charge distribution can be assessed through theoretical means, such as the quantum mechanical semi-empirical energy calculations of the PIXEL approach, which calculates molecule-molecule stabilisation energies.

These two approaches are applied to notable potential interactions highlighted in the structural analysis.

5.1 Atom-to-Atom Intermolecular Interactions

Atom-to-atom interactions are frequently the main focus for crystal engineering, particularly highly directional hydrogen bonding and halogen bonds[29]. The identification of supramolecular synthons relies predominantly on these atom-atom interactions, as discussed in Section 1.1. This approach requires the identification of interactions which are not only attractive but also competitive such that they reliably influence the crystal assembly[208].

Weaker intermolecular interactions, such as the C – H ··· F – C weak hydrogen bonds and "halogen-like" F ··· F interactions present in these crystals, are assumed to have less influence over the crystal assembly due to their weak stabilisation energies. However, in the absence of strong synthons, weak but directional non-covalent interactions may have a significant influence on the initial molecular self-recognition[157]. In the early stages of crystal assembly long-range directionality may have a more significant influence on the arrangement than stronger dispersive forces, which begin to dominate as crystal growth continues.

Potential atom-atom interactions are routinely identified through measurement of close contact distances and angles. This geometric analysis is valuable, but it is important that identified close contacts are also validated by empirical evidence to confirm an attractive interaction, such as experimentally obtained charge distribution models for the structure and semi-empirical energy calculations, e.g. PIXEL.

Four crystal structures were selected for high resolution X-ray diffraction experiments, (2356 – 4), (246 – 35), (34 – 256) and (345 – 26). These structures were of interest as they all exhibited complementary substitution patterns and the pairs (2356 – 4)(246 – 35) and (34 – 256)(345 – 26) were found to be isostructural or 3D similar in standard resolution experiments. The structural similarity makes them ideal for comparison. The charge distribution models obtained from these data sets and multipolar refinement were analysed to confirm and assign interaction energies for proposed atom-atom intermolecular interactions identified in the crystal structures.

PIXEL calculations were performed to evaluate the importance of these interactions relative to the overall crystal lattice energy. These calculations of molecule-molecule energy were also used to infer the presence of attractive atom-atom interactions in structures for which high resolution data collection was not possible, (234 – 25), (24 – 25) and (4 – 25).

In this discussion it is important to identify the specific atom not just relative position on the ring. For this purpose, substituents are given a unique label following the scheme in Figure 5.1.

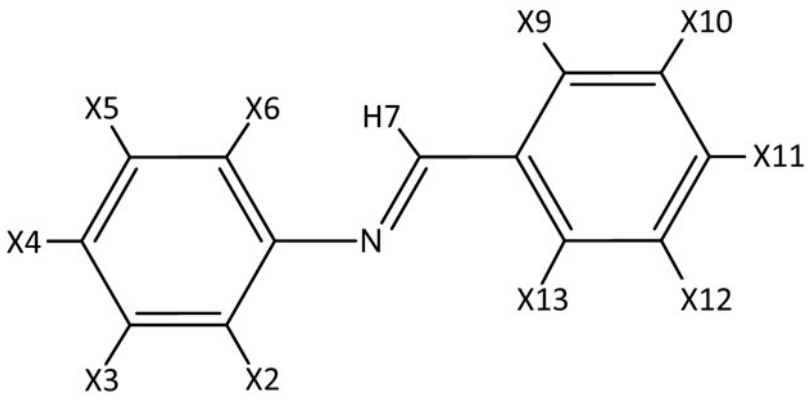

Figure 5.1 Molecular diagram for numbering scheme. Atom X = F or H.

5.1.1 Structures (2356 – 4) and (246 – 35)

Structures (2356 – 4) and (246 – 35) are isostructural complementary structures belonging to Stacking Group 3. A short contact between F2 and H7 has already been identified in both of these structures. This short contact has been highlighted as a potential directing force in the formation of Stacking Group 3 structures. Other short contacts in these structures also become apparent

through investigation of atom-atom geometry. High resolution X-ray diffraction coupled with charge density calculations and PIXEL analysis of the structure will help to reveal the nature of such interactions and the potential influence on the crystal assembly.

5.1.1.1 Identifying Short Contacts

The short contact distance for two atoms is defined by the sum of the van der Waals radii for the atoms. The maximum contact distance is approximately 2.54 Å for F ··· H short contacts and 2.90 Å for F ··· F short contacts[207]. Through investigation of interatomic distance and bond geometry four F ··· H and four F ··· F short contacts were identified for structure (2356 – 4), Table 5.1. One slightly extended contact has been included in this set, H12 ··· F3 at 2.557 Å.

These short contacts are suggestive of an interaction between the atoms. While distance does not provide definite evidence of an interaction it is a reliable indicator[209]. The shortest contacts suggest a particularly attractive interaction, such as F2 ··· H7 at 2.262 Å.

The bond angles are also an important indicator for likely interactions, especially when investigating directional interactions such as hydrogen bonds. The ideal bond geometry for hydrogen bonds is 180°, as described in Section 1.1.3. The C – H ··· F angle is close to linear for the F2 ··· H7 and F3 ··· H4 contacts, 165.82° and 161.30°, respectively. The C – F ··· H geometry has been shown to have less sensitivity to deviations from linearity[135], as described in Section 1.2.3.3.

The ideal geometry for F ··· F "halogen-like" interactions is found to be 90° for both C – F ··· F angles in a mutually orthogonal type I interaction, see Section 1.1.5.2 and 1.2.4 for more detail. The F11 ··· F11 contact exhibits type I geometry with a C – F ··· F bond angle of 113.19°; however, none of the F ··· F contacts in structure (2356 – 4) conform to an ideal geometry.

Table 5.1 Intermolecular short contacts identified in structure (2356 – 4). Symmetry describes the operation relating the two molecules in the intermolecular short contact.

Atom 1	**Atom 2**	**Symmetry**	**Length /Å**	**Length – Van der Waals radii /Å**	**Angle C – H ··· F /°**	**Angle C – F ··· H /°**
H7	F2	-1+x,y,z	2.262	-0.278	165.82	144.27
F5	H4	1-x,1-y,1-z	2.496	-0.044	126.04	118.77
F3	H4	2-x,1-y,1-z	2.53	-0.010	161.30	115.53
H12	F3	2-x,-0.5+y,0.5-z	2.557	0.017	133.99	158.14

Atom 1	Atom 2	Symmetry	Length /Å	Length – Van der Waals radii /Å	Angle C – F_1 ⋯ F_2 /°	Angle C – F_2 ⋯ F_1 /°
F11	F11	-x,1-y,-z	2.900	0.000	113.19	113.19
F11	F5	x,0.5-y,-0.5+z	2.925	0.025	121.93	153.27
F6	F2	-1+x,y,z	2.936	0.036	106.51	89.23
F5	F3	-1+x,y,z	2.938	0.038	89.52	107.38

Structure (246 – 35) was also analysed through investigation of the interatomic distance and bond geometry and five F ⋯ H and three F ⋯ F short contacts were identified, Table 5.2. The shortest contact in this structure is F10 ⋯ H11 at 2.376 Å, again this suggests a particularly attractive interaction.

In structure (246 – 35) there are also two contacts with close to linear bond geometry: F2 ⋯ H7 and F12 ⋯ H3 with C – H ⋯ F bond angles of 165.25° and 162.21°, respectively.

Unlike (2356 – 4), two of the F ⋯ F short contacts in structure (246 – 35) exhibit near orthogonal C – F ⋯ F bond angles, Table 5.2. This suggests a more attractive interaction and is accompanied by a shorter interatomic distance compared to F ⋯ F contacts in (2356 – 4).

Table 5.2 Intermolecular short contacts identified in structure (246 – 35). Symmetry describes the operation relating the two molecules in the intermolecular short contact.

Atom 1	Atom 2	Symmetry	Length /Å	Length – Van der Waals radii /Å	Angle C – H ⋯ F /°	Angle C – F ⋯ H /°
F10	H11	-x,1-y,1-z	2.376	-0.164	151.62	122.87
F6	H9	-x,-0.5+y,1.5-z	2.389	-0.151	150.43	150.29
F12	H3	2-x,-0.5+y,1.5-z	2.398	-0.142	162.21	135.57
H7	F2	-1+x,y,z	2.408	-0.132	165.25	142.60
H5	F10	-x,-0.5+y,1.5-z	2.498	-0.042	146.45	145.96
Atom 1	**Atom 2**	**Symmetry**	**Length /Å**	**Length – Van der Waals radii /Å**	**Angle C – F_1 ⋯ F_2 /°**	**Angle C – F_2 ⋯ F_1 /°**
F6	F2	-1+x,y,z	2.881	-0.019	95.82	90.63
F10	F12	-1+x,y,z	2.892	-0.008	96.35	90.82
F4	F4	2-x,1-y,2-z	2.922	0.022	108.08	108.08

Short contacts are indicative of an attractive interaction but many C – H ··· F contacts are dismissed as a by-product of close-packing requirements; they are rationalised as non-repulsive but ultimately insignificant to the crystal assembly[130,134].

5.1.1.1.1 Surface Enrichment

Geometric analysis of short contacts, such as the above, cannot differentiate attractive interactions from the incidental proximity of atoms, although optimal bond angles and short interatomic distances are good indicators.

Surface enrichment can be used as another indicator to infer the likelihood of a contact to be more significant than chance. The enrichment ratio for a particular type of contact can be calculated from the Hirshfeld surface. The ratio measures the propensity of an atom/chemical species to form intermolecular interactions with another[188]. The methodology for these calculations is described in Section 2.2.2.1.

Enrichment ratios were calculated for the molecules in structures (2356 – 6) and (246 – 35). Details of the Hirshfeld Contact Surfaces and calculations can be found in the appendices.

Table 5.3 Enrichment Ratios for structure (2356 – 4).

Atoms	H	C	F
H	0.84	~	~
C	0.41	2.47	~
F	1.46	0.72	0.75

Table 5.4 Enrichment Ratios for structure (246 – 35).

Atoms	H	C	F
H	0.79	~	~
C	0.61	2.13	~
F	1.38	0.76	0.79

In both structures the H ··· F contacts are shown to be enriched – occurring more often than would be expected by chance. This is also found to be the case in other surface enrichment studies of fluorinated organics (in the absence of strong hydrogen bond acceptors)[135,157,188]. The C ··· C contacts are also shown to be enriched, this is not indicative of atom-atom interactions but instead suggests close stacks of aromatic rings, discussed further in Section 5.2.

Conversely, the F ··· F contacts are shown to be 'impoverished' – occurring less often than would be expected by chance. In part this is due to the propensity for fluorine to engage in contacts with hydrogen. It does not necessarily indicate that F ··· F contacts are unfavourable but rather that H ··· F contacts are preferred. It has also been proposed that there is a statistical bias towards arrangements with many weak C – H ··· F interactions opposed to arrangements in which F ··· F interactions are in an optimal geometry for "halogen-like" bonding[208]. This proposal is based on the assumption that C – H ··· F has weaker directionality than F ··· F. Although hydrogen bonds have strong directional preference for linear arrangements, it does appear that weaker hydrogen bond interactions are observed in a wide range of bond geometries[135].

Surface enrichment ratios quantify the propensity for interactions of a particular type, e.g. C – H ··· F, within a structure. However, there is no insight into the attractive or directing nature of individual interactions, e.g. F2 ··· H7.

The next step in assessment of possible atom-atom interactions is an analysis of the charge distribution to determine the attractive or repulsive nature of specific intermolecular interactions.

5.1.1.2 Identifying Critical Points

As discussed in Section 2.1.3.3, critical points are used to describe the topology of electron density in crystals. Critical points are identified where the gradient vector of the electron density becomes zero, i.e. $\nabla\rho\ (r) = 0$. Critical points of the type (3, -1) are known as bond critical points (BCP). They occur at a saddle point between the electron density maxima of two atomic nuclei.

According to Bader's quantum theory of atoms in molecules (QTAIM), a bond critical point will always be present where there is an interaction between two atomic nuclei[173,176,177]. The nature of the interaction can be analysed from the electron density, $\rho(rBCP)$, and the Laplacian of electron density, $\nabla^2\rho(rBCP)$. A low $\rho(rBCP)$ and $\nabla^2\rho(rBCP) > 0$ indicates a closed-shell interaction such as a hydrogen bond or a van der Waals interaction.

The values for the Laplacian and electron density can also be used to estimate energy at the critical point following the equations 2.11 and 2.12 outlined in Section 2.1.3.3.2. These give approximations for the local kinetic energy density, $G(rBCP)$, and the local potential energy density, $V(rBCP)$.

Geometric analysis of (2356 – 4) and (246 – 35) highlighted a number of close contacts that might correspond to intermolecular interactions. The F2 to H7 contact, present in both, is of particular interest and has already been highlighted as a potential directing influence in the crystal

assembly. Identification of BCPs will distinguish which close contacts represent intermolecular interactions and allow assessment of the corresponding stabilisation energy.

The energy of interactions can be calculated using the values for the local kinetic energy density, $G(rBCP)$, following Equation 5.1[144,145,210].

Equation 5.1 Calculation of the energy of an intermolecular interaction

$$E_{int} = kG_{BCP}\ (in\ atomic\ units)$$

E_{int} is the stabilisation energy of the interaction

G_{BCP} is the local kinetic energy density at the BCP

k = -0.429 for C – H ··· F interactions

k = -0.129 for C – F ··· F interactions

The coefficient value, k, varies for different types of interaction. The value 0.429 is cited for conventional hydrogen bonds as well as organic hydrogen bonds in a number of studies although the approximation $E_{HB} = \frac{1}{2}\ V_{BCP}$ is often given for the stabilisation energy of moderate to strong hydrogen bonds[144,145,210]. The C – F ··· F coefficient value was calculated by Levina *et al.* in 2019[144], who did so by comparing the experimental enthalpy of sublimation to the calculated lattice energy in crystals of perfluorinated molecules. The relative values of the coefficients are consistent with the results of other theoretical studies[211].

Other charge density properties have also been used to calculate the energy of intermolecular bonds. These estimators of interaction energy have varying efficacy for different types of interactions and fitting functions generally only have good agreement with results in the range 3 to 90 kJ mol^{-1}.[210]

Applicability of these types of calculations to weaker interactions is not well established. The standard uncertainty of the experimentally derived $\rho(rBCP)$ and $\nabla^2\rho(rBCP)$ will affect the accuracy of estimations through G_{BCP}. An error of only a few kilojoules would be substantial relative to the weak interactions being studied in these systems. Therefore, the calculated stabilisation energy for identified bond critical points should be interpreted cautiously. Other properties of the proposed interaction should still be considered in analysis, such as interatomic distance and bond geometry.

The charge distribution data for the structures (2356 – 4) and (246 – 35) were obtained experimentally from high resolution X-ray diffraction and multipolar refinement. A critical point

search of the structures yielded the following intermolecular bond critical points, Table 5.5 and 5.6.

Table 5.5 Intermolecular Bond Critical Points identified in structure (2356 – 4)

Contact	**Atomic Distance / Å**	**ρ(r) / *e* Å^{-3}**	**$\nabla^2\rho$(r) / e Å^{-5}**	**G_{BCP} / kJ mol^{-1} Bohr^{-3}**	**V_{BCP} / kJ mol^{-1} Bohr^{-3}**	**E_{int} / kJ mol^{-1}**
F ··· H						
F2 ··· H7	2.2623	0.04654	1.227	24.16	-14.91	-10.36
F5 ··· H4	2.4965	0.04163	0.730	14.82	-9.75	-6.36
F3 ··· H12	2.5573	0.03335	0.616	12.26	-7.75	-5.26
F11 ··· H12	2.6441	0.03122	0.540	10.77	-6.84	-4.62
F3 ··· H4	2.5305	0.01754	0.546	10.29	-5.70	-4.41
F6 ··· H9	2.6608	0.02870	0.513	10.15	-6.34	-4.35
F11 ··· H10	2.7020	0.02467	0.441	8.67	-5.31	-3.72
F2 ··· H13	2.7329	0.01810	0.391	7.49	-4.33	-3.21
F5 ··· H10	2.8459	0.00855	0.244	4.55	-2.44	-1.95
F ··· F						
F2 ··· F6	2.9357	0.03571	0.716	14.22	-8.93	-1.83
F11 ··· F11	2.8999	0.03441	0.713	14.09	-8.75	-1.82
F3 ··· F5	2.9382	0.03549	0.702	13.95	-8.77	-1.80
F5 ··· F11	2.9248	0.03111	0.662	12.98	-7.93	-1.67

Table 5.6 Intermolecular Bond Critical Points identified in structure (246 – 35)

Contact	**Atomic Distance / Å**	**ρ(r) / *e* Å^{-3}**	**$\nabla^2\rho$(r) / e Å^{-5}**	**G_{cp} / kJ mol^{-1} Bohr^{-3}**	**V_{cp} / kJ mol^{-1} Bohr^{-3}**	**E_{int} / kJ mol^{-1}**
F ··· H						
F10 ··· H11	2.3764	0.03232	0.838	16.25	-9.66	-6.97
F2 ··· H7	2.4084	0.02479	0.845	16.00	-8.99	-6.86
F6 ··· H9	2.3890	0.02378	0.793	15.02	-8.43	-6.44
F12 ··· H3	2.3982	0.02784	0.655	12.69	-7.55	-5.44
F4 ··· H5	2.5502	0.03369	0.626	12.47	-7.89	-5.35
F12 ··· H11	2.5263	0.03212	0.623	12.33	-7.69	-5.29
F10 ··· H5	2.4984	0.02407	0.613	11.76	-6.82	-5.05
F2 ··· H13	2.5396	0.01591	0.518	9.72	-5.33	-4.17
F4 ··· H3	2.7545	0.02279	0.391	7.67	-4.70	-3.29
F ··· F						
F2 ··· F6	2.8810	0.04472	0.885	17.83	-11.56	-2.30
F10 ··· F12	2.8916	0.04097	0.853	17.01	-10.79	-2.19
F4 ··· F4	2.922	0.03148	0.660	12.97	-7.96	-1.67
F12 ··· F4	3.253	0.01147	0.243	4.59	-2.57	-0.59

It is important to note that many of the BCPs identified in the critical point search have an interatomic distance significantly longer than the sum of the van der Waals radii, 2.54 Å for F ··· H and 2.90 Å for F ··· F[207]. As such, these potential interactions were not highlighted in the geometric search for short contacts. Some of these contacts can be dismissed from discussion of stabilising interactions as they represent such a small contribution and have unlikely geometries for directing the assembly. For example, in structure (246 – 35) the F12 ··· F4 contact has a large interatomic distance, 3.253 Å, and a very small corresponding E_{int}, -0.59 kJ mol^{-1}. Therefore, this interaction is unlikely to be competitive in crystal formation.

In general, the assertions made about the observed short contacts in Section 5.1.1.1 correlate well with the estimated interaction energies from the BCPs. For example, it was suggested that

F2 ··· H7 in (2356 – 4) and F10 ··· H11 in (246 – 35) would be particularly attractive interactions as indicated by their short interatomic distances. Additionally, interactions F2 ··· F6 and F10 ··· F12 in (246 – 35) were highlighted as having close to mutually orthogonal bond angles, an ideal geometry for fluorine "halogen-like" interactions. This is reflected in the relatively high estimated interaction energies, Table 5.6.

(2356 – 4) and (246 – 35) are isostructural and similar atom-atom contacts are observed between the two structures. This is more apparent in observation of the critical points than geometric close contacts as a wider range of weak interactions have been identified. The estimated bond critical point energies reveal that there is a different hierarchy of interaction strength for the equivalent contacts. For example, the F6 ··· H9 interaction in (246 – 35) is stronger than the same contact in (2356 – 4) both in absolute value and relative to other interactions in the structure. These different hierarchies seem to be primarily connected to changes in interatomic distance for equivalent contacts and deviation from ideal bond geometry. For example, the interatomic distance for the F6 ··· H9 interaction is 2.389 Å and 2.661 Å for (246 – 35) and (2356 – 4), respectively, Table 5.5 and 5.6.

5.1.1.2.1 Nature of the F2 ··· H7 Interaction

While the distance between atoms in a proposed interaction is a reliable indicator of interaction strength[209], the results of this critical point search suggest that energy is not always strictly proportional to distance. The closest contacts are not necessarily the strongest. This is highlighted by the F2 ··· H7 contact in structure (246 – 35). While it is not the strongest interaction in the structure, the estimated stabilisation energy is higher than for contacts with a similar, or slightly shorter, interatomic distance, Table 5.6. This can be rationalised by considering the superior hydrogen bond donor ability of C7 compared to the other carbon donors present in the molecule. The C7 is the carbon atom in the azomethine linker between the aromatic rings. Azomethine carbon is understood to be a better hydrogen bond donor than aromatic carbon; the dipole charge between C7 and H7 is greater than between aromatic carbon and hydrogen.

The F2 ··· H7 interaction in structure (2356 – 4) also shows an enhanced bonding ability. This interaction has the strongest estimated energy observed from charge density experiments in this study, -10.36 kJ mol^{-1}. This observation is in agreement with the proposed influence of the F2 ··· H7 interaction in the crystal assembly of Stacking Group 3 structures.

Figure 5.2 shows the Laplacian map for the F2 ··· H7 interaction in (2356 – 4). The BCPs have been marked with a cross. Also note the presence of the F2 ··· F6 interaction in the same plane.

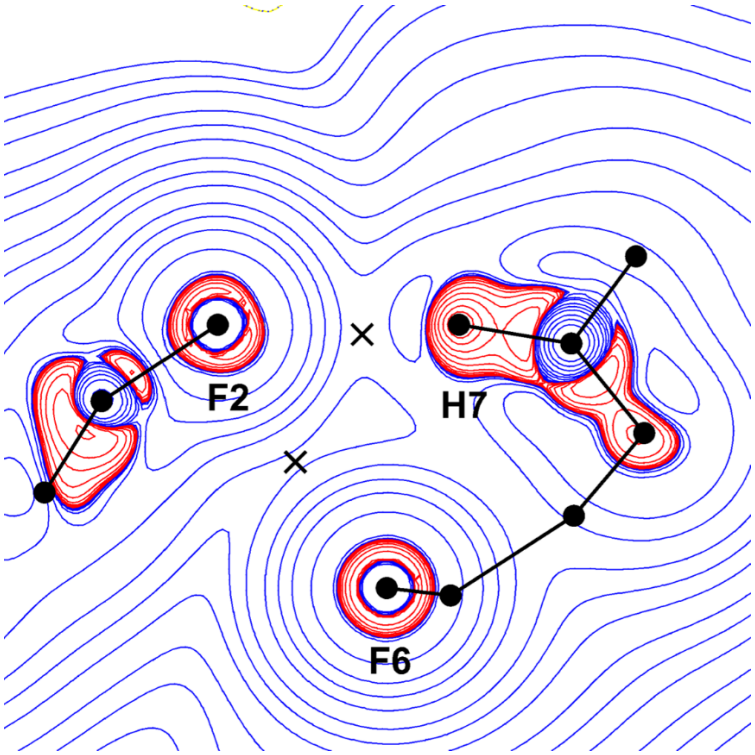

Figure 5.2 Logarithmic Laplacian map in the plane F2 H7 F6 for structure (2356 – 4). Red contours represent negative values (charge accumulation) and blue contours represent positive values (charge depletion). Intermolecular BCP are marked with a cross.

The interaction energies estimated from the charge density properties do not carry specific information about the nature of the individual energetic contributions, i.e. the ratio of dispersive, electrostatic and repulsive forces contributing to the overall energy.

Experimental charge density can be employed to investigate the electrostatic nature of atom-atom interactions through inspection of the electrostatic potential and electron density gradient fields[212,213]. Charge distribution can be partitioned to different nuclei by identifying the zero-flux surface in the gradient vector field[175,213]. The zero-flux surface for the electron density defines the *ρ*-basin for the corresponding atom to which the electron density is partitioned. The zero-flux surface for the electrostatic potential defines the *v*-basin for the corresponding atom, inside of which the electrons are attracted to the nuclei[214].

Superposition of the electrostatic potential gradient field lines on top of the electron density gradient lines reveals where there is interpenetration of the *ρ*- and *v*-basins. This overlap indicates that part of the electron density associated with one atom falls within the electrostatic potential basin of another. Atom-atom interactions with interpenetration of the *ρ*- and *v*-basins therefore exhibit an electrostatic component in attraction.

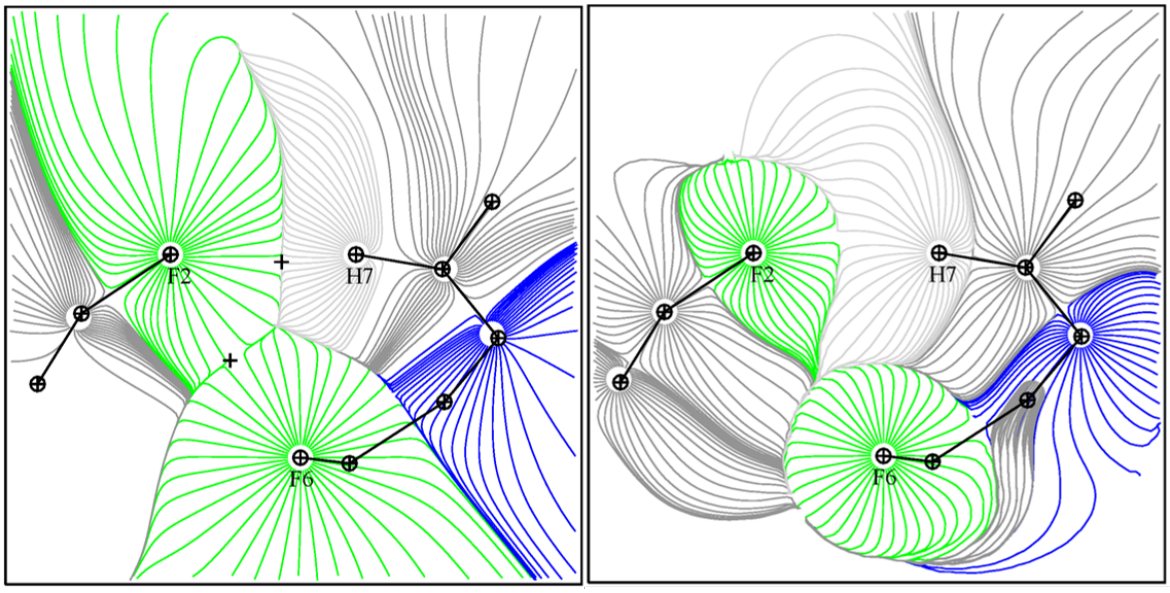

Figure 5.3 Gradient field lines for the electron density (left) and the electrostatic potential (right) in the plane F2 H7 F6 for structure (2356 – 4). The *ρ*-basins and *v*-basins are defined by the boundary of the gradient lines associated with each atom for electron density and electrostatic potential respectively. The gradient lines are coloured according to the corresponding atom: green for F, light grey for H, dark grey for C and dark blue for N. Crosses mark the intermolecular BCPs.

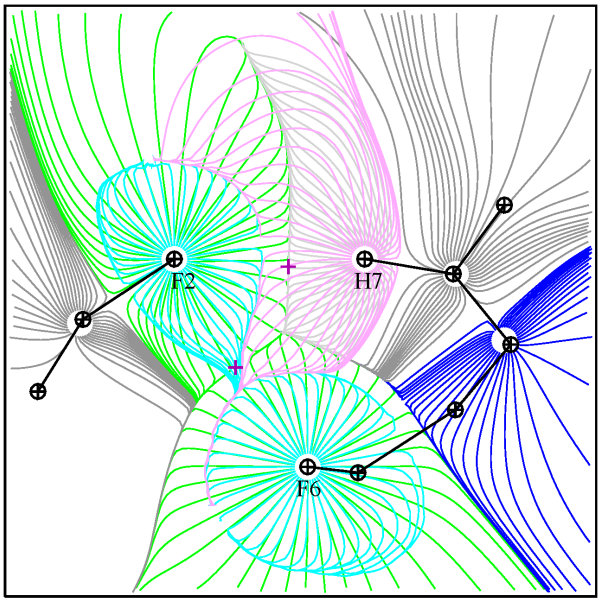

Figure 5.4 Superposition of gradient field lines for the electrostatic potential on top of the electron density in the plane F2 H7 F6 for structure (2356 – 4). The electrostatic potential gradient lines have been coloured differently to distinguish them; turquoise blue for F and pink for H. Crosses mark the intermolecular BCPs.

This methodology was applied to the atom-atom interactions observed in the plane F2 H7 F6 for structure (2356 – 4), Figures 5.3 and 5.4. Inspection of the superimposed gradient field lines reveals substantial interpenetration of the *ρ*-basins and *v*-basins for the F2 ··· H7 interaction. This highlights the importance of the electrostatic component in this interaction. This is consistent with the definition of a hydrogen bond and the Coulombic character is important to the directionality observed in hydrogen bonds. The observation is also consistent with C-F ··· H-C interactions in theoretical studies[144].

The F2 ··· F6 interaction, on the other hand, exhibits a very slight overlap between *ρ*-basins and *v*-basins, one which is interrupted by the electrostatic potential basin of H7. This is indicative of a negligible electrostatic contribution to the interaction. Again this observation is consistent with C-F ··· F-C interactions in theoretical studies[144]. Note this does not invalidate the intermolecular bond path identified between F2 and F6, the formation of bond paths in electron density is not necessarily accompanied by penetration of the atomic basins[212].

A similar picture is observed for the isostructural (246 – 35), Figure 5.5, 5.6 and 5.7. The F2 ··· H7 interaction is weaker but still shows a significant electrostatic component. Whilst the F2 ··· F6 interaction is stronger compared to (2356 – 4), there is no meeting of the *v*-basins for F2 and F6.

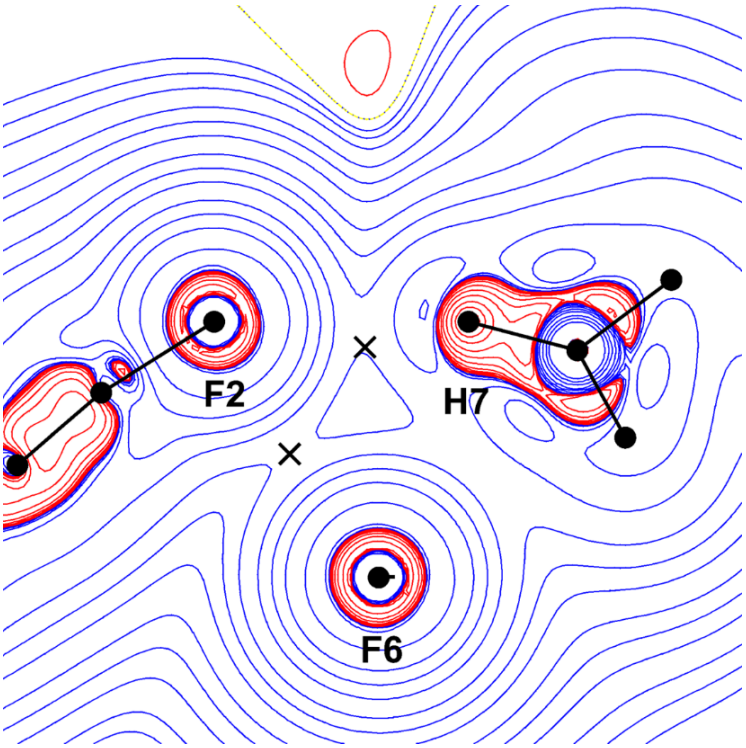

Figure 5.5 Logarithmic Laplacian map in the plane F2 H7 F6 for structure (246 – 35). Red contours represent negative values (charge accumulation) and blue contours represent positive values (charge depletion). Intermolecular BCP are marked with a cross.

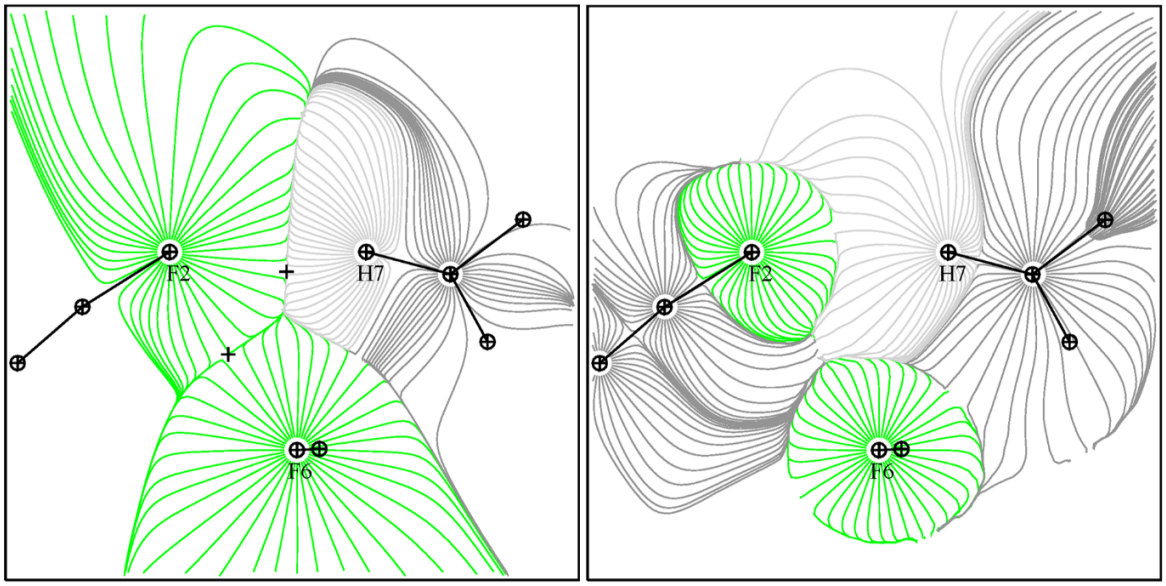

Figure 5.6 Gradient field lines for the electron density (left) and the electrostatic potential (right) in the plane F2 H7 F6 for structure (246 – 35). The *ρ*-basins and *v*-basins are defined by the boundary of the gradient lines associated with each atom for electron density and electrostatic potential respectively. The gradient lines are coloured according to the corresponding atom: green for F, light grey for H and dark grey for C. Crosses mark the intermolecular BCPs.

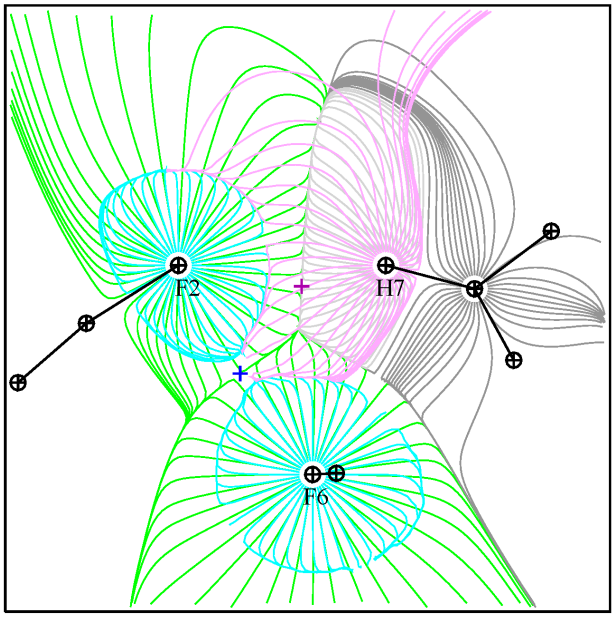

Figure 5.7 Superposition of gradient field lines for the electrostatic potential on top of the electron density in the plane F2 H7 F6 for structure (246 – 35). The electrostatic potential gradient lines have been coloured differently to distinguish them; turquoise blue for F and pink for H. Crosses mark the intermolecular BCPs.

These observations show that the F2 ··· H7 interaction is attractive and has a strong electrostatic component, suggesting a directional character to the bond. This is consistent with speculation of its influence in the crystal assembly of Stacking Group 3 structures. However, the relative importance of this interaction is not known in the context of other forces stabilising the crystal structure as a whole.

For this purpose, the overall lattice energy of the crystal and molecule-molecule energy contributions were calculated using Gavezzotti's PIXEL.

5.1.1.3 Evaluating Contributions through PIXEL Calculations

The PIXEL method calculates molecule-molecule interaction energies broken down into Coulombic, polarisation, dispersion and repulsion contributions as well as the sum of these, which produces the total lattice energy for the crystal and its energetic contributions. The theory behind these calculations is described in detail in Section 2.2.1.

A comparison of the total lattice energy and the calculated BCP energies gives a sense of how significant these interactions are to the total stabilisation of the crystal. The BCP energies suggest that the highlighted atom-atom interactions are attractive but the more important question is whether they are competitive; do they influence the crystal assembly?[208]

The results of PIXEL calculations present the interaction energy between pairwise molecules. These molecule-molecule interaction energies cannot be easily partitioned into individual atom-atom interactions. Often, it is better to avoid such a procedure as the majority of the molecule-molecule stabilisation may have no specific relation to atom-atom features[28,215]. Diffuse molecule-molecule effects will account for a large part of the overall energy, especially in these crystals, which exhibit only weak hydrogen and "halogen-like" bond interactions.

Acknowledging these restrictions, a comparison between the atom-atom BCP energies and their molecule-molecule equivalent can still offer some insight into the nature and role of the atom-atom interactions in the crystal structure.

An initial observation of the total energies suggests that the structures are not only isostructural but also isoenergetic; structure (2356 – 4) has a slightly better stabilisation, predominately arising from better stabilisation between the stacked molecules, Table 5.7 and 5.8. These features will be explored further in Section 5.2, but it is noteworthy that each symmetry equivalent molecule-molecule interaction is energetically similar between the two structures.

Table 5.7 PIXEL calculated energies for structure (2356 – 4) compared against the energies of BCP atom-atom contacts present in the same molecular pair relationships. The column abbreviations represent Coulombic, Polarisation, Dispersion, Repulsion and Total energy contributions. The sum of the BCP interaction energies is denoted "Σ E_{int}". All energies are given in units of kJ mol^{-1}. Not all BCP have been reported here, therefore the sum of the E_{int} values does not include all interactions.

Structure	**Symmetry**	**Coul**	**Pol***	**Disp**	**Rep**	**Total**	**Σ E_{int}**	**Contacts**
2356 – 4	1-x, y-0.5, z+0.5	-14.6	-7.0	-88.4	44.0	-66.0		
	1-x, y+0.5, z+0.5	-14.6	-7.0	-88.4	44.0	-66.0		
	x-1,y,z	-10.1	-4.2	-36.8	17.4	-33.8	-14.00	H7 to F2 F6 to F2 F5 to F3
	x+1,y,z	-10.1	-4.2	-36.8	17.4	-33.8	-14.00	F2 to H7 F2 to F6 F3 to F5
	1-x,1-y,1-z	-4.4	-1.5	-13.5	6.5	-12.9	-12.72	F5 to H4 H4 to F5
	2-x,1-y,1-z	-3.8	-1.4	-11.9	4.7	-12.4	-8.83	F3 to H4 H4 to F3
	-x,y+0.5,0.5-z	-2.5	-0.8	-10.3	2.1	-11.5	-6.31	F6 to H9 F5 to H10
	-x,y-0.5,0.5-z	-2.5	-0.8	-10.3	2.1	-11.5	-6.31	H9 to F6 H10 to F5
	2-x,y+0.5, 0.5-z	-2.3	-0.9	-10.7	2.8	-11.1	-8.47	F3 to H12 F2 to H13
	2-x,y+0.5, 0.5-z	-2.3	-0.9	-10.7	2.8	-11.1	-8.47	H12 to F3 H13 to F2
	1-x,1-y,-z	-3.2	-0.8	-9.5	3.4	-10.1	-9.24	F11 to H12 H12 to F11
	-x,1-y,-z	-2.5	-0.7	-8.3	3.7	-7.8	-9.26	H10 to F11 F11 to H10 F11 to F11
Total		-34.7	-13.4	-182.2	76.1	-154.2	-50.47	

**Total polarisation energy for the crystal structure is calculated by the summation of all molecular polarisations rather than the summation of molecular pair polarisation energies.*

Table 5.8 PIXEL calculated energies for structure (246 – 35) compared against the energies of BCP atom-atom contacts present in the same molecular pair relationships. The column abbreviations represent Coulombic, Polarisation, Dispersion, Repulsion and Total energy contributions. The sum of the BCP interaction energies is denoted "Σ E_{int}". All energies are given in units of kJ mol^{-1}. Not all BCP have been reported here, therefore the sum of the E_{int} values does not include all interactions.

Structure	**Symmetry**	**Coul**	**Pol***	**Disp**	**Rep**	**Total**	**Σ E_{int}**	**Contacts**
246 – 35	1-x,y-0.5,z+1.5	-11.2	-5.4	-79.6	35.7	-60.5		
	1-x,y+0.5,z+1.5	-11.2	-5.4	-79.6	35.7	-60.5		
	x-1,y,z	-7.8	-2.5	-36.2	14.2	-32.2	-11.36	H7 to F2 F6 to F2 F10 to F12
	x+1,y,z	-7.8	-2.5	-36.2	14.2	-32.2	-11.36	F2 to H7 F2 to F6 F12 to F10
	-x,1-y,1-z	-6.8	-1.8	-13.2	8.3	-13.5	-8.25	F4 to H3 H3 to F4 F4 to F4
	-x,y-0.5,1.5-z	-5.4	-1.5	-12.6	6.4	-13.1	-11.49	H9 to F6 F10 to H5
	-x,y+0.5,1.5-z	-5.4	-1.5	-12.6	6.4	-13.1	-11.49	F6 to H9 H5 to F10
	1-x,1-y,1-z	-3.8	-1.4	-13.5	5.6	-13.0	-12.18	F4 to H5 H5 to F4 F4 to F4
	2-x,y-0.5,1.5-z	-4.2	-1.3	-12.3	5.2	-12.6	-9.61	F12 to H3 H13 to F2
	2-x,y+0.5,1.5-z	-4.2	-1.3	-12.3	5.2	-12.6	-9.61	H3 to F12 F2 to H13
	1-x,1-y,2-z	-4.4	-1.1	-11.5	5.9	-11.1	-10.58	F12 to H11 H11 to F12
	2-x,1-y,2-z	-2.3	-0.5	-9.2	3.5	-8.6	-13.94	F10 to H11 H11 to F10
Total		-35.4	-12	-177.2	73.2	-151.3	-55.54	

**Total polarisation energy for the crystal structure is calculated by the summation of all molecular polarisations rather than the summation of molecular pair polarisation energies.*

In both structures, comparison of the two sets of energy calculations reveals that the sum of the atom-atom interaction energy, ΣE_{int}, is uniformly in excess of the Coulombic contribution for the molecule-molecule interaction. This suggests that atom-atom interactions are also composed of other energetic contributions. In some instances it may also reflect an overestimation of the F ··· H interaction energies from the BCP, a problem cited in other studies and not unanticipated for these weak interactions[210,216]. It should also be noted that the C – H bond distances have been normalised for PIXEL calculations, on average making them shorter and increasing the interatomic distance for the F ··· H interactions compared to the coordinates obtained from high resolution data.

In the case of F ··· F interactions, investigation of the gradient field lines suggests there is a negligible electrostatic component. It is likely that these fluorine interactions are driven predominately by dispersive forces[217].

Observation of the different energies also reveals that the molecular pair with the largest sum of the atom-atom interaction energy, ΣE_{int}, does not correspond to the strongest molecule-molecule interaction. This is true even if excluding the two most stabilising molecular pairs, which relate to the aromatic stacking relationship. This reflects the dominant influence of the molecule-molecule diffuse features in these structures.

However, the molecule-molecule relationship which includes the F2 ··· H7 interaction is the next most stabilising contribution to the total crystal lattice energy, after the stacking relationships. Again, this is indicative of an influential role played by the F2 ··· H7 interaction in the crystal assembly of Stacking Group 3 structures.

Additionally, the highest values for Coulombic and polarisation energy contributions are observed in the molecule-molecule relationships related to the aromatic stacking. This suggests electrostatic features between the overlapping rings are more stabilising than any atom-atom interactions and may indicate the presence of the proposed dipole-dipole interactions. These ideas are explored further in Section 5.2.

5.1.2 Structures (34 – 256) and (345 – 26)

The same procedure of identifying likely atom-atom interactions and evaluating their importance in structure determination was applied to the 3D-similar Stacking Group 2 structures (34 – 256) and (345 – 26). In these structures the H7 ··· F2 interaction is absent, as for all the Stacking Group 2 structures, and so this investigation attempts to identify and evaluate alternative atom-atom interactions that may influence the crystal assembly.

5.1.2.1 Identifying Short Contacts

Both structures (34 – 256) and (345 – 26) exhibit fewer short contacts than found in (2356 – 4) and (246 – 35). Structure (345 – 26) only exhibits one true short contact with an interatomic distance shorter than the sum of the van der Waals radii, although the two next closest contacts have been reported in Table 5.10. With the possible exception of H7 ··· F9, the H ··· F short contacts observed in these structures do not exhibit ideal bond geometry; the C – H ··· F angles are far from linear. However, the proximity of the atoms still suggests an attractive interaction, albeit a less directional one.

In contrast, in the F3 ··· F13 short contact in structure (34 – 256) both C – F ··· F angles are very close to 90°, Table 5.9. This mutually orthogonal arrangement has been highlighted as an ideal configuration for "halogen-like" bonding between fluorine atoms[152,155]. This suggests a strongly attractive interaction between these atoms.

Table 5.9 Intermolecular short contacts identified in structure (34 – 256). Symmetry describes the operation relating the two molecules in the intermolecular short contact.

Atom 1	**Atom 2**	**Symmetry**	**Length /Å**	**Length – Van der Waals radii /Å**	**Angle C – H ··· F /°**	**Angle C – F ··· H /°**
H7	F9	-1-x,2-y,-z	2.382	-0.158	163.11	137.03
H10	F13	-1+x,y,z	2.461	-0.079	128.62	130.2
H11	F4	-1+x,y,1+z	2.467	-0.073	123.23	121.89
Atom 1	**Atom 2**	**Symmetry**	**Length /Å**	**Length – Van der Waals radii /Å**	**Angle $C – F_1 ··· F_2$ /°**	**Angle $C – F_2 ··· F_1$ /°**
F9	F13	-1+x,y,z	2.846	-0.054	106.37	159.11
F3	F13	1-x,1-y,-z	2.868	-0.032	87.7	89.81

Table 5.10 Intermolecular short contacts identified in structure (345 – 26). Symmetry describes the operation relating the two molecules in the intermolecular short contact.

Atom 1	**Atom 2**	**Symmetry**	**Length /Å**	**Length – Van der Waals radii /Å**	**Angle C – H ··· F /°**	**Angle C – F ··· H /°**
H12	F5	x,y,z-1	2.423	-0.117	120.70	122.32
H11	F4	-1+x,y,-1+z	2.582	0.042	128.27	126.34
H2	F13	-x,-y,1-z	2.588	0.048	114.73	133.05

5.1.2.1.1 Surface Enrichment

Surface enrichment ratios were also calculated for the molecules in structures (34 – 256) and (345 – 26). Details of the Hirshfeld Contact Surfaces and calculations can be found in the appendices for this chapter.

Table 5.11 Enrichment Ratios for structure (34 – 256).

Atoms	H	C	F
H	0.61	~	~
C	0.41	2.86	~
F	1.67	0.52	0.67

Table 5.12 Enrichment Ratios for structure (345 – 26).

Atoms	H	C	F
H	0.54	~	~
C	0.35	3.08	~
F	1.84	0.30	0.63

The results are similar to those observed for structures (2356 – 4) and (246 – 35), Table 5.3 and 5.4. The H ··· F contacts are highly enriched; the ratio for H ··· F is larger here than in the previous structures and, consequently, the other contacts involving H and F are further 'impoverished' in comparison.

Again, the low ratio for F ··· F seems somewhat counterintuitive given the favourable short contact geometries observed in structure (34 – 256). However, this is the natural consequence of the greater propensity for fluorine to interact with hydrogen and directionality of attractive F ··· F interactions.

Additionally, structures (34 – 256) and (345 – 26) exhibit enriched C ··· C contacts. This indicates the close stacking of aromatic rings in the structure, which is explored in Section 5.2.

5.1.2.2 Identifying Critical Points

As for the previous structures, the charge distribution data for the structures (34 – 256) and (345 - 26) were obtained experimentally from high resolution X-ray diffraction and multipolar refinement. A critical point search of the structures yielded the following intermolecular bond critical points, Table 5.13 and 5.14.

Table 5.13 Intermolecular Bond Critical Points identified in structure (34 – 256).

Contact	**Distance / Å**	***ρ*(r) / *e* Å^{-3}**	**$\nabla^2\rho$(r) / e Å^{-5}**	**G_{cp} / kJ mol^{-1} Bohr^{-3}**	**V_{cp} / kJ mol^{-1} Bohr^{-3}**	**E_{int} / kJ mol^{-1}**
F ··· H						
F9 ··· H7	2.3821	0.04547	0.864	17.49	-11.46	-7.50
F4 ··· H11	2.4673	0.04659	0.813	16.65	-11.15	-7.14
F13 ··· H10	2.4610	0.04164	0.755	15.28	-9.99	-6.56
F12 ··· H11	2.6204	0.04064	0.654	13.39	-8.95	-5.74
F3 ··· H6	2.6866	0.02709	0.492	9.69	-5.99	-4.16
F12 ··· H5	2.7011	0.02620	0.461	9.09	-5.63	-3.90
F4 ··· H5	2.6622	0.01845	0.362	6.97	-4.09	-2.99
F3 ··· H5	2.8362	0.02048	0.351	6.85	-4.14	-2.94
F3 ··· H11	2.7158	0.00770	0.292	5.40	-2.84	-2.32
F9 ··· H2	3.0682	0.00799	0.149	2.81	-1.55	-1.21
F ··· F						
F13 ··· F3	2.8681	0.04850	0.929	18.88	-12.47	-2.44
F13 ··· F9	2.8460	0.03873	0.797	15.87	-10.01	-2.05
F4 ··· F12	2.9838	0.02801	0.574	11.23	-6.83	-1.45
F9 ··· F9	3.0876	0.02268	0.453	8.79	-5.25	-1.13

Table 5.14 Intermolecular Bond Critical Points identified in structure (345 – 26).

Contact	**Distance / Å**	**ρ(r) / *e* Å^{-3}**	**$\nabla^2\rho$(r) / e Å^{-5}**	**G_{cp} / kJ mol^{-1} Bohr^{-3}**	**V_{cp} / kJ mol^{-1} Bohr^{-3}**	**E_{int} / kJ mol^{-1}**
F ··· H						
F5 ··· H12	2.4228	0.06770	0.971	21.15	-15.85	-9.07
F13 ··· H2	2.5885	0.05302	0.630	13.79	-10.40	-5.92
F4 ··· H11	2.5823	0.01666	0.645	12.04	-6.53	-5.17
F3 ··· H12	2.6826	0.03954	0.573	11.84	-8.07	-5.08
F13 ··· H10	2.6458	0.03737	0.540	11.11	-7.52	-4.77
F5 ··· H10	2.6205	0.03454	0.507	10.34	-6.89	-4.44
F3 ··· H6	2.6864	0.03776	0.477	9.99	-6.99	-4.29
F9 ··· H6	2.6355	0.03672	0.427	9.03	-6.42	-3.87
F9 ··· H7	2.7060	0.03742	0.379	8.19	-6.06	-3.51
F9 ··· H2	2.9502	0.02462	0.284	5.8	-3.88	-2.49
F4 ··· H10	2.9960	0.00628	0.262	4.83	-2.51	-2.07
F3 ··· H11	3.0215	0.00895	0.144	2.73	-1.55	-1.17
F ··· F						
F4 ··· F4	3.1645	0.04175	0.294	6.91	-5.82	-0.89

Again, many of the BCPs identified in this critical point search have an interatomic distance significantly longer than the sum of the van der Waals radii, 2.54 Å for F ··· H and 2.90 Å for F ··· F[207]. Consequently, many more atom-atom relationships are highlighted by the critical point search than were found through investigation for short contacts. As for the previous BCP searches, some of these contacts can be dismissed from discussion of influential interactions as they represent such a small stabilising contribution and have unlikely geometries for directing the assembly. For example, in structure (345 – 26) the F3 ··· H11 contact has an elongated interatomic distance, 3.0215 Å, and a small corresponding E_{int}, -1.17 kJ mol^{-1}. Therefore, this interaction is unlikely to be competitive in crystal formation.

Unlike the previous pair of structures, (34 – 256) and (345 – 26) are 3D-similar but non-isostructural. Despite the similar substitution and packing arrangement, the atom-atom interactions highlighted by the critical point search are distinctly different. The most prominent interactions in each structure are also distinct.

Observations of the short contacts in structure (34 – 256) highlighted the F13 ··· F3 interaction as exhibiting a mutually orthogonal arrangement, an ideal geometry for fluorine "halogen-like" interactions. The interaction energy, -2.44 kJ mol^{-1}, estimated from the BCP properties demonstrates the stabilising contribution of this atom-atom interaction, Table 5.13. Whilst lower in estimated energy than the highest F ··· H critical point, there is greater electron density, ρ(r), at the bond critical point for F13 ··· F3. The F13 ··· F3 interaction is the most stabilising F ··· F contact observed in the structures investigated by experimental charge density. The directional nature of the mutually orthogonal arrangement lends this interaction the capacity to be structure directing.

There is also an interaction between the azomethine hydrogen and fluorine, F9 ··· H7, in structure (34 – 256). This is the most stabilising interaction in (34 – 256) according to the estimated interaction energies, -7.50 kJ mol^{-1}. The same interaction is present in (345 – 26). However, the interatomic distance in this relationship is very elongated and the corresponding interaction energy is much lower, -3.51 kJ mol^{-1}.

The most stabilising atom-atom contribution in structure (345 – 26) appears to be the F5 ··· H12 interaction. This was the only contact identified shorter than the sum of the van der Waals radii. The bond geometry for this interaction does not appear to be ideal, Table 5.10, but the associated interaction energy is much higher than any others in the structure, Table 5.14.

These two interactions, F13 ··· F3 in (34 – 256) and F5 ··· H12 in (345 – 26), appear to be the most likely to have a significant influence on the crystal assembly for the respective structures.

5.1.2.2.1 Nature of the F13 ··· F3 Interaction in (34 – 256)

The F13 ··· F3 interaction is a mutually orthogonal type I "halogen-like" interaction. The F13 and F3 atoms are positioned on molecules on different planes, relative to the plane of the aromatic rings. The interacting molecules are related by inversion such that two identical F13 ··· F3 contacts are present in the relationship between the two inter-planar molecules.

Figure 5.8 presents the Laplacian map for one instance of the F13 ··· F3 interaction, alongside an illustration of the location of the short contacts in the context of the molecular pair involved.

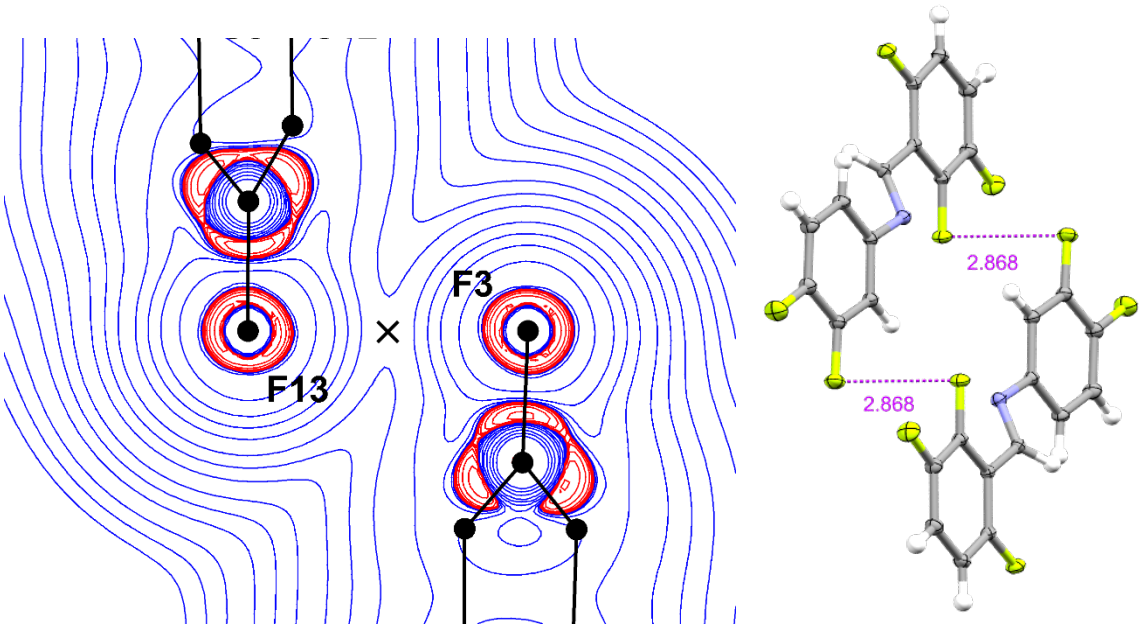

Figure 5.8 Left: Logarithmic Laplacian map in the plane F13 F3 C3 for structure (34 – 256). Red contours represent negative values (charge accumulation) and blue contours represent positive values (charge depletion). Intermolecular BCPs are marked with a cross. Right: Depiction of the (34 – 256) molecular dimer for this interaction with inter-planar F13 ··· F3 short contact distances labelled, units of Å.

The electron density and electrostatic potential gradient field lines were also examined and compared, Figure 5.9 and 5.10.

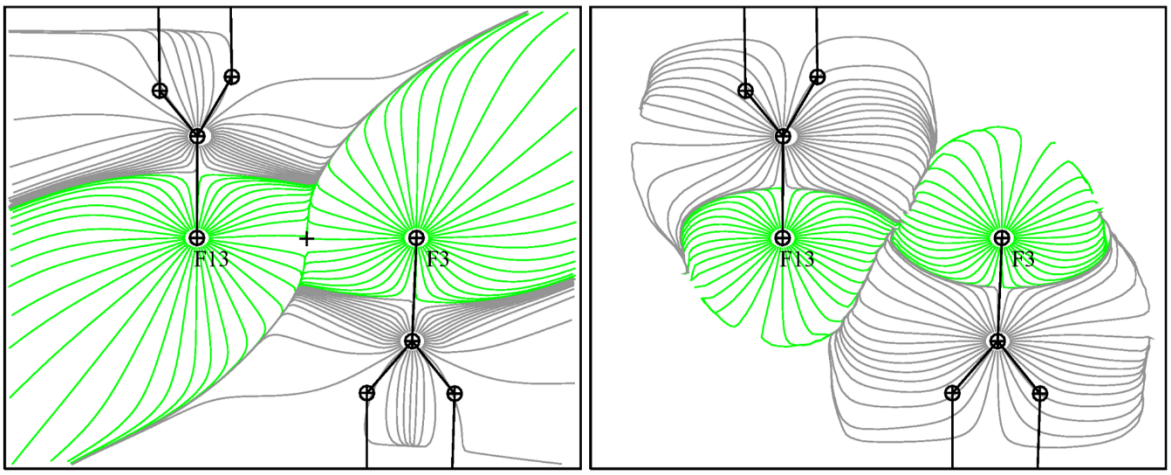

Figure 5.9 Gradient field lines for the electron density (left) and the electrostatic potential (right) in the plane F13 F3 C3 for structure (34 – 256). The *ρ*-basins and *v*-basins are defined by the boundary of the gradient lines associated with each atom for electron density and electrostatic potential respectively. The gradient lines are coloured according to the corresponding atom: green for F and dark grey for C. Crosses mark the intermolecular BCPs.

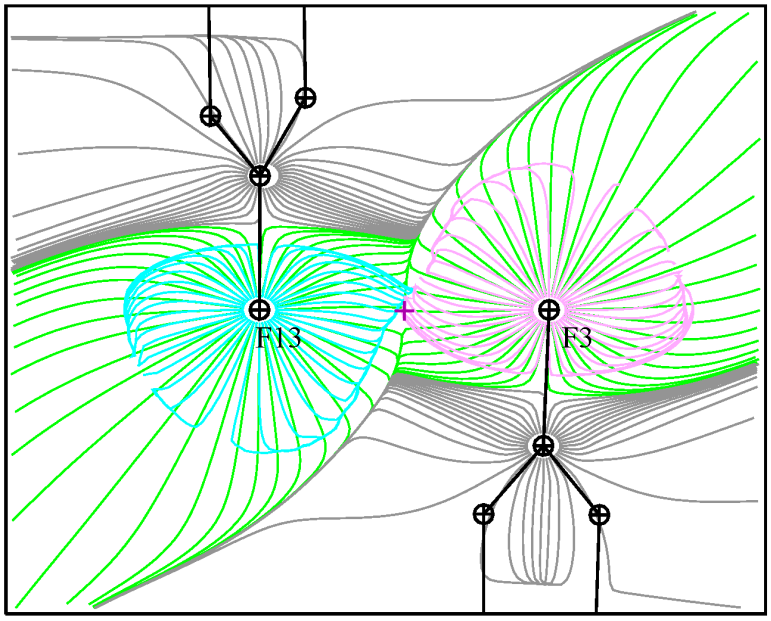

Figure 5.10 Superposition of gradient field lines for the electrostatic potential on top of the electron density in the plane F13 F3 C3 for structure (34 – 256). The electrostatic potential gradient lines have been coloured differently to distinguish them; turquoise blue for F13 and pink for F3. Crosses mark the intermolecular BCPs.

The boundaries of *ρ*-basins and *v*-basins coincide exactly at the bond critical point for the F13 ··· F3 interaction, suggesting that the electrostatic contribution to the interaction is negligible. Although, there is slight interpenetration of the electrostatic potential adjacent to the critical point.

5.1.2.2.2 Nature of F5 ··· H12 in (345 – 26)

The F5 ··· H12 interaction is the most stabilising atom-atom contribution in structure (345 – 26). While this interaction is the only short contact identified which was shorter than the sum of the van der Waals radii, the bond geometry of C – H ··· F is far from linear, 120.70°, Table 5.10.

A cursory inspection of the Laplacian of electron density map reveals a geometrically more favourable arrangement between H12 and F4, in which the C – H ··· F angle is much closer to linear, Figure 5.11. However, the interatomic distance for H12 and F4 is much larger, 2.753 Å, and no BCP is identified between them. It is unclear why the F5 ··· H12 distance is optimised rather than the F4 ··· H12, perhaps due to repulsion from other non-bonded adjacent atoms such as H11 or the loss of other preferable interaction arrangements.

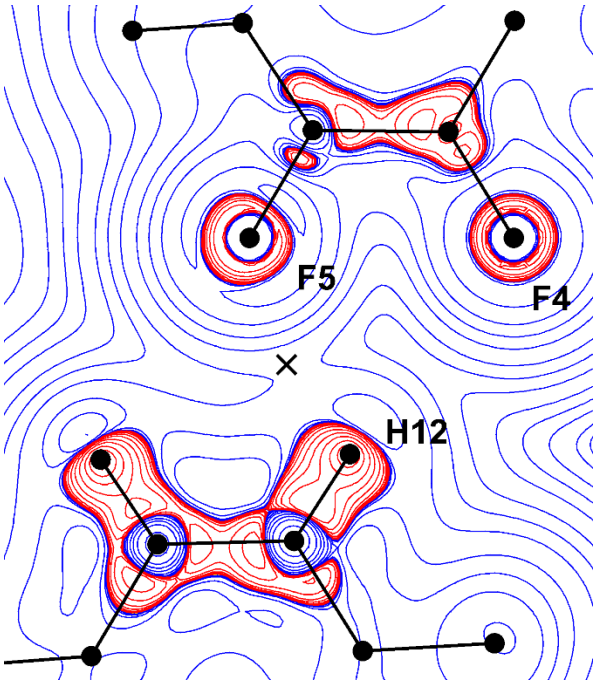

Figure 5.11 Logarithmic Laplacian map in the plane F5 H12 F4 for structure (345 – 26). Red contours represent negative values (charge accumulation) and blue contours represent positive values (charge depletion). Intermolecular BCPs are marked with a cross.

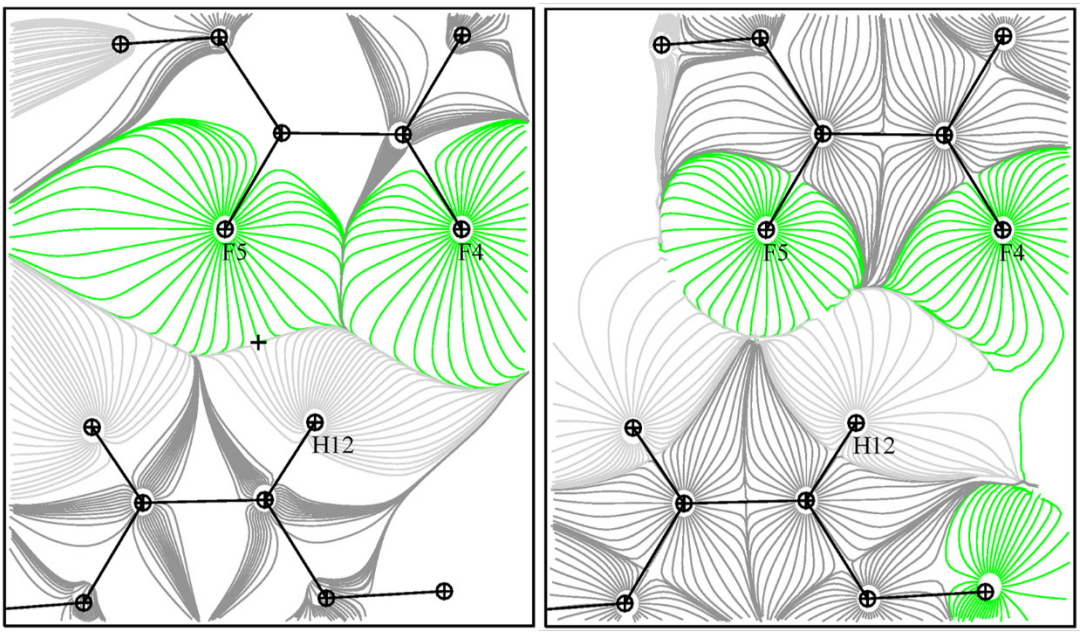

Figure 5.12 Gradient field lines for the electron density (left) and the electrostatic potential (right) in the plane F5 H12 F4 for structure (345 – 26). The *ρ*-basins and *v*-basins are defined by the boundary of the gradient lines associated with each atom for electron density and electrostatic potential respectively. The gradient lines are coloured according to the corresponding atom: green for F, light grey for H and dark grey for C. Crosses mark the intermolecular BCPs.

The directionality of hydrogen bonds is associated with their electrostatic character. Therefore, the geometry of this interaction suggests it has a lesser electrostatic contribution compared to stronger hydrogen bonds. The electron density and electrostatic potential gradient field lines were compared to investigate the electrostatic component of the interaction, Figure 5.12 and 5.13.

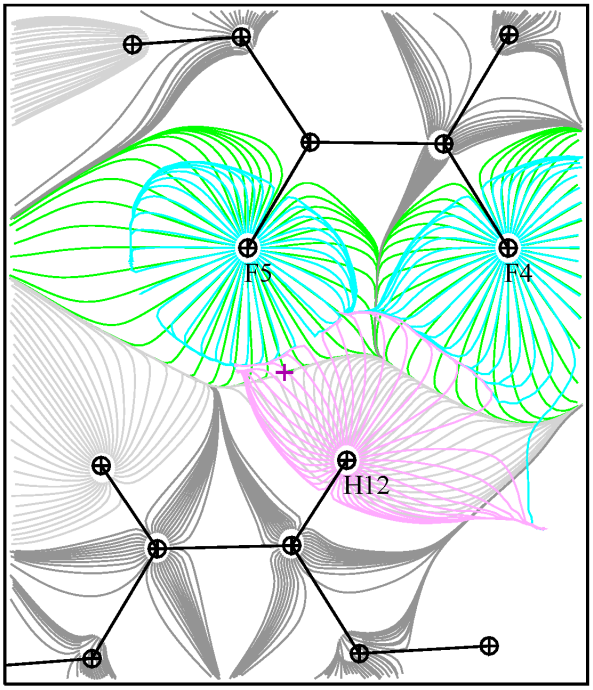

Figure 5.13 Superposition of gradient field lines for the electrostatic potential on top of the electron density in the plane F5 H12 F4 for structure (345 – 26). The electrostatic potential gradient lines have been coloured differently to distinguish them; turquoise blue for F and pink for H. Crosses mark the intermolecular BCPs.

The superposition of the two gradient field lines shows that the F5 ··· H12 interaction still exhibits some electrostatic component but the overlap between the *ρ*-basins and *v*-basins is only small. By contrast there is a large penetration of H12 electrostatic potential into the F4 *ρ*-basin. However, the atoms are significantly separated and there is no BCP identified between them.

The minimal electrostatic character of F5 ··· H12 is consistent with the non-ideal bond geometry. This lack of directing ability means that it is unlikely that the F5 ··· H12 interaction is an influential determinant for the crystal structure. Despite its relative stabilisation strength this atom-atom interaction does not appear to be a competitive synthon in crystal assembly.

5.1.2.3 Evaluating Contributions through PIXEL Calculations

Again, a comparison of the total lattice energy and the calculated BCP energies gives a sense of how significant these interactions are to the total stabilisation of the crystal. The comparison of

the atom-atom and molecule-molecule interactions highlights the differences between these structures, Table 5.15 and 5.16.

Table 5.15 PIXEL calculated energies for (34 – 256) compared against the energies of BCP atom-atom contacts present in the same molecular pair relationships. The column abbreviations represent Coulombic, Polarisation, Dispersion, Repulsion and Total energy contributions. The sum of the BCP interaction energies is denoted "Σ E_{int}". Energies given in units of kJ mol^{-1}. Not all BCP have been reported here, therefore the sum of the E_{int} values does not include all interactions.

Structure	**Symmetry**	**Coul**	**Pol***	**Disp**	**Rep**	**Total**	**Σ E_{int}**	**Contacts**
34 – 256	-x,2-y,-z	-17.7	-7.0	-93.8	45.3	-73.3		
	-x,1-y,-z	-13.1	-5.5	-78.7	33.7	-63.5		
	1-x,1-y,-z	-11.2	-3.7	-36.8	14.4	-37.3	-4.78	F3 to F13 F13 to F3
	-x-1,2-y,-z	-5.9	-2.8	-28.7	12.7	-24.7	-16.14	F9 to H7 H7 to F9 F9 to F9
	x-1,y,z	-4.9	-1.6	-20.8	7.4	-20.0	-16.90	H10 to F13 H6 to F3 H5 to F3 F9 to H2 F9 to F13
	x+1,y,z	-4.9	-1.6	-20.8	7.4	-20.0	-16.90	F13 to H10 F3 to H6 F3 to H5 H2 to F9 F13 to F9
	-x,1-y,1-z	-5.3	-1.3	-13	5.7	-13.9	-11.49	F12 to H11 H11 to F12
	x-1,y,z+1	-6.1	-1.7	-11.4	5.9	-13.3	-7.14	F4 to H11
	x+1,y,z-1	-6.1	-1.7	-11.4	5.9	-13.3	-7.14	H11 to F4
	-x,2-y,-z-1	-4.5	-0.8	-8.3	2.3	-11.3	-5.93	F4 to H5 H5 to F4
	x,y,z-1	1.6	-0.5	-7.1	2.0	-4.1	-5.35	H5 to F12 F4 to F12
	x,y,z+1	1.6	-0.5	-7.1	2.0	-4.1	-5.35	F12 to H5 F12 to F4
Total		-35.7	-12.7	-181.6	72.3	-157.7	-49.80	

**Total polarisation energy for the crystal structure is calculated by the summation of all molecular polarisations rather than the summation of molecular pair polarisation energies.*

Table 5.16 PIXEL calculated energies for (345 – 26) compared against the energies of BCP atom-atom contacts present in the same molecular pair relationships. The column abbreviations represent Coulombic, Polarisation, Dispersion, Repulsion and Total energy contributions. The sum of the BCP interaction energies is denoted "Σ E_{int}". All energies are given in units of kJ mol^{-1}. Not all BCP have been reported here, therefore the sum of the E_{int} values does not include all interactions.

Structure	**Symmetry**	**Coul**	**Pol***	**Disp**	**Rep**	**Total**	**Σ E_{int}**	**Contacts**
345 – 26	1-x,1-y,1-z	-16.5	-6.4	-94.7	44.4	-73.2		
	1-x,-y,1-z	-10.4	-3.8	-75.8	29.5	-60.5		
	2-x,1-y,1-z	-7.7	-1.7	-25.2	7.4	-27.2	-23.63	F5 to H10 H10 to F5 F9 to H6 H6 to F9 F9 to H7 H7 to F9
	-x,-y,1-z	-8.6	-2.3	-25.6	9.7	-26.8	-21.99	F13 to H2 H2 to F13 F3 to H12 H12 to F3
	x-1,y,z	0.3	-1.1	-17.9	3.6	-15.1	-11.54	F13 to H10 F3 to H6 H2 to F9
	x+1,y,z	0.3	-1.1	-17.9	3.6	-15.1	-11.54	H10 to F13 H6 to F3 F9 to H2
	x,y,z-1	-4.5	-1.5	-11.9	6.7	-11.2	-9.07	F5 to H12
	x,y,z+1	-4.5	-1.5	-11.9	6.7	-11.2	-9.07	H12 to F5
	x-1,y,z-1	-4.0	-0.8	-7.8	2.4	-10.3	-5.17	F4 to H11 F4 to H10 F3 to H11
	x+1,y,z+1	-4.0	-0.8	-7.8	2.4	-10.3	-5.17	H11 to F4 H10 to F4 H11 to F3
	-x,-y,-z	0.1	-0.3	-8.3	0.9	-7.7	-0.89	F4 to F4
	2-x,1-y,2-z	1.1	-0.7	-7.6	1	-6.2		
Total		-27.9	-10.1	-168.2	59.1	-147.1	-52.27	

**Total polarisation energy for the crystal structure is calculated by the summation of all molecular polarisations rather than the summation of molecular pair polarisation energies.*

As observed in the previous pair of structures, comparison of the molecule-molecule energies and the sum of atom-atom energies indicates an overestimation of the F ··· H interaction from BCP calculations. Again, it should be noted that the C – H bond distances have been normalised for PIXEL calculations.

Identification of the critical points revealed that despite their 3D similar structural relationship and similar substitution patterns, (34 – 256) and (345 – 26) exhibit very different energies for equivalent atom-atom interactions. This is carried forward to the molecule-molecule relationships.

Symmetry equivalent molecule-molecule relationships are consistently more stabilising for structure (34 – 256). For example, the symmetry relationship (x-1, y, z) has a total stabilisation energy of -20.0 kJ mol^{-1} in (34 – 256), and the equivalent symmetry relationship in (345 – 26), (x+1, y, z), has a total energy of -15.1 kJ mol^{-1}, Table 5.15 and 5.16. This is consistent with the higher overall crystal lattice energy for (34 – 256).

The most notable exception to this trend is the molecule-molecule relationship associated with the F5 ··· H12 interaction in (345 – 26). The relationship is favourable for (345 – 26), -11.2 kJ mol^{-1}, but the equivalent in (34 – 256) has a destabilising Coulombic contribution despite an attractive H5 ··· F12 interaction, Table 5.15 and 5.16.

Whilst more favourable than its (34 – 256) equivalent, this molecule-molecule relationship is less stabilising than might be expected given that it is associated with the strongest atom-atom interaction in (345 – 26), F5 ··· H12. This is largely due to a lack of dispersion energy as the molecules are end-to-end with little surface contact. However, the electrostatic contribution of the atom-atom interaction is still insufficient to elevate the stabilisation of this molecule arrangement; it cannot be considered a structure determining interaction. This is consistent with evaluation of the gradient field lines, Figure 5.12.

By contrast, the most favourable molecule-molecule relationships in structure (34 – 256), excluding the stacking interactions, correspond to the atom-atom interactions thought most likely to be structure determining, F13 ··· F3 and F9 ··· H7.

The relatively high molecule-molecule stabilisation energy associated with the F13 ··· F3 contact invites further investigation of the atom-atom contribution. In the inter-planar arrangement of the molecules only the periphery atoms, F and H, are making surface contact with the interacting molecule. This suggests that while the main contribution to the molecule-molecule stabilisation is dispersion, a substantial amount of this could be attributed to the F13 ··· F3 interaction and it is possible that F··· F interactions may be underestimated by the BCP calculations.

5.1.3 Structures (234 – 25), (24 – 25) and (4 – 25)

Structures (234 – 25), (24 – 25) and (4 – 25) form head-to-head aromatic stacks and belong to Stacking Group 1. They were identified in the structural similarity analysis, Section 4.3.3.2, as being of note due to the similarity between both structure and fluorine substitution pattern. Structures (234 – 25) and (24 – 25) were found to be isostructural while (4 – 25) was 2D similar to them. It was proposed that the F2 atom has greater influence on the structural arrangement than the F3 atom as the absence of the F3 does not significantly change the crystal packing. Whereas, the removal of F2 produces the structurally less similar (4 – 25).

These observations are strongly indicative, but without evidence of attractive non-covalent interactions they are not sufficient to confirm the directing ability of F2 in atom-atom interactions. For this purpose, geometrically determined short contacts and PIXEL calculations of molecule-molecule energies have been compared to infer the presence of attractive interactions involving F2 and other possible directing interactions in the structures.

In these investigations it was not possible to collect high resolution X-ray diffraction data and perform charge density calculations to evaluate the atom-atom contributions, due to unsuitable crystal quality. Instead, this section demonstrates the extent to which standard resolution experiments can be employed with semi-empirical calculation methods to identify non-covalent interactions.

5.1.3.1 Identifying Short Contacts

The isostructural (234 – 25) and (24 – 25) exhibit the same four notable short contacts as one another. The interatomic distances vary such that different contacts are likely to be the most attractive in each structure, but the bond geometries are very similar, Table 5.17 and 5.18.

Table 5.17 Intermolecular short contacts identified in structure (234 – 25). Symmetry describes the operation relating the two molecules in the intermolecular short contact.

Atom 1	Atom 2	Symmetry	Length /Å	Length – Van der Waals radii /Å	Angle C – H ··· F /°	Angle C – F ··· H /°
F2	H5	0.5+x,-y,0.5+z	2.503	-0.037	139.9	124.6
F12	H7	0.5+x,-y,0.5+z	2.54	0.000	158.5	112.7
F12	H6	0.5+x,1-y,0.5+z	2.551	0.011	165.5	119.5
F4	H11	x,y-1,z-1	2.572	0.032	125.6	127.8

Table 5.18 Intermolecular short contacts identified in structure (24 – 25). Symmetry describes the operation relating the two molecules in the intermolecular short contact.

Atom 1	**Atom 2**	**Symmetry**	**Length /Å**	**Length – Van der Waals radii /Å**	**Angle C – H ··· F /°**	**Angle C – F ··· H /°**
F12	H7	0.5+x,-y,0.5+z	2.467	-0.073	157.4	110.5
F4	H11	x,y-1,z+1	2.478	-0.062	134.5	137.6
F12	H6	0.5+x,-1-y,0.5+z	2.505	-0.035	168.2	124.1
F2	H5	0.5+x,-y,0.5+z	2.602	0.062	142.3	124.1

In contrast, structure (4 – 25), which is 2D similar to (234 – 25) and (24 – 25), has only one short contact in common, F4 ··· H11, Table 5.19.

Table 5.19 Intermolecular short contacts identified in structure (4 – 25). Symmetry describes the operation relating the two molecules in the intermolecular short contact.

Atom 1	**Atom 2**	**Symmetry**	**Length /Å**	**Length – Van der Waals radii /Å**	**Angle C – H ··· F /°**	**Angle C – F ··· H /°**
F4	H5	0.5-x,y-0.5,0.5-z	2.529	-0.011	166	116
F9	H6	1.5-x,y-0.5,0.5-z	2.570	0.030	167	119
F4	H11	-1+x,1+y,z	2.590	0.050	128	128
F12	H11	2-x,1-y,-z	2.632	0.092	117	126
F9	H7	1.5-x,y-0.5,0.5-z	2.654	0.114	160	115

The F2 atom, which has been highlighted as a possible structural influence in structures (234 – 25) and (24 – 25), participates only in the F2 ··· H5 short contact.

In structure (4 – 25), in the absence of F2, H5 is seen to participate in a new short contact with F4. While the contact F4 ··· H11 is still observed, there appears to be a shift in bond preference carried through the remaining contacts. It is possible these slight shifts in preference, originating from the absence of F2, are responsible for the different molecular arrangement in the (4 – 25) crystal compared to (234 – 25) and (24 – 25).

This proposal for the importance of F2 in (234 – 25) and (24 – 25) relies on the assumption that these interactions are attractive and structure directing, particularly in the case of the F2 ··· H5 short contact.

5.1.3.2 Evaluating Contributions through PIXEL Calculations

Although it has not been possible to collect high resolution X-ray diffraction data for this set of structures, the results of PIXEL analysis provide specific molecule-molecule energies to which atom-atom relationships can be assigned. As previously emphasised, molecule-molecule energies cannot be partitioned wholly into atom-atom contributions, but they can be used to estimate the relative stabilising influence of the different interactions. In particular, the Coulombic contribution can be used as a measure of electrostatic forces present; these are usually associated with directional intermolecular bonds such as hydrogen bonds.

Table 5.20 PIXEL calculated energies for (234 – 25). The column abbreviations represent Coulombic, Polarisation, Dispersion, Repulsion and Total energy contributions. All energies are given in units of kJ mol^{-1} and distance in Å.

Structure	Symmetry	Distance	Coul	Pol*	Disp	Rep	Total	Contacts
234 – 25	x,y-1,z	3.755	-4.5	-4.5	-80.8	32.7	-57.0	
	x,y+1,z	3.755	-4.5	-4.5	-80.8	32.7	-57.0	
	x+0.5,-y,z+0.5	6.807	-12.5	-5.3	-37.2	20.2	-34.8	F2 to H5 F12 to H7
	x-1,-y,z-1	6.807	-12.5	-5.3	-37.2	20.2	-34.8	H5 to F2 H7 to F12
	x-1,1-y,z-1	7.809	-4.3	-1.7	-16.1	6.6	-15.5	H6 to F12
	x+0.5,1-y, z+0.5	7.809	-4.3	-1.7	-16.1	6.6	-15.5	F12 to H6
	x,y-1,z-1	13.244	-4.0	-1.2	-10.0	4.5	-10.7	F4 to H11
	x,y+1,z+1	13.244	-4.0	-1.2	-10.0	4.5	-10.7	H11 to F4
	x-1,-y,z+0.5	10.609	-2.7	-0.6	-8.9	1.6	-10.5	
	x+0.5,-y,z-1	10.609	-2.7	-0.6	-8.9	1.6	-10.5	
	x,y,z-1	12.701	-0.7	-0.6	-7.0	1.5	-6.9	
	x,y,z+1	12.701	-0.7	-0.6	-7.0	1.5	-6.9	
	x-1,-y-1,z-1	7.739	1.1	-0.3	-5.6	0.4	-4.4	
	x+0.5,-y-1, z+0.5	7.739	1.1	-0.3	-5.6	0.4	-4.4	
	x-1,-y-1,z+0.5	11.229	-0.6	-0.2	-2.9	0.2	-3.5	
	x+0.5,-y-1,z-1	11.229	-0.6	-0.2	-2.9	0.2	-3.5	
Total			-25.4	-11.2	-176.3	67.8	**-152.4**	

Table 5.21 PIXEL calculated energies for (24 – 25). The column abbreviations represent Coulombic, Polarisation, Dispersion, Repulsion and Total energy contributions. All energies are given in units of kJ mol^{-1} and distance in Å.

Structure	Symmetry	Distance	Coul	Pol*	Disp	Rep	Total	Contacts
24 – 25	x,y-1,z	3.778	-5.6	-4.6	-81.6	36.1	-55.7	
	x,y+1,z	3.778	-5.6	-4.6	-81.6	36.1	-55.7	
	x+0.5,-y,z+0.5	6.897	-12.2	-4.9	-36.0	18.8	-34.3	F2 to H5 F12 to H7
	x-1,-y,z-1	6.897	-12.2	-4.9	-36.0	18.8	-34.3	H5 to F2 H7 to F12
	x-1,-y,z+0.5	10.188	-3.3	-1.3	-15.4	5.0	-15.1	
	x+0.5,-y,z-1	10.188	-3.3	-1.3	-15.4	5.0	-15.1	
	x-1,1-y,z-1	7.899	-4.6	-1.7	-14.2	5.9	-14.6	H6 to F12
	x+0.5,1-y, z+0.5	7.899	-4.6	-1.7	-14.2	5.9	-14.6	F12 to H6
	x,y,z-1	12.87	-2.3	-0.9	-8.6	2.8	-8.9	
	x,y,z+1	12.87	-2.3	-0.9	-8.6	2.8	-8.9	
	x-1,1-y,z+0.5	10.841	-2.1	-0.4	-6.5	1.2	-7.8	
	x+0.5,1-y,z-1	10.841	-2.1	-0.4	-6.5	1.2	-7.8	
	x,y-1,z+1	13.414	-3.5	-1.2	-7.5	4.7	-7.5	F4 to H11
	x,y+1,z-1	13.414	-3.5	-1.2	-7.5	4.7	-7.5	H11 to F4
	x-1,1-y,z-1	7.830	0.5	-0.3	-5.3	0.3	-4.8	
	x+0.5,1-y, z+0.5	7.830	0.5	-0.3	-5.3	0.3	-4.8	
Total			-32.5	-12.8	-183.2	74.8	**-157.0**	

**Total polarisation energy for the crystal structure is calculated by the summation of all molecular polarisations rather than the summation of molecular pair polarisation energies.*

The results of PIXEL analysis suggest that the short contacts observed in structures (234 – 25) and (24 – 25) are attractive, Table 5.20 and 5.21. The stabilising molecule-molecule relationships are indicative of the associated short contacts being attractive interactions.

In both structures, the molecular relationships with the highest Coulombic contribution correspond to either the aromatic stacking relationship or molecular pairs with atom-atom close contacts between them. In the case of the F2 ··· H5 and F12 ··· H7 interactions the Coulombic contribution is greater for this molecule-molecule interaction than the aromatic stacking

relationship. This indicates a competitive interaction occurring between these molecules and supports the proposed importance of the F2 atom to this structural arrangement.

While the molecular interaction between the stacking molecules is still the most stabilising, the Coulombic and total energy contribution is significantly less compared to the aromatic stacking relationship observed in the Head-to-Tail structures (2356 – 4), (246 – 35), (34 – 256) and (345 – 26). This is discussed further in Section 5.2.2.

5.1.4 Concluding Remarks

A combination of different methods and calculations have been employed to investigate and evaluate intermolecular atom-atom interactions in these crystal structures.

5.1.4.1 Competitive Weak Hydrogen Bonds

Across the structures investigated in this section, evidence suggests that F ··· H interactions have a stabilising effect on the crystal structure: geometric analysis highlights a number of short contacts; surface enrichment ratios indicate the presence of more F ··· H contacts than predicted by chance; charge density analysis identifies bond critical points between F and H.

However, energetically strong interactions are not always competitive[208]. Lo Presti compared a series of polymorphic structures with weak hydrogen bonds and found that, while C – H ··· F interactions provide a stabilising contribution, they are not conserved between polymorphs[157].

The qualifiers used to identify an attractive atom-atom interaction cannot distinguish whether it is structurally influencing or the result of other stabilising forces, such as close-packing or minimisation of repulsive contacts. Assessment of the directionality provides some insight into the directing and structure determining capacity of an interaction. More directional F ··· H contacts were initially highlighted through inspection of the bond geometry. The F2 ··· H7 interaction observed in (2356 – 4) and (246 – 35) has a close to linear bond geometry which is preferable for hydrogen bonds. The F5 ··· H12 interaction exhibits less directionality and has a C – H ··· F bond angle of 120.7 Å, Table 5.22.

Table 5.22 Intermolecular short contacts and their geometries.

Structure	**Atom 1**	**Atom 2**	**Length /Å**	**Length – Van der Waals radii /Å**	**Angle C – H ··· F /°**	**Angle C – F ··· H /°**
(2356 – 4)	H7	F2	2.262	-0.278	165.82	144.27
(246 – 35)	H7	F2	2.408	-0.132	165.25	142.60

(345 – 26)	H12	F5	2.423	-0.117	120.70	122.32

Directionality in weak hydrogen bonds can also be assessed through comparison of the electron density and electrostatic potential gradient vector field lines. This was performed for the F ··· H interactions listed in Table 5.22. This revealed the significant electrostatic character of the F2 ··· H7 interaction in both (2356 – 4) and (246 – 35), a property associated with the directionality of hydrogen bonds, Section 5.1.1.2.1. Despite being an energetically strong interaction, the F5 ··· H12 contact did not demonstrate strong directionality. While there was some interpenetration of the *ρ*-basins and *v*-basins at the BCP, the overlap was not as significant as observed in the previous structures, Section 5.1.2.2.2.

The structure determining nature of the F2 ··· H7 interaction is also substantiated by observing its persistent presence in the majority of Stacking Group 3 structures. The F2 ··· H7 interaction is conserved across a number of similar structures, including the polymorphs (2356 – 4) and (2356 – 4 II).

5.1.4.2 Fluorine ··· Fluorine Interactions

Attractive F ··· F interactions were also identified in this analysis. While their surface enrichment ratios were reduced due to F ··· H interactions, short contacts were suggestive of stabilising bonds and bond critical points were observed between F atoms.

The F13 ··· F3 interaction exhibited strong directionality as well as favourable stabilisation energy. It was highlighted as a possible structure determinant. PIXEL calculations were used in the analysis in addition to the BCP energies. The F13 ··· F3 interaction coincided with a strongly stabilising molecule-molecule relationship. Observation of the molecular arrangement suggests that a substantial part of the stabilisation energy could be attributed to the F13 ··· F3 contact, which is thought to be dispersive in nature[217].

5.1.4.3 PIXEL Calculations in Atom-Atom Analysis

For the last set of structures, (234 – 25), (24 – 25) and (4 – 25), PIXEL calculations were the only source of energetic data. For these structures, the proposed atom-atom interactions also coincided with stabilising molecule-molecule relationships. The presence of favourable F ··· H short contacts correlated well with the scale of Coulombic contribution to the molecule-molecule stabilisation energy.

However, in all instances, the largest contribution to the overall lattice energy came from the stacked molecule relationship. The aromatic stacking is the most influential intermolecular interaction in the observed structures.

The extent and influence of aromatic stacking on the crystal assembly can be explored further through PIXEL analysis as well as experimental charge distribution observations.

5.2 Aromatic Overlap

The aromatic stacking interaction between phenyls and fluorophenyls is usually very favourable, and has been successfully used as a supramolecular synthon in a number of crystal design strategies[74,75,86,92,95,118,120–124,218], Section 1.2.2.4. The attraction between aromatic rings can be augmented by halogenation of the ring[219].

Surface enrichment ratios show that C ··· C contacts have high enrichment in halogenated aromatic structures compared to unsubstituted aromatics[188,208]. This demonstrates a smaller plane separation between rings and therefore a stronger interaction, revealing the greater affinity for aromatic stacking when electronegative substituents are present.

Differing rationalisations are put forward to explain this interaction enhancement. These different models are described in more detail in Section 1.2.2. The substituents' effect on the π-electron distribution is often cited as the main factor in the improved interaction. However, more recent studies, and the findings of this work, suggest that it is the direct interaction of substituents with the other ring which have the greatest influence on the aromatic stacking.

In addition to the geometric analysis of plane separation and translation distances, the strength of aromatic stacking can be experimentally assessed through investigation of the charge distribution. The identification of cage critical points, (CCP) (3, +3), between aromatic rings indicate the presence of an intermolecular interaction relating to the rings. The electron density, ρ, at the CCP can be used as an estimate of interaction strength[219].

Aromatic stacking interactions in these structures have also been investigated through semi-empirical PIXEL calculations. These calculations provide a stabilisation energy for individual molecule-molecule pairs, so the stacked pairs of aromatic ring-containing molecules can be isolated and their specific energies assessed. The energy is divided into separate contributions: Coulombic, polarisation, dispersion and repulsion. It is known that dispersion is the main contributor to the attraction between aromatic rings[88,91]. However, the smaller electrostatic component is highly orientation dependant, and so, the interplay of these contributors produces the directionality observed in aromatic ring stacking. PIXEL analysis reveals these relationships.

Following the direct substituent interaction model, substituent effects are broadly additive[115]. Consequently, the effect of increased substitution and different fluorine placement should be observable through analysis of the PIXEL energy contributions.

Full data for the PIXEL calculations for each structure analysed are provided in the appendices.

5.2.1 Head-to-Tail Overlap

Anti-parallel head-to-tail overlap is the most frequently observed arrangement of molecules in the fluoroaniline structural library. This arrangement promotes the direct electrostatic attraction between F and the opposing ring by juxtaposing fluorine and hydrogen atoms.

The electrostatic contributions from these direct interactions are additive. As such, a strong aromatic overlap, with a large Coulombic contribution, is expected for structures with an optimal number of juxtaposing F and H atoms and a minimal number of non-bonded proximal F atoms ('F clashes'). These conditions describe the complementary set of structures, outlined in Section 4.3.6.

PIXEL analysis was performed on the complementary structures, as well as a couple of crystals with similar but distinct structures for comparison. The complementary structures consist of a selection of different head-to-tail overlap types, Stacking Group 2, 3 and 4, as well as an anomalous grid structure. Analysis of this set provides insight into the characteristics of the different stacking groups as well as strong complementary overlaps. In all cases the stacking molecule-molecule relationship is the largest contributor to the overall crystal lattice energy.

5.2.1.1 Stacking Group 2

Stacking Group 2 structures exhibit two aromatic overlap molecule-molecule relationships, one nearer and one farther, as detailed in the geometric analysis, Section 4.2.2.2. PIXEL calculations confirm that the nearer relationship has a greater associated stabilisation energy. As expected, the dispersion contributes the most to the total energy but there is a significant Coulombic contribution arising from the direct substituent interactions. For the closer aromatic stacking molecules in Stacking Group 2, the average total energy equals -73.2 kJ mol^{-1} and the average Coulombic energy equals -16.8 kJ mol^{-1}. These molecule-molecule energies are reported in Appendix E.1.1.

The most attractive aromatic overlap in Stacking Group 2 was observed for structure (0 – 23456). Both molecule-molecule relationships have a large stabilisation energy and the Coulombic contribution is significant despite a slightly elongated molecule separation, Table 5.23. This enhanced interaction may be the result of the influence of the fluorine substituents on the π-electron density.

Table 5.23 PIXEL molecule-molecule pair energy for aromatic overlap in structure (0 – 23546), Stacking Group 2.

Structure	Distance / Å	Coulombic / kJ mol^{-1}	Polarisation / kJ mol^{-1}	Dispersion / kJ mol^{-1}	Repulsion / kJ mol^{-1}	Total / kJ mol^{-1}
0 – 23456	4.123	-18.3	-7.7	-89.8	42.3	-73.6
	4.188	-16.2	-7.6	-86.3	39.1	-71.1

Although direct interactions between the substituent on the overlapping rings are considered the primary force influencing aromatic stacking behaviour, the polarising effect of electronegative substituents will still have some influence on the electron distribution.

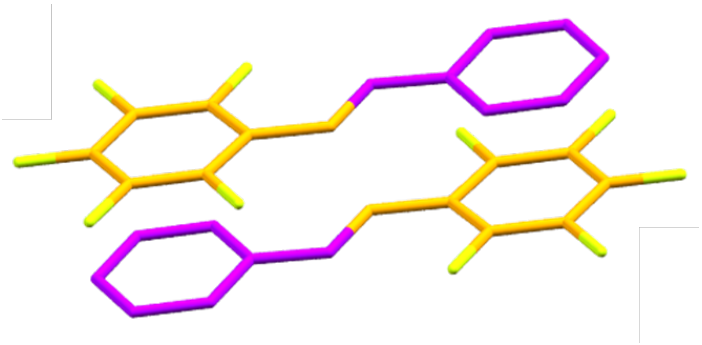

Figure 5.14 Near aromatic stacking relationship in (0 – 23456).

Structures (0 – 23456) and (23456 – 0) have the most polarised substitution patterns – the greatest difference between fluorination number on the opposing rings. The electron withdrawing nature of fluorine will deplete some π-electron density from the substituted aromatic ring, while the unsubstituted ring will remain unaffected. The additional attraction afforded by the interaction of 'electron-poor' and 'electron-rich' aromatic faces is less compared to the direct interactions. However, the effect is most exaggerated for these two structures and an increase in electrostatic attraction is suggested by the greater Coulombic contribution in both, Table 5.23 and 5.24.

Table 5.24 PIXEL molecule-molecule pair energy for aromatic overlaps in (23456 – 0), Stacking Group 4.

Structure	Distance / Å	Coulombic / kJ mol^{-1}	Polarisation / kJ mol^{-1}	Dispersion / kJ mol^{-1}	Repulsion / kJ mol^{-1}	Total / kJ mol^{-1}
23456 – 0	3.965	-16.0	-7.8	-89.7	44.3	-69.1
	4.400	-17.5	-7.8	-91.1	45.6	-70.9

	3.965	-16.0	-7.8	-89.7	44.3	-69.1
	4.400	-17.5	-7.8	-91.1	45.6	-70.9

5.2.1.2 Stacking Group 3

Stacking Group 3 structures only exhibit one unique molecule-molecule aromatic overlap relationship, as depicted in geometric analysis, Section 4.2.2.3. Similar to Stacking Group 2 complementary structures, dispersion factors contribute the most to the total energy but there is a significant Coulombic contribution. The average Coulombic and total energy for the Stacking Group 3 aromatic stacking relationships is lower than the average for the close Stacking Group 2 relationships. The average total energy equals -63.7 kJ mol^{-1} and the Coulombic energy contribution is -13.1 kJ mol^{-1}. These molecule-molecule energies are reported in Appendix E.1.1.

While lower than Stacking Group 2, the Coulombic contribution is still substantial for the complementary structures. The F and H atom juxtaposition is maximised in these structures, optimising the potential direct substituent interactions with the opposing ring.

Comparison between the isostructural (2356 – 4) and the non-complementary (2356 – 0) reveals a loss of overlap attraction and elongated molecule separation distance for (2356 – 0), Table 5.25. This suggests a significant difference in the attraction arising from the absence of just one F and H juxtaposition. However, the stabilisation energy for (2356 – 0) is not too dissimilar to other complementary structures, such as (246 – 35), which is also isostructural with (2356 – 0). Therefore, it is difficult to disambiguate the different influences on the aromatic stack molecule-molecule relationship.

Table 5.25 PIXEL molecule-molecule pair energy for aromatic overlaps in structures (2356 – 4) and (2356 – 0), Stacking Group 3.

Structure	**Distance / Å**	**Coulombic / kJ mol^{-1}**	**Polarisation / kJ mol^{-1}**	**Dispersion / kJ mol^{-1}**	**Repulsion / kJ mol^{-1}**	**Total / kJ mol^{-1}**
2356 – 4	3.873	-14.6	-7.0	-88.4	44.0	-66.0
	3.873	-14.6	-7.0	-88.4	44.0	-66.0
2356 – 0	4.176	-12.0	-6.2	-81.8	38.2	-61.8
	4.176	-12.0	-6.2	-81.8	38.2	-61.8

5.2.1.3 Directionality of the Head-to-Tail Overlap

Anti-parallel head-to-tail overlap is evidently a strongly attractive aromatic stacking interaction. In part this is due to the significant electrostatic component of the interaction, arising from the presence of fluorine substituents. This electrostatic character influences the directionality of the aromatic stacking relationship, increasing the propensity for rings to adopt this head-to-tail configuration.

However, there are some notable exceptions. Structure (4 – 2356) adopts a Grid arrangement of molecules. Despite the complementary substitution pattern, (4 – 2356) forms shifted parallel stacks, Figure 5.15.

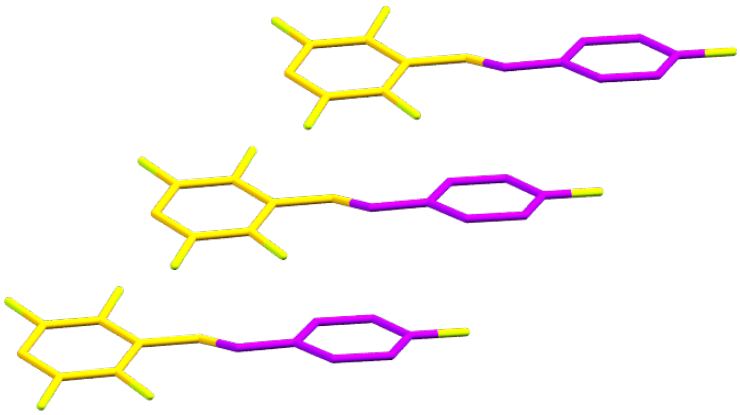

Figure 5.15 Stacking in Grid structure (4 – 2356).

Stacks in Grid arrangements exhibit simultaneous elongated parallel head-to-head and parallel head-to-tail relationships between the adjacent molecules. These relationships are largely dismissed due to the large separation; they seem unlikely to participate in aromatic overlap interactions. Regardless of the large translation distance, the plane separation for the head-to-tail configuration is actually quite favourable for interaction, 3.279 Å. The geometric data is presented in Appendix C.4.

The stacking molecule-molecule relationship is certainly much diminished compared to the other complementary structures, but it is still the most stabilising interaction in the (4 – 2356) structure owing to the high dispersion, Table 5.26. In this structure the directionality of the anti-parallel head-to-tail aromatic stacking is outweighed by other directing influences, producing this Grid arrangement. Other molecule-molecule relationships in the structure have a small Coulombic energy contribution. This indicates the presence of possible atom-atom interactions, which may be supporting the Grid arrangement.

Table 5.26 PIXEL molecule-molecule pair energy for stacking molecules in (4 – 2356), Grid structure.

Structure	Distance / Å	Coulombic / kJ mol^{-1}	Polarisation / kJ mol^{-1}	Dispersion / kJ mol^{-1}	Repulsion / kJ mol^{-1}	Total / kJ mol^{-1}
4 – 2356	4.695	-6.3	-5.2	-75.2	34.6	-52.0
	4.695	-6.3	-5.2	-75.2	34.6	-52.0

There is still a small Coulombic contribution to the stacking molecule-molecule energy, suggesting the presence of some electrostatic attraction between the aromatic rings. It seems likely that this influence comes from the elongated head-to-tail relationship. However, similar values of Coulombic contribution are observed for the head-to-head aromatic overlap relationships in Stacking Group 1 structures. It is unclear where this electrostatic component originates from.

5.2.2 Head-to-Head Overlap

5.2.2.1 Stacking Group 1

While Stacking Group 1 is well populated in the structural library, geometric analysis indicates that parallel head-to-head overlap is not as energetically favourable as head-to-tail aromatic overlap. Specifically, Stacking Group 1 overlap relationships exhibit a larger plane separation than expected given the lateral translation. This suggests the introduction of additional plane separation to mitigate the repulsive effect of non-bonded fluorine atoms in close proximity. Consequently, the interaction between the aromatic rings is expected to be less attractive in comparison to head-to-tail interactions.

The PIXEL-calculated molecule-molecule pair energies, between head-to-head aromatic stacks, support this conclusion. The average total energy and average Coulombic energy contribution is significantly lower than any of the Head-to-Tail stacking types observed. The average total energy is -55.8 kJ mol^{-1} and the average Coulombic contribution is -5.5 kJ mol^{-1}. The molecule-molecule overlap energies of the analysed structures are reported in Appendix E.1.2.

The molecule-molecule pair energy for aromatic overlap in structure (4 – 25) has been reported in Table 5.27 as a good approximation of an average Stacking Group 1 structure. As expected, the vast majority of the stabilisation is from dispersive forces between the stacked molecules. A lower Coulombic contribution was also expected, reflecting the reduced electrostatic attraction. There is still some Coulombic energy observed in the aromatic stacking interaction. This contribution is similar in scale to the Coulombic energy observed in parallel stacked fluorobenzene[19].

Table 5.27 PIXEL molecule-molecule pair energy for aromatic overlap in (4 – 25).

Structure	Distance / Å	Coulombic / kJ mol^{-1}	Polarisation / kJ mol^{-1}	Dispersion / kJ mol^{-1}	Repulsion / kJ mol^{-1}	Total / kJ mol^{-1}
4 – 25	3.747	-5.7	-4.3	-78.1	33.7	-54.5
	3.747	-5.7	-4.3	-78.1	33.7	-54.5

Both the dispersion and repulsion contributions to the head-to-head aromatic interaction are also lower than the head-to-tail stacks. This is rationalised by considering the increased centroid separation and translation distance. Although it should be noted that the distance reported by PIXEL (the distance between the molecules' centre of mass) and the plane separation are comparable to head-to-tail structures.

In parallel head-to-head configurations there is no additional attractive electrostatic energy afforded by a closer arrangement of molecules, as there is no juxtaposition of F and H atoms. Instead, the crystal assembly prioritises the minimisation of repulsion between stacked molecules.

The propensity for some crystals to adopt Stacking Group 1 arrangements rather than head-to-tail arrangements is the result of both minimising repulsion and stabilising contributions from non-stacked molecule pairs and atom-atom interactions in the overall crystal structure.

For some substitution patterns a head-to-tail orientation of the rings would produce the same number of juxtaposed F atoms as a head-to-head orientation, and therefore the same amount of repulsion. The Visual Packing Matrix, Section 4.1.2, and the Overlap Matrix, Section 4.2.7, show that molecules with identical substitution of fluorine on both rings adopt predominately Head-to-Head overlap. This suggests that these arrangements produce more thermodynamically favourable structures than the head-to-tail equivalent.

On average, the total crystal lattice energy is more stabilising for Stacking Group 1 structures than Stacking Group 2 or 3. This stabilisation is derived from diffuse molecule-molecule interactions of non-stacked adjacent molecules, evidenced by the high total dispersion contribution. Additionally, some Coulombic stabilisation energy may also be the product of atom-atom interactions, as examined in Section 5.1.3.2.

The overall crystal lattice energies and energetic contributions for these structures are reported in Appendix E.2.

5.2.2.2 Anti-parallel Head-to-Head Overlap

In addition to parallel configurations, anti-parallel head-to-head aromatic ring stacking is observed in the Interwoven structures, as well as unusual structures such as (234 – 34) and the 'brickwork' structures (23 – 25) and (25 – 25).

These arrangements were highlighted in the geometric analysis section as evidence of the direct substituent interaction model taking precedence over the π-polarisation model, Section 4.2.7.2.

The π-polarisation model asserts that all head-to-head configurations of the aromatic rings will be similarly or less electrostatically attractive than head-to-tail configurations. In head-to-head overlap configurations the electrostatic potential above the interacting rings will be the same, as they have the same number of fluorine substituents.

Conversely, the direct substituent interaction model suggests that identical aromatic rings could interact favourably via electrostatic interaction, provided that favourable direct interactions are still available. In parallel head-to-head stacks the substituted fluorine atoms are necessarily juxtaposed with their equivalents on the opposing ring. However, in anti-parallel head-to-head stacks the conformation may allow the juxtaposition of F and H atoms of the overlapping rings, leading to an attractive interaction.

Structure (234 – 34) exhibits anti-parallel head-to-head interactions, which were highlighted in Section 4.2.7.2 as appearing to be electrostatically attractive, Figure 5.16. Molecule-molecule interaction energies can be calculated using PIXEL to substantiate these assertions and compare the relative stabilisation afforded by different overlap configurations.

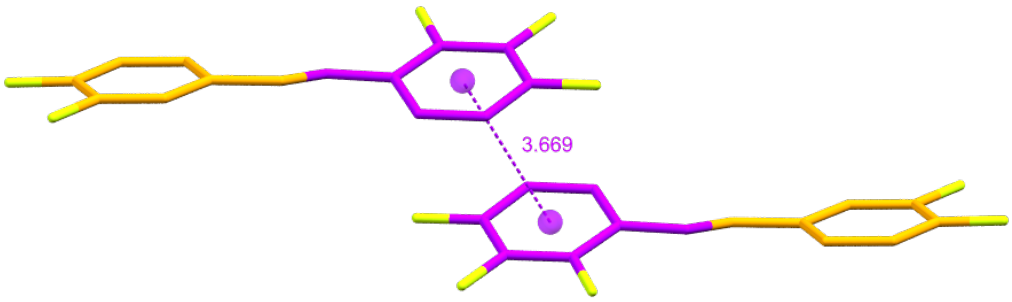

Figure 5.16 Anti-parallel head-to-head offset overlap motif in structure (234 – 34). Centroid separation distances are given in units of Å.

PIXEL calculations were performed on the Interwoven structures, (4 – 236) and (234 – 24), the brickwork structure (23 – 25) and structure (234 – 34). The molecule-molecule overlap energies of

the analysed structures are reported in Appendix E.1.3. These results were also compared against the energies calculated for parallel head-to-head aromatic stacking.

For the purpose of comparison, the average of the energy contributions for the head-to-tail stacks observed in these structures and the parallel head-to-head stacks from the previous data set have been halved in order to represent the stabilisation offered by one aromatic ring interaction. This approach does not account for the diffuse molecule-molecule features likely to be present between stacked molecules. However, it is a sufficient approximation to compare the average stabilisation energy from the different aromatic ring configurations.

These calculations reveal that, on average, the anti-parallel head-to-head configuration is more energetically favourable than parallel head-to-head configurations, Table 5.28. The Coulombic contribution for anti-parallel is approximately twice that seen in the parallel arrangement. This electrostatic component indicates the presence of attractive direct substituent interactions between the overlapping rings. The dispersion contribution is also slightly improved in the anti-parallel arrangement as the centroid separation and translation distances are shorter. This is likely to be the result of decreased repulsion; F atoms are not forced into close proximity.

Table 5.28 PIXEL molecule-molecule energies for different overlap types in Stacking Group 1, Interwoven structures and other anti-parallel head-to-head structures. The results are averaged per aromatic ring.

Overlap Relationship	**Coulombic / kJ mol^{-1}**	**Polarisation / kJ mol^{-1}**	**Dispersion / kJ mol^{-1}**	**Repulsion / kJ mol^{-1}**	**Total / kJ mol^{-1}**
Parallel H-t-H	-2.7	-2.2	-39.9	17.0	-27.9
Anti-Parallel H-t-H	-5.5	-3.1	-44.1	18.3	-34.4
H-t-T by inversion	-6.2	-2.9	-41.9	18.2	-32.8

Similar average stabilisation energies are observed for the anti-parallel head-to-head and the anti-parallel head-to-tail configurations in these structures. The Coulombic attraction is slightly more favourable in the head-to-tail arrangement, but the dispersion component is stronger in the head-to-head arrangement.

These two different configurations are often observed together in the same structure, such as in the Interwoven structures. This is consistent with the similarity of their molecule-molecule energies for the interacting aromatic rings. The two configurations form co-operatively rather than competitively in the crystal assembly.

This is a small data set, but the results are illustrative of the influence of direct substituent interactions in electrostatic attraction between the rings.

As with atom-atom interactions, PIXEL molecule-molecule energies are used to infer the presence of direct interactions and quantify the energetic contributions. However, to confirm individual direct substituent interactions and the strength of aromatic ring interactions it is useful to return to charge density analysis.

5.2.3 Investigating Aromatic Interactions through Charge Density

5.2.3.1 Direct Substituent Interactions

The direct interactions between the fluorine substituents and the opposite stacked aromatic ring appear to be identified in the charge distribution data obtained for the Stacking Group 2 structures (34 – 256) and (345 – 26). In 2011, Wheeler described the substituent effects as arising from "direct interactions of the substituent with the proximal vertex of the other ring"[115]. In the closest stacking dimer of both (34 – 256) and (345 – 26), bond critical points are observed between fluorine substituents and the nearest carbon atom of the opposite ring, i.e. the proximal vertex.

In structure (345 – 26), these BCP are observed between the para position fluorine, F4, and C11 of the opposing ring, Figure 5.17. Similarly, BCP are observed between F13 and C6 of opposing rings in structure (34 – 256).

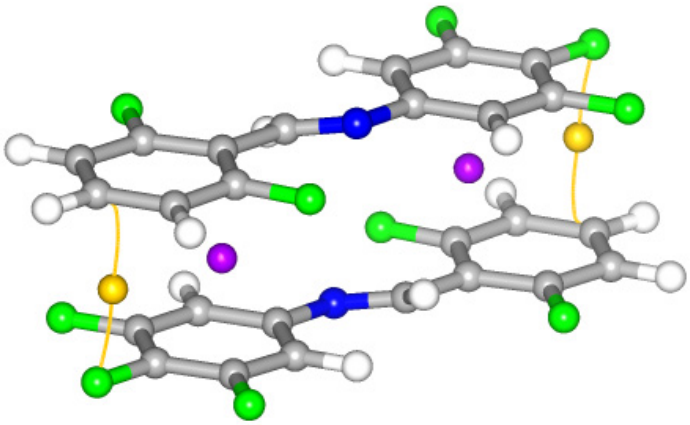

Figure 5.17 Selected critical points in the aromatic interaction in structure (345 – 26). Orange spheres and bond paths represent bond critical points in direct substituent interactions. Purple spheres represent the cage critical points between the rings.

Table 5.29 Bond critical point properties for direct substituent interactions between aromatic rings in structures (345 – 26) and (34 – 256).

Interaction	**Atomic Distance / Å**	**ρ(r) / *e* Å^{-3}**	**$\nabla^2\rho$(r) / e Å^{-5}**	**G_{BCP} / kJ mol^{-1} Bohr^{-3}**	**V_{BCP} / kJ mol^{-1} Bohr^{-3}**
345 – 26					
F4 ··· C11	3.3493	0.02806	0.326	6.73	-4.58
C11 ··· F4	3.3493	0.02798	0.327	6.74	-4.58
34 – 256					
F13 ··· C6	3.3842	0.02891	0.383	7.80	-5.18
C6 ··· F13	3.3842	0.02891	0.383	7.80	-5.18

The direct substituent bond critical point properties indicate the presence of a small but not insignificant stabilising interaction, Table 5.29. The results suggest that the substituent effects are slightly stronger for structure (34 – 256), however, this does not necessarily reflect the total strength of the aromatic ring interaction.

Aromatic ring interactions can also be characterised by the electron density at cage critical points (CCP) observed between the rings.

5.2.3.2 Cage Critical Points

Cage critical points (CCP) are found at a local minimum in the electron-density distribution; all curvatures are positive (3, +3). Analysis of the electron density, $\rho(rCCP)$, and the Laplacian of electron density, $\nabla^2\rho(rCCP)$, at a cage critical point between rings can be used to examine and indicate the strength of an aromatic stacking interaction[219,220].

Cage critical points are observed between the aromatic rings in the close-stacked dimer relationships in both structures (34 – 256) and (345 – 26). These two inter-ring interactions appear to be the strongest in the structures studied through high resolution X-ray diffraction. Cage critical points were not readily identified between rings in the other aromatic ring arrangements.

In structure (345 – 26) two CCPs were identified between the dimer rings, Figure 5.17. In structure (34 – 256) four CCPs were identified, each of the CCPs seems to correspond to one of the rings in

the slipped stack arrangement, Figure 5.18. The electron density and Laplacian associated with each CCP is reported in Table 5.30.

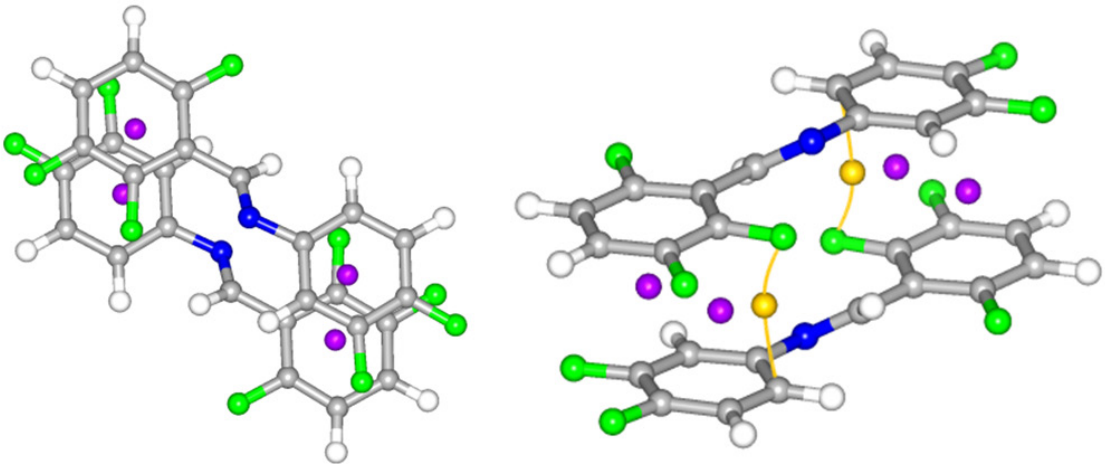

Figure 5.18 Selected critical points in the aromatic interaction in structure (34 – 256). Left: Top-down view to demonstrate the position of the CCP. Right: side view to demonstrate position of the BCP. Orange spheres and bond paths represent bond critical points (BCP) in direct substituent interactions. Purple spheres represent the cage critical points (CCP) between the rings.

Table 5.30 Cage critical point properties for inter-ring critical points. The critical point code labels correspond to the critical point data file for the different structures, provided in the appendices.

CCP	$\rho(r)$ / e Å^{-3}	$\nabla^2\rho(r)$ / e Å^{-5}
345 – 26		
cp185	0.0248	0.2997
cp301	0.0248	0.2997
34 – 256		
cp29	0.0282	0.3305
cp118	0.0282	0.3305
cp283	0.0306	0.3514
cp331	0.0306	0.3515

The greater charge density at the CCP indicates that the aromatic ring interaction in the close dimer of (34 – 256) is stronger than the interaction in (345 – 26).

This result is not reflected in the total energy for the molecule-molecule pair calculated with PIXEL, Table 5.31. However, the Coulombic contribution is greater for structure (34 – 256), which is consistent with the stronger direct substituent interactions and aromatic stacking interaction.

Table 5.31 PIXEL molecule-molecule energies for the close-stacked aromatic interaction dimer in structures (34 – 256) and (345 – 26).

Structure	**Distance / Å**	**Coulombic / kJ mol^{-1}**	**Polarisation / kJ mol^{-1}**	**Dispersion / kJ mol^{-1}**	**Repulsion / kJ mol^{-1}**	**Total / kJ mol^{-1}**
34 – 256	3.350	-17.7	-7.0	-93.8	45.3	-73.3
345 – 26	3.398	-16.5	-6.4	-94.7	44.4	-73.2

Charge distribution analysis of the stacked molecules has revealed that structure (34 – 256) seems to participate in a stronger aromatic interaction than (345 – 26). This is not immediately obvious from the PIXEL molecule-molecule energy, as structure (345 – 26) has a greater dispersion contribution; resulting in a similar total molecule-molecule stabilisation. This increased dispersion appears to arise from better surface contact of the stacked molecules rather than from strictly aromatic interaction, as demonstrated by the enriched C ··· C short contacts reported in Section 5.1.2.1.1.

Charge distribution analysis is valuable in disentangling these sources of interaction. The results here are in good agreement with the direct substituent interaction model and suggest a strong directionality in the formation of substituted aromatic ring interactions. However, these features were only identifiable in the closest aromatic stacks observed. It is not possible to perform this analysis on more separated, or weaker, aromatic stacking arrangements in order to make a comparison.

5.2.4 Aromatic Stacking versus Total Lattice Energy

For each case analysed using PIXEL, the most stabilising molecule-molecule relationship in the structure invariably includes the overlap of aromatic rings (near-overlap in the case of the Grid structure).

Stacking Group 2 dimers and the stacking in structure (23456 – 0) exhibit the strongest aromatic overlap interactions, according to PIXEL calculations, Appendix E.1. However, Stacking Group 2 structures have the lowest average total lattice energy of the different structural groups analysed, Appendix E.2. The average stabilisation energy for the aromatic stack interactions of the different

structural groups were compared against the average total lattice energies. An inverse relationship was revealed between aromatic interaction strength and overall lattice energy, Table 5.32.

Table 5.32 Averaged energies for aromatic overlap and total lattice energy from PIXEL calculations for different structural groups. Structures (0 – 23456) and (23456 – 0) have been excluded, as well as structures with more than one overlap type present. Standard deviation between structures is reported in brackets alongside the average values. The number of structure members in each averaged group is reported as *N*.

	Aromatic Overlap		**Lattice**	***N***
Structural Group	**Coulombic / kJ mol^{-1}**	**Total / kJ mol^{-1}**	**Total / kJ mol^{-1}**	
Stacking Group 2	-14.4 (0.8)	-68.8 (1.7)	-150.6 (5.0)	3
Stacking Group 3	-13.1 (1.5)	-63.7 (2.5)	-152.2 (2.2)	6
Stacking Group 1	-5.45 (0.6)	-55.8 (0.9)	-156.9 (3.1)	4
Grid	-4.95 (1.4)	-51.8 (0.3)	-160.8 (2.8)	2
Angled Overlap	-8.25 (0.5)	-48.1 (0.8)	-165.5 (1.2)	2

The observations suggest that, while aromatic interactions are strongly stabilising, their formation may hinder the crystal structure from adopting a more thermodynamically optimal packing arrangement.

The structural groups with strong overlap relationships also have large Coulombic contributions, reflecting the directional nature of the aromatic stacking and the presence of direct substituent interactions between the rings. An exception to this is the structures belonging to the Angled Overlap group. They exhibit a significant Coulombic contribution although the total aromatic overlap energy is the lowest observed. The weak total overlap energy is the result of limited surface contact between the overlapping molecules, which are only in contact at one face of the molecule, Figure 5.19.

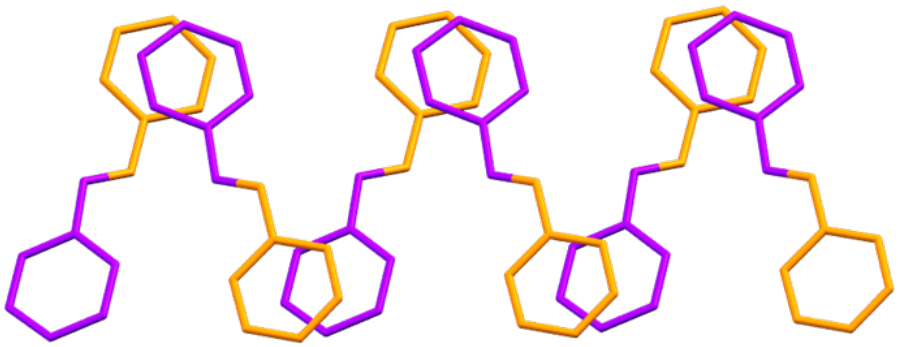

Figure 5.19 Archetype representation of the Angled Overlap structures.

The Angled Overlap arrangement allows the aromatic rings to form favourable aromatic overlap interactions, juxtaposing the F and H atoms, while also reducing the molecule-molecule interactions by limiting the surface contact between them. Divergence from strict stacks may offer the Angled Overlap structures more flexibility in the later stages of crystal assembly, which results in a better total stabilisation.

These observations suggest that, like strong hydrogen bonds, favourable aromatic stacking interactions are structure directing but do not necessarily lead to the most thermodynamically stable crystal structure.

These calculations were only performed on a small number of structures, a larger sample of structures from across the groups would be useful in substantiating these observations and revealing any additional relationships between aromatic stacking relationships and the overall crystal stabilisation.

It should also be noted that these comparisons of the calculated lattice energies do not consider the energetic influence of different intramolecular geometries exhibited by the fluoroaniline molecules, which may be associated with additional destabilisation in the system.

5.2.5 Concluding Remarks

A combination of PIXEL calculations, charge distributions analysis and geometric data have been used to assess the influence and behaviour of aromatic overlap interactions in these crystal structures.

5.2.5.1 Evidence for the Direct Substituent Interaction Model

The geometric analysis highlighted structure (234 – 34) and other examples of anti-parallel head-to-head overlap as evidence of direct substituent interactions between the rings. The favourable electrostatic component of these arrangements relies on direct substituent interactions between

rings because the electrostatic potential of the rings is necessarily the same. The attractive nature of these interactions was confirmed by PIXEL calculations. The stabilisation from the Coulombic contribution was comparable to the stabilisation observed in equivalent head-to-tail stacking overlaps, Table 5.28. This strongly supports the direct substituent interaction model.

Additionally, charge distribution analysis provides evidence of bond critical points between fluorine substituents and the nearest carbon atom in the opposing ring, i.e. the proximal vertex. This is described further in Section 5.2.3.1.

These observations provide experimental evidence to support the direct substituent interaction model. The π-polarisation still influences the interactions to a lesser extent, but the influence of the direct substituent interactions is foremost in the electrostatic contribution to aromatic stack formation.

5.2.5.2 Directionality of Aromatic Stacking

Direct substituent interactions have been shown to control the main electrostatic component of aromatic stacking interactions. Therefore, they have a significant influence on the directionality of the aromatic stacking. Slipped stacking geometries are observed in the categorised stacking groups. Charge density analysis of Stacking Group 2 structures (345 – 26) and (34 – 256) showed that the slipped stacks positioned F substituents above a “vertex” of the opposing ring, here bond critical points were observed between the substituent and the interacting aromatic ring.

The dispersive component of aromatic interactions promotes the planar arrangement of rings, increasing molecule-molecule contact. Preferably, a molecule should align with both rings of an opposing molecule to maximise contact; however, some substitution patterns will lead to a juxtaposition of F atoms in these ‘column stacking’ arrangements. In these instances, offset and angled overlap arrangements may be favoured to reduce repulsion.

Reliable prediction of aromatic overlap type, based on the substitution pattern, would make these aromatic interactions more viable as supramolecular synthons in crystal engineering. However, observations suggest a complex interrelationship of different structure directing kinetic and thermodynamic influences.

Chapter 6 Conclusions and Recommendations for Further Research

6.1 Conclusions

6.1.1 Summary of Work

The aim of the work presented in this thesis is to improve experimental-based understanding of aromatic stacking interactions augmented by fluorine substitution. For this purpose, a select structural database of systematically fluorinated benzylideneanilines was constructed. These structures were categorised and analysed by a number of methods.

Initial categorisation grouped structures with visually similar packing arrangements and centred on the aromatic ring overlap. These stacking groups were further categorised through geometric analysis of the aromatic overlap relationships. A number of varied overlap types were identified and characterised.

These results suggested a relationship between the fluorine substitution pattern and the observed aromatic arrangements. However, a more refined comparison of structural similarity was required to draw associations between the substitution pattern and the structural arrangement of the overall crystal structure. Therefore, spatial similarity analysis was performed with the XPac program. This analysis provided substantial supporting evidence for the correlation between fluorine substitution position and the resulting crystal assembly.

These initial methods relied on atomic coordinates from standard resolution crystallography. As such, they cannot definitively characterise or quantify the stabilising contribution of the proposed interactions. Analysis of the charge distribution between molecules is required to establish the presence of attractive intermolecular interactions and determine their stabilising energy.

Based on the grouping derived from geometric analysis, a select subset of structures was chosen for high resolution X-ray diffraction experiments and theory-based quantum crystallographic analysis. These structures were chosen to exemplify the behaviour of attractive complementary head-to-tail stacking arrangements. Additional structures were selected to complement and extend the analysis using PIXEL calculations. These structures exhibited appropriate characteristics relevant to the objectives of this thesis in the geometric or similarity analysis, but required energetic calculations to confirm the attractive nature of certain proposed interactions.

As stated in the aims in Chapter 3, the main objectives of this work can be summarised by the following questions:

Objectives:

1. *Are fluorine-augmented aromatic stacking interactions structure directing?*
2. *Is there experimental evidence for the direct substituent interaction model?*
3. *How does the placement of fluorine substituents affect aromatic stacking interactions?*
4. *Can C – H ··· F – C or F ··· F interactions influence the crystal assembly and are they competitive with other interactions in the structure?*

Results from each analysis method contribute to addressing these key questions, as outlined in the following sections.

6.1.2 Structure Directing Aromatic Stacking Interactions

The interactions between aromatic rings have been successfully used to inform crystal design in numerous applications, particularly the interactions between fluorinated and unsubstituted aromatic rings[74,75,86,92,95,118,120–124,218].

The prevalence of these interactions is, in part, driven by dispersive forces. The stacking of planar aromatic rings maximises the dispersive forces and satisfies close-packing requirements, leading to a more thermodynamically stable crystal structure. However, there is evidence to suggest that aromatic interactions, specifically fluorine-augmented interactions, have an electrostatic component, which enhances their directionality. This contribution improves the longer-range directionality of the aromatic interactions. Consequently, these interactions may be considered to have a structure directing effect in crystal assembly.

Geometric analysis identified a number of aromatic overlap types. These proved to be a central component in the overall crystal structure, as highlighted by the spatial similarity within each overlap group. The geometric data shows that the average plane separation, lateral translation and centroid separation vary for the different overlap configurations, indicating differences in the relative stabilisation energy of these aromatic interactions. PIXEL calculations on selected structures confirm that the different arrangements correspond to different stabilising contributions.

The directing capability of an interaction is more prominent when the electrostatic component is pronounced, as electrostatic interactions have directionality at a longer range. Therefore,

aromatic interactions associated with a pronounced electrostatic character are likely to have greater influence on the crystal assembly.

PIXEL calculations revealed that the anti-parallel head-to-tail stacking interactions exhibited the strongest molecule-molecule stabilisation as well as the greatest Coulombic contribution. The Coulombic contribution reflects the electrostatic character of the interactions. Although, the dispersion contribution is still the most prominent force in the stabilisation of these molecule-molecule interactions.

The Angled Overlap group also exhibits a strong Coulombic contribution if the interaction energy is considered per each overlapping ring; there is only one aromatic overlap in each molecule-molecule arrangement, compared to two in column stacks. As such, the dispersion contribution associated with the molecule-molecule interaction in this aromatic arrangement is lessened, as there is less surface contact between the molecules.

The formation of the Angled Overlap structures suggests the presence of directional aromatic interactions even in the absence of more significant dispersion and molecule stacking.

PIXEL calculations also revealed that, for each structure analysed, the most stabilising molecule-molecule interaction always corresponded to the overlap of aromatic rings. However, the structures for which the aromatic molecule-molecule interactions were the strongest also exhibited the weakest overall stabilisation energy, Table 6.1

Table 6.1 Averaged energies for aromatic overlap and total lattice energy from PIXEL calculations for different structural groups, repetition of Table 5.32.

	Aromatic Overlap		**Lattice**
Structural Group	**Coulombic / kJ mol^{-1}**	**Total / kJ mol^{-1}**	**Total / kJ mol^{-1}**
Stacking Group 2	-14.4	-68.8	-150.6
Stacking Group 3	-13.1	-63.7	-152.2
Stacking Group 1	-5.45	-55.8	-156.9
Grid	-4.95	-51.8	-160.8
Angled Overlap	-8.25	-48.1	-165.5

This demonstrates that, like strong hydrogen bonds, strong aromatic interactions appear to be influential in the crystal assembly, but their formation does not necessarily lead to the most thermodynamically stable crystal structure.

This is most apparent in the anti-parallel head-to-tail stacking structures, which exhibit strong, directional aromatic interactions with a large Coulombic component but also have relatively low overall stabilisation energies.

6.1.3 Direct Substituent Interaction Model

The directionality of the aromatic interactions appears to originate from their electrostatic component. The direct substituent interaction model attributes the majority of this electrostatic character to the direct interactions between the F and the C – H dipole of the interacting ring.

There is an increasingly large body of computational data in support of the direct substituent interaction model as opposed to the π-polarisation or other models[88,114–116,202,203,221]. More recently some experimental studies have also been conducted that support the direct interaction model[222]. However, there is still much debate as to which models give the most accurate view of aromatic interaction in different systems[223]. In this work, the mechanisms dictating the stabilisation of fluorine-augmented aromatic interactions were experimentally investigated. The results strongly support the direct substituent interaction model.

Favourable anti-parallel head-to-head aromatic overlap arrangements were identified in the geometric analysis. These aromatic arrangements were subsequently analysed through PIXEL energy calculations. This revealed that the molecule-molecule interactions between these head-to-head arrangements exhibited an attractive Coulombic contribution and were energetically stabilising overall. The favourable electrostatic component of these arrangements relies on direct substituent interactions between rings because the electrostatic potential of the rings is necessarily the same.

Charge density analysis of structures (34 – 256) and (345 – 26) also provided support for this model. In the closest stacking dimers of both structures, bond critical points were identified between the fluorine substituents and the nearest carbon atom in the opposing ring. This is in accordance with Wheeler's description of the direct substituent interaction model, in which substituent effects arise from "direct interactions of the substituent with the proximal vertex of the other ring"[115].

More broadly, the direct substituent interaction model emphasises the importance of the specific position of a substituent on the aromatic ring, rather than its effect on the π-electron distribution.

This is reflected in the relationships observed between fluorine substitution patterns and aromatic overlap behaviour in the crystal structure. The mechanisms by which the aromatic arrangements assemble are sensitive to the specific pattern of substitution not merely the number of electron-withdrawing substituents.

6.1.4 Aromatic Overlap Preference

Within the scope of this project, it has not been possible to devise a robust and accurate set of rules to predict exactly how the fluorine substituent placement affects the aromatic stacking interaction. However, some observed relationships between fluorine substitution and aromatic overlap preference have been rationalised, using evidence from the various methods employed.

Anti-parallel head-to-tail stacking, such as Stacking Group 2, 3 and 4, are consistently observed for molecules with substitution patterns that allow the juxtaposition of F and H substituents. This preference is the result of the direct substituent interactions between rings, as reflected by the electrostatic contribution in PIXEL energy calculations between the overlapping stacked molecules. However, there are some exceptions, especially in instances where Angled Overlap or Staggered Overlap arrangements would also fulfil the maximum number of juxtaposed F and H substituents.

Angled overlap and staggered overlap arrangements have a reduced dispersion contribution for the molecule-molecule relationship relating to the aromatic interaction, but the overall crystal lattice energy tends to be more stabilising. Therefore, these arrangements appear to produce more thermodynamically optimal structures. The electrostatic component for these overlap interactions does not appear to be less stabilising than the head-to-tail overlaps. Therefore, these interactions are similarly directional and competitive in the crystal assembly.

Some aromatic ring interactions provide a cooperative, rather than a competitive, effect. For example, in the Interwoven structures both anti-parallel head-to-head offset overlap and anti-parallel head-to-tail overlap (similar to Stacking Group 2 dimers) are observed together. PIXEL analysis showed that the total molecule-molecule energies were similar for these two overlap types. Structures with more than one overlap type present demonstrate the difficulty in reliably understanding which aromatic interaction will be preferable.

Parallel head-to-head interactions were initially difficult to rationalise. The proximity of fluorine atoms on the opposing rings would suggest increased repulsion. However, from geometric analysis, it appears that these repulsion forces in the stack are mitigated by increased lateral translation in relation to the plane separation. These structural arrangements seem to originate

from the two driving forces of minimising repulsion and maximising stabilising contributions from adjacent non-stacked molecules. Indeed, PIXEL calculations reveal that the total crystal lattice energy of Stacking Group 1 is more stabilising than Stacking Groups 2 or 3. The Stacking Group 1 structures exhibit a higher total dispersion contribution and a similar repulsive energy despite the juxtaposition of fluorine atoms. Additionally, Stacking Group 1 structures exhibit Coulombic stabilisation, which may be the product of atom-atom interactions – facilitated by the stacking arrangement.

In all rationalisations of the fluoroaniline structures, the relationship between the fluorine substitution pattern and the aromatic overlap type is complicated by the possibility of structure directing atom-atom intermolecular interactions.

6.1.5 Weak C – H ··· F – C and F ··· F Interactions

In this work, one atom-atom interaction was particularly prominent: the F2 ··· H7 interaction observed in most Stacking Group 3 structures. Charge distribution analysis of the complementary Stacking Group 3 structures (2356 – 4) and (246 – 35) identified bond critical points between the F2 and H7 atoms. Further analysis of the local kinetic energy density suggested that these interactions were relatively strong and investigation of the ρ- and v- gradient field vectors highlighted the significant electrostatic character of the interaction; a property associated with the directionality of hydrogen bonds.

These results are strongly indicative of a favourable, structure directing interaction. The competitive nature of this bond is further substantiated by the observation of its persistent presence throughout Stacking Group 3 structures. The F2 ··· H7 interaction is conserved across a number of similar structural variants, including the polymorphs (2356 – 4) and (2356 – 4 II).

This interaction between the azomethine hydrogen and fluorine (in an ortho position) is also found in the literature for fluoroaniline structures. It was highlighted as a possible weak hydrogen fluorine synthon (synthon I) in the paper by Kaur and Choudhury in 2015[191].

The azomethine hydrogen is significant to the strength and competitive nature of this interaction. The azomethine group is a superior hydrogen bond donor in comparison to the aromatic hydrogens. This observation suggests a strategy for designing enhanced C – H ··· F – C interactions utilising superior hydrogen bond donor groups that are also prohibited from acting as hydrogen bond acceptors.

Charge density analysis of structure (34 – 256) highlighted a particularly strong fluorine interaction, F13 ··· F3. Analysis of the local kinetic energy density indicated that this interaction

was relatively strong. However, there is very little associated electrostatic character; fluorine-centred interactions are largely dispersive. PIXEL calculations show that the F13 ··· F3 interactions coincide with a strongly stabilising molecule-molecule interaction in the (34 – 256) structure. The arrangement of the molecules suggests that a substantial part of this stabilisation could be attributed to the F ··· F interaction. However, there is not sufficient evidence to identify this as a competitive or structure directing interaction.

6.1.6 Concluding Remarks

In conclusion, this thesis presents a comprehensive method for understanding and rationalising the inter-relationship between the aromatic stacking interactions and the fluorine substitution. The systematic characterisation of a representative portion of the molecular structures across the matrix provides a framework for categorising the assembly of this molecular system in the solid state. This framework could be readily applied to other systems in order to rationalise the crystal structures produced.

The interplay of weak intermolecular interactions in these crystal structures creates a complex picture of the crystal assembly. Therefore, it remains difficult to confidently use this framework to generally predict the crystal structure assembly for an unknown. However, there are some common interactions observed within particular members of the matrix that one would have more confidence in predicting.

For example, the weak F2 ··· H7 interaction and the aromatic interaction associated with Stacking Group 3 can be reasonably predicted for fluoroanilines that meet the following conditions:

- the *ortho* position 2 on the aniline ring has a fluorine substituent;
- there are a favourable number of F and H juxtapositions offered by the head-to-tail stacking of the rings – the more of these juxtapositions, the more likely a head-to-tail arrangement will be observed as direct substituent interactions are additive;
- the number of juxtapositions is greater than would be observed in an angled overlap configuration – fluorine substitution in both *ortho* positions 2 and 6 seems to prohibit the formation of angled overlap aromatic interactions.

Following these requirements, complementary structures with fluorine substitution in the 2 and 6 positions on the aniline ring are particularly likely to exhibit these intermolecular interactions.

The complexity of these requirements reflects the subtle interplay of weak intermolecular interactions informing the crystal structure assembly.

6.2 Further Research

The understanding of fluorine augmented aromatic stacking interactions gained in this work could be expanded by investigating a few different avenues in further work.

Firstly, a broader range of fluoroanilines could be examined through charge density analysis, in particular non-head-to-tail overlap arrangements. An example of both the angled overlap and anti-parallel head-to-head overlap configurations would be good candidates for investigation. This analysis would help clarify the factors determining the preferential formation of these overlaps in instances where it appears that an anti-parallel head-to-tail would also be favourable. If possible, the analysis of charge distribution features between the rings, such as CCPs and BCPs between F substituents and the opposing ring, would improve characterisation and comparison of the aromatic interaction behaviour.

Other methods to investigate the topology of the electron density gradient field would also improve understanding of the intermolecular interactions. For example, visualisation of the delocalised non-covalent interactions using the electron density and reduced density gradient (NCI method)[224,225]. These properties can be used to divide the real-space into different bonding regions, which represent non-interacting densities, weak non-covalent interactions, strong hydrogen bonding and repulsive interactions. The NCI method can better visualise the diffuse weak non-covalent interactions than QTAIM critical point identification. Inspection of NCI domains may help characterise the locality and directionality of the non-covalent bonds observed in these crystal structures[225].

Database studies have been utilised in other works to determine the population density of weak hydrogen bonding interactions at different angles and interatomic distances, including C – H ⋯ F interactions[135,226–228]. While the structural library presented in this work is small, it has a comparable number of structures to those included in these database studies[135] and is arguably more coherent. A similar procedure of statistical analysis could be performed on these structures to determine a probability density for the interactions.

Lastly, the methodology outlined in this work could be applied to a slightly different molecular system, one which has a similar set of aromatic stacking behaviours. Repetition of the general methods reported here would test the reproducibility of these finding and their applicability to other fluorine-augmented simple aromatic systems.

Appendix A Experimental

A.1 Synthesis and Crystallisation

The fluoroanilines were synthesised by combination of aniline and benzaldehyde as shown in the reaction scheme, Figure 6.1. The two starting materials began with the desired substitution of fluorine for the final molecule. Ethanol was used as a solvent for the reaction. It was chosen as a suitably volatile liquid for crystallisation by solvent evaporation. A few drops of glacial acetic acid were added to stabilise the anilines, which are sensitive to alkaline hydrolysis. The synthesis and crystallisation of these molecules was carried out by Dr. Terry Threlfall.

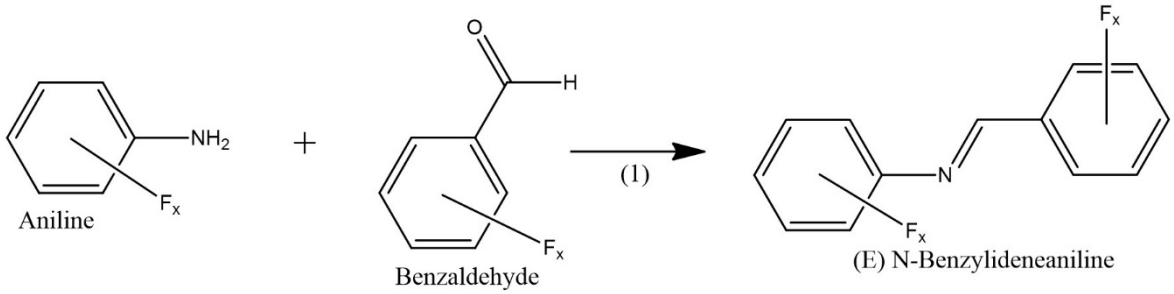

(1) EtOH and a few drops of CH_3CH_2OOH (aq)

Figure 6.1 Reaction scheme for the synthesis of fluoroanilines. Fx represents the various fluorine substitutions.

A.2 Single Crystal X-Ray Diffraction Experiment

A.2.1 Standard Resolution

Crystals were mounted onto a MiTeGen pip with paraffin or silicone oil before being placed on the goniometer of the diffractometer. A number of diffractometers were used in these experiments, all of which are part of the National Crystallographic Service facilities.

These include a molybdenum-based rotating anode source (FR-E+ SuperBright Molybdenum X-Ray generator) diffractometer with an AFC12 goniometer and a Saturn 724+ 18bit CCD detector[229]. A second 'sister' diffractometer on the other port of the anode source has a similar configuration, but was upgraded with a HyPix-600HE detector part-way through this project[230]. Data was collected at 100K for all standard resolution studies using this equipment.

Additionally, a smaller low power 600W molybdenum-based benchtop diffractometer was used, a XtaLAB mini, which has a CCD detector and operates at 170K.

One particularly difficult sample, (23456 – 23546), was referred to the Diamond Light Source synchrotron. This was run at the Diamond beamline I19[231], a facility for small molecule diffraction utilising a high intensity beam, 5 – 28 keV. A solution was found from this data, although the resulting structure was disordered.

A.2.2 High Resolution

Data collection for the high resolution studies were run exclusively on the rotating anode source diffractometer with the HyPix-600HE detector. This diffractometer also has a highly focused beam (70 µm).

The high resolution data were collected under slightly different conditions for each crystal, as detailed in additional materials provided at https://doi.org/10.5258/SOTON/D1348, but in all instances a full sphere of data was collected to a resolution of 0.4 Å.

Appendix B Crystal Data

Crystal structure data is reported at https://doi.org/10.5258/SOTON/D1348

Appendix C Geometric Data

C.1 Stacking Groups

C.1.1 Stacking Group 1

In instances of Stacking Group 1, the translation and plane separation values given are the measured distance, not an average of two measured distances as the intermolecular dihedral angle is 0 and so only one value is produced.

Row A represents the aniline-to-aniline overlap and row B represents the benzylidene-to-benzylidene overlap. In instances where there are two molecules in the asymmetric unit, Z' = 2, the rows are separated into A1, B1, A2 and B2 with the number representing the stack in question.

Table 6.2 Geometric data for Stacking Group 1.

Structure Code		Centroid Separation /Å	Translation /Å	Plane Separation /Å	Inter-molecular Dihedral Angle /°	Intra-molecular Dihedral Angle /°	Nitrogen Separation /Å
4 – 25	A	3.7474(2)	1.615(3)	3.3816(14)	0.00(12)	40.51(7)	3.7474(2)
	B	3.7474(2)	1.476(3)	3.4446(13)	0.00(11)		
4 – 45	A1	3.7652(2)	1.416(3)	3.4886(12)	0.00(16)	34.00(7)	3.7652(2)
Z' = 2	B1	3.7652(2)	1.460(3)	3.4707(13)	0.00(16)		
	A2	3.7652(2)	1.425(3)	3.4853(12)	0.0(3)	40.25(7)	3.7652(2)
	B2	3.7652(2)	1.509(3)	3.4496(12)	0.0(3)		
5 – 35	A	3.7909(6)	1.696(3)	3.3906(18)	0.0(5)	41.50(8)	3.7909(6)
	B	3.7909(6)	1.536(3)	3.4657(16)	0.0(2)		
24 – 23	A	3.7154(2)	1.453(9)	3.420(4)	0.0(3)	39.1(2)	3.7154(2)
	B	3.7154(2)	1.460(10)	3.416(4)	0.0(3)		
24 – 24	A	3.79695(7)	1.432(3)	3.5164(12)	0.000(14)	34.71(7)	3.79695(7)
	B	3.79695(7)	1.724(3)	3.3830(15)	0.00(18)		
24 – 25	A	3.7783(5)	1.682(12)	3.383(6)	0.0(7)	49.3(3)	3.7783(5)
	B	3.7783(5)	1.731(13)	3.358(7)	0.0(8)		

Appendix C

Structure Code		Centroid Separation /Å	Translation /Å	Plane Separation /Å	Inter-molecular Dihedral Angle /°	Intra-molecular Dihedral Angle /°	Nitrogen Separation /Å
26 – 2	A	3.7858(2)	1.392(3)	3.5207(10)	0.00(9)	39.76(6)	3.7858(2)
	B	3.7858(2)	1.584(2)	3.4386(11)	0.00(14)		
34 – 246	A1	3.7441(6)	1.51(3)	3.426(11)	0.0(3)	42.5(6)	3.7441(6)
Z’ = 2	B1	3.7441(6)	1.40(2)	3.471(8)	0.00(12)		
	A2	3.7441(6)	1.46(3)	3.446(11)	0.00(10)	39.3(6)	3.7441(6)
	B2	3.7441(6)	1.54(3)	3.411(12)	0.000(4)		
35 – 24	A	3.6894(2)	1.424(4)	3.4033(19)	0.00(3)	36.72(10)	3.6894(2)
	B	3.6894(2)	1.430(4)	3.4011(16)	0.0(2)		
35 – 35	A1	3.7026(10)	1.354(7)	3.446(3)	0.0(3)	34.81(16)	3.7026(10)
Z’ = 2	B1	3.7026(10)	1.425(7)	3.417(3)	0.0(4)		
	A2	3.7026(10)	1.278(7)	3.475(3)	0.0(4)	38.39(16)	3.7026(10)
	B2	3.7026(10)	1.341(7)	3.451(3)	0.0(5)		
35 – 245	A	3.7381(5)	1.569(3)	3.3929(13)	0.00(14)	43.09(6)	3.7381(5)
	B	3.7381(5)	1.387(3)	3.4713(11)	0.00(19)		
45 – 25	A	3.7616(2)	1.595(5)	3.407(2)	0.0(3)	1.36(11)	3.7616(2)
	B	3.7616(2)	1.618(5)	3.392(2)	0.0(3)		
234 – 23	A	3.6728(2)	1.495(6)	3.355(3)	0.0(3)	41.58(15)	3.6728(2)
	B	3.6728(2)	1.442(6)	3.378(3)	0.00(11)		
234 – 25	A	3.7546(4)	1.587(5)	3.402(2)	0.0(3)	41.24(11)	3.7546(4)
	B	3.7546(4)	1.549(4)	3.420(2)	0.0(5)		
235 – 2356	A	3.7232(3)	1.502(3)	3.4069(11)	0.0(3)	47.57(6)	3.7232(3)
	B	3.7232(3)	1.501(3)	3.4072(12)	0.0(3)		
245 – 245	A	3.6424(2)	1.465(4)	3.3348(17)	0.00(15)	31.52(10)	3.6424(2)
	B	3.6424(2)	1.260(4)	3.4174(16)	0.0(2)		
246 – 23	A	3.6878(3)	1.244(12)	3.472(4)	0.00(10)	41.9(3)	3.6878(3)
	B	3.6878(3)	1.421(12)	3.403(5)	0.0(7)		

Structure Code		Centroid Separation /Å	Translation /Å	Plane Separation /Å	Inter-molecular Dihedral Angle /°	Intra-molecular Dihedral Angle /°	Nitrogen Separation /Å
246 – 25	A1	3.7631(10)	1.607(9)	3.403(4)	0.00(5)	42.1(2)	3.7631(10)
Z’ = 2	B1	3.7631(10)	1.431(10)	3.480(4)	0.00(5)		
	A2	3.7631(10)	1.412(9)	3.488(4)	0.00(5)	43.5(2)	3.7631(10)
	B2	3.7631(10)	1.588(9)	3.412(4)	0.0(4)		
246 – 234	A	3.72403(7)	1.390(2)	3.4547(8)	0.0(3)	46.40(5)	3.72403(7)
	B	3.72403(7)	1.612(2)	3.3570(10)	0.00(11)		
246 – 235	A	3.7670(3)	1.665(3)	3.3790(16)	0.0(3)	29.88(8)	3.7670(3)
	B	3.7670(3)	1.520(3)	3.4469(15)	0.0(3)		
246 – 245	A1	3.73859(17)	1.683(16)	3.338(8)	0.00(13)	39.8(4)	3.73859(17)
Z’ = 2	B1	3.73859(17)	1.609(16)	3.375(8)	0.00(7)		
	A2	3.73859(17)	1.750(16)	3.303(8)	0.00(15)	45.8(4)	3.73859(17)
	B2	3.73859(17)	1.673(17)	3.343(9)	0.00(8)		
345 – 4	A	3.7184(2)	1.559(3)	3.3756(14)	0.0(2)	44.36(7)	3.7184(2)
	B	3.7184(2)	1.561(3)	3.3748(13)	0.0(2)		
345 – 23	A	3.7123(5)	1.576(3)	3.3613(16)	0.0(2)	41.96(8)	3.7123(5)
	B	3.7123(5)	1.535(4)	3.3801(16)	0.0(2)		
345 – 35	A	3.7259(6)	1.399(3)	3.4534(13)	0.0(4)	35.48(7)	3.7259(6)
	B	3.7259(6)	1.326(3)	3.4820(13)	0.0(3)		
345 – 345	A	3.7367(5)	1.436(10)	3.450(4)	0.00(10)	1.2(4)	3.7367(5)
	B	3.7367(5)	1.453(11)	3.443(4)	0.00(17)		
2356 – 24	A1	3.7136(11)	1.436(7)	3.425(3)	0.0(4)	48.49(15)	3.7136(11)
Z’ = 2	B1	3.7136(11)	1.617(6)	3.343(3)	0.0(3)		
	A2	3.7136(11)	1.188(7)	3.518(2)	0.0(4)	42.37(15)	3.7136(11)
	B2	3.7136(11)	1.573(6)	3.364(3)	0.00(3)		

C.1.2 Stacking Group 2

Row 1 represents the first aniline-to-benzylidene overlap and row 2 represents the second aniline-to-benzylidene overlap between separate pairwise molecules.

Table 6.3 Geometric data for Stacking Group 2.

Structure Code		Centroid Separation /Å	Translation Average /Å	Plane Separation Average /Å	Inter-molecular Dihedral Angle /°	Intra-molecular Dihedral Angle /°	Nitrogen Separation /Å
0 – 23456	1	3.5974(6)	1.1723(18)	3.3997(8)	3.16(4)	3.16(4)	4.060(3)
	2	3.6229(6)	1.3370(17)	3.3662(9)	3.16(4)		3.768(3)
34 – 235	1	3.740(2)	1.429(6)	3.456(3)	4.21(14)	4.21(14)	4.079(6)
	2	3.687(2)	1.315(6)	3.445(3)	4.21(14)		3.790(6)
34 – 256	1	3.57526(18)	1.1806(4)	3.3746(2)	4.956(10)	4.956(10)	4.1742(5)
	2	3.71254(18)	1.4259(4)	3.4277(3)	4.956(10)		3.7125(5)
45 – 26	1	3.6198(7)	1.1901(16)	3.4185(8)	3.59(3)	3.59(3)	3.3840(17)
	2	3.6226(7)	1.2807(16)	3.3886(9)	3.59(3)		3.9451(18)
245 – 235	1	3.6323(9)	1.2955(19)	3.3923(11)	6.85(4)	6.85(4)	4.006(2)
	2	3.7416(9)	1.5758(19)	3.3901(12)	6.85(4)		3.801(2)
345 – 2	1	3.6127(11)	1.185(3)	3.4126(14)	0.81(6)	0.81(6)	3.557(3)
	2	3.5843(12)	1.227(3)	3.3680(14)	0.81(6)		3.601(3)
345 – 26	1	3.5948(3)	1.2345(7)	3.3759(4)	1.594(14)	1.594(14)	3.7868(12)
	2	3.6758(3)	1.1097(7)	3.5040(4)	1.594(14)		3.9926(11)
345 – 256	1	3.6509(9)	1.357(2)	3.3891(12)	2.08(5)	2.08(5)	3.677(3)
	2	3.6299(9)	1.236(2)	3.4130(12)	2.08(5)		3.866(3)

C.1.3 Stacking Group 3

Row 1 represents the first aniline-to-benzylidene overlap and row 2 represents the second aniline-to-benzylidene overlap present in every pairwise stack. In instances where there are two molecule in the asymmetric unit, Z' = 2, the rows are separated into 1a, 2a, 1b and 2b with the letter representing the molecule.

Table 6.4 Geometric data for Stacking Group 3.

Structure Code		**Centroid Separation /Å**	**Translation Average /Å**	**Plane Separation Average /Å**	**Inter-molecular Dihedral Angle /°**	**Intra-molecular Dihedral Angle /°**	**Nitrogen Separation /Å**
2 – 245	1 2	3.6287(9) 3.6980(9)	1.191(2) 1.336(2)	3.4264(11) 3.4483(11)	3.03(5) 3.03(5)	25.77(5)	3.9860(11)
2 – 345	1 2	3.6439(8) 3.6326(8)	1.3132(19) 1.3109(19)	3.3980(10) 3.3861(10)	4.81(4) 4.81(4)	32.90(4)	4.0418(10)
2 – 23456	1 2	3.5983(11) 3.8341(12)	1.278(3) 1.783(3)	3.3654(15) 3.3916(18)	4.96(6) 4.96(6)	46.72(7)	3.9722(12)
23 – 235	1 2	4.0000(19) 4.217(2)	2.197(5) 2.581(5)	3.343(4) 3.335(4)	0.79(12) 0.79(12)	61.12(13)	4.0369(17)
23 – 23456	1 2	3.5216(7) 3.7859(7)	1.1443(17) 1.7662(17)	3.3303(8) 3.3468(8)	4.20(4) 4.20(4)	44.69(4)	3.9116(8)
26 – 35	1 2	4.012(2) 3.975(2)	2.248(6) 2.188(6)	3.323(4) 3.320(4)	2.18(11) 2.18(11)	62.70(12)	4.0122(16)
26 – 345	1 2	3.7061(12) 3.7315(12)	1.600(3) 1.436(3)	3.3421(18) 3.4444(17)	3.34(7) 3.34(7)	44.28(7)	3.8338(10)
35 – 246	1 2	3.862(3) 3.915(3)	1.905(7) 1.963(7)	3.360(5) 3.388(5)	3.16(17) 3.16(17)	59.24(13)	4.182(3)
35 – 345 Z’ = 2	1a 2a 1b 2b	3.676(3) 3.604(2) 3.565(2) 3.659(2)	1.354(4) 1.000(4) 1.048(4) 1.291(4)	3.418(3) 3.460(3) 3.407(3) 3.423(3)	4.30(8) 4.30(8) 3.84(8) 3.84(8)	29.67(10) 32.56(10)	3.958(3) 3.911(2)
35 – 2356	1 2	3.693(3) 3.821(3)	1.451(8) 1.686(8)	3.396(4) 3.428(4)	4.80(17) 4.80(17)	48.49(18)	4.021(3)

Appendix C

Structure Code		**Centroid Separation /Å**	**Translation Average /Å**	**Plane Separation Average /Å**	**Inter-molecular Dihedral Angle /°**	**Intra-molecular Dihedral Angle /°**	**Nitrogen Separation /Å**
234 – 235	1a	3.6891(13)	1.345(3)	3.4333(18)	4.44(7)	39.70(8)	3.7493(9)
Z' = 2	2a	3.7021(13)	1.490(3)	3.3892(19)	4.44(7)		
	1b	3.5749(13)	1.147(3)	3.3841(17)	5.59(7)	39.47(8)	3.8477(12)
	2b	3.6860(13)	1.318(3)	3.4404(18)	5.59(7)		
235 – 234	1a	3.6835(12)	1.308(3)	3.4419(16)	5.53(7)	39.02(7)	4.0099(15)
Z' = 2	2a	3.6291(12)	1.433(3)	3.3297(17)	5.53(7)		
	1b	3.6087(12)	1.178(3)	3.4084(16)	4.73(7)	40.23(7)	3.8369(12)
	2b	3.5994(12)	1.309(3)	3.3393(17)	4.73(7)		
236 – 45	1	3.6443(9)	1.309(2)	3.3986(13)	6.29(5)	44.81(5)	3.9003(9)
	2	3.7013(9)	1.513(2)	3.3762(13)	6.29(5)		
246 – 35	1	3.8527(8)	1.908(3)	3.3474(16)	3.42(5)	58.02(7)	4.0511(9)
	2	3.8638(8)	1.856(3)	3.3892(16)	3.42(5)		
2345 – 2	1	3.6278(8)	1.362(2)	3.3561(11)	6.46(4)	40.63(5)	3.9704(9)
	2	3.6580(8)	1.417(2)	3.3704(11)	6.46(4)		
2356 – 0	1	3.805(3)	1.680(8)	3.412(5)	5.96(18)	51.00(17)	3.984(3)
	2	3.721(3)	1.571(8)	3.371(5)	5.96(18)		
2356 – 4	1	3.7336(2)	1.5658(6)	3.3870(3)	4.929(11)	49.548(12)	3.9740(2)
	2	3.6740(2)	1.5633(5)	3.3216(3)	4.929(11)		
2356 – 4 II	1	3.8697(17)	1.771(5)	3.439(3)	5.63(8)	52.54(9)	4.0594(15)
	2	3.8064(17)	1.643(5)	3.432(3)	5.63(8)		
2356 – 5	1	3.808(2)	1.685(6)	3.414(3)	4.45(11)	48.59(13)	3.9372(18)
	2	3.635(2)	1.382(6)	3.361(3)	4.45(11)		
2356 – 35	1	3.671(4)	1.504(5)	3.349(4)	3.12(7)	48.05(12)	3.883(4)
	2	3.710(4)	1.513(5)	3.388(4)	3.12(7)		

C.1.4 Stacking Group 4

Rows numbered 1, 2, 3 and 4 represent the four aniline-to-benzylidene overlap relationships. Two intramolecular dihedral angles describe the molecular conformations in each overlap.

Table 6.5 Geometric data for Stacking Group 4.

Structure Code		Centroid Separation /Å	Translation Average /Å	Plane Separation Average /Å	Inter-molecular Dihedral Angle /°	Intra-molecular Dihedral Angle /°	Nitrogen Separation /Å
23 – 245	1	3.6930(12)	1.266(3)	3.4685(16)	5.04(7)	39.18(7) 39.52(7)	3.741(3)
	2	3.7349(12)	1.550(3)	3.3977(18)	3.42(7)	39.18(7) 39.52(7)	3.741(3)
	3	3.7081(12)	1.401(3)	3.4328(17)	5.04(7)	39.18(7) 39.52(7)	4.047(2)
	4	3.6630(12)	1.423(3)	3.3752(17)	3.42(7)	39.18(7) 39.52(7)	4.047(2)
24 – 35	1	3.7123(11)	1.171(3)	3.5224(15)	2.73(6)	35.87(6) 37.51(6)	4.067(2)
	2	3.7201(11)	1.335(3)	3.4707(15)	5.71(6)	35.87(6) 37.51(6)	4.067(2)
	3	3.6887(11)	1.323(3)	3.4429(15)	2.73(6)	35.87(6) 37.51(6)	3.858(2)
	4	3.6772(11)	1.321(3)	3.4304(15)	5.71(6)	35.87(6) 37.51(6)	3.858(2)
24 – 235	1	3.6918(6)	1.3683(16)	3.4286(8)	1.82(3)	37.44(4) 37.98(4)	4.0345(12)
	2	3.6891(6)	1.4744(16)	3.3809(9)	5.61(3)	37.44(4) 37.98(4)	4.0345(12)
	3	3.6592(6)	1.4220(16)	3.3713(9)	1.82(3)	37.44(4) 37.98(4)	3.7162(12)
	4	3.6627(6)	1.5732(16)	3.3069(9)	5.61(3)	37.44(4) 37.98(4)	3.7162(12)

Appendix C

Structure Code		**Centroid Separation /Å**	**Translation Average /Å**	**Plane Separation Average /Å**	**Inter-molecular Dihedral Angle /°**	**Intra-molecular Dihedral Angle /°**	**Nitrogen Separation /Å**
25 – 235	1	3.7286(15)	1.325(3)	3.4855(17)	3.45(7)	24.56(8)	
Disorder						29.23(8)	
	2	3.7332(15)	1.627(3)	3.3597(19)	1.72(7)	24.56(8)	
						29.23(8)	
	3	3.7104(15)	1.368(3)	3.4489(18)	3.45(7)	24.56(8)	
						29.23(8)	
	4	3.7048(14)	1.522(4)	3.3780(19)	1.72(7)	24.56(8)	
						29.23(8)	
235 – 24	1	3.6560(8)	1.268(2)	3.4290(10)	4.40(4)	38.03(4)	4.0038(15)
Z’ = 3						39.01(4)	
	2	3.5755(7)	1.4012(19)	3.3020(10)	2.05(4)	38.03(4)	4.0038(15)
						39.01(4)	
	3	3.6452(8)	1.079(2)	3.4820(10)	4.40(4)	38.03(4)	3.6691(15)
						39.01(4)	
	4	3.7099(7)	1.511(2)	3.3880(11)	2.05(4)	38.03(4)	3.6691(15)
						39.01(4)	
	1	3.6735(7)	1.383(2)	3.3973(11)	4.67(4)	43.30(5)	3.9219(8)
	2	3.6301(7)	1.335(2)	3.3740(11)	4.67(4)		
245 – 24	1	3.7461(17)	1.280(5)	3.517(3)	6.04(9)	33.13(10)	4.354(4)
						36.13(10)	
	2	3.8174(17)	1.727(5)	3.402(3)	4.77(9)	33.13(10)	4.354(4)
						36.13(10)	
	3	3.8789(17)	1.750(5)	3.458(3)	6.04(9)	33.13(10)	3.735(4)
						36.13(10)	
	4	3.8144(17)	1.650(5)	3.436(3)	4.77(9)	33.13(10)	3.735(4)
						36.13(10)	

Structure Code		Centroid Separation /Å	Translation Average /Å	Plane Separation Average /Å	Inter-molecular Dihedral Angle /°	Intra-molecular Dihedral Angle /°	Nitrogen Separation /Å
245 – 25	1	3.6915(9)	1.553(3)	3.3480(15)	2.98(5)	27.74(6) 24.43(6)	3.602(2)
	2	3.6703(9)	1.414(3)	3.3873(14)	3.84(6)	27.74(6) 24.43(6)	3.602(2)
	3	3.6288(9)	1.423(3)	3.3378(14)	2.98(5)	27.74(6) 24.43(6)	4.068(2)
	4	3.6497(9)	1.109(3)	3.4773(13)	3.84(6)	27.74(6) 24.43(6)	4.068(2)
246 – 345	1	3.7160(13)	1.432(4)	3.427(2)	3.92(8)	31.66(8) 33.40(8)	3.931(3)
	2	3.6033(13)	1.282(4)	3.367(2)	3.23(8)	31.66(8) 33.40(8)	3.931(3)
	3	3.6846(13)	1.420(4)	3.398(2)	3.92(8)	31.66(8) 33.40(8)	3.570(3)
	4	3.8069(13)	1.759(4)	3.375(2)	3.23(8)	31.66(8) 33.40(8)	3.570(3)
346 – 35	1	3.7577(8)	1.731(2)	3.3353(12)	4.16(5)	38.86(5) 36.60(5)	4.1831(16)
	2	3.6609(8)	1.057(2)	3.5044(11)	8.51(5)	38.86(5) 36.60(5)	4.1831(16)
	3	3.7011(8)	1.498(2)	3.3846(12)	4.16(5)	38.86(5) 36.60(5)	3.6014(17)
	4	3.7774(8)	1.196(2)	3.5780(12)	8.51(5)	38.86(5) 36.60(5)	3.6014(17)

Appendix C

Structure Code		**Centroid Separation /Å**	**Translation Average /Å**	**Plane Separation Average /Å**	**Inter-molecular Dihedral Angle /°**	**Intra-molecular Dihedral Angle /°**	**Nitrogen Separation /Å**
2345 – 24	1	3.6846(7)	1.3449(17)	3.5309(9)	6.56(4)	30.66(4) 28.97(4)	3.5281(13)
	2	3.6536(7)	1.5120(17)	3.3238(10)	3.86(4)	30.66(4) 28.97(4)	3.5281(13)
	3	3.6308(7)	1.3088(17)	3.3867(9)	6.56(4)	30.66(4) 28.97(4)	4.0344(13)
	4	3.6637(7)	1.5998(17)	3.2944(10)	3.86(4)	30.66(4) 28.97(4)	4.0344(13)
2356 – 45 Disorder	1	3.7727(18)	1.668(4)	3.382(3)	6.61(9)	46.62(9) 48.51(10)	3.992(4)
	2	3.668(2)	1.426(5)	3.378(3)	4.26(9)	46.62(9) 48.51(10)	3.992(4)
	3	3.7021(18)	1.493(5)	3.387(3)	6.61(9)	46.62(9) 48.51(10)	3.838(4)
	4	3.804(2)	1.671(5)	3.416(3)	4.26(9)	46.62(9) 48.51(10)	3.838(4)
23456 – 0	1	3.641(3)	1.332(6)	3.386(3)	4.95(14)	45.40(13) 45.16(13)	3.904(5)
	2	3.623(3)	1.377(6)	3.349(3)	4.59(13)	45.40(13) 45.16(13)	3.904(5)
	3	3.759(3)	1.699(7)	3.353(4)	4.95(14)	45.40(13) 45.16(13)	3.725(5)
	4	3.770(3)	1.728(6)	3.348(4)	4.59(13)	45.40(13) 45.16(13)	3.725(5)

Structure Code		Centroid Separation /Å	Translation Average /Å	Plane Separation Average /Å	Inter-molecular Dihedral Angle /°	Intra-molecular Dihedral Angle /°	Nitrogen Separation /Å
23456 – 4	1	3.8109(18)	1.776(5)	3.372(3)	5.09(10)	49.84(10) 49.39(10)	3.827(4)
	2	3.8032(19)	1.791(5)	3.352(3)	5.10(10)	49.84(10) 49.39(10)	3.827(4)
	3	3.6981(18)	1.544(5)	3.359(3)	5.09(10)	49.84(10) 49.39(10)	3.946(4)
	4	3.7037(19)	1.530(5)	3.371(3)	5.10(10)	49.84(10) 49.39(10)	3.946(4)
23456 – 25	1	3.654(8)	1.28(2)	3.422(12)	4.1(5)	39.9(5) 39.2(5)	3.680(14)
	2	3.686(8)	1.39(2)	3.422(12)	4.8(5)	39.9(5) 39.2(5)	3.680(14)
	3	3.661(8)	1.35(2)	3.403(11)	4.1(5)	39.9(5) 39.2(5)	3.862(14)
	4	3.629(8)	1.21(5)	3.420(12)	4.8(5)	39.9(5) 39.2(5)	3.862(14)

C.2 Offset Overlap Groups

C.2.1 Staggered Overlap

Table 6.6 Geometric data for the Staggered Overlap structures. In addition to the Head-to-Tail parallel overlap, structure (23 – 24) also exhibits Head-to-Head anti-parallel overlap.

Structure Code		**Centroid Separation /Å**	**Translation Average /Å**	**Plane Separation Average /Å**	**Intermolecular Dihedral Angle /°**	**Intramolecular Dihedral Angle /°**
0 – 234	1 2	4.015(4) 3.727(4)	2.209(8) 1.43(3)	3.345(8) 3.440(8)	6.42(4) 6.42(4)	6.24(4)
4 – 234	1 2	3.7781(8) 3.8817(9)	1.571(2) 1.986(2)	3.4467(13) 3.3246(16)	8.19(5) 8.19(5)	8.19(5)
5 – 246	1 2	3.760(2) 4.138(2)	1.472(7) 2.464(7)	3.459(4) 3.376(5)	5.44(14) 5.44(14)	5.44(14)
23 – 24	H-t-T H-t-H 1 H-t-H 2	3.7044(9) 3.6291(12) 3.6929(12)	1.407(3) 1.278(3) 1.479(3)	3.4162(14) 3.3965(14) 3.3837(12)	8.60(5) 0.0(3) 0.0(3)	8.60(5)

C.2.2 Interwoven

Table 6.7 Geometric data for the Interwoven structures.

Structure Code		Centroid Separation /Å	Translation Average /Å	Plane Separation Average /Å	Inter-molecular Dihedral Angle /°	Intra-molecular Dihedral Angle /°
4 – 236	H-t-T H-t-H 1 H-t-H 2	3.6833(16) 3.791(2) 3.675(2)	1.397(4) 1.522(5) 1.501(4)	3.408(2) 3.409(3) 3.354(3)	1.89(9) 0.0(3) 0.0(3)	1.89(9)
23 – 234	H-t-T H-t-H 1 H-t-H 2	3.7295(17) 3.635(2) 3.734(3)	1.321(5) 1.485(5) 1.180(5)	3.470(3) 3.318(3) 3.543(3)	14.35(11) 0.00(3) 0.0(2)	14.35(11)
24 – 236	H-t-T H-t-H 1 H-t-H 2	3.6012(9) 3.8761(13) 3.7802(14)	1.209(3) 1.892(3) 1.592(3)	3.3903(13) 3.3829(18) 3.4285(18)	4.89(5) 0.0(3) 0.00(13)	4.89(5)
25 – 23	H-t-T H-t-H 1 H-t-H 2	3.831(2) 3.893(3) 3.844(3)	1.353(6) 1.807(6) 1.794(6)	3.565(3) 3.448(4) 3.400(4)	16.10(13) 0.0(2) 0.0(4)	16.10(13)
234 – 24	H-t-T H-t-H 1 H-t-H 2	3.7001(11) 3.7187(16) 3.6831(15)	1.154(3) 1.516(3) 1.336(3)	3.4902(16) 3.3959(19) 3.4321(18)	13.54(7) 0.00(17) 0.00(10)	13.54(7)
234 – 246	H-t-T H-t-H 1 H-t-H 2	3.6523(9) 3.5832(12) 3.7243(12)	1.253(2) 1.175(2) 1.533(2)	3.4205(12) 3.3852(12) 3.3941(14)	8.86(5) 0.00(18) 0.00(16)	8.86(5)
245 – 234	H-t-T H-t-H 1 H-t-H 2	3.7571(12) 3.6515(17) 3.7732(17)	1.347(3) 1.448(3) 1.594(4)	3.4922(19) 3.3522(19) 3.420(2)	15.60(7) 0.00(12) 0.00(19)	15.60(7)

C.2.3 Other Offset Overlap

Table 6.8 Geometric data for structures (23 – 25) and (25 – 25).

Structure Code		**Centroid Separation /Å**	**Translation Average /Å**	**Plane Separation Average /Å**	**Inter-molecular Dihedral Angle /°**	**Intra-molecular Dihedral Angle /°**
23 – 25	H-t-T H-t-H	3.5808(9) 3.6984(14)	1.120(3) 1.405(3)	3.3965(12) 3.4211(18)	6.17(6) 0.00(8)	6.17(6)
25 – 25	H-t-T H-t-H	4.1084(7) 3.8067(9)	2.2527(18) 1.7469(17)	3.3577(14) 3.3822(12)	21.53(4) 0.000(3)	21.53(4)

Table 6.9 Geometric data for structure (234 – 26).

Structure Code		**Centroid Separation /Å**	**Translation Average /Å**	**Plane Separation Average /Å**	**Inter-molecular Dihedral Angle /°**	**Intra-molecular Dihedral Angle /°**
234 – 26 Molecule A	1 2	3.8312(8) 3.8560(8)	1.657(2) 1.663(2)	3.4531(12) 3.4772(12)	4.00(4) 4.00(4)	4.00(4)
234 – 26 Molecule B	H-t-H A1 H-t-H A2 H-t-H B1 H-t-H B2	4.0712(10) 4.1971(10) 4.2241(11) 3.6555(11)	2.325(2) 2.655(2) 2.385(2) 1.183(2)	3.3420(15) 3.2506(16) 3.4861(16) 3.4588(13)	0.000(5) 0.0(2) 0.00(8) 0.000(5)	33.99(4)

Table 6.10 Geometric data for structure (234 – 34).

Structure Code		**Centroid Separation /Å**	**Translation /Å**	**Plane Separation /Å**	**Inter-molecular Dihedral Angle /°**	**Intra-molecular Dihedral Angle /°**
234 – 34	H-t-H 1 H-t-H 2	3.669(2) 3.656(2)	1.524(4) 1.322(4)	3.337(3) 3.409(3)	0.00(2) 0.0(3)	17.35(7)

C.3 Angled Overlap

C.3.1 Conventional Angled Overlap

Table 6.11 Geometric data for conventional Angled Overlap structures.

Structure Code		Centroid Separation /Å	Translation Average /Å	Plane Separation Average /Å	Inter-molecular Dihedral Angle /°	Intra-molecular Dihedral Angle /°
24 – 4	AO	3.846(4)	1.742(11)	3.428(6)	0.7(2)	37.5(2)
45 – 4	AO	3.791(5)	1.596(15)	3.439(8)	1.6(3)	40.6(3)
24 – 2356 Z' = 2	A AO 1 AO 2 B AO 1 AO 2	3.871(7) 3.598(6) 3.854(7) 3.618(7)	1.70(2) 1.22(2) 1.679(17) 1.289(16)	3.479(11) 3.387(9) 3.469(10) 3.380(9)	3.1(4) 3.1(4) 2.3(4) 2.3(4)	3.5(4) 4.0(4)
25 – 35	AO 1 AO 2	3.7603(13) 3.9246(13)	1.625(3) 1.985(3)	3.388(2) 3.386(2)	4.77(7) 4.77(7)	32.47(8)
234 – 0	AO	3.748(3)	1.599(8)	3.391(4)	2.74(16)	31.69(16)
234 – 4	AO	3.7756(12)	1.651(3)	3.3955(19)	4.33(7)	32.59(7)
245 – 3	AO	3.7921(9)	1.752(2)	3.3632(13)	0.82(5)	22.19(5)
245 – 4	AO	3.742(3)	1.553(8)	3.405(4)	0.45(16)	35.94(16)
345 – 234	AO 1 AO 2	4.0951(12) 4.3227(12)	2.278(3) 2.793(3)	3.403(2) 3.295(3)	5.20(6) 5.20(6)	35.06(7)
2345 – 35	AO	3.7154(16)	1.524(4)	3.385(2)	5.29(9)	21.06(9)

C.3.2 Angled Overlap with Offset

Table 6.12 Geometric data for structure (25 – 245).

Structure Code		Centroid Separation /Å	Translation Average /Å	Plane Separation Average /Å	Inter-molecular Dihedral Angle /°	Intra-molecular Dihedral Angle /°
25 – 245	AO H-t-H	3.939(2) 3.604(3)	1.938(6) 1.370(6)	3.428(4) 3.334(4)	4.74(13) 0.0(3)	27.8(13)

C.3.3 Angled Overlap with Stacking

Table 6.13 Geometric data for Angled Overlap structures with head-to-tail stacks.

Structure Code		Centroid Separation /Å	Translation Average /Å	Plane Separation Average /Å	Inter-molecular Dihedral Angle /°	Intra-molecular Dihedral Angle /°
234 – 245 Z' = 3	BC AO 1 BC AO 2 AB H-t-T 1 AB H-t-T 2	3.724(2) 3.929(2) 3.763(2) 3.584(2)	1.531(6) 1.942(6) 1.715(6) 1.224(6)	3.395(3) 3.416(4) 3.345(4) 3.368(3)	2.83(13) 3.56(14) 10.03(13) 4.37(13)	16.35(13) 19.33(14) 16.35(13) 19.33(14) 3.52(13) 16.35(13) 3.52(13) 16.35(13)
2345 – 234	AO H-t-T	4.0355(9) 3.9220(9)	2.253(2) 1.596(3)	3.3477(17) 3.5216(15)	2.74(5) 23.45(5)	23.45(5)

Table 6.14 Geometric data for Angled Overlap structures with twisted stacks.

Structure Code		**Centroid Separation /Å**	**Translation Average /Å**	**Plane Separation Average /Å**	**Inter-molecular Dihedral Angle /°**	**Intra-molecular Dihedral Angle /°**
24 – 234	AA AO	3.6982(10)	1.484(3)	3.3852(13)	4.96(6)	20.15(6)
Z′ = 2	AB H-t-H 1	3.9071(9)	1.751(2)	3.4919(15)	4.55(5)	20.15(6)
						20.58(5)
	AB H-t-H 2	3.9655(10)	1.597(3)	3.6272(16)	4.67(5)	20.15(6)
						20.58(5)
	BB AO	3.7502(9)	1.644(2)	3.3701(14)	3.33(5)	20.58(5)
234 – 234	AA AO	3.5820(8)	1.331(2)	3.3255(11)	1.20(5)	16.49(5)
Z′ = 2	AB H-t-H 1	3.9795(8)	1.796(2)	3.5511(13)	3.14(4)	19.13(5)
						16.49(5)
	AB H-t-H 2	3.9621(8)	1.859(2)	3.4977(13)	5.61(4)	19.13(5)
						16.49(5)
	BB AO	3.7011(8)	1.646(2)	3.3149(12)	2.02(4)	19.13(5)
245 – 0	AO	3.8091(13)	1.639(3)	3.4374(18)	3.01(7)	22.39(7)
	H-t-T	3.9356(12)	1.764(3)	3.5182(19)	3.01(7)	
245 – 2	AB AO 1	3.799(2)	1.604(6)	3.444(3)	1.26(12)	20.89(13)
Z′ = 2						22.12(13)
	AB AO 2	3.970(2)	1.965(7)	3.448(4)	3.81(15)	20.89(13)
						22.12(13)
	AB H-t-T 1	3.872(2)	1.660(6)	3.499(3)	1.26(12)	20.89(13)
						22.12(13)
	AB H-t-T 2	4.201(2)	2.252(7)	3.547(4)	3.81(15)	20.89(13)
						22.12(13)

C.3.4 Other Angled Overlap

Table 6.15 Geometric data for structure (2345 – 0).

Structure Code		Centroid Separation /Å	Translation Average /Å	Plane Separation Average /Å	Inter-molecular Dihedral Angle /°	Intra-molecular Dihedral Angle /°
2345 – 0	AC AO 1	3.6729(10)	1.444(3)	3.3772(14)	2.98(5)	31.24(6)
Z' = 3						31.62(6)
	AC AO 2	3.6848(10)	1.540(3)	3.3480(14)	3.29(6)	31.24(6)
						31.62(6)
	AB H-t-T 1	3.8883(11)	1.730(3)	3.4820(15)	3.99(6)	31.24(6)
						31.22(6)
	AB H-t-T 2	3.6901(10)	1.312(3)	3.4430(14)	6.73(6)	31.24(6)
						31.22(6)
	BC H-t-T 1	3.6715(11)	1.380(3)	3.4023(14)	2.83(6)	31.22(6)
						31.62(6)
	BC H-t-T 2	3.8088(10)	1.590(3)	3.4606(15)	3.92(5)	31.22(6)
						31.62(6)

C.4 Grid Structures

Table 6.16 Geometric data for the Grid structures.

Structure Code		Centroid Separation /Å	Translation Average /Å	Plane Separation Average /Å	Intermolecular Dihedral Angle /°	Intramolecular Dihedral Angle /°
4 – 235	H-t-H	4.7218(5)	3.301(3)	3.376(3)	0.0(3)	11.44(8)
	H-t-T	4.7863(15)	3.300(4)	3.466(3)	11.44(8)	
4 – 2356	H-t-H	4.6948(2)	3.175(4)	3.459(4)	0.0(5)	10.22(9)
	H-t-T	4.6791(16)	3.338(4)	3.279(4)	10.22(9)	
23 – 45	H-t-H	4.5675(5)	3.048(6)	3.402(6)	0.0(6)	3.99(15)
	H-t-T	4.822(7)	3.449(7)	3.402(7)	3.99(15)	

23 – 345	H-t-H H-t-T	4.6420(4) 4.720(3)	3.170(7) 3.268(7)	3.392(7) 3.419(7)	0.0(8) 0.94(17)	0.94(17)
34 – 23	H-t-H H-t-T	4.6873(2) 4.746(3)	3.270(6) 3.252(7)	3.359(6) 3.456(7)	0.0(9) 5.29(15)	5.29(15)
234 – 256	H-t-H H-t-T	4.7263(2) 4.7254(12)	3.360(3) 3.223(3)	3.324(3) 3.451(3)	0.0(2) 15.78(7)	15.78(7)
246 – 246	H-t-H H-t-T	4.4806(3) 4.7959(9)	2.995(9) 3.587(8)	3.333(8) 3.184(10)	0.00(4) 2.39(5)	2.39(5)

C.4.1 Other Grid Structures

Table 6.17 Geometric data for structure (234 – 23456).

Structure Code		**Centroid Separation /Å**	**Translation Average /Å**	**Plane Separation Average /Å**	**Intermolecular Dihedral Angle /°**	**Intramolecular Dihedral Angle /°**
234 – 23456	H-t-H H-t-T	4.5670(4) 4.739(2)	3.182(4) 3.330(5)	3.276(4) 3.279(5)	0.0(4) 9.25(11)	9.25(11)

C.5 Other Structures

Table 6.18 Geometric data for structure (4 – 345). H-t-H describes a near overlap in an offset anti-parallel head-to-head arrangement. However, the centroid separation and translational displacement make this unlikely to be a significant interaction.

Structure Code		**Centroid Separation /Å**	**Translation Average /Å**	**Plane Separation Average /Å**	**Intermolecular Dihedral Angle /°**	**Intramolecular Dihedral Angle /°**
4 – 345	H-t-H	4.0743(14)	2.261(3)	3.389(2)	0.00(12)	43.11(6)

Table 6.19 Geometric data for structures (2345 – 23) and (23456 – 23). Unbalanced stacks, one close and one far overlap relationship in a head-to-tail arrangement. H-t-T 1 represents the close stacking overlap, while H-t-T 2 represents the far stacking overlap.

Structure Code		**Centroid Separation /Å**	**Translation Average /Å**	**Plane Separation Average /Å**	**Intermolecular Dihedral Angle /°**	**Intramolecular Dihedral Angle /°**
2345 – 23	H-t-T 1 H-t-T 2	3.6531(10) 4.5805(12)	1.543(3) 3.339(2)	3.3097(15) 3.134(3)	3.34(5) 3.34(5)	43.33(6)
23456 – 23	H-t-T 1 H-t-T 2	3.6380(6) 4.7422(7)	1.5307(16) 3.5833(15)	3.2969(9) 3.0996(17)	5.09(3) 5.09(3)	43.45(4)

Table 6.20 Geometric data for structure (2356 – 26). Perpendicular stacking indicated by ⊥.

Structure Code		**Centroid Separation /Å**	**Translation Average /Å**	**Plane Separation Average /Å**	**Inter-molecular Dihedral Angle /°**	**Intra-molecular Dihedral Angle /°**
2356 – 26 Z’ = 2	AB H-t-T	3.7003(10)	1.425(3)	3.4139(14)	3.31(6)	67.31(6) 31.62(6)
	AB H-t-T ⊥	3.7147(10)	0.978(3)	3.5824(13)	3.40(6)	67.31(6) 31.62(6)
	AA H-t-H	3.7492(14)	1.426(3)	3.4673(16)	0.0(2)	67.31(6)
	BB H-t-H	3.9673(13)	2.112(3)	3.3586(18)	0.00(6)	31.62(6)

Table 6.21 Geometric data for structures (256 – 2356) and (2356 – 2356).

Structure Code		**Centroid Separation /Å**	**Translation Average /Å**	**Plane Separation Average /Å**	**Inter-molecular Dihedral Angle /°**	**Intra-molecular Dihedral Angle /°**
256 – 2356	H-t-H 1 H-t-H 2	3.572(3) 3.574(3)	1.278(6) 1.277(6)	3.336(4) 3.336(3)	0.0(6) 0.00(5)	65.51(12)
2356 – 2356	H-t-H 1 H-t-H 2	3.5330(14) 3.5352(14)	1.308(3) 1.311(3)	3.2820(16) 3.2834(16)	0.0(1) 0.0(1)	70.58(5)

Appendix D Charge Density Data

Charge density data is reported at https://doi.org/10.5258/SOTON/D1348

Appendix E PIXEL Calculations

E.1 Aromatic Overlap Pairs

E.1.1 Head-to-Tail Overlap

Table 6.22 PIXEL molecule-molecule pair energy for aromatic overlaps in Stacking Group 2.

Structure	Distance / Å	Coulombic / kJ mol^{-1}	Polarisation / kJ mol^{-1}	Dispersion / kJ mol^{-1}	Repulsion / kJ mol^{-1}	Total / kJ mol^{-1}
0 – 23456	4.123	-18.3	-7.7	-89.8	42.3	-73.6
	4.188	-16.2	-7.6	-86.3	39.1	-71.1
34 – 256	3.350	-17.7	-7.0	-93.8	45.3	-73.3
	4.045	-13.1	-5.5	-78.7	33.7	-63.5
345 – 26	3.398	-16.5	-6.4	-94.7	44.4	-73.2
	4.368	-10.4	-3.8	-75.8	29.5	-60.5
345 – 256	3.480	-14.5	-6.5	-92.1	40.4	-72.7
	3.887	-14.1	-5.7	-87.7	38.1	-69.4

Table 6.23 PIXEL molecule-molecule pair energy for aromatic overlaps in Stacking Group 3.

Structure	Distance / Å	Coulombic / kJ mol^{-1}	Polarisation / kJ mol^{-1}	Dispersion / kJ mol^{-1}	Repulsion / kJ mol^{-1}	Total / kJ mol^{-1}
26 – 345	4.238	-13.6	-5.5	-83.6	38.0	-64.8
	4.238	-13.6	-5.5	-83.6	38.0	-64.8
35 – 246	3.887	-11.8	-5.3	-76.9	32.4	-61.5
	3.887	-11.8	-5.3	-76.9	32.4	-61.5
236 – 45	3.717	-15.4	-6.6	-87.2	41.8	-67.4
	3.717	-15.4	-6.6	-87.2	41.8	-67.4

246 – 35	3.851	-11.2	-5.4	-79.6	35.7	-60.5
	3.851	-11.2	-5.4	-79.6	35.7	-60.5
2356 – 4	3.873	-14.6	-7.0	-88.4	44.0	-66.0
	3.873	-14.6	-7.0	-88.4	44.0	-66.0
2356 – 0	4.176	-12.0	-6.2	-81.8	38.2	-61.8
	4.176	-12.0	-6.2	-81.8	38.2	-61.8

Table 6.24 PIXEL molecule-molecule pair energy for aromatic overlaps in (23456 – 0), Stacking Group 4.

Structure	**Distance / Å**	**Coulombic / kJ mol^{-1}**	**Polarisation / kJ mol^{-1}**	**Dispersion / kJ mol^{-1}**	**Repulsion / kJ mol^{-1}**	**Total / kJ mol^{-1}**
23456 – 0	3.965	-16.0	-7.8	-89.7	44.3	-69.1
	4.400	-17.5	-7.8	-91.1	45.6	-70.9
	3.965	-16.0	-7.8	-89.7	44.3	-69.1
	4.400	-17.5	-7.8	-91.1	45.6	-70.9

E.1.2 Parallel Head-to-Head Overlap

Table 6.25 PIXEL molecule-molecule pair energy for aromatic overlaps in Stacking Group 1.

Structure	**Distance / Å**	**Coulombic / kJ mol^{-1}**	**Polarisation / kJ mol^{-1}**	**Dispersion / kJ mol^{-1}**	**Repulsion / kJ mol^{-1}**	**Total / kJ mol^{-1}**
4 – 25	3.747	-5.7	-4.3	-78.1	33.7	-54.5
	3.747	-5.7	-4.3	-78.1	33.7	-54.5
45 – 25	3.762	-6.0	-4.5	-78.4	33.1	-55.8
	3.762	-6.0	-4.5	-78.4	33.1	-55.8
24 – 25	3.778	-5.6	-4.6	-81.6	36.1	-55.7
	3.778	-5.6	-4.6	-81.6	36.1	-55.7

234 – 25	3.755	-4.5	-4.5	-80.8	32.7	-57.0
	3.755	-4.5	-4.5	-80.8	32.7	-57.0

E.1.3 Anti-Parallel Head-to-Head Overlap

H-t-H represents anti-parallel head-to-head overlap.

H-t-T represents anti-parallel head-to-tail overlap related by inversion.

Table 6.26 PIXEL molecule-molecule pair energy for anti-parallel head-to-head overlaps.

Structure	**Overlap Type**	**Distance / Å**	**Coulombic / kJ mol^{-1}**	**Polarisation / kJ mol^{-1}**	**Dispersion / kJ mol^{-1}**	**Repulsion / kJ mol^{-1}**	**Total / kJ mol^{-1}**
234 – 34	H-t-H	8.484	-7.6	-3.6	-42.1	20.0	-33.3
	H-t-H	7.144	-3.2	-3.7	-51.8	19.7	-39.0
23 – 25	H-t-T	3.400	-14.0	-6.1	-89.0	41.3	-67.8
	H-t-H	8.414	-6.4	-2.2	-36	16.1	-28.5
234 – 24	H-t-T	3.636	-10.1	-5.5	-80.8	33.6	-62.8
	H-t-H	7.128	-8.7	-3.8	-55.5	23.0	-44.9
	H-t-H	8.063	-4.5	-2.4	-38.2	14.3	-30.8
4 – 236	H-t-T	3.665	-13.3	-5.6	-81.7	34.3	-66.3
	H-t-H	8.238	-5.4	-2.4	-38.2	14	-31.9
	H-t-H	7.126	-3	-3.3	-46.9	20.7	-32.5

E.1.4 Angled Overlap

Table 6.27 PIXEL molecule-molecule pair energy for aromatic ring overlap in Angled Overlap structures.

Structure	Distance / Å	Coulombic / kJ mol^{-1}	Polarisation / kJ mol^{-1}	Dispersion / kJ mol^{-1}	Repulsion / kJ mol^{-1}	Total / kJ mol^{-1}
234 – 0	4.638	-8.7	-6.2	-62.0	28.0	-48.8
	4.638	-8.7	-6.2	-62.0	28.0	-48.8
234 – 4	4.778	-7.8	-5.8	-60.9	27.2	-47.3
	4.778	-7.8	-5.8	-60.9	27.2	-47.3

E.2 Overall Crystal Lattice Energies

Table 6.28 PIXEL calculated total crystal lattice energies for Stacking Group 1 structures.

Structure	Coulombic / kJ mol^{-1}	Polarisation / kJ mol^{-1}	Dispersion / kJ mol^{-1}	Repulsion / kJ mol^{-1}	Total / kJ mol^{-1}
4 – 25	-29.8	-12.7	-184.8	70.3	-157.1
45 – 25	-29.1	-13.7	-186	67.7	-161.1
24 – 25	-32.5	-12.8	-183.2	74.8	-157.0
234 – 25	-25.4	-11.2	-176.3	67.8	-152.4

Table 6.29 PIXEL calculated total crystal lattice energies for Stacking Group 2 structures.

Structure	Coulombic / kJ mol^{-1}	Polarisation / kJ mol^{-1}	Dispersion / kJ mol^{-1}	Repulsion / kJ mol^{-1}	Total / kJ mol^{-1}
0 – 23456	-29.4	-12.7	-185.1	69.4	-157.8
34 – 256	-35.7	-12.7	-181.6	72.3	-157.7
345 – 26	-27.9	-10.1	-168.2	59.1	-147.1
345 – 256	-24.5	-9.7	-170.8	58.1	-147.0

Table 6.30 PIXEL calculated total crystal lattice energies for Stacking Group 3 structures.

Structure	**Coulombic / kJ mol^{-1}**	**Polarisation / kJ mol^{-1}**	**Dispersion / kJ mol^{-1}**	**Repulsion / kJ mol^{-1}**	**Total / kJ mol^{-1}**
26 – 345	-31.3	-11.9	-172.9	67.6	-148.5
35 – 246	-33.0	-10.9	-173.4	66.7	-150.6
236 – 45	-34.7	-13.8	-178.5	73.0	-154.0
246 – 35	-35.4	-12.0	-177.2	73.2	-151.3
2356 – 4	-34.7	-13.4	-182.2	76.1	-154.2
2356 – 0	-31.7	-13.7	-179.5	70.5	-154.4

Table 6.31 PIXEL calculated total crystal lattice energies for Stacking Group 4 structures.

Structure	**Coulombic / kJ mol^{-1}**	**Polarisation / kJ mol^{-1}**	**Dispersion / kJ mol^{-1}**	**Repulsion / kJ mol^{-1}**	**Total / kJ mol^{-1}**
23456 – 0	-34.5	-14.1	-183.6	76.2	-156.2

Table 6.32 PIXEL calculated total crystal lattice energies for Grid structures.

Structure	**Coulombic / kJ mol^{-1}**	**Polarisation / kJ mol^{-1}**	**Dispersion / kJ mol^{-1}**	**Repulsion / kJ mol^{-1}**	**Cell dipole / kJ mol^{-1}**	**Total / kJ mol^{-1}**
4 – 2356	-37.6	-13.4	-193.6	81.1	0	-163.6
23 – 45	-23.7	-10.1	-177.3	65.1	-11.9	-158

Table 6.33 PIXEL calculated total crystal lattice energies for Angled Overlap structures.

Structure	**Coulombic / kJ mol^{-1}**	**Polarisation / kJ mol^{-1}**	**Dispersion / kJ mol^{-1}**	**Repulsion / kJ mol^{-1}**	**Total / kJ mol^{-1}**
234 – 0	-35.0	-16.2	-183.8	70.7	-164.3
234 – 4	-34.5	-17.1	-184.5	69.4	-166.7

Table 6.34 PIXEL calculated total crystal lattice energies for structures with anti-parallel head-to-head overlap.

Structure	**Coulombic / kJ mol^{-1}**	**Polarisation / kJ mol^{-1}**	**Dispersion / kJ mol^{-1}**	**Repulsion / kJ mol^{-1}**	**Total / kJ mol^{-1}**
23 – 25	-37.1	-16.0	-184.6	73.8	-163.9
234 – 24	-30.2	-12.4	-171.5	62.9	-151.3
4 – 236	-38.1	-16.0	-180	73.9	-160.3
234 – 34	-32.1	-13.4	-181.2	65.3	-161.4

List of References

1 S. Datta and D. J. W. Grant, Crystal structures of drugs: advances in determination, prediction and engineering, *Nat. Rev. Drug Discov.*, 2004, **3**, 42–57.

2 N. K. Duggirala, M. L. Perry, Ö. Almarsson and M. J. Zaworotko, Pharmaceutical cocrystals: along the path to improved medicines, *Chem. Commun.*, 2016, **52**, 640–655.

3 D.-K. Bučar, Engineering Molecular Crystals: Backbreaking, yet Gratifying, *Cryst. Growth Des.*, 2017, **17**, 2913–2918.

4 G. R. Desiraju, Crystal engineering: From molecule to crystal, *J. Am. Chem. Soc.*, 2013, **135**, 9952–9967.

5 M. K. Corpinot and D. K. Bučar, A Practical Guide to the Design of Molecular Crystals, *Cryst. Growth Des.*, 2019, **19**, 1426–1453.

6 M. K. Mishra, U. Ramamurty and G. R. Desiraju, Mechanical property design of molecular solids, *Curr. Opin. Solid State Mater. Sci.*, 2016, **20**, 361–370.

7 R. Taylor, Which intermolecular interactions have a significant influence on crystal packing?, *CrystEngComm*, 2014, **16**, 6852.

8 C. P. Brock and J. D. Dunitz, Towards a Grammar of Crystal Packing, *Chem. Mater.*, 1994, **6**, 1118–1127.

9 J. Perlstein, Molecular Self-Assemblies. 2. A Computational Method for the Prediction of the Structure of One-Dimensional Screw, Glide, and Inversion Molecular Aggregates and Implications for the Packing of Molecules in Monolayers and Crystals, *J. Am. Chem. Soc.*, 1994, **116**, 455–470.

10 A. I. Kitaigorodskii, The principle of close packing and the condition of thermodynamic stability of organic crystals, *Acta Crystallogr.*, 1965, **18**, 585–590.

11 A. I. Kitaigorodskii, *Organic chemical crystallography*, Consultants Bureau, New York, 1961.

12 L. Pauling and M. Delbrück, The Nature of Intermolecular Forces Operative in Biological Processes, *Science*, 1940, **92**, 77–9.

13 J. A. R. P. Sarma and J. D. Dunitz, Structures of three crystalline phases of p-

(trimethylammonio)benzenesulfonate and their interconversions, *Acta Crystallogr. Sect. B*, 1990, **46**, 784–794.

14 G. R. Desiraju, Polymorphism: The Same and Not Quite the Same, *Cryst. Growth Des.*, 2008, **8**, 3–5.

15 J.-P. Brog, C.-L. Chanez, A. Crochet and K. M. Fromm, Polymorphism, what it is and how to identify it: a systematic review, *RSC Adv.*, 2013, **3**, 16905.

16 S. L. Price, Predicting crystal structures of organic compounds, *Chem. Soc. Rev.*, 2014, **43**, 2098–2111.

17 A. Gavezzotti, Structure and energy in organic crystals with two molecules in the asymmetric unit: Causality or chance?, *CrystEngComm*, 2008, **10**, 389–398.

18 A. J. Cruz-Cabeza, S. M. Reutzel-Edens and J. Bernstein, Facts and fictions about polymorphism, *Chem. Soc. Rev.*, 2015, **44**, 8619–8635.

19 J. D. Dunitz and A. Gavezzotti, Molecular recognition in organic crystals: Directed intermolecular bonds or nonlocalized bonding?, *Angew. Chemie - Int. Ed.*, 2005, **44**, 1766–1787.

20 A. Gavezzotti and G. Filippini, Geometry of the Intermolecular X-H-Y (X, Y = N, O) Hydrogen Bond and the Calibration of Empirical Hydrogen-Bond Potentials, *J. Phys. Chem*, 1994, **98**, 4831–4837.

21 W. T. M. Mooij, B. P. van Eijck, S. L. Price, P. Verwer and J. Kroon, Crystal structure predictions for acetic acid, *J. Comput. Chem.*, 1998, **19**, 459–474.

22 A. M. Reilly, R. I. Cooper, C. S. Adjiman, S. Bhattacharya, A. D. Boese, J. G. Brandenburg, P. J. Bygrave, R. Bylsma, J. E. Campbell, R. Car, D. H. Case, R. Chadha, J. C. Cole, K. Cosburn, H. M. Cuppen, F. Curtis, G. M. Day, R. A. DiStasio Jr, A. Dzyabchenko, B. P. van Eijck, D. M. Elking, J. A. van den Ende, J. C. Facelli, M. B. Ferraro, L. Fusti-Molnar, C.-A. Gatsiou, T. S. Gee, R. de Gelder, L. M. Ghiringhelli, H. Goto, S. Grimme, R. Guo, D. W. M. Hofmann, J. Hoja, R. K. Hylton, L. Iuzzolino, W. Jankiewicz, D. T. de Jong, J. Kendrick, N. J. J. de Klerk, H.-Y. Ko, L. N. Kuleshova, X. Li, S. Lohani, F. J. J. Leusen, A. M. Lund, J. Lv, Y. Ma, N. Marom, A. E. Masunov, P. McCabe, D. P. McMahon, H. Meekes, M. P. Metz, A. J. Misquitta, S. Mohamed, B. Monserrat, R. J. Needs, M. A. Neumann, J. Nyman, S. Obata, H. Oberhofer, A. R. Oganov, A. M. Orendt, G. I. Pagola, C. C. Pantelides, C. J. Pickard, R. Podeszwa, L. S. Price, S. L. Price, A. Pulido, M. G. Read, K. Reuter, E. Schneider, C. Schober, G. P. Shields, P. Singh,

I. J. Sugden, K. Szalewicz, C. R. Taylor, A. Tkatchenko, M. E. Tuckerman, F. Vacarro, M. Vasileiadis, A. Vazquez-Mayagoitia, L. Vogt, Y. Wang, R. E. Watson, G. A. de Wijs, J. Yang, Q. Zhu and C. R. Groom, Report on the sixth blind test of organic crystal structure prediction methods, *Acta Crystallogr. Sect. B Struct. Sci. Cryst. Eng. Mater.*, 2016, **72**, 439–459.

23 S. Mohamed, in *Monographs in Supramolecular Chemistry*, 2019, pp. 1–31.

24 J. Perlstein, K. Steppe, S. Vaday and E. M. N. Ndip, Molecular self-assemblies. 5. Analysis of the vector properties of hydrogen bonding in crystal engineering, *J. Am. Chem. Soc.*, 1996, **118**, 8433–8443.

25 C. O'Dowd, J. D. Kennedy and M. Thornton-Pett, The use of Kitaigorodskii's Aufbau principle in the solid-state study of crystalline borane compounds. A preliminary account, *J. Organomet. Chem.*, 2002, **657**, 20–39.

26 J. Perlstein, in *Crystal Engineering: From Molecules and Crystals to Materials*, 1999, pp. 11420–11432.

27 P. Hobza, Calculations on noncovalent interactions and databases of benchmark interaction energies, *Acc. Chem. Res.*, 2012, **45**, 663–672.

28 A. Gavezzotti, The 'sceptical chymist': Intermolecular doubts and paradoxes, *CrystEngComm*, 2013, **15**, 4027–4035.

29 A. Bauzá, T. J. Mooibroek and A. Frontera, Towards design strategies for anion-π interactions in crystal engineering, *CrystEngComm*, 2015, **18**, 10–23.

30 M. J. Turner, S. Grabowsky, D. Jayatilaka and M. A. Spackman, Accurate and efficient model energies for exploring intermolecular interactions in molecular crystals, *J. Phys. Chem. Lett.*, 2014, **5**, 4249–4255.

31 A. Gavezzotti, *Molecular aggregation : structure analysis and molecular simulation of crystals and liquids*, Oxford University Press, 2007.

32 P. Atkins and J. de Paula, in *Elements of Physical Chemistry*, Oxford University Press, Oxford, 5th edn., 2009, pp. 351–363.

33 A. G. P. Maloney, The University of Edinburgh, 2015.

34 A. G. P. Maloney, P. A. Wood and S. Parsons, Competition between hydrogen bonding and dispersion interactions in the crystal structures of the primary amines, *CrystEngComm*, 2014, **16**, 3867–3882.

35 T. Steiner, The Hydrogen Bond in the Solid State, *Angew. Chemie Int. Ed.*, 2002, **41**, 48–76.

36 E. Arunan, G. R. Desiraju, R. A. Klein, J. Sadlej, S. Scheiner, I. Alkorta, D. C. Clary, R. H. Crabtree, J. J. Dannenberg, P. Hobza, H. G. Kjaergaard, A. C. Legon, B. Mennucci and D. J. Nesbitt, Defining the hydrogen bond: An account (IUPAC Technical Report), *Pure Appl. Chem.*, 2011, **83**, 1619–1636.

37 J. D. Dunitz and A. Gavezzotti, Supramolecular synthons: Validation and ranking of intermolecular interaction energies, *Cryst. Growth Des.*, 2012, **12**, 5873–5877.

38 G. R. Desiraju, Supramolecular Synthons in Crystal Engineering—A New Organic Synthesis, *Angew. Chemie Int. Ed. English*, 1995, **34**, 2311–2327.

39 J. D. Dunitz, Phase transitions in molecular crystals from a chemical viewpoint, *Pure Appl. Chem*, 1991, **63**, 177–185.

40 J.-M. Lehn, Supramolecular Chemistry—Scope and Perspectives Molecules, Supermolecules, and Molecular Devices(Nobel Lecture), *Angew. Chemie Int. Ed. English*, 1988, **27**, 89–112.

41 G. R. Desiraju, Crystal Engineering: A Holistic View, *Angew. Chemie Int. Ed.*, 2007, **46**, 8342–8356.

42 A. Mukherjee, Building upon supramolecular synthons: Some aspects of crystal engineering, *Cryst. Growth Des.*, 2015, **15**, 3076–3085.

43 P. T. A. Galek, L. Fábián, W. D. S. Motherwell, F. H. Allen and N. Feeder, Knowledge-based model of hydrogen-bonding propensity in organic crystals, *Acta Crystallogr. Sect. B Struct. Sci.*, 2007, **63**, 768–782.

44 M. C. Etter, Encoding and Decoding Hydrogen-Bond Patterns of Organic Compounds, *Acc. Chem. Res.*, 1990, **23**, 120–126.

45 A. Gavezzotti, The lines-of-force landscape of interactions between molecules in crystals; Cohesive versus tolerant and collateral damage contact, *Acta Crystallogr. Sect. B Struct. Sci.*, 2010, **66**, 396–406.

46 S. Wang, X. H. Ding, Y. H. Li and W. Huang, Effects of strong hydrogen bonds and weak intermolecular interactions on supramolecular assemblies of 4-fluorobenzylamine, *J. Mol. Struct.*, 2015, **1091**, 98–108.

47 M. K. Corpinot, S. A. Stratford, M. Arhangelskis, J. Anka-Lufford, I. Halasz, N. Judaš, W.

Jones and D.-K. Bučar, On the predictability of supramolecular interactions in molecular cocrystals – the view from the bench, *CrystEngComm*, 2016, **18**, 5434–5439.

48 E. J. C. de Vries, S. Kantengwa, A. Ayamine and N. B. Báthori, Testing the limits of synthon engineering: salts of salicylic and sulfosalicylic acid with nucleobases and derivatives, *CrystEngComm*, 2016, **18**, 7573–7579.

49 D. Chopra and T. N. G. Row, Role of organic fluorine in crystal engineering, *CrystEngComm*, 2011, **13**, 2175–2186.

50 G. R. Desiraju, The C-H···O Hydrogen Bond: Structural Implications and Supramolecular Design, *Acc. Chem. Res.*, 1996, **29**, 441–449.

51 S. Chakraborty, L. Rajput and G. R. Desiraju, Designing Ternary Co-crystals with Stacking Interactions and Weak Hydrogen Bonds. 4,4'-Bis-hydroxyazobenzene, *Cryst. Growth Des.*, 2014, **14**, 2571–2577.

52 M. Pérez-Torralba, M. Á. García, C. López, M. C. Torralba, M. R. Torres, R. M. Claramunt and J. Elguero, Structural investigation of weak intermolecular interactions (Hydrogen and Halogen Bonds) in fluorine-substituted benzimidazoles, *Cryst. Growth Des.*, 2014, **14**, 3499–3509.

53 M. Albrecht, M. Müller, A. Valkonen and K. Rissanen, Weak non-covalent interactions control the relative molecular orientation in the crystals of N-pentafluorobenzyl aniline derivatives, *CrystEngComm*, 2010, **12**, 3698–3702.

54 L. Wang, Y. Hu, W. Wang, F. Liu and K. Huang, Energetic multi-component molecular solids of tetrafluoroterephthalic acid with some aza compounds by strong hydrogen bonds and weak intermolecular interactions of C–H···F and C–H···O, *CrystEngComm*, 2014, **16**, 4142–4161.

55 R. Du, J. Wu, L. Chen, H. Huang, X. Zhang and J. Zhang, Hierarchical Hydrogen Bonds Directed Multi-Functional Carbon Nanotube-Based Supramolecular Hydrogels, *Small*, 2014, **10**, 1387–1393.

56 N. Kumar, S. Khullar, Y. Singh and S. K. Mandal, Hierarchical importance of coordination and hydrogen bonds in the formation of homochiral 2D coordination polymers and 2D supramolecular assemblies, *CrystEngComm*, 2014, **16**, 6730–6744.

57 C. R. Groom, I. J. Bruno, M. P. Lightfoot and S. C. Ward, The Cambridge structural database, *Acta Crystallogr. Sect. B Struct. Sci. Cryst. Eng. Mater.*, 2016, **72**, 171–179.

58 C. Dalvit, C. Invernizzi and A. Vulpetti, Fluorine as a Hydrogen-Bond Acceptor: Experimental Evidence and Computational Calculations, *Chem. - A Eur. J.*, 2014, **20**, 11058–11068.

59 P. Panini and D. Chopra, Experimental and theoretical characterization of short h-bonds with organic fluorine in molecular crystals, *Cryst. Growth Des.*, 2014, **14**, 3155–3168.

60 K. Müller-Dethlefs and P. Hobza, Noncovalent Interactions: A Challenge for Experiment and Theory, *Chem. Rev.*, 2000, **100**, 143–168.

61 A. Mukherjee, S. Tothadi and G. R. Desiraju, Halogen bonds in crystal engineering: Like hydrogen bonds yet different, *Acc. Chem. Res.*, 2014, **47**, 2514–2524.

62 Corradi, Meille, Messina, Metrangolo and Resnati, Halogen Bonding versus Hydrogen Bonding in Driving Self-Assembly Processes Perfluorocarbon-hydrocarbon self-assembly, part IX. This work was supported by MURST (Cofinanziamento ’99) and EU (COST-D12-0012). We thank Dr. A. Lunghi and Dr. P. Cardillo (Stazi, *Angew. Chem. Int. Ed. Engl.*, 2000, **39**, 1782–1786.

63 C. B. Aakeröy, M. Fasulo, N. Schultheiss, J. Desper and C. Moore, Structural competition between hydrogen bonds and halogen bonds, *J. Am. Chem. Soc.*, 2007, **129**, 13772–13773.

64 G. R. Desiraju, P. Shing Ho, L. Kloo, A. C. Legon, R. Marquardt, P. Metrangolo, P. Politzer, G. Resnati and K. Rissanen, Definition of the halogen bond (IUPAC recommendations 2013), *Pure Appl. Chem.*, 2013, **85**, 1711–1713.

65 P. Politzer, J. S. Murray and T. Clark, Halogen bonding and other σ-hole interactions: A perspective, *Phys. Chem. Chem. Phys.*, 2013, **15**, 11178–11189.

66 T. Clark, M. Hennemann, J. S. Murray and P. Politzer, Halogen bonding: The σ-hole, *J. Mol. Model.*, 2007, **13**, 291–296.

67 G. R. Desiraju and R. Parthasarathy, The Nature of Halogen•••Halogen Interactions: Are Short Halogen Contacts Due to Specific Attractive Forces or Due to Close Packing of Nonspherical Atoms?, *J. Am. Chem. Soc.*, 1989, **111**, 8725–8726.

68 A. Mukherjee and G. R. Desiraju, Halogen bonds in some dihalogenated phenols: Applications to crystal engineering, *IUCrJ*, 2014, **1**, 49–60.

69 P. Metrangolo and G. Resnati, Type II halogen···halogen contacts are halogen bonds, *IUCrJ*, 2014, **1**, 5–7.

70 F. Meyer and P. Dubois, Halogen bonding at work: Recent applications in synthetic

chemistry and materials science, *CrystEngComm*, 2013, **15**, 3058–3071.

71 Sushila, P. Venugopalan, R. Kataria, D. K. Das, A. Chaudhary and R. Patra, Wheel and Axle Topology Driven Halogen Bonds for the Construction of Molecular Arrays in Hexacoordinated Sn(IV)Porphyrins: A Structural and Theoretical Investigation, *Cryst. Growth Des.*, 2019, **19**, 942–951.

72 K. Shimizu and J. Ferreira da Silva, Halogen and hydrogen bonding interplay in the crystal packing of halometallocenes, *Molecules*, , DOI:10.3390/molecules23112959.

73 K. Eskandari and M. Lesani, Does fluorine participate in halogen bonding?, *Chem. - A Eur. J.*, 2015, **21**, 4739–4746.

74 L. M. Salonen, M. Ellermann and F. Diederich, Aromatic rings in chemical and biological recognition: Energetics and structures, *Angew. Chemie - Int. Ed.*, 2011, **50**, 4808–4842.

75 E. A. Meyer, R. K. Castellano and F. Diederich, Interactions with Aromatic Rings in Chemical and Biological Recognition, *Angew. Chemie Int. Ed.*, 2003, **42**, 1210–1250.

76 V. L. Malinovskii, F. Samain and R. Häner, Helical arrangement of interstrand stacked pyrenes in a DNA framework, *Angew. Chemie - Int. Ed.*, 2007, **46**, 4464–4467.

77 R. Fasan, R. L. A. Dias, K. Moehle, O. Zerbe, D. Obrecht, P. R. E. Mittl, M. G. Grütter and J. A. Robinson, Structure-activity studies in a family of β-hairpin protein epitope mimetic inhibitors of the p53-HDM2 protein-protein interaction, *ChemBioChem*, 2006, **7**, 515–526.

78 C. R. Martinez and B. L. Iverson, Rethinking the term 'pi-stacking', *Chem. Sci.*, 2012, **3**, 2191–2201.

79 Z. F. Yao, J. Y. Wang and J. Pei, Control of π-π Stacking via Crystal Engineering in Organic Conjugated Small Molecule Crystals, *Cryst. Growth Des.*, 2018, **18**, 7–15.

80 K. Daze and F. Hof, in *Encyclopedia of Physical Organic Chemistry, 5 Volume Set*, John Wiley & Sons, Inc., Hoboken, NJ, USA, 2016, pp. 26–31.

81 S. Tsuzuki, K. Honda, T. Uchimaru, M. Mikami and K. Tanabe, Origin of attraction and directionality of the π/π interaction: Model chemistry calculations of benzene dimer interaction, *J. Am. Chem. Soc.*, 2002, **124**, 104–112.

82 W. B. Jennings, B. M. Farrell and J. F. Malone, Attractive intramolecular edge-to-face aromatic interactions in flexible organic molecules, *Acc. Chem. Res.*, 2001, **34**, 885–894.

83 C. A. Hunter and J. K. M. Sanders, The Nature of π-π Interactions, *J. Am. Chem. Soc.*, 1990, **112**, 5525–5534.

84 F. Cozzi, F. Ponzini, R. Annunziata, M. Cinquini and J. S. Siegel, Polar Interactions between Stacked π Systems in Fluorinated 1,8-Diarylnaphthalenes: Importance of Quadrupole Moments in Molecular Recognition, *Angew. Chemie Int. Ed. English*, 1995, **34**, 1019–1020.

85 N. M. D. Brown and F. L. Swinton, The importance of quadrupolar interactions in determining the structure of solid hydrocarbon–fluorocarbon compounds, *J. Chem. Soc., Chem. Commun.*, 1974, 770–771.

86 B. A. Ikkanda and B. L. Iverson, Exploiting the interactions of aromatic units for folding and assembly in aqueous environments, *Chem. Commun.*, 2016, **52**, 7752–7759.

87 C. A. Hunter, K. R. Lawson, J. Perkins and C. J. Urch, Aromatic interactions, *J. Chem. Soc. Perkin Trans. 2*, 2001, 651–669.

88 S. E. Wheeler and J. W. G. Bloom, Toward a more complete understanding of noncovalent interactions involving aromatic rings, *J. Phys. Chem. A*, 2014, **118**, 6133–6147.

89 M. O. Sinnokrot and C. D. Sherrill, High-accuracy quantum mechanical studies of π-π interactions in benzene dimers, *J. Phys. Chem. A*, 2006, **110**, 10656–10668.

90 J. wun Hwang, P. Li and K. D. Shimizu, Synergy between experimental and computational studies of aromatic stacking interactions, *Org. Biomol. Chem.*, 2017, **15**, 1554–1564.

91 J. D. Dunitz, A. Gavezzotti and W. B. Schweizer, Molecular Shape and Intermolecular Liaison: Hydrocarbons and Fluorocarbons, *Helv. Chim. Acta*, 2003, **86**, 4073–4092.

92 S. R. Shaikh, R. L. Gawade, D. Kumar, A. Kotmale, R. G. Gonnade and T. Stürzer, Crystal Engineering for Intramolecular π-π Stacking: Effect of Sequential Substitution of F on Molecular Geometry in Conformationally Flexible Sulfonamides, *Cryst. Growth Des.*, 2019, **19**, 5665–5678.

93 D. M. Cho, S. R. Parkin and M. D. Watson, Partial fluorination overcomes herringbone crystal packing in small polycyclic aromatics, *Org. Lett.*, 2005, **7**, 1067–1068.

94 A. Hori and T. Arii, Cation-π and arene-perfluoroarene interactions between Cu(II) fluorine-substituted β-diketonate complex and benzenes, *CrystEngComm*, 2007, **9**, 215–217.

95 M. D. Blanchard, R. P. Hughes, T. E. Concolino and A. L. Rheingold, π-Stacking between pentafluorophenyl and phenyl groups as a controlling feature of intra- and intermolecular

crystal structure motifs in substituted ferrocenes. Observation of unexpected face-to-face stacking between pentafluorophenyl rings, *Chem. Mater.*, 2000, **12**, 1604–1610.

96 J. R. Lane, G. C. Saunders and S. J. Webb, Engineering of a polar crystal structure exclusively by π-π Stacking between aryl and polyfluoroaryl groups, *CrystEngComm*, 2013, **15**, 1293–1295.

97 L. M. Henling, J. W. Ziller, A. R. Dunn, R. H. Grubbs, G. W. Coates, E. B. Lobkovsky, A. R. Dunn, L. M. Henling, R. H. Grubbs and J. W. Ziller, Phenyl-perfluorophenyl stacking interactions: Topochemical [2+2] photodimerization and photopolymerization of olefinic compounds, *J. Am. Chem. Soc.*, 2002, **120**, 3641–3649.

98 B. W. Gung and J. C. Amicangelo, Substituent effects in C6F6-C6H5X stacking interactions, *J. Org. Chem.*, 2006, **71**, 9261–9270.

99 M. Karanam and A. R. Choudhury, Study of halogen-mediated weak interactions in a series of halogen-substituted azobenzenes, *Cryst. Growth Des.*, 2013, **13**, 4803–4814.

100 J. D. Dunitz, Organic fluorine: Odd man out, *ChemBioChem*, 2004, **5**, 614–621.

101 R. Berger, G. Resnati, P. Metrangolo, E. Weber and J. Hulliger, Organic fluorine compounds: a great opportunity for enhanced materials properties, *Chem. Soc. Rev. Chem. Soc. Rev*, 2011, **40**, 3496–3508.

102 K. Reichenbächer, H. I. Süss and J. Hulliger, Fluorine in crystal engineering - 'The little atom that could', *Chem. Soc. Rev.*, 2005, **34**, 22–30.

103 M. Cametti, B. Crousse, P. Metrangolo, R. Milani and G. Resnati, The fluorous effect in biomolecular applications, *Chem. Soc. Rev.*, 2012, **41**, 31–42.

104 J.-P. Bégué and D. Bonnet-Delpon, *Bioorganic and medicinal chemistry of fluorine*, John Wiley & Sons, Hoboken, New Jersey, 2008.

105 L. Pauling, *The Nature of the Chemical Bond and the Structure of Molecule and Crystals: An Introduction to Modern Structural Chemistry*, Cornell University Press, Ithaca, New York, 1939.

106 D. O'Hagan, Understanding organofluorine chemistry. An introduction to the C-F bond, *Chem. Soc. Rev.*, 2008, **37**, 308–319.

107 C. R. PATRICK and G. S. PROSSER, A Molecular Complex of Benzene and Hexafluorobenzene, *Nature*, 1960, **187**, 1021–1021.

108 J. H. Williams, J. K. Cockcroft and A. N. Fitch, Structure of the Lowest Temperature Phase of the Solid Benzene–Hexafluorobenzene Adduct, *Angew. Chemie Int. Ed. English*, 1992, **31**, 1655–1657.

109 C. J. Pace and J. Gao, Exploring and exploiting polar-π interactions with fluorinated aromatic amino acids, *Acc. Chem. Res.*, 2013, **46**, 907–915.

110 J. C. Ma and D. A. Dougherty, The cation-π interaction, *Chem. Rev.*, 1997, **97**, 1303–1324.

111 S. L. Cockroft, C. A. Hunter, K. R. Lawson, J. Perkins and C. J. Urch, Electrostatic control of aromatic stacking interactions, *J. Am. Chem. Soc.*, 2005, **127**, 8594–8595.

112 S. L. Cockroft, J. Perkins, C. Zonta, H. Adams, S. E. Spey, C. M. R. Low, J. G. Vinter, K. R. Lawson, C. J. Urch and C. A. Hunter, Substituent effects on aromatic stacking interactions, *Org. Biomol. Chem.*, 2007, **5**, 1062–1080.

113 S. E. Wheeler and K. N. Houk, Through-space effects of substituents dominate molecular electrostatic potentials of substituted arenes, *J. Chem. Theory Comput.*, 2009, **5**, 2301–2312.

114 A. L. Ringer and D. Sherrill, Substituent effects in sandwich configurations of multiply substituted benzene dimers are not solely governed by electrostatic control, *J. Am. Chem. Soc.*, 2009, **131**, 4574–4575.

115 S. E. Wheeler, Local nature of substituent effects in stacking interactions, *J. Am. Chem. Soc.*, 2011, **133**, 10262–10274.

116 S. E. Wheeler and K. N. Houk, Substituent effects in the benzene dimer are due to direct interactions of the substituents with the unsubstituted benzene, *J. Am. Chem. Soc.*, 2008, **130**, 10854–10855.

117 P. B. Lutz and C. A. Bayse, Interpreting geometric preferences in π-stacking interactions through molecular orbital analysis, *Int. J. Quantum Chem.*, 2018, **118**, e25513.

118 S. W. Watt, C. Dai, A. J. Scott, J. M. Burke, R. L. Thomas, J. C. Collings, C. Viney, W. Clegg and T. B. Marder, Structure and phase behavior of a 2:1 complex between arene- and fluoroarene-based conjugated rigid rods, *Angew. Chemie - Int. Ed.*, 2004, **43**, 3061–3063.

119 O. S. Bushuyev, A. Tomberg, J. R. Vinden, N. Moitessier, C. J. Barrett and T. Friščić, Azo···phenyl stacking: A persistent self-assembly motif guides the assembly of fluorinated cis-azobenzenes into photo-mechanical needle crystals, *Chem. Commun.*, 2016, **52**, 2103–

2106.

120 J. M. Serrano-Becerra, S. Hernández-Ortega, D. Morales-Morales and J. Valdés-Martínez, Bottom-up design and construction of a non-centrosymmetric network through π-π stacking interactions, *CrystEngComm*, 2009, **11**, 226–228.

121 T. Rasmusson, L. J. P. Martyn, G. Chen, A. Lough, M. Oh and A. K. Yudin, Aromatic fluorine as a versatile control element for the construction of molecules with helical chirality, *Angew. Chemie - Int. Ed.*, 2008, **47**, 7009–7012.

122 K. Kishikawa, K. Oda, S. Aikyo and S. Kohmoto, Columnar superstructures of non-disc-shaped molecules generated by arene-perfluoroarene face-to-face interactions, *Angew. Chemie - Int. Ed.*, 2007, **46**, 764–768.

123 C. E. Smith, P. S. Smith, R. L. Thomas, E. G. Robins, J. C. Collings, C. Dai, A. J. Scott, S. Borwick, A. S. Batsanov, S. W. Watt, S. J. Clark, C. Viney, J. A. K. Howard, W. Clegg and T. B. Marder, Arene-perfluoroarene interactions in crystal engineering: structural preferences in polyfluorinated tolans, *J. Mater. Chem.*, 2004, **14**, 413–420.

124 S. Zhu, S. Zhu, G. Jin and Z. Li, Strong phenyl-perfluorophenyl π-π stacking and C-H···F-C hydrogen bonding interactions in the crystals of the corresponding aromatic aldimines, *Tetrahedron Lett.*, 2005, **46**, 2713–2716.

125 E. Espinosa, I. Alkorta, J. Elguero and E. Molins, From weak to strong interactions: A comprehensive analysis of the topological and energetic properties of the electron density distribution involving X-H···F-Y systems, *J. Chem. Phys.*, 2002, **117**, 5529–5542.

126 P. A. Champagne, J. Desroches and J. F. Paquin, Organic fluorine as a hydrogen-bond acceptor: Recent examples and applications, *Synth.*, 2015, **47**, 306–322.

127 P. Murray-Rust, W. C. Stallings, C. T. Monti, R. K. Preston and J. P. Glusker, Intermolecular interactions of the carbon-fluorine bond: the crystallographic environment of fluorinated carboxylic acids and related structures, *J. Am. Chem. Soc.*, 1983, **105**, 3206–3214.

128 L. Shimoni, J. P. Glusker, L. Shimonia and J. P. Glusker, in *Science of Crystal Structures: Highlights in Crystallography*, Kluwer Academic Publishers-Plenum Publishers, 1994, vol. 5, pp. 383–397.

129 J. A. K. Howard, V. J. Hoy, D. O'Hagan and G. T. Smith, How good is fluorine as a hydrogen bond acceptor?, *Tetrahedron*, 1996, **52**, 12613–12622.

130 J. D. Dunitz and R. Taylor, Organic fluorine hardly ever accepts hydrogen bonds, *Chem. - A Eur. J.*, 1997, **3**, 89–98.

131 R. Taylor, The hydrogen bond between N-H or O-H and organic fluorine: Favourable yes, competitive no, *Acta Crystallogr. Sect. B Struct. Sci. Cryst. Eng. Mater.*, 2017, **73**, 474–488.

132 A. Gavezzotti and L. Lo Presti, Building blocks of crystal engineering: A large-database study of the intermolecular approach between C-H donor groups and O, N, Cl, or F acceptors in organic crystals, *Cryst. Growth Des.*, 2016, **16**, 2952–2962.

133 R. Taylor and P. A. Wood, A Million Crystal Structures: The Whole Is Greater than the Sum of Its Parts, *Chem. Rev.*, 2019, **119**, 9427–9477.

134 J. D. Dunitz and A. Gavezzotti, How molecules stick together in organic crystals: Weak intermolecular interactions, *Chem. Soc. Rev.*, 2009, **38**, 2622–2633.

135 B. K. Saha, A. Saha, D. Sharada and S. A. Rather, F or O, Which One Is the Better Hydrogen Bond (Is It?) Acceptor in C-H···X-C (X- = F-, O=) Interactions?, *Cryst. Growth Des.*, 2018, **18**, 1–6.

136 V. R. Thalladi, H. C. Weiss, D. Bläser, R. Boese, A. Nangia and G. R. Desiraju, C-H···F interactions in the crystal structures of some fluorobenzenes, *J. Am. Chem. Soc.*, 1998, **120**, 8702–8710.

137 A. R. Choudhury and T. N. Guru Row, How Realistic Are Interactions Involving Organic Fluorine in Crystal Engineering? Insights from Packing Features in Substituted Isoquinolines, *Cryst. Growth Des.*, 2004, **4**, 47–52.

138 Y. Sakamoto and T. Suzuki, Perfluorinated and Half-Fluorinated Rubrenes: Synthesis and Crystal Packing Arrangements, *J. Org. Chem.*, 2017, **82**, 8111–8116.

139 T. S. Thakur, M. T. Kirchner, D. Bläser, R. Boese and G. R. Desiraju, C-H···F-C hydrogen bonding in 1,2,3,5-tetrafluorobenzene and other fluoroaromatic compounds and the crystal structure of alloxan revisited, *CrystEngComm*, 2010, **12**, 2079–2085.

140 R. Mariaca, N. R. Behrnd, P. Eggli, H. Stoeckli-Evans and J. Hulliger, Synthesis and crystal engineering of fluorinated stilbenes, *CrystEngComm*, 2006, **8**, 222–232.

141 M. Y. Anzahaee, J. K. Watts, N. R. Alla, A. W. Nicholson and M. J. Damha, Energetically important C-H · · · F-C pseudohydrogen bonding in water: Evidence and application to rational design of oligonucleotides with high binding affinity, *J. Am. Chem. Soc.*, 2011, **133**,

728–731.

142 H.-J. J. Schneider, M. Karplus, G. Dolgonos, J. Lipkowski, H.-J. J. Schneider, B. Schulz, J. G. Vinter, S. Kirpekar, O. L. Malkina and H. H. Limbach, Hydrogen bonds with fluorine. Studies in solution, in gas phase and by computations, conflicting conclusions from crystallographic analyses, *Chem. Sci.*, 2012, **3**, 1381.

143 D. Gurka, R. W. Taft, L. Joris and P. V. R. Schleyer, Regarding Proton Transfer in Hydrogen-Bonded Complexes as Measured by Fluorine Nuclear Magnetic Resonance, *J. Am. Chem. Soc.*, 1967, **89**, 5957–5958.

144 E. O. Levina, I. Y. Chernyshov, A. P. Voronin, L. N. Alekseiko, A. I. Stash and M. V. Vener, Solving the enigma of weak fluorine contacts in the solid state: A periodic DFT study of fluorinated organic crystals, *RSC Adv.*, 2019, **9**, 12520–12537.

145 M. V. Vener, A. N. Egorova, A. V. Churakov and V. G. Tsirelson, Intermolecular hydrogen bond energies in crystals evaluated using electron density properties: DFT computations with periodic boundary conditions, *J. Comput. Chem.*, 2012, **33**, 2303–2309.

146 J. Shang, N. M. Gallagher, F. Bie, Q. Li, Y. Che, Y. Wang and H. Jiang, Aromatic triazole foldamers induced by C-H...X (X = F, Cl) intramolecular hydrogen bonding, *J. Org. Chem.*, 2014, **79**, 5134–5144.

147 R. Taylor, It Isn't, It Is: The C-H···X (X = O, N, F, Cl) Interaction Really Is Significant in Crystal Packing, *Cryst. Growth Des.*, 2016, **16**, 4165–4168.

148 J. McKenzie and C. A. Hunter, Competitor analysis of functional group H-bond donor and acceptor properties using the Cambridge Structural Database, *Phys. Chem. Chem. Phys.*, 2018, **20**, 25324–25334.

149 P. Panini and D. Chopra, Quantitative insights into energy contributions of intermolecular interactions in fluorine and trifluoromethyl substituted isomeric N-phenylacetamides and N-methylbenzamides, *CrystEngComm*, 2013, **15**, 3711–3733.

150 P. Panini, R. G. Gonnade and D. Chopra, Experimental and computational analysis of supramolecular motifs involving Csp2(aromatic)-F and CF3 groups in organic solids, *New J. Chem.*, 2016, **40**, 4981–5001.

151 M. Barceló-Oliver, C. Estarellas, A. García-Raso, A. Terrón, A. Frontera, D. Quiñonero, I. Mata, E. Molins and P. M. Deyà, Experimental and theoretical study of uracil derivatives: The crucial role of weak fluorine-fluorine noncovalent interactions, *CrystEngComm*, 2010,

12, 3758–3767.

152 R. M. Osuna, V. Hernández, J. T. L. Navarrete, E. D'Oria and J. J. Novoa, Theoretical evaluation of the nature and strength of the F···F intermolecular interactions present in fluorinated hydrocarbons, *Theor. Chem. Acc.*, 2011, **128**, 541–553.

153 R. J. Baker, P. E. Colavita, D. M. Murphy, J. A. Platts and J. D. Wallis, Fluorine-fluorine interactions in the solid state: An experimental and theoretical study, *J. Phys. Chem. A*, 2012, **116**, 1435–1444.

154 V. R. Hathwar and T. N. Guru Row, Charge density analysis of heterohalogen (Cl···F) and homohalogen (F···F) intermolecular interactions in molecular crystals: Importance of the extent of polarizability, *Cryst. Growth Des.*, 2011, **11**, 1338–1346.

155 V. A. Karnoukhova, I. V. Fedyanin and K. A. Lyssenko, Directionality of intermolecular C-F···F-C interactions in crystals: Experimental and theoretical charge density study, *Struct. Chem.*, 2016, **27**, 17–24.

156 H. R. Khavasi and N. Rahimi, Are fluorine-based contacts predictable? A case study in three similar coordination compounds, *CrystEngComm*, 2017, **19**, 1361–1365.

157 L. Lo Presti, On the significance of weak hydrogen bonds in crystal packing: A large databank comparison of polymorphic structures, *CrystEngComm*, 2018, **20**, 5976–5989.

158 P. Ganguly and G. R. Desiraju, Long-range synthon Aufbau modules (LSAM) in crystal structures: Systematic changes in C6H6-nFn (0 ≤ n ≤ 6) fluorobenzenes, *CrystEngComm*, 2010, **12**, 817–833.

159 G. Chapuis and C. P. Brock, *IUCr Online Dictionary of Crystallography*, Commission for Crystallographic Nomenclature, 2017.

160 H. Burzlaff and H. Zimmermann, in *International Tables for Crystallography Volume A: Space-group symmetry*, ed. T. Hahn, Springer, Dordrecht, 2006, pp. 742–749.

161 T. Hahn, Ed., *International Tables for Crystallography: Volume A, Space-Group Symmetry*, Springer, Dordrecht, 5th edn., 2006.

162 W. Bragg and L. Bragg, The structure of some crystals as indicated by their diffraction of X-rays, *Proc. R. Soc. London. Ser. A, Contain. Pap. a Math. Phys. Character*, 1913, **89**, 248–277.

163 C. Hammond, in *The Basics of Crystallography and Diffraction*, Oxford University Press,

Oxford, 4th edn., 2015, pp. 329–362.

164 G. Rossman and E. Arnold, in *International Tables for Crystallography Volume B: Reciprocal space*, ed. U. Shmueli, Springer, Dordrecht, 2006, pp. 244–281.

165 C. Giacovazzo, in *International Tables for Crystallography Volume B: Reciprocal space*, ed. U. Shmueli, Springer Netherlands, Dordrecht, 2001, pp. 210–234.

166 L. Palatinus, The charge-flipping algorithm in crystallography, *Acta Crystallogr. Sect. B Struct. Sci. Cryst. Eng. Mater.*, 2013, **69**, 1–16.

167 T. S. Koritsanszky and P. Coppens, Chemical applications of X-ray charge-density analysis, *Chem. Rev.*, 2001, **101**, 1583–1627.

168 A. Ø. Madsen, in *Electron Density and Chemical Bonding I: Experimental Charge Density Studies*, ed. D. Stalke, Springer Berlin Heidelberg, Berlin, Heidelberg, 2012, pp. 21–52.

169 I. L. Kirby, M. B. Pitak, S. J. Coles and P. A. Gale, Systematic Experimental Charge Density: Linking Structural Modifications to Electron Density Distributions, *Chem. Lett.*, 2014, **44**, 2–9.

170 N. K. Hansen and P. Coppens, Testing aspherical atom refinements on small-molecule data sets, *Acta Crystallogr. Sect. A*, 1978, **34**, 909–921.

171 F. L. Hirshfeld, Can X-ray data distinguish bonding effects from vibrational smearing?, *Acta Crystallogr. Sect. A*, 1976, **32**, 239–244.

172 L. J. Farrugia, *IUCrJ*, 2014, 1, 265–266.

173 R. F. W. Bader, *Atoms in molecules : a quantum theory*, Clarendon Press, Oxford, 1990.

174 A. Krawczuk and P. Macchi, Charge density analysis for crystal engineering, *Chem. Cent. J.*, 2014, **8**, 68.

175 R. F. W. Bader, The zero-flux surface and the topological and quantum definitions of an atom in a molecule, *Theor. Chem. Acc.*, 2001, **105**, 276–283.

176 R. F. W. Bader, A bond path: A universal indicator of bonded interactions, *J. Phys. Chem. A*, 1998, **102**, 7314–7323.

177 P. S. V. Kumar, V. Raghavendra and V. Subramanian, Bader's Theory of Atoms in Molecules (AIM) and its Applications to Chemical Bonding, *J. Chem. Sci.*, 2016, **128**, 1527–1536.

178 Y. A. Abramov, On the Possibility of Kinetic Energy Density Evaluation from the Experimental Electron-Density Distribution, *Acta Crystallogr. Sect. A Found. Crystallogr.*, 1997, **53**, 264–272.

179 E. Espinosa, E. Molins and C. Lecomte, Hydrogen bond strengths revealed by topological analyses of experimentally observed electron densities, *Chem. Phys. Lett.*, 1998, **285**, 170–173.

180 A. Gavezzotti, Non-conventional bonding between organic molecules. The 'halogen bond' in crystalline systems, *Mol. Phys.*, 2008, **106**, 1473–1485.

181 A. Gavezzotti, Calculation of intermolecular interaction energies by direct numerical integration over electron densities. 2. An improved polarization model and the evaluation of dispersion and repulsion energies, *J. Phys. Chem. B*, 2003, **107**, 2344–2353.

182 A. Gavezzotti, Calculation of intermolecular interaction energies by direct numerical integration over electron densities. 1. Electrostatic and polarization energies in molecular crystals, *J. Phys. Chem. B*, 2002, **106**, 4145–4154.

183 A. Gavezzotti, Computational studies of crystal structure and bonding, *Top. Curr. Chem.*, 2012, **315**, 1–32.

184 G. Maitland, M. Rigby, E. Smith, W. Wakeham and D. Henderson, *Intermolecular Forces: Their Origin and Determination*, Oxford University Press, Oxford, 1983.

185 M. A. Spackman and P. G. Byrom, A novel definition of a molecule in a crystal, *Chem. Phys. Lett.*, 1997, **267**, 215–220.

186 F. L. Hirshfeld, Bonded-atom fragments for describing molecular charge densities, *Theor. Chim. Acta*, 1977, **44**, 129–138.

187 M. A. Spackman and D. Jayatilaka, Hirshfeld surface analysis, *CrystEngComm*, 2009, **11**, 19–32.

188 C. Jelsch, K. Ejsmont and L. Huder, The enrichment ratio of atomic contacts in crystals, an indicator derived from the Hirshfeld surface analysis, *IUCrJ*, 2014, **1**, 119–128.

189 G. Kaur, P. Panini, D. Chopra and A. Roy Choudhury, Structural investigation of weak intermolecular interactions in fluorine substituted isomeric N-benzylideneanilines, *Cryst. Growth Des.*, 2012, **12**, 5096–5110.

190 G. Kaur and A. R. Choudhury, Understanding of the weak intermolecular interactions

involving halogens in substituted N-benzylideneanilines: Insights from structural and computational perspectives, *Cryst. Growth Des.*, 2014, **14**, 1600–1616.

191 G. Kaur and A. R. Choudhury, A comprehensive understanding of the synthons involving C-H···F-C hydrogen bond(s) from structural and computational analyses, *CrystEngComm*, 2015, **17**, 2949–2963.

192 H. J. Schneider, Crystallographic searches for weak interactions – the limitations of data mining, *Acta Crystallogr. Sect. B Struct. Sci. Cryst. Eng. Mater.*, 2018, **74**, 322–324.

193 E. M. García-Frutos, U. K. Pandey, R. Termine, A. Omenat, J. Barberá, J. L. Serrano, A. Golemme and B. Gõmez-Lor, High charge mobility in discotic liquid-crystalline triindoles: Just a core business?, *Angew. Chemie - Int. Ed.*, 2011, **50**, 7399–7402.

194 H. Xu, K. Sohlberg and Y. Wei, Conformation of protonated trans-N-benzylideneaniline: A revisit, *J. Mol. Struct. THEOCHEM*, 2003, **634**, 311–314.

195 H. Bednarski, M. Domański, J. Weszka and K. Sohlberg, First-principles studies of internal rotation in protonated trans-N-benzylideneaniline, *J. Mol. Struct. THEOCHEM*, 2009, **908**, 122–124.

196 T. E. Souza, I. M. L. Rosa, A. O. Legendre, D. Paschoal, L. J. Q. Maia, H. F. Dos Santos, F. T. Martins and A. C. Doriguetto, Non-centrosymmetric crystals of new N-benzylideneaniline derivatives as potential materials for non-linear optics, *Acta Crystallogr. Sect. B Struct. Sci. Cryst. Eng. Mater.*, 2015, **71**, 416–426.

197 H. B. Bürgi and J. D. Dunitz, Molecular conformation of benzylideneanilines; Relation to electronic structure and spectra, *J. Chem. Soc. D Chem. Commun.*, 1969, 472–473.

198 M. Kaipio, M. Patzschke, H. Fliegl, F. Pichierri and D. Sundholm, Effect of fluorine substitution on the aromaticity of polycyclic hydrocarbons, *J. Phys. Chem. A*, 2012, **116**, 10257–10268.

199 T. Okazaki and K. K. Laali, Transannular π-π Interactions in janusenes and in related rigid systems with cofacial aromatic rings; Gauging aromaticity in the hydrocarbons and in model carbocations; A DFT study, *Org. Biomol. Chem.*, 2006, **4**, 3085–3095.

200 A. Tokatlı and S. Akyürekli, Aromatic character of fluorinated pyridines, *Struct. Chem.*, 2013, **24**, 445–454.

201 S. Gümüş, The aromaticity of substituted diazanaphthalenes, *Comput. Theor. Chem.*, 2011,

963, 263–267.

202 S. E. Wheeler, Understanding substituent effects in noncovalent interactions involving aromatic rings, *Acc. Chem. Res.*, 2013, **46**, 1029–1038.

203 A. L. Ringer, M. O. Sinnokrot, R. P. Lively and C. D. Sherrill, The effect of multiple substituents on sandwich and T-shaped π-π interactions, *Chem. - A Eur. J.*, 2006, **12**, 3821–3828.

204 T. Gelbrich and M. B. Hursthouse, A versatile procedure for the identification, description and quantification of structural similarity in molecular crystals, *CrystEngComm*, 2005, **7**, 324–336.

205 T. Gelbrich and M. B. Hursthouse, Systematic investigation of the relationships between 25 crystal structures containing the carbamazepine molecule or a close analogue: A case study of the XPac method, *CrystEngComm*, 2006, **8**, 448–460.

206 L. Fábián and A. Kálmán, Isostructurality in one and two dimensions: isostructurality of polymorphs, *Acta Crystallogr. Sect. B Struct. Sci.*, 2004, **60**, 547–558.

207 R. S. Rowland and R. Taylor, Intermolecular nonbonded contact distances in organic crystal structures: Comparison with distances expected from van der Waals Radii, *J. Phys. Chem.*, 1996, **100**, 7384–7391.

208 R. Taylor, Identifying intermolecular atom···atom interactions that are not just bonding but also competitive, *CrystEngComm*, , DOI:10.1039/d0ce00270d.

209 T. S. Thakur, R. Dubey and G. R. Desiraju, Intermolecular atom-atom bonds in crystals-a chemical perspective, *IUCrJ*, 2015, **2**, 159–160.

210 I. Mata, I. Alkorta, E. Espinosa and E. Molins, Relationships between interaction energy, intermolecular distance and electron density properties in hydrogen bonded complexes under external electric fields, *Chem. Phys. Lett.*, 2011, **507**, 185–189.

211 M. L. Kuznetsov, Can halogen bond energy be reliably estimated from electron density properties at bond critical point? The case of the (A) n Z—Y•••X − (X, Y = F, Cl, Br) interactions, *Int. J. Quantum Chem.*, 2019, **119**, e25869.

212 A. V. Shishkina, A. I. Stash, B. Civalleri, A. Ellern and V. G. Tsirelson, Electron-density and electrostatic-potential features of orthorhombic chlorine trifluoride, *Mendeleev Commun.*, 2010, **20**, 161–164.

213 F. Bertolotti, A. V. Shishkina, A. Forni, G. Gervasio, A. I. Stash and V. G. Tsirelson, Intermolecular bonding features in solid iodine, *Cryst. Growth Des.*, 2014, **14**, 3587–3595.

214 V. G. Tsirelson, A. S. Avilov, G. G. Lepeshov, A. K. Kulygin, J. Stahn, U. Pietsch and J. C. H. Spence, Quantitative analysis of the electrostatic potential in rock-salt crystals using accurate electron diffraction data, *J. Phys. Chem. B*, 2002, **105**, 5068–5074.

215 A. J. Edwards, C. F. Mackenzie, P. R. Spackman, D. Jayatilaka and M. A. Spackman, Intermolecular interactions in molecular crystals: What's in a name?, *Faraday Discuss.*, 2017, **203**, 93–112.

216 M. A. Spackman, How Reliable Are Intermolecular Interaction Energies Estimated from Topological Analysis of Experimental Electron Densities?, *Cryst. Growth Des.*, 2015, **15**, 5624–5628.

217 A. Varadwaj, H. M. Marques and P. R. Varadwaj, Is the fluorine in molecules dispersive? Is molecular electrostatic potential a valid property to explore fluorine-centered non-covalent interactions?, *Molecules*, 2019, **24**, 379.

218 T. Chen, M. Li and J. Liu, π–π Stacking Interaction: A Nondestructive and Facile Means in Material Engineering for Bioapplications, *Cryst. Growth Des.*, 2018, **18**, 2765–2783.

219 H. Li, Y. Lu, Y. Liu, X. Zhu, H. Liu and W. Zhu, Interplay between halogen bonds and π-π Stacking interactions: CSD search and theoretical study, *Phys. Chem. Chem. Phys.*, 2012, **14**, 9948–9955.

220 C. Estarellas, A. Frontera, D. Quiñonero and P. M. Deyà, Can lone pair-π and cation-π interactions coexist? A theoretical study, *Cent. Eur. J. Chem.*, 2011, **9**, 25–34.

221 R. M. Parrish and C. D. Sherrill, Quantum-mechanical evaluation of π-π Versus substituent-π interactions in π stacking: Direct evidence for the Wheeler-Houk picture, *J. Am. Chem. Soc.*, 2014, **136**, 17386–17389.

222 J. Hwang, P. Li, E. C. Vik, I. Karki and K. D. Shimizu, Study of through-space substituent-π interactions using: N -phenylimide molecular balances, *Org. Chem. Front.*, 2019, **6**, 1266–1271.

223 R. Thakuria, N. K. Nath and B. K. Saha, The Nature and Applications of π-π Interactions: A Perspective, *Cryst. Growth Des.*, 2019, **19**, 523–528.

224 J. Contreras-García, E. R. Johnson, S. Keinan, R. Chaudret, J. P. Piquemal, D. N. Beratan and

W. Yang, NCIPLOT: A program for plotting noncovalent interaction regions, *J. Chem. Theory Comput.*, 2011, **7**, 625–632.

225 A. Otero-De-La-Roza, E. R. Johnson and J. Contreras-García, Revealing non-covalent interactions in solids: NCI plots revisited, *Phys. Chem. Chem. Phys.*, 2012, **14**, 12165–12172.

226 L. Brammer, E. A. Bruton and P. Sherwood, Understanding the Behavior of Halogens as Hydrogen Bond Acceptors, *Cryst. Growth Des.*, 2001, **1**, 277–290.

227 J. A. Van Den Berg and K. R. Seddon, Critical evaluation of C-H···X hydrogen bonding in the crystalline state, *Cryst. Growth Des.*, 2003, **3**, 643–661.

228 T. V. Rybalova and I. Y. Bagryanskaya, C-F...π, F...H, and F...F intermolecular interactions and F-aggregation: Role in crystal engineering of fluoroorganic compounds, *J. Struct. Chem.*, 2009, **50**, 741–753.

229 S. J. Coles and P. A. Gale, Changing and challenging times for service crystallography, *Chem. Sci.*, 2012, **3**, 683–689.

230 S. J. Coles, in *Structure and Bonding*, 2020.

231 H. Nowell, S. A. Barnett, K. E. Christensen, S. J. Teat and D. R. Allan, I19, the small-molecule single-crystal diffraction beamline at Diamond Light Source, *J. Synchrotron Radiat.*, 2012, **19**, 435–441.